

**Functional insights into the architecture and  
TRAF6-mediated regulation of the CBM signalosome  
in lymphocytes**

**Dissertation**

der Fakultät für Biologie  
der Ludwig-Maximilians-Universität München

angefertigt am

**Helmholtz Zentrum München**

Deutsches Forschungszentrum für Gesundheit und Umwelt

Institut für Molekulare Toxikologie und Pharmakologie

Abteilung Zelluläre Signalintegration

vorgelegt von

**Thomas Seeholzer**

München, den 5. September 2019

Diese Dissertation wurde angefertigt  
unter der Leitung von **Prof. Dr. Daniel Krappmann**  
am Helmholtz Zentrum München  
Deutsches Forschungszentrum für Gesundheit und Umwelt  
Institut für Molekulare Toxikologie und Pharmakologie  
Abteilung Zelluläre Signalintegration

**Erstgutachter/in:** Prof. Dr. Daniel Krappmann

**Zweitgutachter/in:** Prof. Dr. Michael Boshart

**Tag der Abgabe:** 5. September 2019

**Tag der mündlichen Prüfung:** 12. November 2020

#### Eidesstattliche Erklärung

Ich versichere hiermit an Eides statt, dass meine Dissertation selbstständig und ohne unerlaubte Hilfsmittel angefertigt worden ist.

Die vorliegende Dissertation wurde weder ganz, noch teilweise bei einer anderen Prüfungskommission vorgelegt.

Ich habe noch zu keinem früheren Zeitpunkt versucht, eine Dissertation einzureichen oder an einer Doktorprüfung teilzunehmen.

München, den 5. September 2019

Thomas Seeholzer

---

Thomas Seeholzer

**TABLE OF CONTENTS**

TABLE OF CONTENTS..... III

LIST OF PUBLICATIONS..... V

LIST OF FIGURES..... VI

1 SUMMARY..... 1

2 ZUSAMMENFASSUNG ..... 4

3 INTRODUCTION..... 7

    3.1 The adaptive immune system..... 7

        3.1.1 Cell-mediated immunity ..... 7

        3.1.2 Humoral immunity ..... 8

    3.2 TCR- and BCR-induced activation of signaling pathways..... 9

    3.3 The CARD11/CARMA1-BCL10-MALT1 signalosome..... 12

        3.3.1 Multidomain structure and function of CBM components ..... 12

        3.3.2 Higher-order filament assembly of the CBM complex..... 15

        3.3.3 Physiological and pathological relevance of the CBM signalosome ..... 16

    3.4 The dual role of MALT1..... 18

        3.4.1 MALT1 scaffolding function induces canonical NF- $\kappa$ B signaling by recruitment of TRAF6 ..... 18

        3.4.2 MALT1 protease function ..... 21

4 AIMS OF THE RESEARCH PROJECT ..... 26

5 PUBLICATIONS..... 28

    5.1 Publication I ..... 28

    5.2 Publication II ..... 51

    5.3 Manuscript I ..... 83

6 DISCUSSION..... 117

    6.1 Structural and functional insights into the architecture of the CBM complex..... 117

---

6.1.1	Formation of the CARD11 seed and BCL10 filaments are highly interconnected processes.....	117
6.1.2	Dynamics of BCL10 filament formation .....	123
6.1.3	Structural organization and function of BCL10-MALT1 filaments .....	124
6.1.4	<i>In vivo</i> relevance of BCL10 filaments for signal propagation in lymphocytes .....	127
6.1.5	Disassembly of the CBM complex.....	128
6.2	Regulation of NF- $\kappa$ B and MALT1 activity by TRAF6 .....	129
6.2.1	TRAF6 is essential for NF- $\kappa$ B activation in Jurkat and primary CD4 T cells.....	129
6.2.2	TRAF6 counteracts constitutive MALT1 paracaspase activity in T cells.....	130
6.2.3	The autoimmune phenotype in <i>Traf6<sup>fl/fl</sup>;CD4-Cre</i> mice .....	134
6.3	Conclusion and outlook .....	137
7	REFERENCES .....	139
8	ABBREVIATIONS .....	149
9	APPENDIX .....	152
9.1	Declaration of individual contribution.....	152
9.2	Further publications.....	155
9.3	Acknowledgments.....	156

## LIST OF PUBLICATIONS

### Publication I

**Thomas Seeholzer\***, Susanne Kurz\*, Florian Schlauderer, Simone Woods, Torben Gehring, Simon Widmann, Katja Lammens, Daniel Krappmann (2018). BCL10-CARD11 Fusion Mimics an Active CARD11 Seed That Triggers Constitutive BCL10 Oligomerization and Lymphocyte Activation. *Front. Immunol.* 9:2695. \* equal contribution

### Publication II

Florian Schlauderer\*, **Thomas Seeholzer\***, Ambroise Desfosses\*, Torben Gehring, Mike Strauss, Karl-Peter Hopfner, Irina Gutsche, Daniel Krappmann, Katja Lammens (2018). Molecular architecture and regulation of BCL10-MALT1 filaments. *Nat Commun.* 9:4041. \* equal contribution

### Manuscript I

**Thomas Seeholzer**, Andreas Gewies, Thomas J. O'Neill, Carina Graß, Katrin Demski, Aurelia Weber, Daniel Krappmann (in preparation). Homeostatic control of MALT1 protease activity by the ubiquitin ligase TRAF6. *In preparation.*

**LIST OF FIGURES**

Figure 3.1: Proximal T and B cell receptor signaling induces activation of the transcription factors NFAT, AP-1 and NF- $\kappa$ B. .... 10

Figure 3.2: Molecular structure of CARD11, BCL10, MALT1A and TRAF6. .... 13

Figure 3.3: Model for CARD11 activation and higher order assembly of the CBM complex..... 15

Figure 3.4: MALT1 scaffolding function in NF- $\kappa$ B activation. .... 20

Figure 3.5: MALT1 protease function contributes to optimal adaptive immune responses..... 23

Figure 6.1: Modes of CBM complex formation..... 118

Figure 6.2: “Paddle wheel-like” architecture of the BCL10-MALT1 filament. .... 125

Figure 6.3: Model for the dual function of the E3 ubiquitin ligase TRAF6..... 131

Figure 6.4: Model for MALT1 scaffold and protease function in balancing activation of immune cells. .... 135

## 1 SUMMARY

Assembly of the CARD11/CARMA1-BCL10-MALT1 (CBM) complex bridges proximal T or B cell receptor (TCR/BCR) signaling to the canonical I $\kappa$ B kinase (IKK)/NF- $\kappa$ B pathway in lymphocytes. CARD11 phosphorylation upon antigenic stimulation induces conformational changes and allows the recruitment of pre-assembled BCL10-MALT1 heterodimers. The caspase recruitment domain (CARD) of CARD11 mediates association with BCL10 through heterotypic CARD-CARD interactions, and thereby functions as a seed to nucleate the assembly of BCL10 filaments. Homotypic BCL10-BCL10 CARD interfaces are critical for BCL10 oligomerization, and assembly of the CBM signalosome serves as a scaffolding platform for the integration of downstream signaling mediators like the E3 ubiquitin ligase TRAF6 and the IKK complex to activate NF- $\kappa$ B. Within the complex, MALT1 serves a dual function, acting as a scaffold and protease. TRAF6 binding motifs (T6BMs) within MALT1 recruit TRAF6 to the CBM complex and thereby promote MALT1 ubiquitination and activation of the IKK complex. In addition, MALT1 paracaspase activity is induced upon antigen stimulation and triggers cleavage of a set of protein substrates. Although the proteolytic activity of MALT1 does not directly contribute to canonical NF- $\kappa$ B signaling, it is essential for optimal activation and differentiation of lymphocytes.

Both processes of BCL10 oligomerization and its recruitment to CARD11 are tightly interconnected, and it is unclear, whether CARD11 nucleates BCL10 filaments, or if filament formation happens prior to or at the same time CARD11-BCL10 interaction occurs. To investigate the cellular relevance of CARD11 seeding function for BCL10 oligomerization and the order of events upon antigenic stimulation, we uncoupled the processes of BCL10 recruitment to CARD11 and BCL10 filament formation by designing a system that bypasses the inducible CARD11-BCL10 association (**Publication I**). For this, we covalently fused BCL10 to the N-terminus of CARD11 and lentivirally expressed the chimeric protein in CRISPR/Cas9-generated CARD11 and BCL10 knockout (KO) Jurkat T cells and CARD11 KO BJAB B cells. By using structure-guided destructive mutations targeting the CARD11-BCL10 or BCL10-BCL10 interfaces we determined their functional impact on NF- $\kappa$ B and MALT1 activity. Stable expression of the BCL10-CARD11 fusion in Jurkat T cells promoted strong and constitutive MALT1 protease activity, and its transient expression activated NF- $\kappa$ B comparably to oncogenic variants of CARD11. In line, BJAB B cells stably expressing the fusion construct induced strong and chronic MALT1 and NF- $\kappa$ B activation, highlighting that the proximity of BCL10 and CARD11 alone is sufficient to induce downstream signaling events. While chronic activation by the fusion was independent of the CARD of CARD11, it strictly relied on the ability of BCL10 to form filaments. Collectively, we show that the recruitment of BCL10 to CARD11 and BCL10 filament formation are highly interconnected processes, and that the initial weak heterotypic interaction

between BCL10 and CARD11 needs to be further stabilized by the oligomerized CARD11 seed and the helical BCL10 filaments.

Although the cryo-electron microscopy (cryo-EM) structure of BCL10 filaments has been determined, there is no structural information for the integration of its constitutive binding partner MALT1 into the filament available, and the exact nature of the BCL10-MALT1 interface remains unresolved. To gain deeper insights into the CBM signalosome assembly, our collaboration partners at the Gene Center of the LMU solved the cryo-EM structure of the BCL10-MALT1 complex (**Publication II**). To confirm the exactly defined interfaces for BCL10-MALT1 and BCL10-BCL10 interaction, we used viral reconstitution assays of BCL10 or MALT1 KO Jurkat T cells or murine CD4 T cells from MALT1 KO mice and investigated their contribution to CBM complex formation, MALT1 paracaspase activation and downstream signaling events. Using cryo-EM, we solved the core structure of the BCL10-MALT1 filament at 4.9 Å resolution and thereby identified the exact binding interface between the CARD of BCL10 and the death domain (DD) of MALT1. Structure-guided missense mutations confirmed the physiological importance of the identified interface. Further, the structural organisation of the BCL10-MALT1 holo-complex at lower resolution indicated how the stable inner core, which is formed by the N-terminal domains of BCL10 and MALT1, orchestrates the flexible outer MALT1 platform with its C-terminal domains that protrude from the core structure. Our model for the assembly and architecture of the CBM signalosome provides detailed insights into the exact BCL10-MALT1 interface and how it functions as a signaling platform for the recruitment of mediators to foster NF- $\kappa$ B signaling in T lymphocytes.

Controversial results regarding TRAF6 for TCR-triggered NF- $\kappa$ B signaling have been obtained. T6BMs on MALT1 are critical for antigen-receptor NF- $\kappa$ B signaling in Jurkat and primary T cells. In addition, siRNA-mediated knockdown of TRAF6 impairs NF- $\kappa$ B signaling in Jurkat T cells. In contrast, T cell-specific deletion of TRAF6 was suggested to not affect NF- $\kappa$ B activation. To clarify the role of TRAF6 in TCR-induced MALT1 and NF- $\kappa$ B activation, we generated TRAF6 KO Jurkat T cells by CRISPR/Cas9-technology and obtained a mouse line with a conditional T cell-specific ablation of TRAF6 (**Manuscript I**). TRAF6 deficiency in Jurkat T cells abolished TCR-induced NF- $\kappa$ B signaling, and mice with conditional deletion of TRAF6 in CD4 T cells were strongly compromised in NF- $\kappa$ B activation upon stimulation. Surprisingly, we found that MALT1 protease is constitutively activated in the absence of TRAF6 leading to chronic substrate cleavage. The observed results in TRAF6 deficient Jurkat and CD4 T cells could be reproduced by mutation of T6BMs in MALT1, which induced chronic MALT1 activation, but abolished NF- $\kappa$ B signaling upon stimulation. Constitutive MALT1 proteolytic activity relied on MALT1-BCL10 association, MALT1 dimerization and mono-ubiquitination and

therefore the same mechanisms as inducible MALT1 catalytic activity upon T cell activation. Moreover, we show that MALT1 paracaspase activity was critical for accurate activation of distinct target genes. Hence, by attributing a new role to TRAF6 in the homeostatic control of MALT1 protease activity in resting cells, we provide a possible explanation for the observed autoimmune and inflammatory phenotype of mice with T cell-specific deletion of TRAF6.

## 2 ZUSAMMENFASSUNG

Die Assemblierung des CARD11/CARMA1-BCL10-MALT1 (CBM) Komplexes in Lymphozyten verknüpft Signale von T- oder B-Zell Rezeptoren (TCR/BCR) mit dem kanonischen I $\kappa$ B Kinase (IKK)/NF- $\kappa$ B Signalweg. Die Phosphorylierung von CARD11 nach Antigenstimulation induziert strukturelle Veränderungen, die zur Rekrutierung von bereits assemblierten BCL10-MALT1 Heterodimeren führt. Die Caspase Rekrutierungsdomäne (CARD) von CARD11 vermittelt die Assoziation mit BCL10 durch heterotypische CARD-CARD Interaktionen und dient als Ansatzpunkt für die Ausbildung von BCL10 Filamenten. Homotypische BCL10-BCL10 CARD Kontaktstellen sind entscheidend für die Oligomerisierung von BCL10. Die Assemblierung des CBM Signalosoms dient als Plattform für die Rekrutierung nachgeschalteter Signalmoleküle wie die E3 Ubiquitin Ligase TRAF6 und den IKK Komplex, um NF- $\kappa$ B zu aktivieren. MALT1 ist sowohl ein Gerüstprotein als auch eine Protease und besitzt daher im CBM Komplex eine duale Funktion. Durch TRAF6 Bindemotive (T6BMs) in MALT1 wird TRAF6 zum CBM Komplex rekrutiert und fördert durch Ubiquitinierung von MALT1 die Aktivierung des IKK Komplexes. Zusätzlich wird die Paracaspase Aktivität von MALT1 durch Stimulation induziert und die Spaltung einer Reihe von Proteinsubstraten veranlasst. Auch wenn die proteolytische Aktivität von MALT1 keinen direkten Beitrag zum kanonischen NF- $\kappa$ B Signalweg leistet, so ist sie dennoch essenziell für die optimale Aktivierung und Differenzierung von Lymphozyten.

BCL10 Oligomerisierung und dessen Rekrutierung zu CARD11 sind eng miteinander verknüpft. Bisher ist unklar, ob CARD11 den Kern für die Bildung von BCL10 Filamenten darstellt, oder ob die Formierung der Filamente vor oder gleichzeitig mit der CARD11-BCL10 Interaktion stattfindet. Um die zelluläre Relevanz der CARD11 Keimfunktion für die BCL10 Oligomerisierung, als auch die zeitliche Reihenfolge der Abläufe nach Antigenstimulation zu untersuchen, haben wir die Prozesse der BCL10 Rekrutierung zu CARD11 sowie der BCL10 Filamentbildung entkoppelt. Hierzu entwickelten wir ein System, das die induzierbare CARD11-BCL10 Assoziation überbrückt (**Publikation I**): BCL10 wurde kovalent an den N-Terminus von CARD11 fusioniert und das chimäre Protein lentiviral in CRISPR/Cas9-generierten CARD11 und BCL10 Knockout (KO) Jurkat T-Zellen und CARD11 KO BJAB B-Zellen exprimiert. Mit Hilfe von strukturbasierten Mutationen, die die CARD11-BCL10 oder BCL10-BCL10 Assoziationen unterbinden, haben wir den funktionellen Einfluss der Kontaktstellen auf die NF- $\kappa$ B und MALT1 Aktivität bestimmt. Stabile Expression der BCL10-CARD11 Fusion in Jurkat T-Zellen führte zu starker und konstitutiver MALT1 Protease Aktivität, und die transiente Expression aktivierte NF- $\kappa$ B im gleichen Maße wie onkogene CARD11 Varianten. BJAB B-Zellen, die das Fusionskonstrukt stabil exprimieren, induzierten eine starke und persistente MALT1 und NF- $\kappa$ B Aktivierung. Dieses Ergebnis deutet darauf hin, dass allein die Nähe von BCL10 und

CARD11 ausreicht, um nachgeschaltete Signalereignisse auszulösen. Die chronische Aktivierung durch das Fusionsprotein war unabhängig von der CARD Domäne von CARD11, benötigte jedoch die Fähigkeit von BCL10, Filamente zu bilden. Zusammenfassend zeigen wir, dass die Rekrutierung von BCL10 zu CARD11 und die BCL10 Filamentausbildung hochgradig miteinander vernetzte Prozesse sind und dass der oligomerisierte CARD11 Kern und die helikalen BCL10 Filamente essentiell für die Stabilisierung der anfänglich schwachen heterotypischen Interaktion zwischen BCL10 und CARD11 sind.

Obwohl die Struktur von BCL10 Filamenten mittels Kryo-Elektronenmikroskopie (Kryo-EM) Struktur bereits gelöst wurde, ist bisher nicht beschrieben, in welcher Weise der konstitutive BCL10 Bindungspartner MALT1 mit den Filamenten interagiert. Die genaue Beschaffenheit des BCL10-MALT1 Interfaces bleibt somit ungeklärt. Um tiefere Einblicke in die CBM Signalosom Assemblierung zu gewinnen, haben unsere Kooperationspartner am Genzentrum der LMU die Kryo-EM Struktur des BCL10-MALT1 Komplexes gelöst (**Publikation II**). Wir verwendeten virale Rekonstitutionsverfahren von BCL10 oder MALT1 KO Jurkat T-Zellen oder murinen CD4 T-Zellen aus MALT1 KO Mäusen, um die identifizierten BCL10-MALT1 und BCL10-BCL10 Interaktionsstellen zu bestätigen und deren Einfluss auf CBM Komplexbildung, MALT1 Paracaspase Aktivierung und nachgelagerte Signalereignisse zu untersuchen. Mit Hilfe der Kryo-EM Struktur haben wir die genaue Beschaffenheit des Kerns innerhalb des BCL10-MALT1 Filaments mit einer Auflösung von 4.9 Å analysiert und die exakte Bindungsstelle zwischen der CARD Domäne von BCL10 und der Todesdomäne (DD) von MALT1 identifiziert. Strukturbasierte Missense-Mutationen bestätigten die physiologische Bedeutung der identifizierten Interaktionsstelle. Darüber hinaus zeigte die strukturelle Organisation des BCL10-MALT1 Holo-Komplexes mit geringerer Auflösung, wie der stabile innere Kern, der aus den N-terminalen Domänen von BCL10 und MALT1 gebildet wird, die flexible äußere MALT1 Plattform mit ihren aus der Kernstruktur herausragenden C-terminalen Domänen orchestriert. Unser Modell für den Aufbau und die Architektur des CBM Signalosoms liefert detaillierte Einblicke in die genaue BCL10-MALT1 Kontaktstelle und wie es als Signalplattform für die Rekrutierung von Mediatoren zur Förderung des NF-κB Signalwegs in T-Lymphozyten fungiert.

Es wurden kontroverse Resultate bezüglich TRAF6 und seiner Rolle für die TCR-induzierte NF-κB Aktivierung erzielt. T6BMs von MALT1 sind maßgeblich am Antigenrezeptor-induzierten NF-κB Signalweg in Jurkat und primären T-Zellen beteiligt. Zusätzlich beeinträchtigt ein siRNA-induzierter Knockdown von TRAF6 NF-κB Aktivierung in Jurkat T-Zellen. Im Gegensatz dazu deutet die T-Zell-spezifische Deletion von TRAF6 darauf hin, dass NF-κB Aktivierung nicht durch TRAF6 beeinflusst

wird. Um die Rolle von TRAF6 in TCR-induzierter MALT1 und NF- $\kappa$ B Aktivierung zu klären, erzeugten wir mit Hilfe von CRISPR/Cas9 Technologie TRAF6 KO Jurkat T-Zellen und generierten eine Mauslinie, in denen TRAF6 spezifisch in T-Zellen eliminiert wurde (**Manuskript I**). Das Fehlen von TRAF6 in Jurkat T-Zellen führte zu einem Verlust des TCR-induzierten NF- $\kappa$ B Signalwegs und Mäuse mit konditionaler Deletion von TRAF6 in T-Zellen zeigten nach Stimulation stark eingeschränkte NF- $\kappa$ B Aktivierung. Erstaunlicherweise führte der Verlust von TRAF6 zu konstitutiver MALT1 Protease Aktivität und chronischer Spaltung von Substraten. Die in TRAF6-defizienten Jurkat und CD4 T-Zellen erzielten Resultate konnten mittels Mutation von T6BMs in MALT1 reproduziert werden, welche chronische MALT1 Aktivierung induzierten, jedoch keine NF- $\kappa$ B Aktivierung nach Stimulation auslösen konnten. Konstitutive proteolytische MALT1 Aktivität war abhängig von der MALT1-BCL10 Interaktion, der MALT1 Dimerisierung sowie der MALT1 Monoubiquitinierung und ist somit auf die gleichen Mechanismen angewiesen wie induzierbare MALT1 Aktivität nach T-Zell Aktivierung. Darüber hinaus zeigen wir, dass die Paracaspase Aktivität von MALT1 entscheidend für die präzise Aktivierung von bestimmten Zielgenen war. Indem wir eine neue Rolle von TRAF6 in der homöostatischen Kontrolle der MALT1 Protease Aktivität in ruhenden Zellen beschreiben, liefern wir eine mögliche Erklärung für den Autoimmun- und Entzündungsphänotyp in Mäusen mit T-Zellspezifischer Deletion von TRAF6.

### 3 INTRODUCTION

The immune system is the most important defence mechanism against pathogens like bacteria or viruses. In order to detect antigenic structures foreign to the body and trigger an immune response, two part systems are known that mammals use to counteract these invaders: the innate and the adaptive immune system (Janeway and Medzhitov 2002; Parkin and Cohen 2001). The innate immune system (also known as the immediate defence) is activated and mediated by complement proteins, natural killer (NK) cells and different phagocytes like neutrophils, dendritic cells and macrophages which detect pathogens via specific pattern-recognition receptors (PRRs) on their cell surface. At the site of injury or infection, resident sentinel cells (mostly mast cells, macrophages and dendritic cells) induce inflammation by releasing pro-inflammatory mediators like chemokines and cytokines (e.g. tumor necrosis factor alpha (TNF $\alpha$ ) and interleukins). This attracts granulocytes, macrophages and neutrophils to the sites of inflammation, and foreign antigens are taken up by antigen presenting cells (i.e. dendritic cells and macrophages). These antigen presenting cells finally migrate to lymph nodes and induce activation of the adaptive immune system. This second line of defence relies on T and B lymphocytes which control specificity and memory of the immune system (long-lasting and protective immunity). Therefore, the adaptive immune system uses a clonal selection of lymphocytes, carrying highly specific antigen receptors. Stimulation of these immune cell receptors activates cellular signal transduction pathways in order to induce transcription of pro-inflammatory cytokines and chemokines in the nucleus, thereby triggering the humoral (production of antibodies by B cells) and the cell-mediated (activation of helper and killer T cells) response. Dysregulation of either the innate or the adaptive immune system contributes to the development of autoimmune diseases or cancer (Warrington et al. 2011).

#### 3.1 The adaptive immune system

##### 3.1.1 Cell-mediated immunity

Main function of the adaptive immune system is the specific recognition of antigens by B and T cells. Progenitor lymphoid cells in the bone marrow give rise to naïve CD4<sup>+</sup>CD8<sup>+</sup> T cells (Gerondakis et al. 2014). These cells harbour specific T cell receptors (TCRs) on their surface which are able to bind to antigens, and so called clusters of differentiation (CD), which are critical co-receptors for the antigen recognition (Wucherpfennig et al. 2010). The TCR complex itself is composed of a membrane-bound  $\alpha\beta$  heterodimer (TCR $\alpha\beta$ ), complemented by four CD3 chains (CD3 $\delta\epsilon$  and CD3 $\gamma\epsilon$ ) as well as a  $\zeta$ -chain dimer ( $\zeta\zeta$ ), which harbour intracellular immunoreceptor tyrosine-based activation motifs (ITAMs) (Figure 3.1A). If a naïve T cell recognizes a self-antigen, it will be destroyed during clonal deletion to avoid autoimmunity. Naïve CD4<sup>+</sup>CD8<sup>+</sup> T cells that are not auto-reactive migrate to the thymus, the organ where T cells mature and differentiate into either single-positive CD4 T cells or CD8 T cells.

These cells further passage to the site of lymph nodes and the spleen, where they differentiate into CD4 effector T helper ( $T_H1$ ,  $T_H2$ ,  $T_H17$ ) or regulatory T (Treg) cells, and CD8 cytotoxic T cells, respectively. While  $T_H1$  cells target intracellular pathogens such as viruses,  $T_H2$  cells induce immune reactions in response to extracellular pathogens and parasites (Zhu and Paul 2008).  $T_H17$  cells mediate host defence mechanisms against extracellular bacteria and fungi, and deregulations of  $T_H17$  responses are related to the development of autoimmune diseases (Weaver et al. 2007). In contrast, Tregs suppress pro-inflammatory responses, and therefore are critical for immune tolerance and lymphocyte homeostasis (Chen et al. 2003; Curotto de Lafaille et al. 2004).

$T_H$  cells bind by help of the co-receptor CD4 to antigen presenting cells (APCs) like dendritic cells, which present antigens via another protein complex, the so called major histocompatibility complex class II (MHCII) (Figure 3.1A) (Vyas et al. 2008; Warrington et al. 2011). Additionally, the APC expresses the surface protein B7 on its surface, and associates with the co-receptor CD28 expressed on the T cell. The contact point of  $T_H$  cell and APC is termed immunological synapse (Alarcon et al. 2011). Recognition of a specific antigen via the TCR at this region, in combination with the costimulatory signals, leads to the activation and proliferation of the T cell (clonal expansion), and production of cytokines like interleukin-2 (IL-2) (Chang et al. 2014). IL-2 synthesis requires the transcription factor nuclear factor of activated T cells (NFAT), which is activated via the  $Ca^{2+}$ -dependent phosphatase Calcineurin (Crabtree 1999). IL-2 stimulates cytotoxic and helper T cell growth and induces thereby a positive feedback loop. In contrast to  $T_H$  cells, cytotoxic T cells become activated by binding of CD8 to MHCI, leading to the secretion of perforins and granzymes, which trigger lysis of the cell membrane and induce apoptosis (Parkin and Cohen 2001).

### 3.1.2 Humoral immunity

In addition to  $CD4^+CD8^+$  T cells, the bone marrow also produces naïve B cells (Parkin and Cohen 2001). Each B cell possesses an antigen-binding receptor of unique specificity on its surface, which is able to recognize specific soluble antigens of pathogens. The B cell receptor (BCR) consists of membrane coupled immunoglobulin (Ig) M or IgD molecules, linked to CD79A/B heterodimers which harbour intracellular ITAM motifs similar to T cells (Figure 3.1B) (Burger and Wiestner 2018). Activated  $T_H$  cells stimulate proliferation of the B cell and lead to its differentiation into either a plasma cell or a memory B cell (Parkin and Cohen 2001). Plasma cells are able to produce and secrete specific classes of antibodies, for instance IgG, which can lead to neutralization (preventing bacterial adhesion), opsonisation (which promotes phagocytosis by macrophages) or complement activation (Casadevall and Pirofski 2003). Each antibody is comprised of two identical heavy (H) and light (L) chains, which are connected and stabilized via disulphide bonds. Moreover, each H and L chain contains a variable (V) and a constant (C) region. While these variable regions confer the

antigen specificity and allow specific recognition of a part of the respective antigen (epitope), the constant regions dictate effector functions of the antibody like recruitment of immune cells (Narciso et al. 2011). Basis for the recognition of the high number of possible antigen structures is the ability of T and B cells to produce a large diversity of antigen-specific receptors and antibodies. This is achieved by somatic recombination of gene segments and, in case of antibodies, somatic hypermutation (Jung et al. 2006; Maul and Gearhart 2010). In addition, class-switch recombination of the immunoglobulin heavy-chain locus allows the switch from one to another isotype of immunoglobulin, thereby modulating the functional properties of the antibody without changing its antigenic specificity (Bonilla and Oettgen 2010).

### **3.2 TCR- and BCR-induced activation of signaling pathways**

In T cells, formation of the immunological synapse upon TCR/CD28 co-stimulation triggers activation of several signaling cascades. Upon antigen recognition, lymphocyte-specific protein tyrosine kinase (LCK) and fibroblast yes-related non receptor kinase (FYN), both members of the sarcoma (Src) family of kinases, are recruited and phosphorylate the CD3 subunits of the TCR via their ITAM motifs (Schulze-Luehrmann and Ghosh 2006) (Figure 3.1A). Following recruitment and activation of zeta-chain-associated protein kinase 70 kDa (ZAP70), the adaptor proteins linker for the activation of T cells (LAT) and SH2 containing leukocyte phosphoprotein of 76 kDa (SLP-76) are phosphorylated and serve as scaffolding proteins for the recruitment of effector molecules such as phospholipase C  $\gamma$ 1 (PLC $\gamma$ 1) (Paul and Schaefer 2013; H. Wang et al. 2010). Activation of PLC $\gamma$ 1 induces hydrolysis of phosphatidylinositol-4,5-bisphosphate (PIP<sub>2</sub>) and formation of the second messengers inositol-1,4,5-triphosphate (IP<sub>3</sub>) and diacylglycerol (DAG). IP<sub>3</sub> triggers the release of calcium from the endoplasmic reticulum into the cytosol, thereby activating the protein phosphatase Calcineurin, which induces activation and nuclear translocation of the transcription factor NFAT (Macian 2005; Oh-hora and Rao 2008). In parallel, DAG, in combination with upstream phosphorylation events and recruitment of the guanine nucleotide exchange factor son of sevenless (SOS), induces activation of the rat sarcoma (Ras) - extracellular signal-regulated kinase 1/2 (ERK1/2) pathway, which results in the activation of the transcription factor activator protein-1 (AP-1) (Smith-Garvin et al. 2009). In addition, DAG promotes activation of protein kinase C  $\theta$  (PKC $\theta$ ). PKC $\theta$ , which is also activated by CD28 co-stimulation via phosphoinositide-dependent kinase 1 (PDK1) (Isakov and Altman 2002; Schmitz and Krappmann 2006), induces phosphorylation of caspase recruitment domain (CARD)-containing coiled-coil protein 11 (CARD11/CARMA1). Phosphorylation of CARD11 triggers conformational changes within the protein, leading to its activation and oligomerization, and recruitment of pre-assembled B cell lymphoma 10 (BCL10) and mucosa-associated lymphoid tissue lymphoma translocation protein 1 (MALT1) heterodimers to form the CARD11-BCL10-MALT1 (CBM)

signaling complex, which is essential for activation of the canonical nuclear factor kappa B (NF- $\kappa$ B) signaling pathway (Thome et al. 2010). In addition to NF- $\kappa$ B activation, the CBM complex also triggers activation of c-Jun N-terminal kinase 1/2 (JNK1/2) (Blonska et al. 2007; Hara et al. 2003), which regulates activity of AP-1 (Dong et al. 2000). Hence, TCR/CD28 co-engagement triggers activation of the transcription factors NFAT, AP-1 and NF- $\kappa$ B, which mediate target gene expression of inflammatory cytokines, chemokines and factors that control survival, differentiation and proliferation of T cells (Bhatt and Ghosh 2014; Weil and Israel 2004).

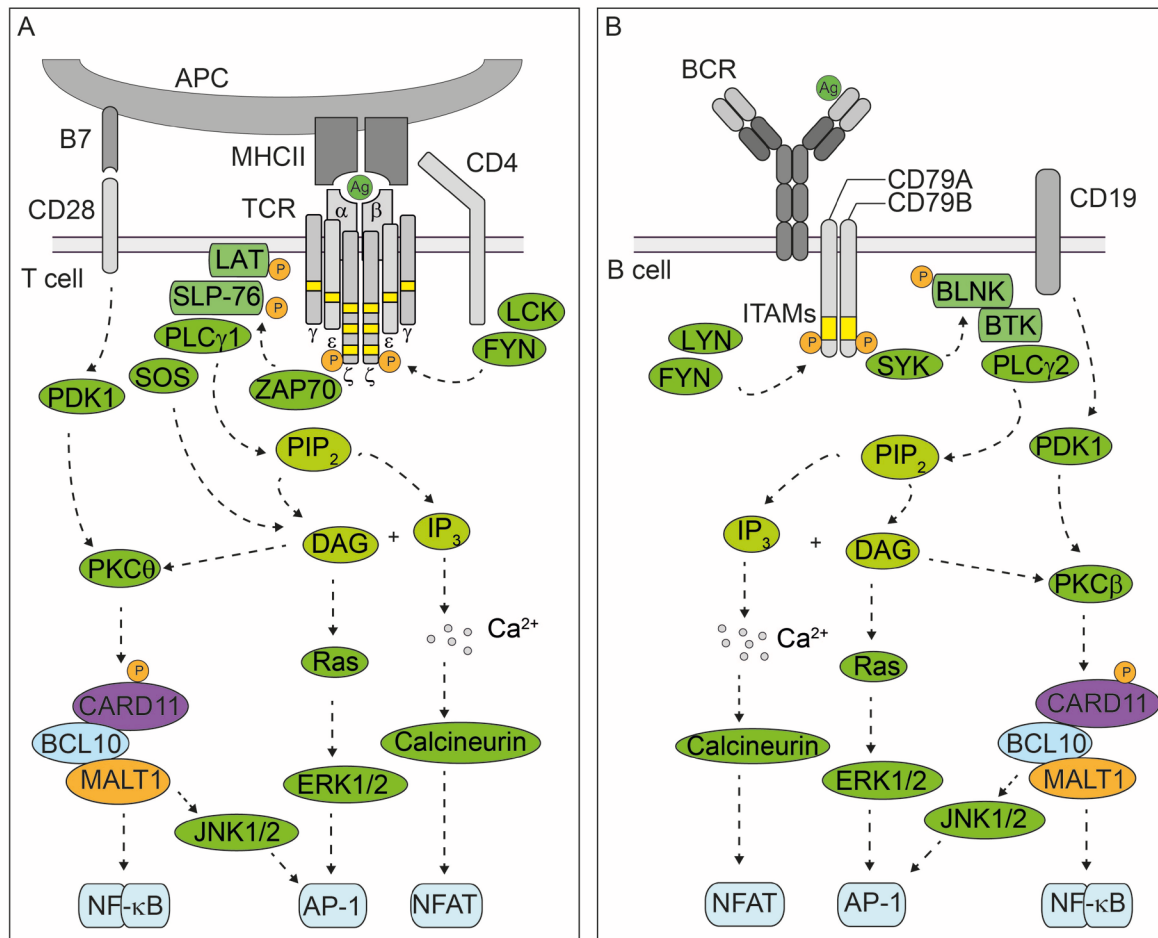


**Figure 3.1: Proximal T and B cell receptor signaling induces activation of the transcription factors NFAT, AP-1 and NF- $\kappa$ B.** (A) Antigen (Ag) presentation via the MHC class II complex on an antigen presenting cell (APC) triggers T cell receptor (TCR) engagement and T cell activation. Phosphorylation of ITAM motifs (marked as yellow bars) within the TCR CD3 subunits by the Src family kinases FYN and LCK allows recruitment of ZAP70, which phosphorylates the adaptor proteins LAT and SLP-76 that serve as scaffold for the activation of PLC $\gamma$ 1. Hydrolysis of PIP $_2$  by PLC $\gamma$ 1 induces formation of the second messengers IP $_3$  and DAG. IP $_3$  triggers release of calcium ions (Ca $^{2+}$ ) from the endoplasmic reticulum and induces activation of NFAT via Calcineurin. DAG, together with the guanine nucleotide exchange factor SOS, activates the Ras-ERK1/2 pathway and results in activation of AP-1. In parallel, DAG promotes activation of PKC $\theta$ , which is supported by CD28 co-stimulation and activation of PDK1. PKC $\theta$  phosphorylates CARD11, triggering CARD11-BCL10-MALT1 (CBM)-complex formation and activation of NF- $\kappa$ B. In addition, the CBM complex also triggers activation of JNK1/2, which leads to activation of AP-1. (B) Recognition of an antigen via the B cell receptor (BCR) on B cells induces phosphorylation of ITAM motifs within the CD79A/B heterodimers by the Src tyrosine-kinase family members FYN and LYN. Recruitment of SYK induces phosphorylation of BLNK, which recruits the effector protein BTK and its substrate PLC $\gamma$ 2. Likewise to T cells, hydrolysis of PIP $_2$  to IP $_3$  and DAG induces activation of NFAT and AP-1, and activation of PKC $\beta$  by DAG and co-receptor engagement triggers formation of the CBM complex and activation of NF- $\kappa$ B.

In contrast to the activation of the TCR in T cells, which relies on the presentation of processed antigens via presenting cells, activation of the BCR in B cells is directly triggered by antigen recognition. Encountering an antigen induces phosphorylation of ITAM motifs within the CD79A/B heterodimers of the BCR by members of the Src tyrosine-kinase family, FYN and Lck/Yes-related novel protein tyrosine kinase (LYN) (Figure 3.1B) (Burger and Wiestner 2018). Recruitment of the tyrosine kinase spleen tyrosine kinase (SYK) induces phosphorylation of the adaptor protein B cell linker (BLNK), which serves as a scaffolding platform. Recruitment of the effector protein bruton's tyrosine kinase (BTK) and its substrate PLCy2 induces, analogous to proximal TCR signaling, the generation of IP<sub>3</sub> and DAG (Cambier et al. 1994). However, phosphorylation of CARD11 is mediated by PKC $\beta$ , which is the functional homolog of PKC $\theta$ . Similar to T cells, this leads to the activation of the transcription factors NFAT, AP-1 and NF- $\kappa$ B (Dal Porto et al. 2004; Harwood and Batista 2010).

Activation of the transcription factor NF- $\kappa$ B is critical for lymphocyte activation, differentiation and survival. This family of transcription factors comprises the five members p65 (RelA), RelB, c-Rel, p105/p50 (NF- $\kappa$ B1) and p100/p52 (NF- $\kappa$ B2), which are ubiquitously expressed (Hayden and Ghosh 2012). Dimeric binding of NF- $\kappa$ B to its cognate DNA sequences ( $\kappa$ B sites) within the nucleus induces target gene expression. However, activation of these transcription factors is tightly controlled by inhibitor of NF- $\kappa$ B (I $\kappa$ B) proteins, for instance I $\kappa$ B $\alpha$ , which retain NF- $\kappa$ B dimers in the cytoplasm by masking their nuclear localization sequences (NLS) (Gerondakis et al. 2014; Oeckinghaus and Ghosh 2009). TCR/BCR engagement triggers phosphorylation of I $\kappa$ B $\alpha$ , inducing its K48-linked polyubiquitination and subsequent degradation by the proteasome. Thereby, NF- $\kappa$ B dimers are liberated and translocate into the nucleus where they induce expression of target genes. In a negative regulatory feedback mechanism, active NF- $\kappa$ B promotes expression and re-synthesis of *NFKBIA*/I $\kappa$ B $\alpha$ , which dissociates DNA-bound NF- $\kappa$ B dimers and causes their nuclear export (Oeckinghaus and Ghosh 2009). NF- $\kappa$ B can be activated by either the canonical or the non-canonical NF- $\kappa$ B pathway. While canonical NF- $\kappa$ B signaling depends on the transcription factors p50, p65 and c-Rel, the non-canonical NF- $\kappa$ B pathway induces translocation of p52-RelB heterodimers into the nucleus to induce target gene expression (Bonizzi and Karin 2004). Antigenic stimulation of lymphocytes mainly drives canonical NF- $\kappa$ B signaling and relies on activation of the I $\kappa$ B kinase (IKK) complex, which consists of the two catalytic subunits IKK $\alpha$  (IKK1) and IKK $\beta$  (IKK2) and the regulatory subunit NF- $\kappa$ B essential modulator (NEMO) (Hinz and Scheidereit 2014).

### 3.3 The CARD11/CARMA1-BCL10-MALT1 signalosome

Bridging antigen-dependent stimulation of lymphocytes to the canonical IKK/NF- $\kappa$ B pathway relies on formation of the high molecular weight CBM complex which is comprised of CARD11/CARMA1, BCL10 and MALT1 (Meininger and Krappmann 2016). CARD11 serves as a multi-domain scaffolding protein and functions as a molecular seed or nucleator for the recruitment of pre-assembled BCL10-MALT1 heterodimers inducing BCL10 filament formation, which links MALT1 functions to the CBM signalosome.

#### 3.3.1 Multidomain structure and function of CBM components

##### 3.3.1.1 CARD11 – A molecular seed for BCL10 filament formation

CARD11/CARMA1 is a ~130 kDa protein and encodes a N-terminal caspase recruitment domain (CARD), followed by a coiled-coil (CC) and a linker region (Figure 3.2). The C-terminus encodes a membrane associated guanylate kinase (MAGUK) domain, comprising a PSD95/Dlg1/ZO-1 (PDZ), Src homology 3 (SH3) and catalytically inactive guanylate kinase (GUK) domain.

In general, CARDS mediate protein-protein interactions that belong to the caspase-recruitment domain subfamily of the death domain (DD) superfamily (Weber and Vincenz 2001). All members of this subfamily are characterized by their conserved structure of six helices, forming an acidic and basic patch on different sides, which is prerequisite for interaction of different CARD domains. The crystal structure of the CARD11 CARD contains six  $\alpha$ -helices arranged around a conserved hydrophobic core, analogous to all members of the CARD family (Li et al. 2012; Qiao et al. 2013). Additionally, a cluster of positively charged residues on the electrostatic surface (R35, R72) is stabilized by two sulphate ions through multiple hydrogen bonds (Li et al. 2012). Indeed, BCL10 is recruited by CARD11 via heterotypic CARD-CARD interaction upon antigen receptor stimulation (Gaide et al. 2002; Li et al. 2012). Furthermore, oligomerization of CARD11 itself is mediated by CARD-CARD interaction via a disulphide bond formed by C28 from each molecule (Jang et al. 2013).

Although no structural information about the CC and linker regions of CARD11 are available, oligomerization of the CC is critical for CBM formation and TCR-induced NF- $\kappa$ B activation (Tanner et al. 2007). Additionally, the CC exerts an auto-inhibitory function on CARD11, as evident from various oncogenic mutations in this region triggering chronic CBM assembly (Lamason et al. 2010; Lenz et al. 2008). For instance, the mutations L225LI and L244P in the CC domain disrupt the interaction between the CARD/CC domain and the inhibitory linker region, thereby driving NF- $\kappa$ B activation in absence of receptor engagement. Accordingly, deletion of the linker region induces constitutive CARD11 activity (Jattani et al. 2016; McCully and Pomerantz 2008). Phosphorylation of the serine residues S645 and S552 by PKC $\beta$ / $\theta$  and S555 by IKK $\beta$  within the linker region upon stimulation are

essential for the interaction with BCL10-MALT1 and stabilize CARD11 in its active conformation (Matsumoto et al. 2005; Shinohara et al. 2007; Sommer et al. 2005). The MAGUK domain, located in the C-terminus of CARD11, mediates association with the membrane, and allows recruitment of CARD11 to PKC $\theta$  at the immunological synapse (Hara et al. 2004; Hara et al. 2015; D. Wang et al. 2004).

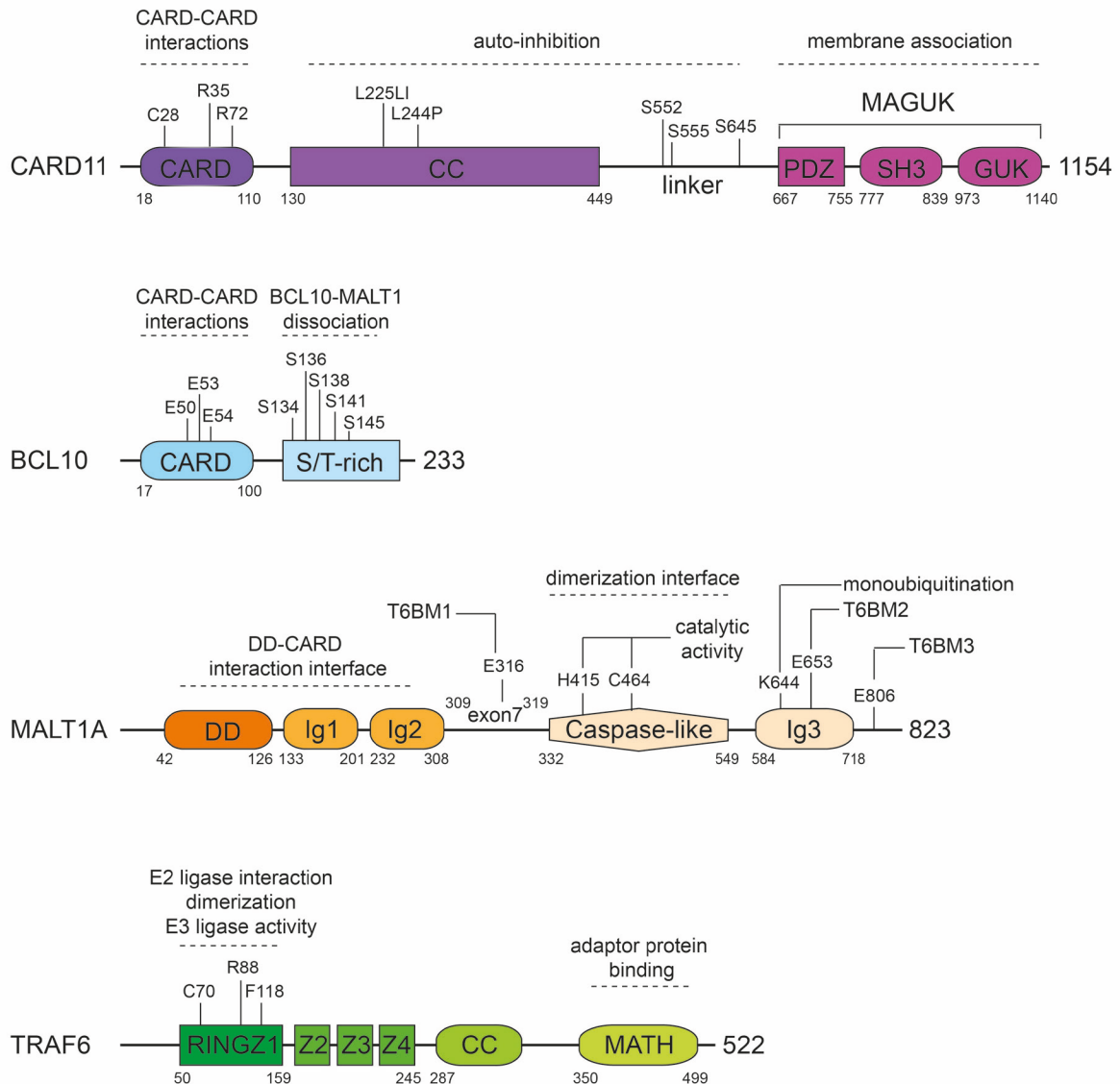


**Figure 3.2: Molecular structure of CARD11, BCL10, MALT1A and TRAF6.**

Individual domains are highlighted in colours and the localization of amino acid residues critical for various protein functions indicated by numbers and dotted lines. Abbreviations: CARD, caspase recruitment domain; CC, coiled-coil; MAGUK, membrane associated guanylate kinase; PDZ, PSD95/Dlg1/ZO-1; SH3, Src homology 3; GUK, guanylate kinase; S/T-rich, Serine/Threonine-rich; DD, death domain; Ig, immunoglobulin-like; T6BM, TRAF6 binding motif; RING, really interesting new gene; Z, Zinc finger; MATH, Meprin and TRAF6 homology; C, Cysteine; R, Arginine; L, Leucine; I, Isoleucine; P, Proline; S, Serine; E, Glutamic acid; H, Histidine; K, Lysine; F, Phenylalanine.

### 3.3.1.2 BCL10 – A linking factor to bridge different CARDs

BCL10 is a ~27 kDa protein and comprises a N-terminal CARD domain followed by a C-terminal Ser/Thr-rich region (Figure 3.2). An acidic stretch (E50, E53, E54) in the CARD of BCL10 allows inducible association with the CARD of CARD11 (Li et al. 2012), and these heterotypic CARD-CARD interactions induce aggregation and filament formation of BCL10 (Qiao et al. 2013). Formation of BCL10 filaments is mediated by different types of homotypic CARD-CARD interactions between the BCL10 molecules and culminates in the formation of the higher order CBM complex (David et al. 2018; Qiao et al. 2013). BCL10 constitutively binds to MALT1, and mutational analysis suggested that the CARD of BCL10 and adjacent residues are critical for MALT1 association (Langel et al. 2008; Lucas et al. 2001). The Ser/Thr-rich region in the C-terminus of BCL10 stabilizes the BCL10-MALT1 interaction (Wegener et al. 2006). Antigen-induced phosphorylation of multiple phosphorylation sites in this region (S134/S136/S138/S141/S145) by IKK $\beta$  interferes with BCL10-MALT1 association, and thereby functions as a negative feedback mechanism which impairs NF- $\kappa$ B and T cell activation (Wegener et al. 2006).

### 3.3.1.3 MALT1 – Scaffold and protease for signal transmission

MALT1, also known as paracaspase1 (PCASP1), encodes a ~92 kDa protein and harbours a N-terminal death domain (DD), three immunoglobulin-like (Ig) domains and a paracaspase domain (Figure 3.2). Again, mutational analysis suggested that BCL10 interaction is mediated by the N-terminal Ig1 and Ig2 domains of MALT1 and is further stabilized by the DD (Langel et al. 2008; Lucas et al. 2001). Three putative TRAF6 binding motifs (T6BMs) have been mapped on MALT1 (E316, E653 and E806) (Noels et al. 2007; L. Sun et al. 2004), and binding of TRAF6 promotes MALT1 ubiquitination and activation of the IKK complex (Oeckinghaus et al. 2007). Besides its scaffolding function, the paracaspase domain of MALT1 confers proteolytic activity upon antigen stimulation (Coornaert et al. 2008; Rebeaud et al. 2008). Determination of the crystal structure of the 228-amino-acid-long catalytic domain shows a similar fold compared to caspases in general, with the initiator caspase-9 as the closest structural relative (Wiesmann et al. 2012). In line with classical caspases, dimerization of the paracaspase domain and formation of a catalytic dyad between C464 and H415 upon substrate binding is prerequisite for its proteolytic activity (Wiesmann et al. 2012). However, while caspases cleave substrates C-terminal of aspartate, MALT1 is an arginine-specific protease and does not induce apoptosis (Hachmann et al. 2012). Additionally, monoubiquitination of K644 in the Ig3 domain, which is a critical step for MALT1 paracaspase activation upon T cell stimulation, requires an intact dimerization interface (Cabalzar et al. 2013; Pelzer et al. 2013).

### 3.3.2 Higher-order filament assembly of the CBM complex

Upon TCR/BCR engagement, CARD11, BCL10 and MALT1 assembly leads to the formation of the higher order CBM complex (Qiao et al. 2013). Prerequisite for formation of the CBM signalosome are structural rearrangements within CARD11 (Figure 3.3). In resting cells, the linker region interacts with the CARD/CC domain of CARD11 to keep it in a closed and inactive conformation (Jattani et al. 2016; McCully and Pomerantz 2008). Upon antigenic stimulation and recruitment of CARD11 to the immunological synapse, multiple phosphorylation events in the linker region induce conformational changes and convert CARD11 in an open and active form (Matsumoto et al. 2005; Sommer et al. 2005). The conformational changes within CARD11 allow the recruitment of preassembled BCL10-MALT1 heterodimers via heterotypic CARD-CARD interactions between CARD11 and BCL10 (Li et al. 2012). Subsequent formation of BCL10 filaments via homotypic CARD-CARD interactions between the BCL10 molecules provides a platform for MALT1 dimerization, thereby bridging MALT1 scaffold and protease function to the CBM complex (Qiao et al. 2013).

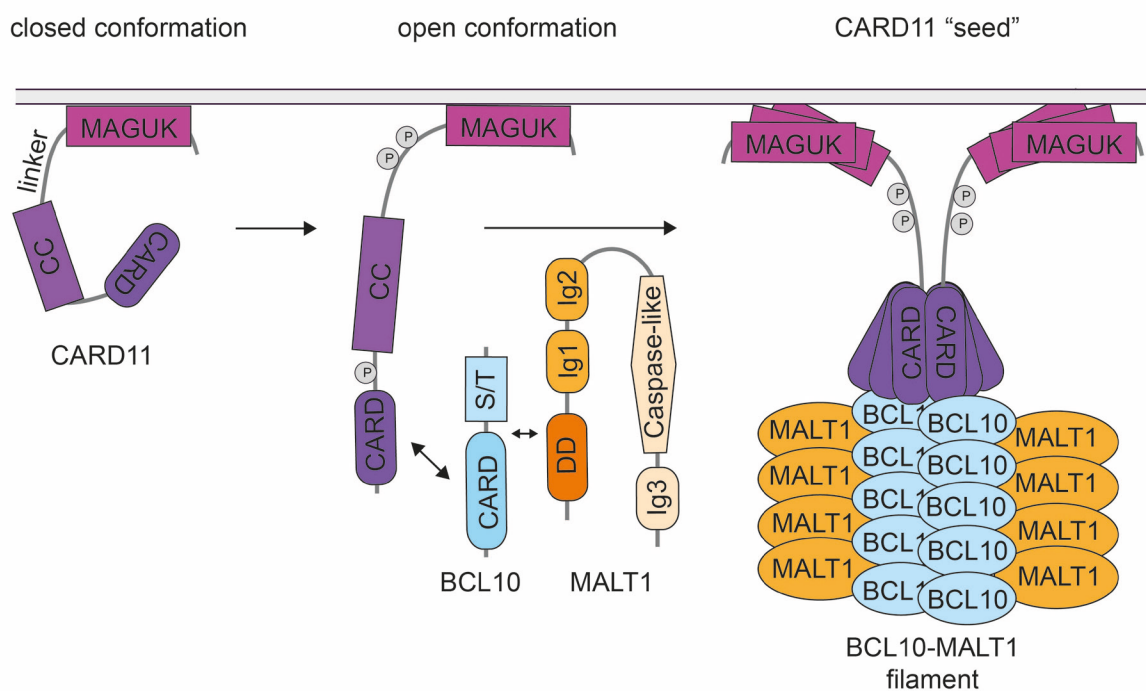


**Figure 3.3: Model for CARD11 activation and higher order assembly of the CBM complex.**

In resting cells, CARD11 is kept in an inactive, closed conformation by intramolecular interactions between the CARD/CC and the linker region, and associates with the cell membrane via its MAGUK domain. Upon antigen receptor ligation on lymphocytes, phosphorylation of CARD11 induces conformational changes and allows its oligomerization via homotypic CARD-CARD interactions. In its open, active conformation, oligomerized CARD11 serves as a molecular seed and induces the recruitment of pre-assembled BCL10-MALT1 complexes via heterotypic CARD-CARD interactions between CARD11 and BCL10. CARD11 thereby nucleates the formation of BCL10 filaments by homotypic CARD-CARD interactions between the BCL10 molecules, thereby bridging MALT1 scaffold and protease function to the higher order signalosome. Double-headed arrows represent protein-protein interactions. Abbreviations: CARD, caspase recruitment domain; CC, coiled-coil; MAGUK, membrane associated guanylate kinase; S/T-rich, Serine/Threonine-rich; DD, death domain; Ig, immunoglobulin-like.

Indeed, formation of high molecular weight structures by components of the CBM complex could be observed by immunofluorescence microscopy: overexpression of BCL10 in HeLa cells shows a clear pattern of distinct and interconnecting cytoplasmic filaments, resembling death-effector filaments in general (Güet and Vito 2000). Mutations in the CARD domain of BCL10 abrogate these filamentous structures and NF- $\kappa$ B activation, highlighting that filament formation is a critical step for BCL10 activation. Subsequent work in T cells could show that BCL10 is enriched in cytoplasmic structures, termed POLKADOTS (punctate and oligomeric killing or activating domains transducing signals) upon TCR stimulation (Rossman et al. 2006; Schaefer et al. 2004). These focal sites of highly dynamic information exchange integrate BCL10 and its partner signaling proteins of the CBM signalosome such as CARD11 and TRAF6 (tumor necrosis factor receptor associated factor 6) to foster TCR-mediated signaling towards NF- $\kappa$ B. Again, mutations in the CARD of BCL10 interfered with POLKADOT formation and correlated with the ability of BCL10 to activate NF- $\kappa$ B (Rossman et al. 2006).

By use of cryo-electron microscopy (cryo-EM), the architecture and assembly of these filamentous structures could be resolved in the nanometer range (Qiao et al. 2013). *In vitro*, BCL10 forms helical filaments with left-handed symmetry and three to four BCL10 subunits per turn. The helix is formed by three different types of homotypic CARD-CARD interactions between the BCL10 molecules, and mutation of these interfaces abrogates BCL10 filament formation. Moreover, mutations within these interfaces not only abolish BCL10 oligomerization, but impair MALT1 and NF- $\kappa$ B activation in T cells, and emphasizes the role of BCL10 filament assembly *in vivo* (Qiao et al. 2013). CARD11 resides selectively on one tip of the BCL10 filaments, highlighting its role as a molecular seed to nucleate BCL10 filament formation via heterotypic CARD-CARD contacts between CARD11 and BCL10 (David et al. 2018; Qiao et al. 2013). Finally, formation of the BCL10 filaments provides a platform for the incorporation of MALT1, and the recruitment and integration of additional mediators to foster downstream signaling events.

### **3.3.3 Physiological and pathological relevance of the CBM signalosome**

The requirement of each CBM component for adaptive immune signaling via T and B cell activation has been underscored by the generation of mouse cell lines with specific ablations of CARD11, BCL10 or MALT1. CARD11 and BCL10 knockout (KO) mice show defects for the activation of NF- $\kappa$ B and JNK in both T and B cells, and therefore fail to proliferate upon antigen stimulation (Egawa et al. 2003; Hara et al. 2003; Ruland et al. 2001). Similarly, MALT1 KO mice show abolished NF- $\kappa$ B signaling and strong defects in T and B cell activation, proliferation and survival in response to antigens (Ruefli-Brasse et al. 2003; Ruland et al. 2003). Consequently, the lack of any component of the CBM

complex leads to severe defects in adaptive immunity. Although deletion of CARD11, BCL10 or MALT1 in mice do not affect total lymphocyte numbers, differentiation of specific lymphocyte subsets critically depends on the CBM complex. For instance, development of the Treg lineage relies on all components of the CBM signalosome (Barnes et al. 2009; Brustle et al. 2017; Molinero et al. 2009; Schmidt-Supprian et al. 2004), and differentiation of T<sub>H</sub>17 cells is strongly impaired in MALT1 KO mice (Brustle et al. 2012; Molinero et al. 2012). Hence, the CBM complex is also important in balancing the development of both effector and regulatory T cells and thereby contributes to the maintenance of immune homeostasis.

The pathological relevance for proper CBM complex signaling is evident from genetic alterations of the CBM causing human disease. Both gain- or loss-of-function mutations in CARD11, BCL10 and MALT1 can frequently be found in human pathology and contribute to the development of lymphoma or immunodeficiency, respectively. B cell lymphoid malignancies, including MALT1 lymphoma and diffuse large B cell lymphoma (DLBCL), are characterized by frequent somatic mutations that enhance NF- $\kappa$ B signaling and thereby sustain lymphoma growth and survival.

MALT1 was originally identified from the chromosomal translocation t(11;18)(q21;q21) that leads to the generation of the API2-MALT1 fusion protein by fusing the C-terminal caspase-like domain of MALT1 to the N-terminus of the inhibitor of apoptosis 2 (cIAP2 or API2) (Morgan et al. 1999). This oncogenic gain-of-function fusion protein drives aberrant antigen-independent activation of NF- $\kappa$ B and MALT1 paracaspase activity and is the most frequent translocation detected in MALT lymphoma (Lucas et al. 2001). Interestingly, the chimeric fusion protein not only cleaves typical MALT1 substrates, but activates oncogenic non-canonical NF- $\kappa$ B signaling by cleaving and thereby stabilizing the NF- $\kappa$ B-inducing kinase (NIK) (Rosebeck et al. 2011).

Additionally, oncogenic activation of the NF- $\kappa$ B pathway contributes to the development of many lymphoid malignancies (Nagel et al. 2014). DLBCL, a class of non-Hodgkin lymphoma (NHL), accounts for 30% to 40% of all NHL cases and can be classified into various subtypes via their gene expression (Lenz and Staudt 2010; Shaffer et al. 2012). In contrast to the activated B cell (ABC) like subtype, that strictly depends on constitutive activation of the NF- $\kappa$ B pathway, the germinal center B cell (GCB) like subtype is devoid of NF- $\kappa$ B activity under basal conditions (Davis et al. 2001; Lam et al. 2005). Constitutive activation of NF- $\kappa$ B in the ABC-type of DLBCL is triggered by a variety of mutations, which include the B cell receptor associated CD79 chains or in the CC domain of the CBM component CARD11 itself (Davis et al. 2010; Lenz et al. 2008). Mechanistically, mutations in the CC in CARD11 disrupt interaction with its linker region (Lamason et al. 2010). Since the linker region keeps CARD11 in an inactive state in resting cells, loss of this interaction converts CARD11 in its active conformation

and drives NF- $\kappa$ B and MALT1 activation by bypassing the requirement of BCR engagement. Interestingly, overexpression of the oncogenic CARD11 mutants L225LI and L244P in GCB DLBCL induces strong constitutive NF- $\kappa$ B and MALT1 activity (Bognar et al. 2016). Of note, patients with germline activating CARD11 mutations cause a phenotype known as B cell expansion with NF- $\kappa$ B and T cell anergy (BENTA), which activates B cells but renders T cells anergic (Brohl et al. 2015; Buchbinder et al. 2015; Snow et al. 2012).

In contrast to gain-of-function mutations, germline loss-of-function mutations in CARD11, BCL10 or MALT1 are associated with combined immunodeficiency (CID), a syndrome in which the function of T and B lymphocytes, and therefore adaptive immunity, is severely impaired. For instance, destructive CARD11 mutations lead to a complete loss of CARD11 protein expression and strongly reduce proliferation of T cells and development of B cells (Greil et al. 2013; Stepensky et al. 2013). Additionally, patients are strongly compromised in the development of Tregs. In line, patients who are deficient of BCL10 have similar impairments in adaptive immune responses (Torres et al. 2014). Homozygous missense mutations in MALT1 result in either decreased or complete loss of MALT1 expression or protease activity, thereby impairing NF- $\kappa$ B activation and T cell proliferation (Jabara et al. 2013; McKinnon et al. 2014; Turvey et al. 2014). Interestingly, several patients with MALT1 loss-of-function mutations developed an autoimmune phenotype, which is possibly caused by partially functional T cell responses in combination with the complete absence of Tregs that fail to maintain immune homeostasis (Charbit-Henrion et al. 2017).

### **3.4 The dual role of MALT1**

#### **3.4.1 MALT1 scaffolding function induces canonical NF- $\kappa$ B signaling by recruitment of TRAF6**

Upon TCR/BCR engagement and formation of the CBM complex, the E3 ubiquitin ligase TRAF6 is recruited to MALT1 via TRAF6 binding sites and induces MALT1 polyubiquitination (Figure 3.4) (Noels et al. 2007; Oeckinghaus et al. 2007; L. Sun et al. 2004). TRAF6 belongs to the family of RING (really interesting new gene) E3 ligases and is ubiquitously expressed (Arch et al. 1998). RING ligases catalyze the direct transfer of ubiquitin by bridging ubiquitin, which is bound by an ubiquitin-conjugating enzyme (UBC) E2, to the substrate (Deshaies and Joazeiro 2009; Metzger et al. 2014). Structurally, TRAF6 is characterized by an N-terminal RING and Zinc Finger 1 (Z1) domain, which confers ubiquitin ligase activity, followed by several zinc fingers (Z2-4) (Ha et al. 2009) (Figure 3.2). The C-terminal region (also termed TRAF domain) can be subdivided into an N-terminal coiled-coil (CC) and a C-terminal MATH (Meprin and TRAF6 homology) domain, and primarily mediates binding to adaptor proteins by forming trimeric structures (Rothe et al. 1994; Ye et al. 2002). Structural

studies indicate that the N-terminal RING/Z1-domain is necessary for catalyzing K63-linked polyubiquitin chains *in vitro*, with the UBC13/UEV1A complex serving as the E2 conjugating enzyme, and residues in the TRAF6-UBC13 interaction site (e.g. C70) are crucial for TRAF6 E3 ligase activity (Lamothe et al. 2008; Walsh et al. 2008; Ye et al. 2002; Yin et al. 2009). In addition to its function in bridging E2s to substrates, the RING domain mediates TRAF6 dimerization, which is required for higher-order oligomerization and polyubiquitination of TRAF6 (Yin et al. 2009).

Several putative TRAF6 binding motifs on MALT1 have been described and are located between the Ig2 and paracaspase domain (T6BM1) or in vicinity of the C-terminal Ig3 domain (T6BM2 and 3) (Figure 3.2) (Noels et al. 2007; L. Sun et al. 2004). Importantly, alternative splicing of MALT1 modulates its scaffolding function by inclusion (isoform A, MALT1A) or exclusion (isoform B, MALT1B) of exon7, which encodes an additional TRAF6 binding site (T6BM1) (Figure 3.2) (Meininger et al. 2016). Only T6BM1 and T6BM3 have been shown to serve as functional TRAF6 binding motifs that control NF- $\kappa$ B signaling in T cells, and presence of the additional binding site in MALT1A (T6BM1) enhances recruitment of TRAF6 and therefore activation of NF- $\kappa$ B (Meininger et al. 2016).

Upon binding, activated TRAF6 initiates K63-linked polyubiquitination of MALT1, thereby providing a docking platform that facilitates recruitment and activation of the IKK complex with its two catalytic subunits IKK $\alpha$  and IKK $\beta$  and the regulatory subunit NEMO (Figure 3.4) (Duwel et al. 2009; Hinz and Scheidereit 2014; Oeckinghaus et al. 2007). In addition, attachment of K63-linked ubiquitin chains to BCL10 by a yet undefined ubiquitin ligase facilitates recruitment of NEMO (C. J. Wu and Ashwell 2008). Further, K63-linked ubiquitination of NEMO by TRAF6 sustains recruitment and activation of the IKK complex (Shambharkar et al. 2007). The following engagement of the TAB/TAK1 complex induces activation of the IKK complex by phosphorylation of IKK $\beta$  (Oeckinghaus et al. 2007; L. Sun et al. 2004). Ultimately, the IKK complex phosphorylates I $\kappa$ B $\alpha$ , inducing its K48-linked polyubiquitination and subsequent degradation by the proteasome. Thereby, previously repressed NF- $\kappa$ B dimers are liberated and translocate into the nucleus where they induce expression of target genes.

Of note, inconsistent results have been obtained regarding the role of TRAF6 for TCR/CD28-triggered NF- $\kappa$ B signaling. For instance, siRNA-mediated knockdown of TRAF6 delays I $\kappa$ B $\alpha$  degradation and impairs NF- $\kappa$ B signaling in Jurkat T cells (Bidere et al. 2006; Oeckinghaus et al. 2007). Additionally, TRAF6 binding motifs in both MALT1 isoforms are essential for the recruitment of TRAF6, and mutation of T6BMs abolishes NF- $\kappa$ B signaling in Jurkat and primary T cells (Meininger et al. 2016; Noels et al. 2007). Contradictory, conditional ablation of TRAF6 in murine CD4 T cells was suggested not to affect NF- $\kappa$ B signaling (King et al. 2006). This questions the relevance of TRAF6 for TCR-

induced NF- $\kappa$ B signaling and led to the prediction that other E3 ubiquitin ligases may compensate for loss of TRAF6 in T cells. Nevertheless, the physiological relevance of TRAF6 is highlighted by the phenotype of mice which are deprived or harbour a T cell specific deletion of TRAF6: ablation in mice leads to defects in osteoclast development, which results in thickening of bones (osteopetrosis) (Lomaga et al. 1999; Naito et al. 1999). Additionally, TRAF6-deficient mice lack lymph nodes, are compromised in the development of thymic stroma and died after three weeks (Akiyama et al. 2005; Naito et al. 1999). Moreover, CD4 T cell-selective deletion of TRAF6 in mice leads to the development of a multi-organ inflammatory disease after ten weeks, attended by upregulation of activated and effector-memory T cells (King et al. 2006). However, which exact mechanisms contribute to the observed autoimmune and inflammatory phenotype of mice lacking TRAF6 in T cells is largely unclear.

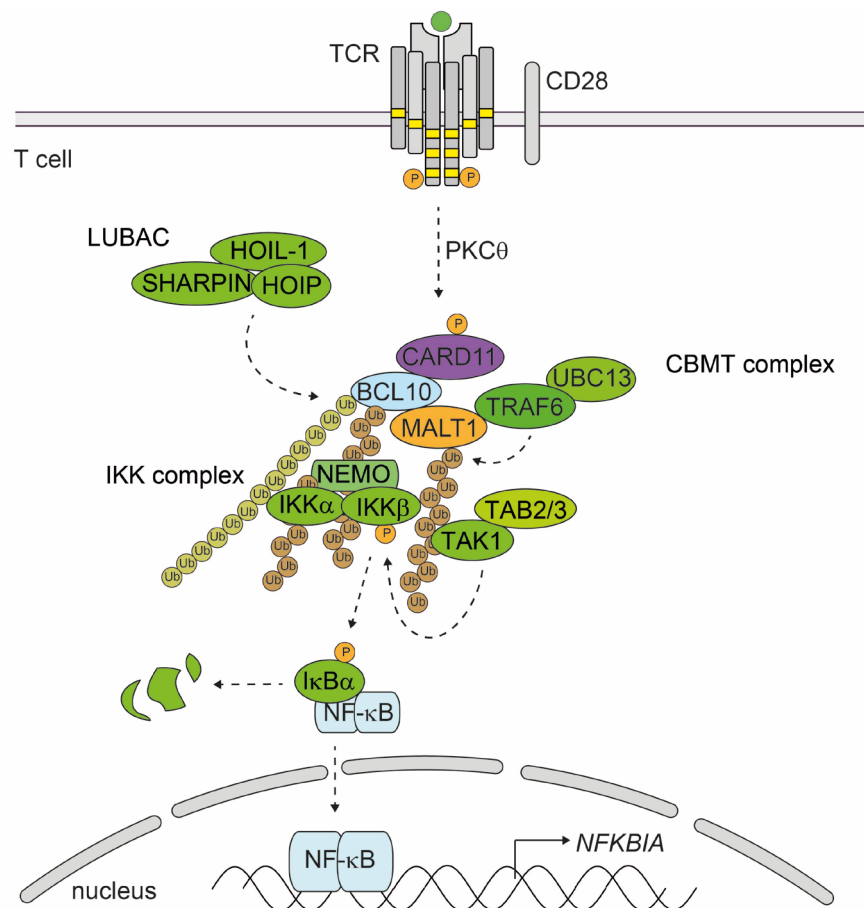


**Figure 3.4: MALT1 scaffolding function in NF- $\kappa$ B activation.**

Upon TCR engagement, phosphorylation of CARD11 by PKC $\theta$  induces formation of the CARD11-BCL10-MALT1 (CBM) complex. MALT1 recruits the E3 ubiquitin ligase TRAF6 via TRAF6 binding sites, which induces in cooperation with the E2 conjugating enzyme UBC13 the K63-linked poly-ubiquitination of MALT1. Ubiquitin chains on MALT1 facilitate the recruitment of the IKK complex, which is further sustained by attachment of K63-linked ubiquitin chains on BCL10. Additionally, BCL10 is potentially decorated with linear ubiquitin chains by the linear ubiquitin chain assembly complex (LUBAC) and contributes to the interaction with NEMO. Following recruitment of the TAB2/3-TAK1 complex induces phosphorylation and activation of IKK $\beta$ , triggering I $\kappa$ B $\alpha$  phosphorylation, ubiquitination and its proteasomal degradation. Thereby, NF- $\kappa$ B translocates into the nucleus and induces target gene expression, for instance re-synthesis of *NFKBIA*/I $\kappa$ B $\alpha$ .

In addition to TRAF6 recruitment to the CBM complex and induced K63-linked ubiquitination, linear M1-linked ubiquitination in response to tumor necrosis factor receptor (TNFR), IL-1R or toll-like receptor (TLR) stimulation facilitates NF- $\kappa$ B activation (Ikeda 2015). The only known E3 ligase complex which is able to generate linear ubiquitin chains is the linear ubiquitin chain assembly complex (LUBAC) (Kirisako et al. 2006). LUBAC consists of the three proteins heme-oxidized IRP2 ubiquitin ligase 1 (HOIL-1 aka RBCK1), HOIL-1-interacting protein (HOIP aka RNF31) and Shank-associated RH domain-interacting protein (SHARPIN), with HOIP as the subunit which confers E3 ligase activity to the complex (Emmerich et al. 2011; Tokunaga and Iwai 2012).

Recently, association of LUBAC to the CBM signalosome upon T cell stimulation was reported, suggesting a role in the adaptive immune response (Dubois et al. 2014): LUBAC components HOIP and SHARPIN contribute to efficient NF- $\kappa$ B activation, independently of the catalytic activity of HOIP (Figure 3.4). Moreover, a system-wide analysis of BCR signalosomes delineated that BCL10 is modified by linear ubiquitination, indicating a possible role of LUBAC in BCR-induced NF- $\kappa$ B signaling (Satpathy et al. 2015). Similar to B cells, BCL10 is conjugated with linear-linked polyubiquitin chains upon TCR stimulation, which is prerequisite for interaction with the IKK complex subunit NEMO, and suggests a role of linear ubiquitination for antigen-receptor induced NF- $\kappa$ B activation (Y. K. Yang et al. 2016b). However, further investigations will be needed to clarify the role and contribution of linear ubiquitination for TCR-induced NF- $\kappa$ B activation in T cells.

### **3.4.2 MALT1 protease function**

#### **3.4.2.1 MALT1 paracaspase activity mediates cleavage of various substrates**

*In silico* studies showed that MALT1 shares high sequence homology to caspases and metacaspases and is therefore categorized as a caspase-like protease or paracaspase (Hulpiau et al. 2016; Uren et al. 2000). Since initial studies could not attribute proteolytic activity to MALT1, it was suggested that MALT1 solely functions as a scaffold protein (Snipas et al. 2004; Uren et al. 2000). However, protease activity, induced upon CBM complex assembly, could be described for the first time by identification of the MALT1 substrates BCL10 and A20 (Coornaert et al. 2008; Rebeaud et al. 2008). In contrast to caspases, which cleave substrates C-terminal of aspartate, MALT1 is an arginine-specific protease, and therefore more closely related to arginine/lysine-specific metacaspases from plants and fungi (Hachmann et al. 2012; Uren et al. 2000; Wiesmann et al. 2012). In its ligand-free, substrate-unbound form, MALT1 is kept inactive by several mechanisms to prevent activation of its protease activity (Wiesmann et al. 2012). For instance, the C-terminal Ig3 domain forms a lid-like structure and interacts with the caspase domain, thereby retaining it in an inactive state. Upon substrate binding, structural rearrangements throughout the molecule, especially changes which affect

interaction between the Ig3 domain and the caspase-domain, release the paracaspase from its auto-inhibition (Wiesmann et al. 2012; J. W. Yu et al. 2011). Moreover, activation of MALT1 paracaspase activity requires its dimerization within the BCL10-MALT1 filaments and mono-ubiquitination in the Ig3 domain (Pelzer et al. 2013; Qiao et al. 2013; Wiesmann et al. 2012).

In recent years, a set of MALT1 substrates has been identified and comprises components of the CBM complex, regulators of NF- $\kappa$ B signaling or post-transcriptional modulators (Figure 3.5). Cleavage of BCL10, the constitutive interaction partner of MALT1 and one of the first substrates that has been described, removes the last five amino acids from the C-terminus of BCL10 (Rebeaud et al. 2008). Although cleavage of BCL10 is required for integrin-dependent adhesion of T cells to fibronectin and therefore the efficient contact of T cells to APCs, its cleavage is not required for expression of NF- $\kappa$ B target genes. Self-cleavage of MALT1 between its DD and Ig1 domain (after residue R149) results in generation of an active p76 fragment, which dissociates from BCL10 and promotes TRAF6-dependent NF- $\kappa$ B activation, without influencing its protease activity (Baens et al. 2014). In addition, a second auto-cleavage site of MALT1 after R781 was reported, and was suggested to contribute to downregulation of NF- $\kappa$ B (Ginster et al. 2017). However, the exact biological effects of BCL10 cleavage and MALT1 auto-proteolysis remain unclear.

The identification of several substrates that are involved in NF- $\kappa$ B and JNK signaling led to the assumption that MALT1 paracaspase activity contributes to optimal T cell activation by fine-tuning TCR-induced signaling pathways. For instance, A20, a deubiquitinase (DUB) that removes K63-linked polyubiquitin chains from MALT1, TRAF6 and NEMO and thereby negatively regulates NF- $\kappa$ B activation, is cleaved by MALT1 upon TCR stimulation (Coornaert et al. 2008; Duwel et al. 2009). Like A20, the deubiquitinase cylindromatosis (CYLD) negatively regulates NF- $\kappa$ B and JNK signaling following various stimuli, and removes K63-linked polyubiquitin chains from NEMO or TRAF6 (Reiley et al. 2007; S. C. Sun 2010; Yoshida et al. 2005). Cleavage of CYLD seems not to be directly implicated in TCR-dependent NF- $\kappa$ B signaling, but was suggested to be required for TCR-induced JNK activation and expression of AP-1-dependent target genes (Staal et al. 2011). Moreover, MALT1-dependent cleavage of RelB appears to promote RelA- and c-Rel-dependent NF- $\kappa$ B activation by removing transcriptionally inactive RelB-RelA and RelB-c-Rel dimers (Hailfinger et al. 2011). More recently, cleavage of the LUBAC component HOIL-1 was suggested to provide a negative feedback loop on NF- $\kappa$ B signaling: cleavage of HOIL-1 by MALT1 reduces linear ubiquitination of several proteins, for instance NEMO, and thereby dampens NF- $\kappa$ B activation and, at the same time, prevents its reactivation (Klein et al. 2015). In a second study, it was proposed that MALT1-induced cleavage of HOIL-1 provides a gain-of-function mechanism and that generation of the C-terminal HOIL-1

fragment itself possesses LUBAC inhibitory properties, thereby negatively regulating NF- $\kappa$ B signaling (Elton et al. 2016).

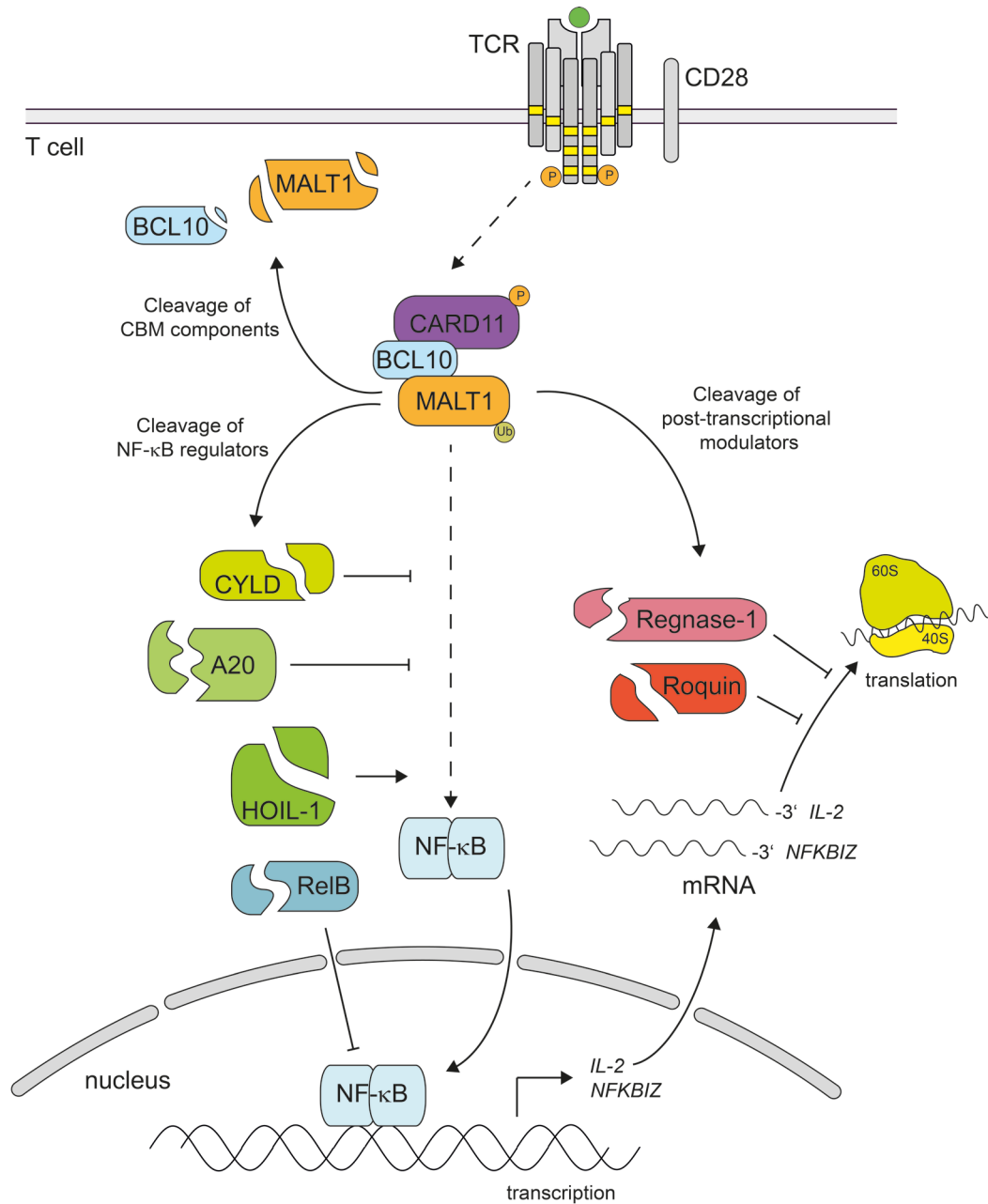


**Figure 3.5: MALT1 protease function contributes to optimal adaptive immune responses.**

Upon TCR stimulation, formation of the CBM signalosome induces NF- $\kappa$ B activation. In parallel, MALT1 protease is activated by its mono-ubiquitination and induces the cleavage of various cellular targets. Substrates comprise the CBM complex components BCL10 and MALT1, both positive (HOIL-1) and negative regulators (CYLD, A20, RelB) of NF- $\kappa$ B signaling, and the post-transcriptional modulators Regnase-1 and Roquin. Hence, MALT1-induced cleavage of Regnase-1 and Roquin stabilizes pro-inflammatory transcripts including *IL-2* and *NFKBIZ*, thereby contributing to the post-transcriptional regulation of genes and optimal T cell activation.

Besides cleavage of signaling mediators, the paracaspase activity of MALT1 additionally targets substrates which regulate the stability of particular subsets of mRNA transcripts (Figure 3.5). Cleavage of the RNase Regnase-1 (also known as MCP1P1 or Zc3h12a) and the RNA binding proteins Roquin-1 and Roquin-2 by MALT1 stabilizes mRNAs of a number of pro-inflammatory genes, which are crucial for cell differentiation (Jeltsch et al. 2014; Uehata et al. 2013). While Regnase-1 directly targets the 3'-untranslated region (UTR) of mRNAs (Matsushita et al. 2009), Roquin proteins bind to mRNA via special domains and recruit a mRNA deadenylase complex which mediates the decay of transcripts (Glasmacher et al. 2010; Leppek et al. 2013). However, they both share a set of transcripts that encode for inflammatory cytokines (IL-2, IL-6, TNF), co-stimulatory surface receptors (ICOS, OX40) and intracellular signaling molecules ( $\text{I}\kappa\text{BNS}$ ,  $\text{I}\kappa\text{B}\zeta$ ) (Fu and Blakeshear 2017; Jeltsch et al. 2014). Hence, MALT1-induced cleavage of Regnase-1 and Roquin-1/2 stabilizes pro-inflammatory transcripts, including the transcriptional regulators  $\text{I}\kappa\text{BNS}$  and  $\text{I}\kappa\text{B}\zeta$ , which promote generation of  $\text{T}_\text{H}17$  cells (Jeltsch et al. 2014). The crucial role for of Regnase-1 and Roquin-1/2 in adaptive immunity is demonstrated by T cell specific Regnase-1 knockout mice and sanroque mice (which harbour a Roquin mutant that is unable to bind to mRNAs) that suffer from spontaneous inflammation, autoimmunity and premature death (Uehata et al. 2013; D. Yu et al. 2007). Thus, MALT1 paracaspase activity contributes to optimal T cell activation by regulating gene expression on a post-transcriptional level.

#### **3.4.2.2 Pathophysiological relevance of MALT1 paracaspase activity**

Despite both negative and positive regulators of NF- $\kappa$ B signaling are targets of MALT1 proteolytic activity, the generation of protease mutant (PM) MALT1 knock-in mice, which express a catalytically inactive form of MALT1, revealed that upstream NF- $\kappa$ B signaling is largely independent of MALT1 protease activity (Bornancin et al. 2015; Gewies et al. 2014; Jaworski et al. 2014; J. W. Yu et al. 2015). Similarly, MALT1 PM mice show no defect in JNK activation, and the physiological role of CYLD cleavage is yet to be explored (Gewies et al. 2014; Jaworski et al. 2014). However, loss of MALT1 paracaspase activity leads to defects in both the adaptive and the innate immune system. Similar to MALT1 KO mice, MALT1 PM mice show severe defects in IL-2 production and proliferation of T cells, as well as deficits in  $\text{T}_\text{H}17$  and Treg differentiation (Brustle et al. 2012; Brustle et al. 2017; Molinero et al. 2012) (Bornancin et al. 2015; Gewies et al. 2014; Jaworski et al. 2014; J. W. Yu et al. 2015). Due to the impaired generation of  $\text{T}_\text{H}17$  cells, both MALT1 KO and PM mice are protected from  $\text{T}_\text{H}17$ -driven experimental autoimmune encephalomyelitis (EAE), which is a model for multiple sclerosis. In line, also pharmacological inhibition of MALT1 protease activity alleviated symptoms and interfered with EAE development (Mc Guire et al. 2014). Importantly, while MALT1 KO mice show an immune suppressive phenotype, MALT1 PM mice develop a severe autoimmune disease (Bornancin et al.

2015; Gewies et al. 2014; Jaworski et al. 2014; J. W. Yu et al. 2015). This autoimmune phenotype in MALT1 protease defective mice could be explained by the preserved MALT1 scaffolding function, which causes residual immune activation which is no longer counterbalanced due to the reduced numbers of Tregs. Consequently, transfer of wildtype Tregs rescues the autoimmune phenotype (Bornancin et al. 2015; Jaworski et al. 2014). Thus, MALT1 not only promotes immune activation, but also is a critical regulator of cell fate decisions and immune homeostasis.

Since gain-of-function mutations in the BCR machinery upstream of MALT1 induce upregulation of MALT1 proteolytic activity in ABC DLBCL, targeting constitutive MALT1 activity via small molecule MALT1 inhibitors may be a promising therapeutic target to treat lymphoma (Ferch et al. 2009; Hailfinger et al. 2009). For instance, the non-competitive inhibitor Mepazine binds allosterically between the paracaspase and Ig3 domain and thereby interferes with the conformational changes necessary for MALT1 activation (Nagel et al. 2012; Schlauderer et al. 2013). Indeed, treatment of the ABC-type of DLBCL cells showed a selective anti-proliferative activity (Nagel et al. 2012). However, as mentioned above, mice expressing catalytically inactive MALT1 show reduced numbers of natural Treg cells, attended by multi-organ inflammation (Bornancin et al. 2015; Gewies et al. 2014; Jaworski et al. 2014; J. W. Yu et al. 2015). This questions the assumption that pharmacological inhibition of MALT1 will generally suppress immune responses. Therefore, a deeper knowledge about the molecular, structural and biological functions of the CBM machinery, and how MALT1 scaffold and paracaspase function individually contribute to immune homeostasis will be mandatory to evaluate the potential for future therapeutic applications targeting autoimmune diseases and cancer.

## 4 AIMS OF THE RESEARCH PROJECT

Formation of the CARD11/CARMA1-BCL10-MALT1 (CBM) complex bridges immune stimulation of B and T cell receptors to  $\text{I}\kappa\text{B}$  kinase/NF- $\kappa\text{B}$  and JNK signaling in lymphocytes. Upon activation, CARD11 acts as a molecular seed and recruits preassembled BCL10-MALT1 complexes via its CARD domain, inducing the formation of BCL10 filaments. However, since these processes are extensively interconnected, it is unclear if CARD11 nucleates BCL10 filaments, or whether BCL10 filament formation, either prior to or at the same time of CARD11 recruitment, is necessary for their interaction. To elucidate the order of events that occur following antigenic stimulation, we uncoupled these processes by generating a direct fusion of BCL10 to CARD11 that bypasses inducible recruitment. Using structure-guided missense mutations in the putative CARD11-BCL10 or BCL10-BCL10 interfaces alone, we aimed to investigate the functional impact of putatively homo- or heterotypic CARD-CARD interactions in a clean genetic setup under physiological conditions in T and B cells. Therefore we intended to generate KO Jurkat T cells by CRISPR/Cas9-technology, and use viral transduction for reconstitution with the respective mutants. In addition, by introducing a combination of point mutations in the CARDS of the fusion protein, conclusions on the cooperativity of these proteins in response to physiological or pathological activation of T and B cells could be drawn (**Publication I: Seeholzer et al., 2018**).

Although a cryo-EM structure of the BCL10 filaments has been determined, no structural information regarding the integration of MALT1 into the BCL10 filaments is available. Hence, a detailed description of the BCL10-MALT1 interface is lacking. To gain further insights into the exact interfaces for BCL10 oligomerization and BCL10-MALT1 interaction, our collaboration partners at the Gene Center of the LMU determined the cryo-EM structure of the BCL10-MALT1 complex. By using structure-guided mutational analysis in combination with viral reconstitution of CRISPR/Cas9-generated KO Jurkat T cells, we aimed to determine the significance of the identified BCL10-BCL10 as well as BCL10-MALT1 interaction sites for CBM complex formation, activation of MALT1 paracaspase activity and downstream signaling events, and confirm their importance in a physiological setting (**Publication II: Schlauderer et al., 2018**).

MALT1 has a dual function, serving as a molecular scaffold and a protease. Recruitment and integration of the E3 ubiquitin ligase TRAF6 into the CBM complex via TRAF6 binding motifs (T6BMs) in MALT1 is critical for canonical NF- $\kappa\text{B}$  signaling in Jurkat and primary T cells. However, it was reported that T cell-specific deletion of TRAF6 does not affect NF- $\kappa\text{B}$  activation, suggesting that other E3 ligases could compensate for its loss. To investigate this controversy, we aimed to generate TRAF6 KO Jurkat T cells and obtain a mouse line with a conditional T cell-specific ablation of TRAF6.

Utilising this, we could unravel how loss of TRAF6, in comparison to prevented binding via TBMs, affects MALT1 scaffold and protease function prior and post antigenic stimulation, and how this might contribute to the up to now unexplained autoimmune and inflammatory phenotype of mice lacking TRAF6 in T cells (**Manuscript I: Seeholzer et al., in preparation**).

## 5 PUBLICATIONS

### 5.1 Publication I

**Thomas Seeholzer\***, Susanne Kurz\*, Florian Schlauderer, Simone Woods, Torben Gehring, Simon Widmann, Katja Lammens & Daniel Krappmann (2018). \* equal contribution

**BCL10-CARD11 Fusion Mimics an Active CARD11 Seed That Triggers Constitutive BCL10 Oligomerization and Lymphocyte Activation.**

Front Immunol. 2018 Nov 20;9:2695. doi: 10.3389/fimmu.2018.02695. eCollection 2018.



# BCL10-CARD11 Fusion Mimics an Active CARD11 Seed That Triggers Constitutive BCL10 Oligomerization and Lymphocyte Activation

Thomas Seeholzer<sup>1†</sup>, Susanne Kurz<sup>1†</sup>, Florian Schlauderer<sup>2</sup>, Simone Woods<sup>1</sup>, Torben Gehring<sup>1</sup>, Simon Widmann<sup>1</sup>, Katja Lammens<sup>2</sup> and Daniel Krappmann<sup>1\*</sup>

<sup>1</sup> Research Unit Cellular Signal Integration, Institute of Molecular Toxicology and Pharmacology, Helmholtz Zentrum München - German Research Center for Environmental Health, Neuherberg, Germany, <sup>2</sup> Gene Center, Ludwig-Maximilians University, Munich, Germany

## OPEN ACCESS

### Edited by:

Andrew L. Snow,  
Uniformed Services University of the  
Health Sciences, United States

### Reviewed by:

Lawrence Kane,  
University of Pittsburgh, United States  
Joel L. Pomerantz,  
Johns Hopkins University,  
United States  
Liron David,  
Boston Children's Hospital, Harvard  
Medical School, United States

### \*Correspondence:

Daniel Krappmann  
daniel.krappmann@  
helmholtz-muenchen.de

<sup>†</sup>These authors have contributed  
equally to this work

### Specialty section:

This article was submitted to  
T Cell Biology,  
a section of the journal  
Frontiers in Immunology

Received: 14 August 2018

Accepted: 31 October 2018

Published: 20 November 2018

### Citation:

Seeholzer T, Kurz S, Schlauderer F,  
Woods S, Gehring T, Widmann S,  
Lammens K and Krappmann D (2018)  
BCL10-CARD11 Fusion Mimics an  
Active CARD11 Seed That Triggers  
Constitutive BCL10 Oligomerization  
and Lymphocyte Activation.  
*Front. Immunol.* 9:2695.  
doi: 10.3389/fimmu.2018.02695

Assembly of the CARD11/CARMA1-BCL10-MALT1 (CBM) signaling complex upon T or B cell antigen receptor (TCR or BCR) engagement drives lymphocyte activation. Recruitment of pre-assembled BCL10-MALT1 complexes to CARD11 fosters activation of the MALT1 protease and canonical NF- $\kappa$ B signaling. Structural data and *in vitro* assays have suggested that CARD11 acts as a seed that nucleates the assembly of BCL10 filaments, but the relevance of these findings for CBM complex assembly in cells remains unresolved. To uncouple cellular CARD11 recruitment of BCL10 and BCL10 filament assembly, we generated a BCL10-CARD11 fusion protein that links the C-terminus of BCL10 to the N-terminus of CARD11. When stably expressed in CARD11 KO Jurkat T cells, the BCL10-CARD11 fusion induced constitutive MALT1 activation. Furthermore, in CARD11 KO BJAB B cells, BCL10-CARD11 promoted constitutive NF- $\kappa$ B activation to a similar extent as CARD11 containing oncogenic driver mutations. Using structure-guided destructive mutations in the CARD11-BCL10 (CARD11 R35A) or BCL10-BCL10 (BCL10 R42E) interfaces, we demonstrate that chronic activation by the BCL10-CARD11 fusion protein was independent of the CARD11 CARD. However, activation strictly relied upon the ability of the BCL10 CARD to form oligomers. Thus, by combining distinct CARD mutations in the context of constitutively active BCL10-CARD11 fusion proteins, we provide evidence that BCL10-MALT1 recruitment to CARD11 and BCL10 oligomerization are interconnected processes, which bridge the CARD11 seed to downstream pathways in lymphocytes.

**Keywords:** lymphocyte signaling, CARMA1-BCL10-MALT1 (CBM) signalosome complex, CARD11, NF- $\kappa$ B, MALT1 paracaspase

## INTRODUCTION

Assembly of the CARD11/CARMA1-BCL10-MALT1 (CBM) signalosome channels T and B cell antigen-receptor (TCR/BCR) ligation to MALT1 protease activation and canonical NF- $\kappa$ B signaling (1, 2). CARD11 phosphorylation, primarily in the central linker region, following antigenic stimulation induces conformational changes that expose the N-terminal CARD (Caspase Recruitment Domain) to recruit pre-assembled BCL10-MALT1 complexes (3, 4). Oncogenic

CARD11 variants have been identified mainly in the coiled-coil domain, and these activating mutations promote chronic CBM assembly and NF- $\kappa$ B-driven survival in diffuse large B cell lymphomas (DLBCL) in the absence of antigenic stimulation (5, 6).

It is well established that BCL10 associates with the CARD-containing scaffold protein CARD11 through heterotypic CARD-CARD interactions (7, 8). Overexpression studies indicate that BCL10, via its N-terminal CARD, forms filament-like clusters in cells, which are required for proper activation of canonical NF- $\kappa$ B signaling (9). Aggregation of BCL10 in foci was also observed following TCR ligation in T cells (10). More recent *in vitro* structural studies, combined with molecular modeling, have demonstrated that the CARD of CARD11 can function as a seed to nucleate the assembly of BCL10 CARD filaments (11–13). *In vitro* BCL10 filaments can also form in the absence of CARD11, but CARD11 decreases the lag period of BCL10 polymerization and thus appears to function as an initiator of the process (11). Impaired MALT1 activity and NF- $\kappa$ B signaling upon overexpression of CARD11 or BCL10 mutants, targeting either the heterotypic CARD11-BCL10 or the homotypic BCL10-BCL10 CARD interfaces, highlights the importance of the different CARD surfaces (12, 13). These experiments, however, did not address the contribution of the different interfaces to antigenic activation when expressed at endogenous levels. We have demonstrated that BCL10 oligomerization is also required for its recruitment to CARD11, indicating that both processes are highly interconnected (14). Thus, the cellular relevance of the CARD11 seeding function for BCL10 filament formation, as well as, the order of events after antigenic stimulation, have not been resolved.

Here, we used CRISPR/Cas9 technology to generate CARD11 and BCL10 KO T and B cell lines and stable lentiviral reconstitution, to investigate the cellular necessity of the CARD11 seed and BCL10 filaments in a clean genetic setup under physiological conditions. As noted earlier, we have been unable to definitively determine whether CARD11 nucleates BCL10 filaments or, if BCL10 filament formation happens prior to, or at the same time as CARD11 recruitment in stimulated T cells using missense mutations in the putative CARD11-BCL10 or BCL10-BCL10 interfaces alone (14). Thus, we uncoupled these processes by fusing BCL10 to CARD11 to bypass inducible recruitment and thereby were able to investigate the cellular necessity of CARD11 seeding and BCL10 oligomerization.

## RESULTS

### BCL10 Recruitment to CARD11 and BCL10 Filament Assembly Are Interconnected Processes

In order to predict mutations that would selectively interfere with CARD11 seed function or BCL10 self-assembly, we used structural modeling to fit the CARD11 seed onto the structure of BCL10 CARD filaments (Figure 1A). Therefore, the CARD11 CARD domain crystal structure was superimposed on to three BCL10 CARD domains at the bottom of the BCL10 filament

cryo EM structure [Figure 1A; (13, 14)]. Since the structure of the CARD11-BCL10 interface has not been determined, the CARD11 BCL10 CARD/CARD interaction was modeled in consideration of the surface charge complementarity analysis of the BCL10-MALT1 filament cryo-EM structure and the crystal structure of the CARD11 (Supplementary Figures 1A–C). As noted earlier, distinct interfaces between the CARDS are required to mediate heterotypic CARD11-BCL10 interactions or homotypic BCL10-BCL10 interactions (12, 13). On the CARD11 side, R35 serves as a critical contact point to multiple residues in BCL10 including E53 and mediates recruitment of BCL10 to CARD11 [Figure 1B; (12)]. On BCL10, R42 contributes to the association at the BCL10-BCL10 interface I that controls BCL10 oligomerization (Figures 1C,D). The structure reveals that R42 is not predicted to confer CARD11-BCL10 interaction (11, 13, 14). *In vitro*, the BCL10 CARD mutation R42E prevents oligomerization of the BCL10-MALT1 complex (14). We expressed BCL10 WT and R42E in adherent U2OS cells to monitor formation of cellular clusters. Indeed, whereas overexpressed BCL10 WT forms cytosolic aggregates in U2OS cells, BCL10 R42E fails to cluster, indicating that oligomerization and filament formation is prevented by the mutation (Figure 1E). We performed co-immunoprecipitation (IP) of HA-BCL10 WT, together with Flag-BCL10 WT or R42E in HEK293 cells (Figure 1F). Despite the higher expression of BCL10 R42E, only Flag-BCL10 WT co-precipitated with HA-BCL10, validating that the mutation abolishes BCL10 self-association.

To rigorously test the function of CARD11 as a molecular seed and BCL10 as a filament forming CARD11 adaptor in B and T cells, we generated CARD11 and BCL10 KO Jurkat T cells, as well as CARD11 KO BJAB B cells, by CRISPR/Cas9 technology (Supplementary Figure 2). CARD11 KO Jurkat T and BJAB B cells were generated using sgRNA targeting Exon3, which induces double stranded breaks and frame shift mutations due to non-homologous end-joining (NHEJ) repair (Supplementary Figure 2A). An exon1-intron1 deletion strategy using two sgRNA was employed to knockout BCL10 from Jurkat T cells (Supplementary Figure 2B). Using these approaches, we obtained several clones that displayed loss of CARD11 or BCL10 expression as determined by Western Blot analysis (Supplementary Figures 2C–E). Destructive frame shift mutations in CARD11 or deletions of BCL10 in both alleles were confirmed by sequencing of the genomic loci in the respective KO cell clones (data not shown). We used PMA/Ionomycin (P/I) stimulation, which bypasses upstream TCR or BCR signaling by directly activating PKC $\theta$  or PKC $\beta$  in T and B cells and increasing cytosolic calcium levels. In line with the key role of the CBM complex, CARD11 or BCL10 deficiency abolished P/I-induced NF- $\kappa$ B signaling in Jurkat T or BJAB B cells as evident from lack of I $\kappa$ B $\alpha$  degradation and NF- $\kappa$ B DNA binding (Supplementary Figures 2C–E). In contrast, CBM-independent, TNF $\alpha$ -driven NF- $\kappa$ B signaling as well as ERK activation were not affected by the absence of CARD11 in Jurkat T cells, demonstrating that loss of the CBM complex selectively affects antigenic signaling. Thus, the absence of CARD11 or BCL10 in Jurkat and BJAB cells faithfully mirrors the signaling

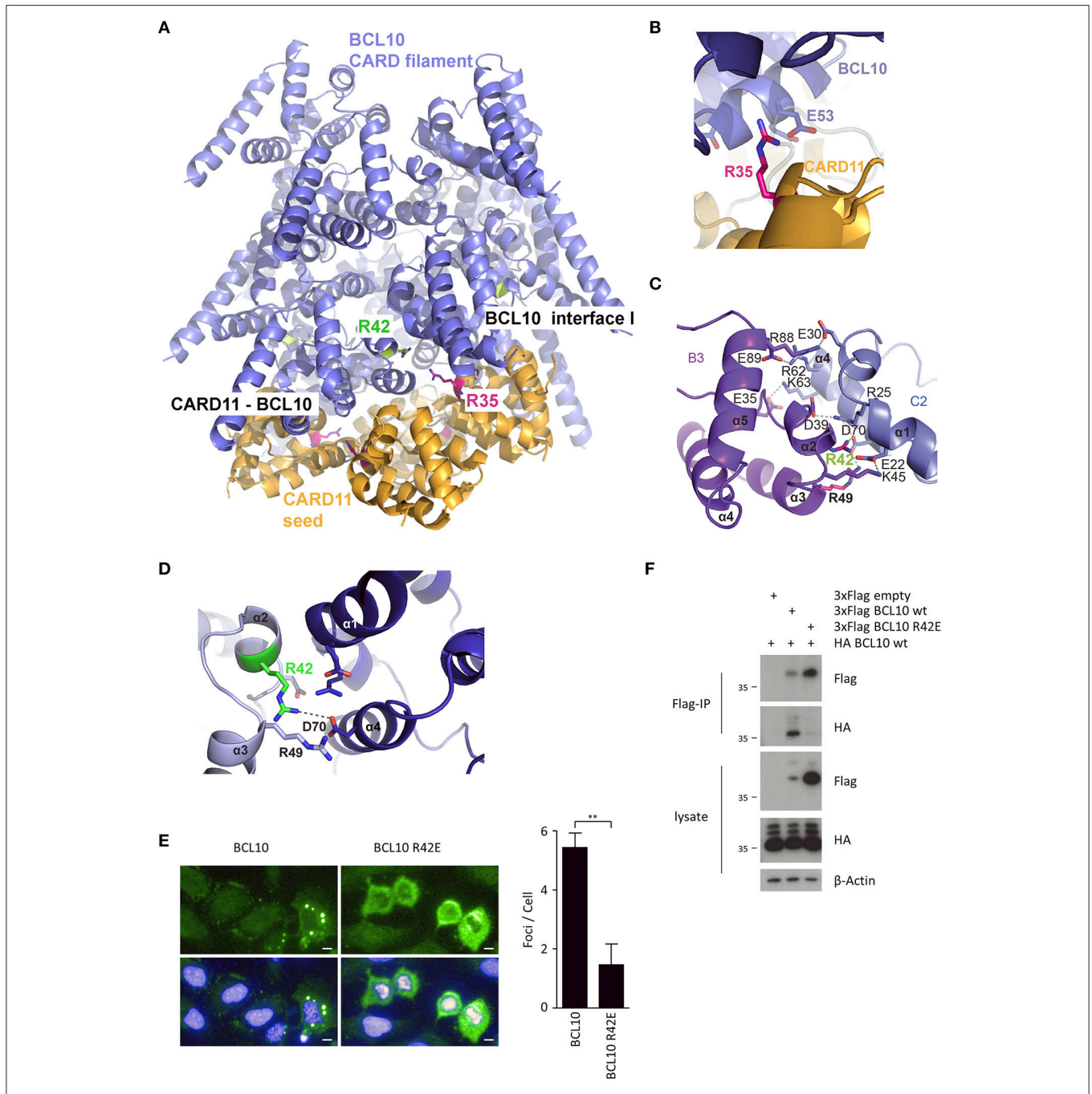


**FIGURE 1 |** CARD-CARD interfaces in the CARD11-BCL10 structure. **(A)** Model of the CARD11-BCL10 filament structure. The oligomeric CARD11 seed (PDB 4LWD, orange) induces BCL10 (PDB 6GK2, blue) filament assembly through the heterotypic CARD11-BCL10 interface. **(B)** Close-up view of CARD11 R35 (magenta) contacting BCL10 E53 in the modeled CARD11-BCL10 interface. **(C,D)** Close-up view of the BCL10-BCL10 interface I. Residues involved in homotypic CARD-CARD association as observed in the cryo-EM structure (EMD-0013, PDB 6GK2) (14) are shown as sticks. The mutated residue R42 is highlighted in green. **(E)** Cellular distribution of BCL10 in U2OS cells was determined after transfection of BCL10-FS or BCL10 R42E-FS and aggregate clustering was detected by indirect confocal immunofluorescence microscopy. Scale bars depict 10  $\mu$ m. Average number of aggregated foci was quantified by blinded counting >30 cells per condition (mean  $\pm$  s.e.m.; \*\* $p \leq 0.01$ ). **(F)** HEK 293 cells were transfected with Flag- and HA-tagged BCL10 constructs as indicated, and self-association of HA-BCL10 WT to Flag-BCL10 WT or R42E mutant was determined after Flag-IP.

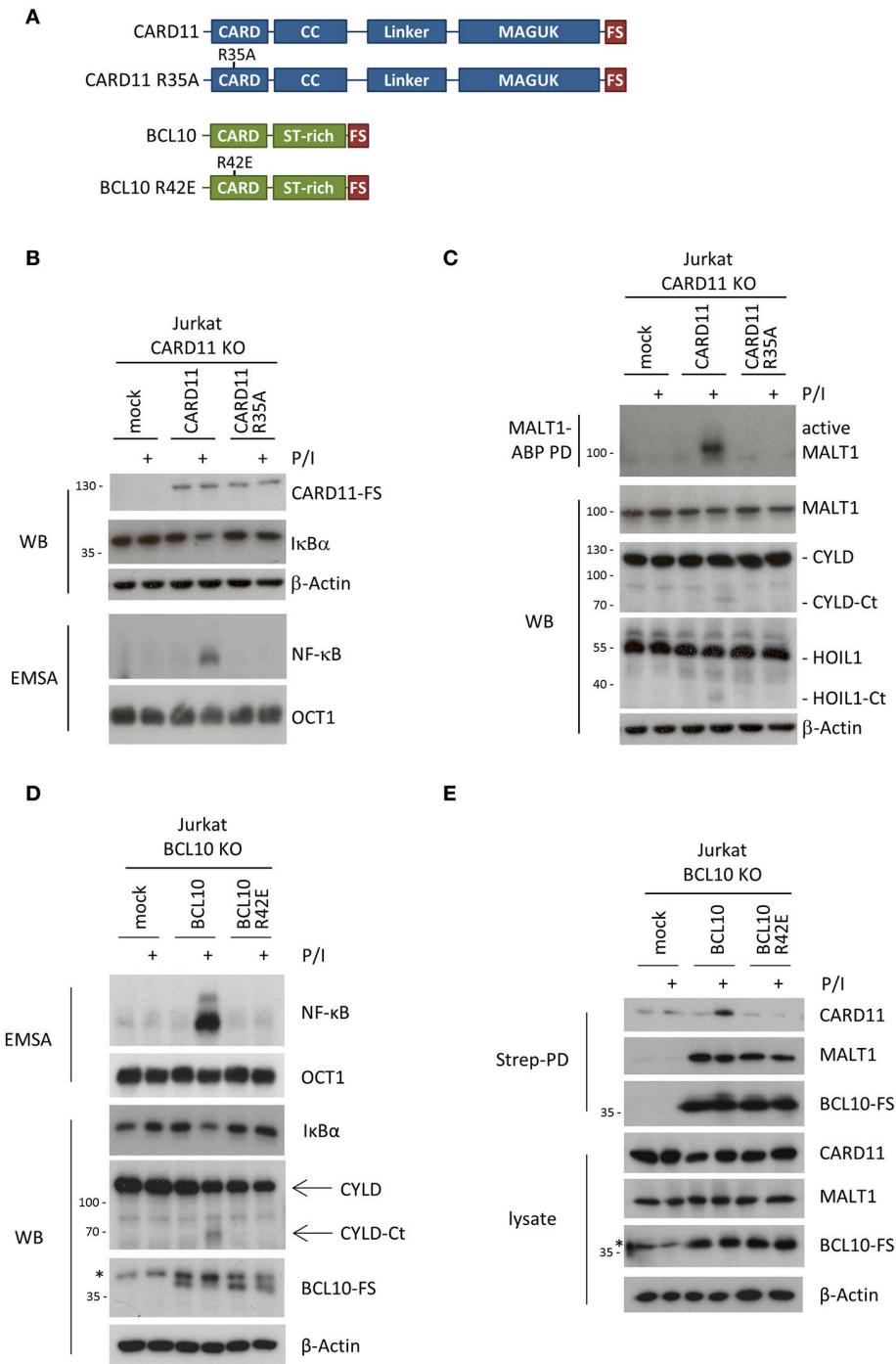


**FIGURE 2 |** Effects of destructive heterotypic and homotypic CARD-CARD interface mutants. **(A)** Schematic presentation of CARD11 and BCL10 WT proteins and the respective CARD mutants R35A and R42E. **(B)** CARD11 KO Jurkat T cells were reconstituted with CARD11 WT or R35A. Cells were stimulated with P/I (30 min) and effects on NF-κB signaling were determined by following IκBα degradation by WB and NF-κB activation by EMSA. **(C)** CARD11 KO Jurkat T cells were reconstituted as in **(B)**, stimulated with P/I (30 min), and MALT1 protease activity was determined via MALT1-ABP PD assay and assessment of substrate cleavage (CYLD and HOIL1) by WB. **(D)** BCL10 KO Jurkat T cells were reconstituted with BCL10 or BCL10 R42E. Cells were stimulated with P/I (30 min) and NF-κB signaling was analyzed as in **(B)**. MALT1 protease activity was determined by CYLD substrate cleavage by WB. **(E)** Recruitment of BCL10 or BCL10 R42E to CARD11 after P/I stimulation (15 min) in Jurkat T cells was monitored by ST-PD and subsequent WB. The asterisks indicate an unspecific band in the BCL10 WB.

CARD11 or BCL10 KO T cells were reconstituted by lentiviral transduction and comparable infection rates for epitope-tagged (FS: Flag-StrepTag2) CARD11 and BCL10 constructs were obtained, as determined by co-expression of the surface marker  $\Delta$ CD2 (**Supplementary Figures 3A,B**). Equivalent expression of WT and mutant CARD11 or BCL10 proteins at close to endogenous levels was confirmed by Western Blotting (**Supplementary Figures 3A,B**). Functionally, lack of CARD11-dependent NF- $\kappa$ B activation after P/I stimulation in CARD11 KO cells was rescued upon reconstitution with CARD11 WT, but not with the CARD11 R35A mutant (**Figure 2B**). We also assessed activation of the MALT1 protease by substrate cleavage (CYLD and HOIL-1) (18) and labeling of active MALT1 by a biotinylated MALT1 activity-based probe (ABP) followed by biotin pull-down (PD) to capture active MALT1 [**Figure 2C**; (19)]. Again, CARD11 WT, but not R35A, could rescue P/I stimulated MALT1 protease activation in Jurkat T cells, revealing that this mutation abolishes all CARD11 downstream function. On the side of BCL10, we confirmed that rescue of BCL10 WT, but not BCL10 R42E, was able to trigger MALT1 activation and mediate NF- $\kappa$ B downstream signaling in response to P/I stimulation [**Figure 2D**; (14)]. Since the structural analyses suggested that BCL10 R42E would selectively disrupt the BCL10-BCL10 but not the CARD11-BCL10 interface (13), we asked if BCL10 R42E could still be recruited to CARD11 upon stimulation. However, no stimulation-dependent binding to CARD11 was detected with BCL10 R42E mutant [**Figure 2E**; (14)]. The data demonstrate that CARD11 recruitment and BCL10 filament formation are interconnected processes. Thus, destructive mutations in the CARD11-BCL10 or BCL10-BCL10 interfaces alone are unable to resolve whether CARD11 acts as a seed to induce BCL10 oligomerization or if an initial BCL10 filament assembly may be required for the recruitment of BCL10-MALT1 to CARD11.

### BCL10-CARD11 Fusion Drives Constitutive MALT1 Activation Through BCL10 Oligomerization in Jurkat T Cells

To test the necessity for BCL10 self-association downstream of CARD11, we designed a system that bypasses inducible CARD11-BCL10 association. For this we cloned chimeric proteins that covalently fuse BCL10 through its C-terminus to the N-terminus of CARD11 (**Figure 3A**). We lentivirally transduced CARD11 KO Jurkat T cells with the SF-tagged BCL10-CARD11 construct (herein referred to as B10-C11 fusion) (**Figure 3B**). We detected a faint but distinct band corresponding to the expected size of the B10-C11 fusion using  $\alpha$ BCL10 and  $\alpha$ CARD11 antibodies (**Figure 3C**). Notably, expression of the B10-C11 protein triggered constitutive cleavage of CYLD and A20, as well as a reduction in endogenous BCL10, which are all MALT1 substrates (18). However, the BCL10-CARD11 fusion itself, which contains a MALT1 cleavage site at R228 in the BCL10 moiety (20), was also prone to processing, giving rise to a fragment the size of endogenous CARD11 (**Figure 3C**). Thus, the data clearly indicate that fusion of BCL10 to CARD11 is sufficient to induce MALT1 activation.

To avoid the indirect reconstitution of CARD11 from the cleaved B10-C11 fusion, we designed all further BCL10-CARD11 fusion constructs so that they contained the MALT1 cleavage resistant BCL10 R228A mutation (**Figure 3A**). The fusion constructs include the destructive mutations R42E in the BCL10 CARD, and R35A in the CARD11 CARD, both alone and in combination. All B10-C11 fusion constructs were transduced into CARD11 KO Jurkat T cells, yielding equivalent infection efficiencies as judged by  $\Delta$ CD2 expression (**Figure 3D**). The chimeric proteins were expressed below the level of endogenous CARD11 and moreover, the fusions containing a functional WT BCL10 CARD were consistently expressed at lower levels compared to the BCL10 mutants R42E that prevent BCL10 oligomerization (**Figure 3E**). StrepTactin pull-downs (ST-PD) demonstrated that the BCL10-CARD11 fusion proteins retained the ability to bind endogenous MALT1, excluding that the fusion or point mutations in the CARDS interfere with MALT1 recruitment (**Figure 3E**).

Using biotin-PD after incubation with bio-MALT1-ABP, we tested MALT1 protease activity in extracts of untreated and P/I stimulated Jurkat T cells (**Figure 3F**). Expression of B10 R228A-C11, containing two functional CARDS, as well as the B10 R228A-C11 R35A fusion, with an inactivation only in the CARD11 CARD, induced strong MALT1 protease activity that was equivalent to the activation obtained in Jurkat T cells after P/I stimulation. Despite robust MALT1 activation, the R228A exchange in BCL10 prevented cleavage of the fusion constructs and thus the appearance of CARD11 (**Figure 3E**). Constitutive MALT1 activation was abrogated in the B10-C11 fusion proteins carrying the oligomerization-defective BCL10 R42E mutation, providing evidence that constitutive MALT1 activation is driven through oligomerization of endogenous BCL10 via the BCL10 CARD (**Figure 3F**). Interestingly, MALT1 activity was further enhanced after stimulation of B10 R228A-C11 expressing cells and this strictly relied on the CARD11 CARD, because the R35A mutation prevented stimulation-dependent induction. In line, even though the B10 R42E/R228A-C11 fusion containing an intact CARD11 CARD was unable to induce constitutive MALT1 activation, it was still able to mediate MALT1 activation in P/I-stimulated Jurkat T cells. Thus, stimulation dependent activation seems to rely on the recruitment of endogenous BCL10 to the CARD11 CARD in the context of the BCL10-CARD11 fusion protein. In fact, the B10 R42E/R228A-C11 fusion acted completely independently of the BCL10 CARD and exactly mirrored the rescue observed when using CARD11 WT (see **Figures 2B,C**). In agreement with these data, the triple mutant B10 R42E/R228A-C11 R35A neither promoted constitutive, nor rescued, stimulus-dependent MALT1 activation.

To confirm these findings on the level of MALT1 substrates, we assessed cleavage of CYLD, HOIL1 and A20 in B10-C11 expressing cells (**Figure 3G**). Cleavage of the three substrates was observed in Jurkat T cells expressing the fusions with an intact BCL10 CARD (B10 R228A-C11 and B10 R228A-C11 R35A), confirming that constitutive MALT1 protease activity relies on BCL10 oligomerization. The intact CARD11 CARD in B10 R42E R228A-C11 still conferred inducible substrate cleavage, which was especially evident for HOIL1 that is also most strongly

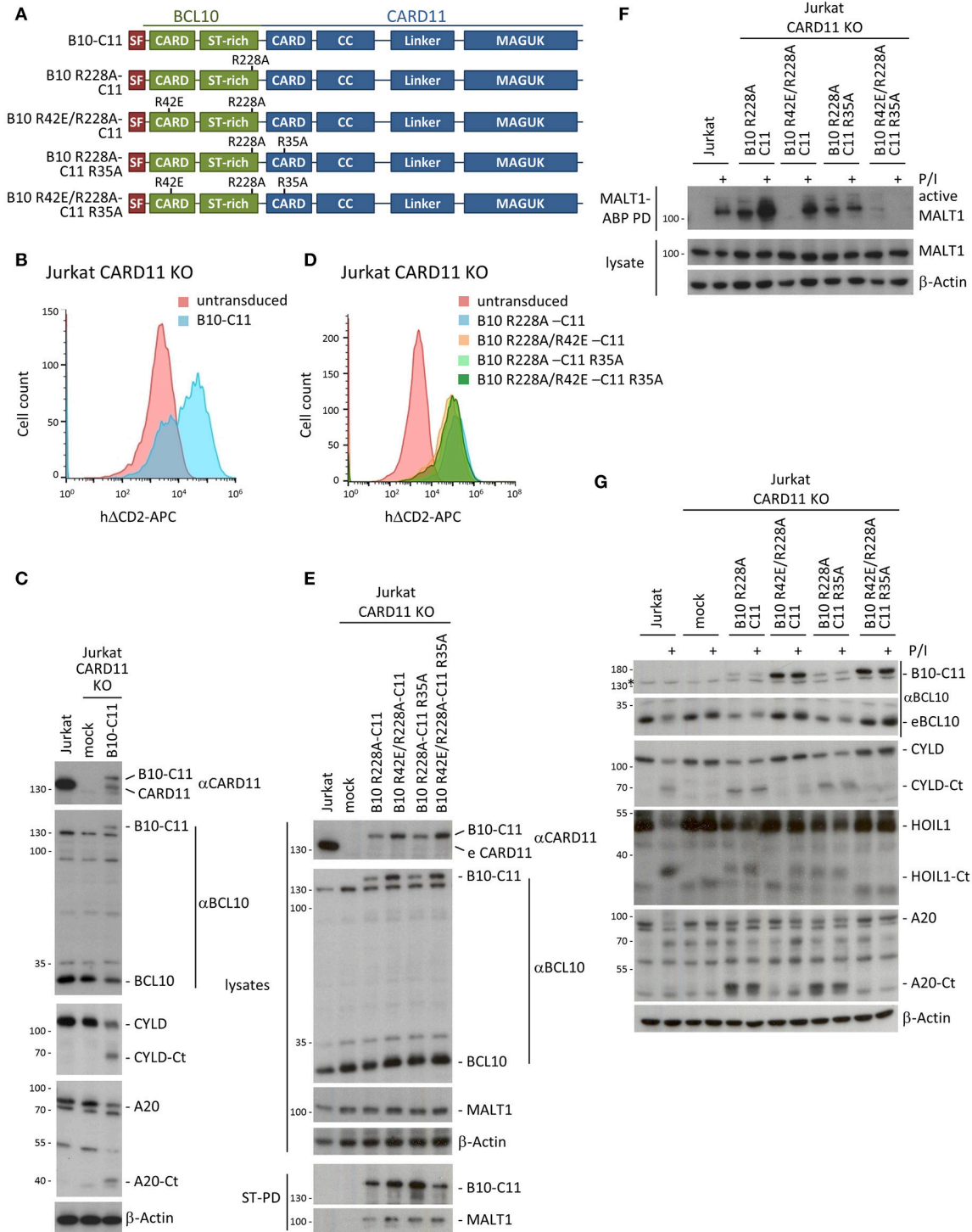


**FIGURE 3 |** A chimeric BCL10-CARD11 fusion protein induces constitutive MALT1 protease activity in Jurkat T cells through the BCL10 oligomerization interface. **(A)** Schematic representation of BCL10-CARD11 (B10-C11) fusion proteins with the respective CARD mutants. **(B)** Transduction efficiency of CARD11 KO Jurkat T cells with BCL10-CARD11 (B10-C11) was analyzed by FACS using the surface marker  $\Delta$ CD2. **(C)** Protein expression of B10-C11 fusion construct and cleavage of MALT1 substrates compared to mock and parental Jurkat T cells was analyzed by WB. **(D)** Transduction efficiency of CARD11 KO Jurkat T cells with different B10 R228A-C11 fusion constructs as in **(B)**. **(E)** Expression of the different B10 R228A-C11 fusion proteins compared to mock and parental Jurkat T cells was analyzed by WB and binding to MALT1 assessed by Strep-PD. **(F)** CARD11 KO Jurkat T cells were reconstituted with B10 R228A-C11 fusion proteins as indicated. Active MALT1 prior or after P/I stimulation (30 min) was detected in the extracts with biotin-labeled MALT1-ABP and MALT1-ABP PD followed by WB. **(G)** CARD11 KO Jurkat T cells were reconstituted and treated as in **(F)** and cleavage of MALT1 substrates (CYLD, HOIL1, A20) was detected by WB.

cleaved after P/I stimulation of Jurkat T cells. Again, destruction of both CARDS in B10 R42E/R228A-C11 R35A led to complete loss of constitutive and inducible MALT1 activation. Thus, covalent attachment of BCL10 to the N-terminus of CARD11 is sufficient to induce MALT1 protease activation, which still relies on the oligomerization interface of the fused BCL10 moiety. These data support the concept that, in cells, CARD11 acts as a seed to induce BCL10 filament assembly.

## Transient Expression of BCL10-CARD11 Induces NF- $\kappa$ B Activation in Jurkat T Cells

Interestingly, when we tested activation of NF- $\kappa$ B by B10-C11 fusion constructs in CARD11 or BCL10 KO Jurkat T cells we noticed a severely blunted response in EMSA (**Figure 4A**). There was a weak induction of constitutive NF- $\kappa$ B DNA binding in B10 R228A-C11, but I $\kappa$ B $\alpha$  degradation and NF- $\kappa$ B activation was only mildly triggered after P/I stimulation, revealing that stable expression of the active BCL10-CARD11 fusion may promote a stage of unresponsiveness in Jurkat T cells. Again, missense mutations in both CARDS completely prevented constitutive, as well as, inducible NF- $\kappa$ B activation in the context of the B10-C11 fusion protein. We switched to a transient transfection system and NF- $\kappa$ B reporter assays to investigate if BCL10-CARD11 fusion proteins can activate NF- $\kappa$ B. Indeed, NF- $\kappa$ B was strongly induced by the expression of B10 R228A-C11 fusion activated in parental Jurkat T cells or CARD11 KO Jurkat T cells (**Figures 4B,C**). However, in line with the EMSA results overall NF- $\kappa$ B activation was strongly diminished when the reporter assay was performed in CARD11 KO Jurkat T cells that stably express the B10-C11 fusion constructs (**Figure 4C**). Further, the oligomerization-deficient BCL10 R42E mutant severely reduced NF- $\kappa$ B activation by the BCL10-CARD11 fusion protein. Again, also in transient transfection we observed that BCL10-CARD11 was expressed at much lower levels compared to the B10 R42E/R228A-C11 protein, suggesting that there is a counter-selection against the expression of the active BCL10-CARD11 fusion. NF- $\kappa$ B induction of BCL10-CARD11 fusion protein was comparable to the induction achieved by oncogenic CARD11 L225LI or CARD11  $\Delta$ linker, especially taking into account the much weaker expression of the fusion protein [**Figure 4C**; (6, 21)]. To check if the generated BCL10-CARD11 fusion construct does not trigger unphysiological NF- $\kappa$ B that bypasses the necessity of known regulators, we determined the requirement for MALT1 and for TRAF6 recruitment to MALT1 (**Figure 4D**). NF- $\kappa$ B activation in response to antigenic stimulation is abolished MALT1 KO Jurkat T cells and signaling can be rescued by transduction of MALT1A or MALT1B, but not the respective MALT1 TRAF6 binding mutants (22). As expected, expression of B10 R228A-C11 or CARD11  $\Delta$ linker was unable to activate NF- $\kappa$ B in MALT1 KO Jurkat T cell (**Figure 4D**). While NF- $\kappa$ B activity was recovered by viral complementation with MALT1B WT, the MALT1B E795A mutant that destroys the only functional TRAF6 binding motif on MALT1B failed to rescue reporter gene expression, proving that MALT1 and TRAF6 are utilized by the BCL10-CARD11 fusion protein to activate NF- $\kappa$ B [**Figure 4D**; (22–24)]. Thus,

while transient expression of the BCL10-CARD11 fusion protein promotes NF- $\kappa$ B activation, NF- $\kappa$ B responses are dampened in Jurkat T cells after stable expression of the fusion proteins. To corroborate whether the BCL10-CARD11 fusion protein can also compensate for BCL10 deficiency, we transduced BCL10 KO Jurkat T cells with the B10 R228A-C11 fusion protein (**Supplementary Figure 4A**). Indeed, fusion of BCL10 to CARD11 was able to trigger constitutive CYLD, A20, and HOIL1 cleavage and thus to drive MALT1 protease activation in BCL10 deficient cells (**Supplementary Figure 4B**). Again, mutation of BCL10 and CARD11 CARD (B10 R42E/R228A-C11 R35A) prevented constitutive and inducible MALT1 activation, underscoring that dimerization/oligomerization of the fusion proteins is required. Similar to the situation in CARD11 KO cells, NF- $\kappa$ B activation was blunted upon stable expression of B10 R228A-C11 in BCL10 KO Jurkat T cells.

## BCL10-CARD11 Fusion Acts Like Oncogenic CARD11 in BJAB B Cells

To better explore the impact of stable BCL10-CARD11 fusion on NF- $\kappa$ B activation, we switched to GCB DLBCL derived BJAB B cells, which under basal conditions are devoid of NF- $\kappa$ B activity, but overexpression of oncogenic CARD11 mutants induces strong chronic NF- $\kappa$ B activity (5, 6, 25). We generated CARD11 KO BJAB B cells (**Supplementary Figure 2D**) and confirmed that the phenotype of the BJAB KO cells was caused by loss of CARD11. For this we reconstituted the cells with CARD11 WT, or the oncogenic CARD11 coiled-coil (CC) mutant L225LI that induces robust NF- $\kappa$ B and proliferation upon overexpression in B cells [**Figure 5A**; (25, 26)]. After viral transduction, BJAB B cells expressed CARD11 WT and CARD11 L225LI slightly above endogenous levels (**Figures 5B,C**). CARD11 WT was able to recover P/I-inducible NF- $\kappa$ B and MALT1 protease activation, but was not associated with constitutive activation (**Figures 5D,E**). In contrast, transduction of CARD11 L225LI was sufficient to promote constitutive NF- $\kappa$ B activation, as well as cleavage of the MALT1 substrates BCL10, CYLD, A20 and HOIL1. This effect was not further augmented by P/I stimulation (**Figures 5D,E**). Thus, CARD11 KO BJAB B cells represent a valid system to elucidate the impact of BCL10-CARD11 fusions on NF- $\kappa$ B signaling.

Next, we expressed B10 R228A-C11 and B10 R42E/R228A-C11 in CARD11 KO BJAB B cells (**Figure 6A**). In addition, we sought to determine whether an oncogenic mutant of CARD11 also relies on BCL10 oligomerization. We have previously shown that the activating potential of CARD11 L225LI is abolished by the R35A mutation (25). Therefore, we expressed the B10-C11 L225LI fusion constructs in the context of the CARD destructive R35A mutation so that they should rely on the BCL10 CARD (B10 R228A-C11 R35A/L225LI and B10 R42E/R228A-C11 R35A/L225LI) (**Figure 6A**). All constructs were transduced in BJAB B cells to a similar extent, as determined by the surface marker  $\Delta$ CD2, but protein expression was far below endogenous CARD11 (**Figures 6B,C**). As observed in Jurkat T cells, B10 R228A-C11 constructs containing an intact BCL10 CARD were expressed at much lower levels and the variant containing

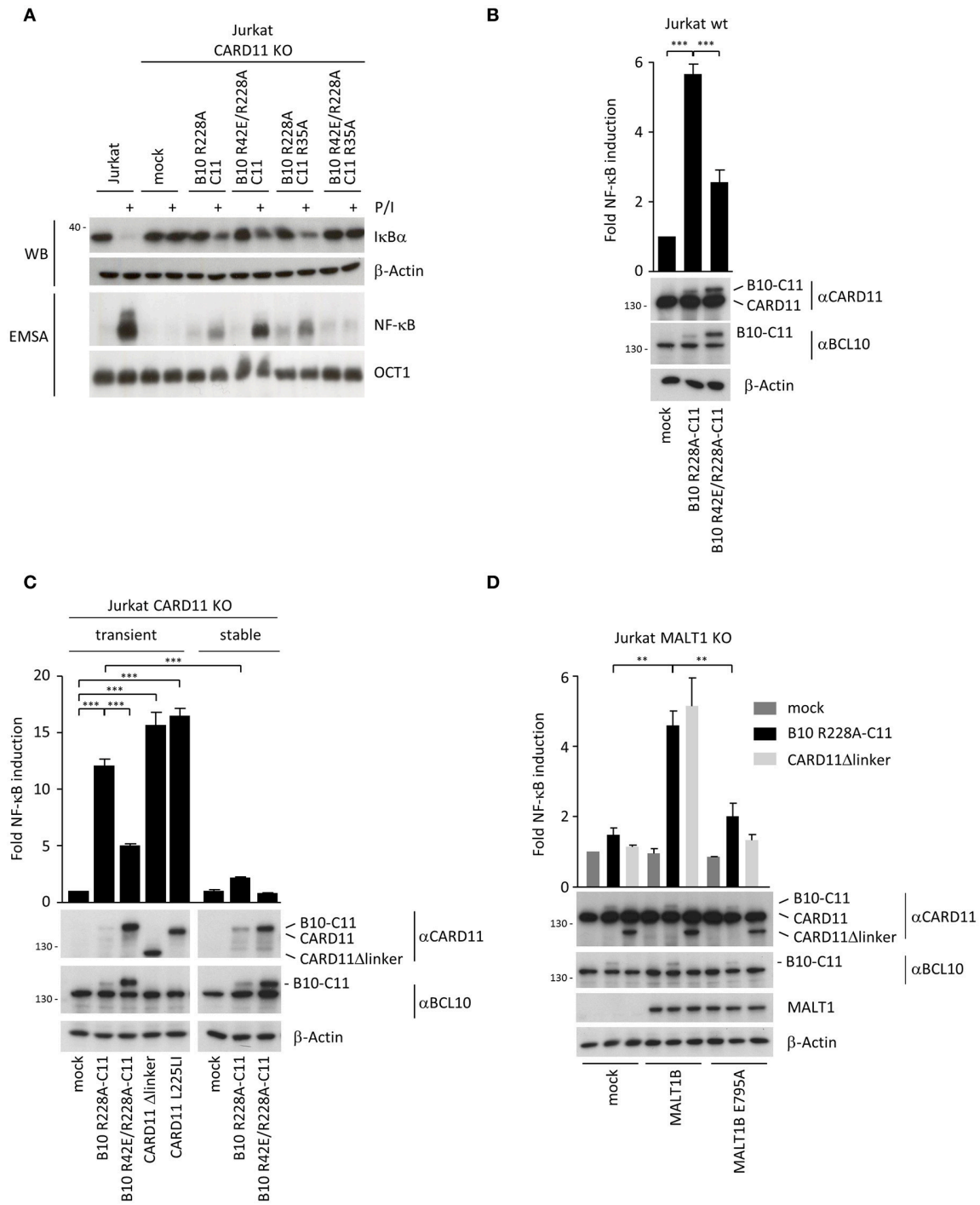
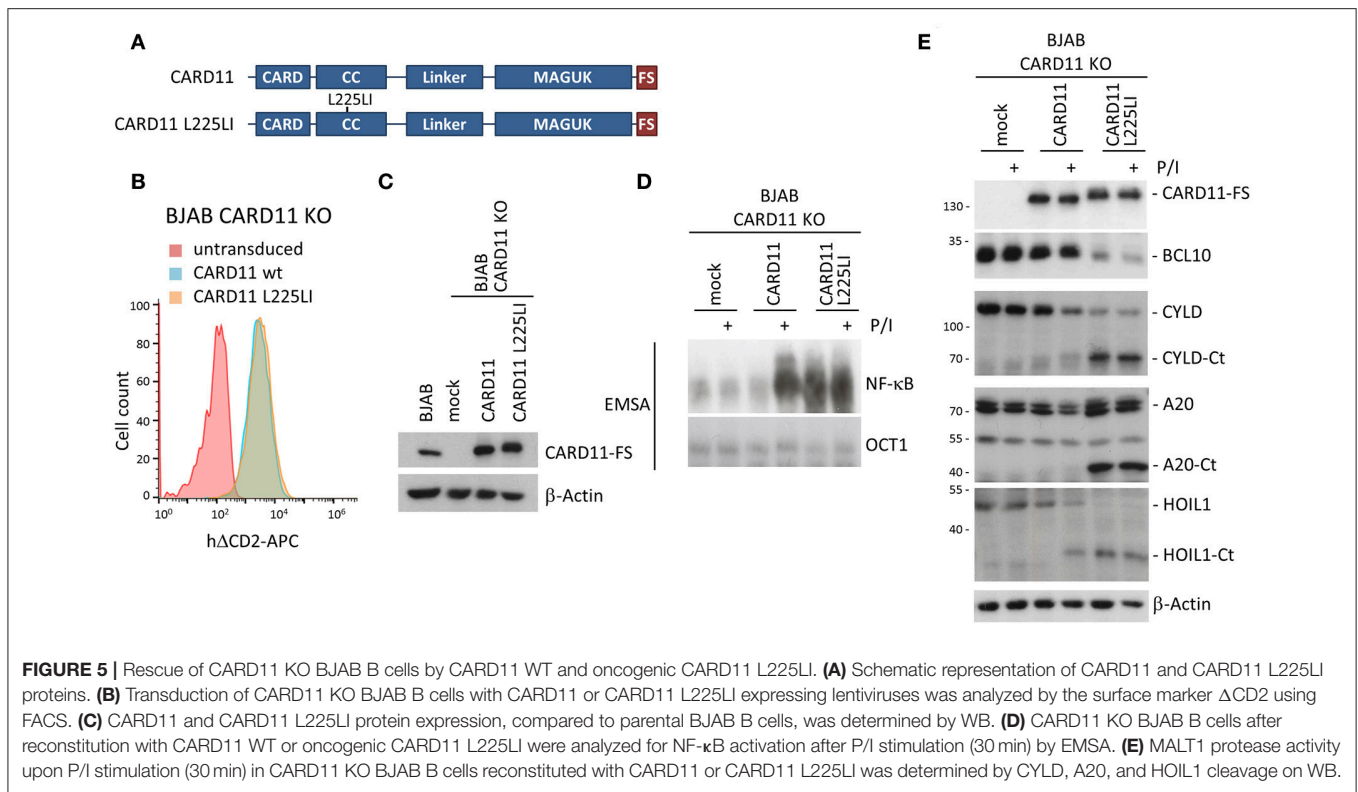


**FIGURE 4 |** Transient expression of chimeric BCL10-CARD11 fusion protein in Jurkat T cells triggers NF-κB activation. **(A)** NF-κB signaling was analyzed in CARD11 KO Jurkat T cells stably reconstituted with different B10 R228A-C11 fusion proteins as indicated. IκBα degradation was determined by WB and NF-κB activation was analyzed by EMSA. **(B)** B10-C11 fusion constructs were transiently expressed in Jurkat T cells together with a dual NF-κB reporter, and NF-κB induction was assessed by a dual luciferase reporter assay. Protein levels were analyzed by WB. Results are displayed relative to mock-transfected cells (mean ± s.e.m.; n = 5). **(C)** Jurkat CARD11 KO cells were transiently or stably reconstituted with B10-C11 fusion or CARD11 constructs and NF-κB activity determined as in **(B)**. Expression of the fusion constructs was verified by WB (mean ± s.e.m.; n = 3). **(D)** Transient expression of B10 R228A-C11 and CARD11 Δlinker in Jurkat MALT1 KO cells stably reconstituted with mock, MALT1 IsoB1 wildtype and the TRAF6 binding motif mutant E795A, respectively. NF-κB activity was determined as described in **(B)** and protein levels visualized on WB (mean ± s.e.m.; n = 3). \*\*p ≤ 0.01, \*\*\*p ≤ 0.001.



the oncogenic mutation (B10 R228A-C11 R35A/L225LI) was hardly detectable (**Figure 6C** lane 5). However, just like in Jurkat T cells, the B10 R228A-C11 fusion induced strong constitutive MALT1 activation, as evident from CYLD, HOIL1 and A20 cleavage, which strictly relied upon the BCL10 CARD interface (**Figure 6D**). Furthermore, the BCL10-CARD11 fusion combined with the oncogenic mutation L225LI (B10 R228A-C11 R35A/L225LI) induced MALT1 activation, despite its very low expression in the BJAB B cells. Again, constitutive MALT1 activation in the oncogenic BCL10-CARD11 fusion required BCL10 oligomerization, but was independent of the CARD11 CARD (**Figure 6D**).

Further, the fusion of BCL10 to CARD11 was sufficient to induce constitutive NF- $\kappa$ B activation in the BJAB B cells that was not further enhanced by P/I treatment (**Figure 6E**). Constitutive NF- $\kappa$ B activation was equivalent to that induced by the oncogenic CARD11 variant L225LI (**Figure 5D**). Despite its very weak expression, the oncogenic fusion construct B10 R228A-C11 R35A/L225LI also induced strong NF- $\kappa$ B activation, suggesting that the combination of fusion with the oncogenic mutant can generate a super-activator that is capable of further boosting CBM signaling. The weak expression of the B10 R228A-C11 R35A/L225LI suggests that there is a strong counter-selection against expression of the hyper-active fusion protein. Again, the constitutive activation observed with expression of the fusion constructs was solely driven by the BCL10 filament interface and was severely reduced in cells expressing the double CARD mutant B10 R42E/R228A-C11 R35A/L225LI. Finally, we confirmed that the fusion constructs also induce NF- $\kappa$ B-dependent gene expression by demonstrating that the

prototype NF- $\kappa$ B target gene, NFKBIA/ $\text{I}\kappa\text{B}\alpha$ , is upregulated to a similar degree in the BJAB B cells expressing either CARD11 L225LI or the activating B10-C11 fusion constructs (**Figure 6F**). Thus, with respect to signaling, the fusion of BCL10 to CARD11 acts like an oncogenic CARD11 variant in B cells, through oligomerization of the BCL10 CARD interface.

## DISCUSSION

BCL10 CARD filaments are formed *in vitro* and the molecular architecture of these clusters has been elucidated by cryo-electron microscopy (11, 13, 14). Although it is possible for BCL10 filaments to form in the absence of CARD11, the CARD of CARD11 appears to promote the initiation of BCL10 clustering in a cell free system. Further, CARD11 is solely located at the tip of the BCL10 filaments, lending support to the hypothesis that CARD11 functions as the molecular seed for BCL10 oligomerization (11, 13). Structure-guided missense mutations in the CARDS of CARD11 or BCL10 have been generated to show that destruction of putatively homotypic (BCL10-BCL10) or heterotypic (CARD11-BCL10) CARD-CARD interactions impedes NF- $\kappa$ B signaling and MALT1 protease activation after overexpression in cells (13, 14).

The functional impact of missense mutations in the CARDS of CARD11 or BCL10 on stimulus-dependent CBM complex signaling has not been thoroughly investigated. By reconstituting CARD11 or BCL10 KO Jurkat T cells, we assessed how destruction of putative CARD11-BCL10 or BCL10-BCL10 interfaces would affect signaling when expressed at endogenous levels. As expected, the CARD11 mutation R35A prevented T

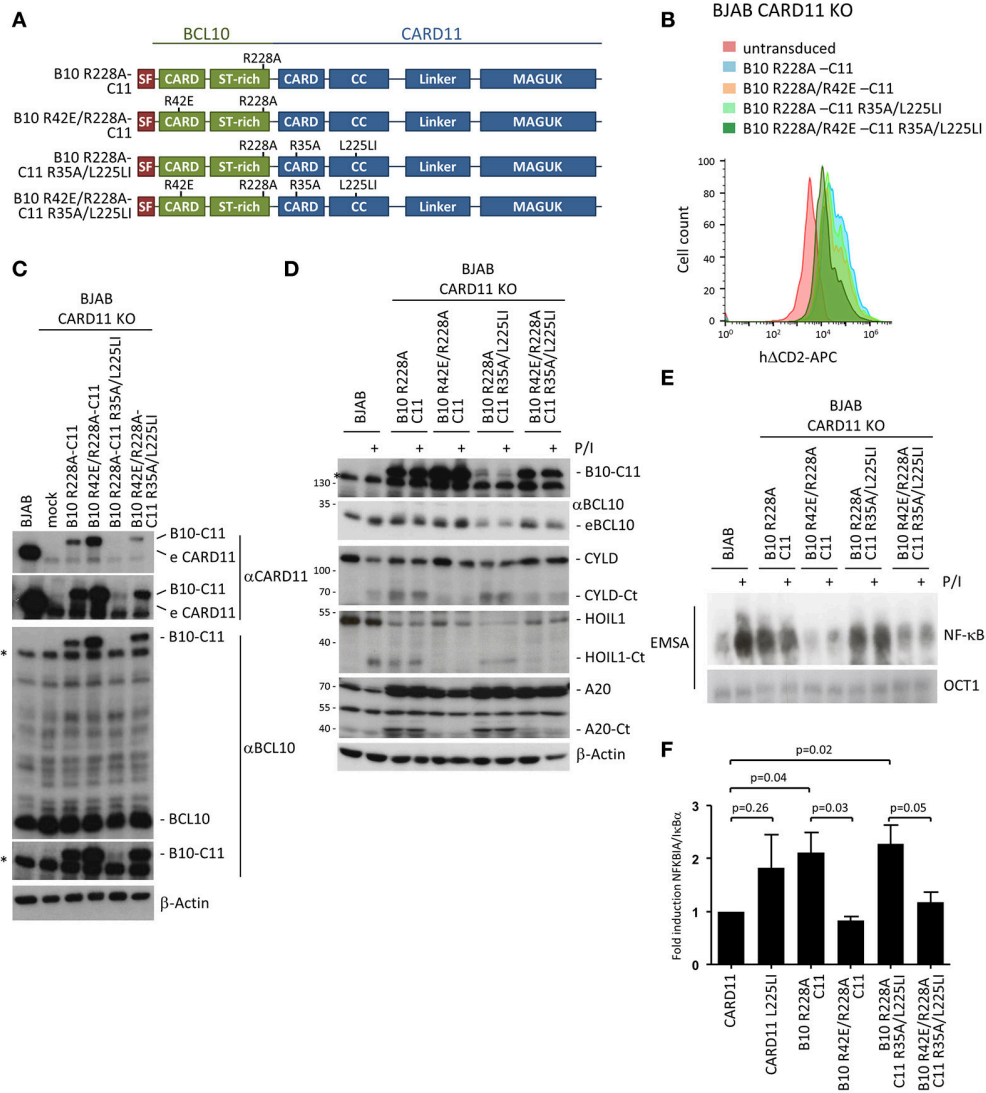


**FIGURE 6 |** Constitutive NF-κB and MALT1 activation by an oncogenic BCL10-CARD11 fusion protein relies on the BCL10 CARD interface in BJAB B cells. **(A)** Schematic representation of BCL10-CARD11 (B10-C11) fusion proteins containing CARD and oncogenic coiled-coil (CC) mutations. **(B)** Transduction of CARD11 KO BJAB B cells with B10 R228A-C11 fusion constructs, as depicted, was analyzed for the ΔCD2 surface marker by FACS. **(C)** Protein expression of the fusion constructs compared to parental BJAB B cells was determined by WB. **(D)** CARD11 KO BJAB B cells were reconstituted with B10 R228A-C11 fusion proteins as indicated. Constitutive and P/I-inducible (30 min) MALT1 activity was detected by CYLD, A20, and HOIL1 cleavage. **(E)** CARD11 KO BJAB B cells were reconstituted as in **(D)** and NF-κB activity was analyzed by EMSA. **(F)** Expression of the NF-κB target gene NFKBIA/κBα in CARD11 and B10 R228A-C11 expressing BJAB B cells was determined by quantitative RT-PCR. All values were normalized to the housekeeping gene RPII and related to CARD11 (mean ± s.e.m., p-values as indicated).

cell stimulation due to its inability to recruit BCL10 (12, 25). In addition, the BCL10-BCL10 interface mutant R42E could not rescue NF-κB signaling in BCL10 KO cells, which confirms the critical function of BCL10-BCL10 interface I for filament assembly and signaling (13). Recently, we have been able to solve the architecture of the BCL10-MALT1 filaments using cryo-EM (14). Surprisingly, we found that different mutations in the interface I that lead to loss of BCL10 filament assembly also abolished CARD11 recruitment of BCL10 and thus CBM complex formation (14). Thus, our results question if CARD11 acts as the seed to nucleate BCL10 filaments, or whether an

initial oligomerization of BCL10 is required for the recruitment to CARD11 in cells. Alternatively, our data would also be in line with a model in which CARD11-BCL10 association, but not BCL10 oligomerization, is critical to promote signaling in lymphocytes, and that filament formation is only observed with recombinant BCL10 or after high overexpression of BCL10.

To clarify the necessity of the CARD11 seed and BCL10 filaments for T and B cell activation, we fused BCL10 to CARD11 to bypass the initial step of heterotypic CARD-CARD interaction between CARD11 and BCL10. Even though this is an artificial system, it provided the first opportunity to examine

the contribution of the individual CARDS in CARD11 and BCL10. Remarkably, stable expression of the BCL10-CARD11 fusion protein promoted strong and chronic MALT1 protease activity in Jurkat T cells. While NF- $\kappa$ B activation was blunted in transduced Jurkat T cells, the transient transfection of BCL10-CARD11 activated NF- $\kappa$ B to a similar extent as an oncogenic CARD11 variant or CARD11 lacking the negative regulatory linker region (CARD11  $\Delta$ linker) (5, 6, 21). Interestingly, the BCL10-CARD11 fusion is not prone to auto-inhibition by the CARD11 linker, which acts as an inhibitory domain (27). In the fusion protein the BCL10 CARD is exposed and most likely not accessible for the CARD11 linker, especially when considering that an additional CARD cannot be bound by the linker in a 1:1 stoichiometry. Moreover, CARD11 and BCL10 CARDS are homologous, but also quite distinct and the BCL10 CARD may complex with the CARD11 linker, which would be critical for auto-inhibition (5, 27). Despite the disrupted auto-inhibition, the BCL10-CARD11 fusion protein signals to NF- $\kappa$ B via MALT1 and the TRAF6 binding motif on MALT1, underscoring that it utilizes the same mechanisms as a physiological CBM complex following T cell activation.

Despite the structural elucidation of BCL10-MALT1 filaments *in vitro*, the nature and relevance of cellular BCL10 oligomeric structures has not been fully resolved. BCL10 tends to aggregate via its CARD into oligomeric clusters and extended filaments after overexpression in cells (7, 9). Endogenous BCL10 forms oligomeric structures in antigen-stimulated T cells termed POLKADOTS (“punctuated and oligomeric killing or activating domains transducing signals”), which are cellular foci that serve as functional platforms for recruiting NF- $\kappa$ B signaling mediators following TCR stimulation (10, 28). Size exclusion chromatography demonstrated that in stimulated Jurkat T cells or ABC DLBCL tumor cells CARMA1, BCL10, and MALT1 assemble into higher order complexes with an apparent molecular weight >1 Mio. Da and the purified CBM complex displayed a filament-like structure in electron microscopy (13, 29). However, by increasing the concentration of BCL10 during the process of CBM purification, BCL10 filament formation may be initiated *in vitro* rather than taking place in living cells. Thus, there is good evidence that BCL10 can cluster via the CARD in cells, but the existence of large helical BCL10 filaments under physiological conditions in antigen-stimulated T or B cells has not been formally demonstrated. Since it may be difficult to imagine that the BCL10-CARD11 fusion itself can form long filaments in the absence of endogenous BCL10, activation by the fusion in BCL10 KO cells may indicate that BCL10-dependent dimerization or short oligomerization may be sufficient for lymphocyte activation. As for endogenous CARD11-associated BCL10, monitoring of BCL10 filament formation in the context of BCL10-CARD11 fusion is difficult with current methods, because of low expression levels. High resolution imaging techniques will be necessary to solve the extent of oligomerization and the cellular architecture of the BCL10 clusters. However, so far imaging in lymphocytes has been hampered by the unavailability of high quality antibodies as well as the small and round-shaped T and B cells that contain very little cytoplasm.

An important question that remains is the *in vivo* necessity for the formation of large, extended BCL10 filaments for signal propagation. The lack of NF- $\kappa$ B and MALT1 activation in BCL10 R42E in the context of the BCL10-CARD11 fusion reflects the need for BCL10 dimerization/oligomerization, but does not prove the requirement for higher order filaments. Alternatively, BCL10-MALT1 recruitment to CARD11 and BCL10 dimerization or short oligomers may be sufficient to facilitate cellular processes such as ubiquitination of CBM complex components. A number of ubiquitin ligases [e.g., TRAF6, LUBAC (linear ubiquitin chain assembly complex) and cIAP2] are recruited to the CBM complex and conjugation of mono-ubiquitin or poly-ubiquitin chains of different topology on all subunits has been implicated in triggering MALT1 activation and/or downstream signaling (1, 2). The complexity of ubiquitin-dependent regulation is exemplified by BCL10. K48-, K63-, or M1-linked ubiquitin chains are primarily conjugated on K17, K31, and/or K63 in the BCL10 CARD (30–32). Ubiquitination of these lysine residues is required for NF- $\kappa$ B activation in T cells and pro-survival signaling in ABC DLBCL cells (31–33). Deficiency in HOIP/RNF31, the catalytic subunit of LUBAC, suppresses NF- $\kappa$ B signaling in Jurkat T cells whereas HOIP activating mutations enhance NF- $\kappa$ B-dependent pro-survival in ABC DLBCL cells, supporting that M1-linked ubiquitin chains on BCL10 are enhancing CBM complex signaling (32, 34). However, at the same time BCL10 is degraded by lysosomal or proteasomal pathways and these processes are controlled by at least partially overlapping ubiquitination sites (31, 35–37). In addition, K48-linked poly-ubiquitination of CARD11 induces its degradation (38). Thus, the BCL10-CARD11 fusion protein is most likely strongly affected by regulatory ubiquitination and ubiquitin conjugation in each moiety may be responsible for activation, as well as the high turnover of the active BCL10-CARD11 fusions. Due to the multi-layered ubiquitin regulation and the uneven expression levels of active vs. inactive BCL10-CARD11 fusions, this system is not an ideal tool to study the relevance of BCL10 ubiquitination. However, it will be important to clarify in how far BCL10 oligomerization and potential filament formation cooperate with ubiquitination processes to induce downstream signaling or alternatively, if BCL10 ubiquitination may also facilitate CBM complex assembly.

In BJAB B cells stable BCL10-CARD11 expression activates MALT1 and NF- $\kappa$ B as strong as oncogenic variants of CARD11 derived from DLBCL tumor patients (5, 6, 25, 26), clearly showing that the proximity of BCL10 and CARD11 alone is sufficient to activate downstream signaling pathways. Thus, the BCL10-CARD11 fusion already provides compelling evidence that CARD11 acts as a seed in cells to boost lymphocyte activation. By introducing point mutations we were also now able to unravel the contribution of the two different CARD interfaces. Constitutive activity of the BCL10-CARD11 fusion no longer required the presence of an intact CARD11 CARD, but was solely driven by the BCL10 oligomerization interface. In contrast, stimulus-dependent MALT1 activation of the BCL10-CARD11 fusion protein relied on an intact CARD11 CARD, which most likely as in CARD11 WT serves as a platform for recruitment and oligomerization of endogenous BCL10.

Interestingly, introduction of the active oncogenic mutation L225LI into the CARD11 coiled-coil (CC) region in the context of the BCL10-CARD11 resulted in a fusion protein that was hyper-active, despite the very low expression level in the BJAB B cells. Indeed, all active BCL10-CARD11 fusion proteins were expressed at a lower level compared to their inactive counterparts. However, the very low expression of the hyper-active fusion constructs indicates that there is a strong counter-selection against the expression of these constitutively active variants in T and B cells. Since all fusions constitutively activate the MALT1 paracaspase in the two cell types, it is possible that the sustained MALT1 cleavage of mRNA processing factors Regnase-1 and Roquin1/2 may exert toxic effects that impair T and B cell survival (39, 40). More work is needed to understand under which circumstances chronic activation induces cell survival or toxicity.

While expression of BCL10-CARD11 fusion drives NF- $\kappa$ B activation in BJAB B cells, constitutive and inducible NF- $\kappa$ B signaling is severely impaired in Jurkat T cells expressing the fusion protein. Even though NF- $\kappa$ B activation is impaired in Jurkat T cells, MALT1 protease is still strongly activated by BCL10-CARD11 fusions, demonstrating that not all CBM downstream effects are affected. Further, the reduced responsiveness relies on the stable expression of the BCL10-CARD11 fusion protein and it needs to be explored what cell-intrinsic mechanisms operate in Jurkat T cells that counteract constitutive activation of the canonical NF- $\kappa$ B pathway downstream of the CBM complex. Of note, T lymphocytes from patients with germline activating CARD11 mutations are anergic, while the B cells are activated and expanding, causing a phenotype called BENTA (B cell expansion with NF- $\kappa$ B and T cell anergy) (41, 42). It will be interesting to see whether similar negative regulatory mechanisms observed in Jurkat T cells driven by an active BCL10-CARD11 fusion could also operate in primary T cells.

Our data suggest that upon the initial BCL10 recruitment to CARD11, the weak heterotypic interaction of the monomeric CARDs needs to be stabilized by further interactions arising from the oligomerized CARD11 seed and the helical BCL10 filaments. The additional contact points within this multimeric complex are essential for a high affinity binding and the formation of a stable CBM complex that is competent to trigger downstream signaling. Furthermore, the structural rigidity in the core BCL10-MALT1 filament may stabilize the binding, which is in line with the observation that CARD11 binding is also reduced when BCL10 is not complexed with MALT1 (14). In conclusion, we demonstrate that the recruitment of BCL10-MALT1 to CARD11 and BCL10-MALT1 filament formation are highly interconnected processes that cooperate to drive CBM downstream effects in response to physiological or pathological activation of T and B cells.

## MATERIALS AND METHODS

### Cell Lines and Treatments

Cell lines were maintained at 37°C in a humidified atmosphere at 5% CO<sub>2</sub>. Jurkat T cells and BJAB B cells were cultured in RPMI 1640 Medium, and U2OS and HEK293T cells in DMEM. Media were supplemented with 10% (Jurkat T cells, U2OS, HEK293T)

or 15% (BJAB B cells) fetal calf serum, 100 U/ml penicillin and 100  $\mu$ g/ml streptomycin. U2OS, HEK293T and BJAB B cells were obtained from the DSMZ, Jurkat T cells were authenticated by the Authentication Service of the Leibniz Institute DSMZ. Jurkat T cells were stimulated with Phorbol 12-Myristate 13-Acetate (PMA: 200 ng/ml; Merck) and Ionomycin (300 ng/ml; Calbiochem) for 30 min, except if otherwise stated.

### DNA Constructs and Antibodies

DNA constructs and antibodies used in this study are listed in Tables 1, 2, respectively.

### Generation and Reconstitution of Knock-Out Cells

Bicistronic expression vector px458 expressing Cas9 and sgRNA (45, 46) was digested with *BbsI* and the linearized vector

**TABLE 1 |** DNA constructs.

pHAGE- $\Delta$ CD2-T2A	Lentiviral transfer vector used (43)
pMD2.G	Lentiviral packaging construct (Addgene: Plasmid #12259)
psPAX2	Lentiviral packaging construct (Addgene: Plasmid #12260)
pHAGE- $\Delta$ CD2-T2A-SF CARD11-FS constructs	Lentiviral transfer vector (mock) CARD11, CARD11 R35A, and CARD11 L225LI in pHAGE- $\Delta$ CD2-T2A (25)
BCL10-FS constructs SF-BCL10-CARD11 (B10-C11) constructs	BCL10 and BCL10 R42E in pHAGE- $\Delta$ CD2-T2A CARD11 and CARD11 mutants (R35A, R35A/L225LI) in SF-BCL10, SF-BCL10 R42E, SF-BCL10 R228A, or SF-BCL10 R42E/R228A containing pHAGE- $\Delta$ CD2-T2A
pGL3-6xNF- $\kappa$ B luc	NF- $\kappa$ B reporter firefly luciferase (44)
pRL-TKluc	TK reporter renilla luciferase (Promega)

**TABLE 2 |** Antibodies.

Primary antibodies	Source
A20/TNFAIP3 (D13H3)	Cell Signaling
BCL10 (C-17)	Santa Cruz
BCL10 (H-197)	Santa Cruz
CARMA1/CARD11 (1D12)	Cell Signaling
CYLD (E-10)	Santa Cruz
HOIL-1 (S150D)	MRC
I $\kappa$ B $\alpha$ (L35A5)	Cell Signaling
I $\kappa$ B $\alpha$ (phospho-Ser32/36) (5A5)	Cell Signaling
MALT1 (B-12)	Santa Cruz
StrepTagII	IBA
$\beta$ -Actin (I-19)	Santa Cruz
anti-CD2-APC (RPA-2.10)	eBioscience

Secondary antibodies	Source
HRP-conjugated anti-goat	Jackson ImmunoResearch
HRP-conjugated anti-mouse	Jackson ImmunoResearch
HRP-conjugated anti-rabbit	Jackson ImmunoResearch
HRP-conjugated anti-sheep	Jackson ImmunoResearch
Alexa Fluor488-donkey anti-mouse	Invitrogen

was gel purified. Targeting oligos (CARD11: 5'CTCATCA ATGACCTTACTGACGCAGGTAGG 3'BCL10: 5'AGT GAGGTCCTCCTCGGTGA 3' and 5'TTCCGCTTTCGTCTC CCGCT 3') for each targeting site positioned as depicted in **Supplementary Figures 2A,B**, were annealed and ligated to the linearized vector. Jurkat T cells or BJAB B cells ( $4\text{--}8 \times 10^6$ ) were electroporated (220 V and 1,000  $\mu\text{F}$ ) using a Gene pulser X (Biorad) with px458 plasmids expressing sgRNA targeting CARD11 or BCL10, as well as a EGFP expression cassette. Twenty-four to forty-eight hours after electroporation, GFP positive cells were sorted using a MoFlow sorting system. Isolation of clonal cell lines was achieved by serial dilutions and was followed by an appropriate expansion period. KO cell clones were initially identified by detecting CARD11 or BCL10, respectively, by Western Blot. Clones lacking protein expression were genotyped by genomic PCR using intronic primers flanking targeting sites.

For reconstitution, lentivirus was produced in HEK293T cells.  $1 \times 10^6$  HEK293T cells were seeded in 8 ml DMEM medium (10% FCS, 1% Pen/Strep) in 10  $\text{cm}^2$  dishes and grown overnight at 37°C. The next day, the cells were transfected with 1.5  $\mu\text{g}$  of the packaging vector psPAX2, 1.0  $\mu\text{g}$  of the lentiviral envelope plasmid pMD2.G and 2  $\mu\text{g}$  pHAGE transfer vector using XtremeGENE HP DNA Transfection Reagent (Roche) according to the manufacturer's protocol. After 3 days the supernatant of the HEK293T cells containing the virus was sterile filtered (0.45  $\mu\text{m}$ ). For transduction, virus supernatant was transferred to  $5 \times 10^5$  Jurkat T cells or BJAB B cells. For BJAB B cells, supernatant was concentrated with Amicon centrifugal filter units (100 K) prior to transduction. The solution was filled up with RPMI medium (10% FCS, 1% Pen/Strep) to a final volume of 2–2.5 ml and mixed with Polybrene (8  $\mu\text{g}/\text{ml}$ ). To enhance transduction efficiency, BJABs were centrifuged for 1 h at 500  $\times$  g. Forty to seventy-two hours later, cells were washed with PBS (without calcium and magnesium) and re-suspended in 1–2 ml RPMI medium (10% FCS, 1% Pen/Strep). Seven to ten days after transduction infection was analyzed by determining  $\Delta\text{CD}2$  surface expression by FACS and CARD11 or BCL10 protein expression by Western Blot. Only cells yielding a transduction efficiency of >90% as determined by FACS analysis, were used for further analyses.

Generation and reconstitution of MALT1-deficient Jurkat T cells has been described (22).

### Flow Cytometry (FACS)

Surface expression of  $\Delta\text{CD}2$  after lentiviral transduction of BJAB B cells or Jurkat T cells was assessed by incubating 200  $\mu\text{l}$  of the cell culture for 15 min at room temperature with 2  $\mu\text{l}$  anti-CD2-APC (RPA-2.10) antibody. Cells were centrifuged (1,100 rpm, 5 min) and re-suspended in 250  $\mu\text{l}$  PBS before FACS using Attune Acoustic Focusing Flow Cytometer.

### Cell Lysis and Precipitations

For analysis of expression via Western Blot or EMSA, cells ( $1\text{--}3 \times 10^6$ ) were harvested (300  $\times$  g, 5 min, 4°C) and washed once with ice cold PBS. The pellet was resuspended in 80–100  $\mu\text{l}$  high salt buffer (20 mM HEPES pH 7.9, 350 mM NaCl, 20%

glycerol, 1 mM  $\text{MgCl}_2$ , 0.5 mM EDTA, 0.1 mM EGTA, 1% NP-40, 1 mM DTT, 10 mM sodium fluoride, 8 mM  $\beta$ -glycerophosphate, 300  $\mu\text{M}$  sodium vanadate and Roche protease inhibitor cocktail). For binding studies, cells ( $1\text{--}5 \times 10^7$ ) were lysed in co-IP buffer (25 mM HEPES pH 7.5, 150 mM NaCl, 0.2% NP-40, 10% glycerol, 1 mM DTT, 10 mM sodium fluoride, 8 mM  $\beta$ -glycerophosphate, 300  $\mu\text{M}$  sodium vanadate and protease inhibitor cocktail). Lysate controls were mixed with 4xSDS loading dye and boiled. For StrepTactin pull-downs (ST-PD), 20–40  $\mu\text{l}$  Strep-Tactin Sepharose (1:1 suspension) was used for binding of Strep-tagged BCL10 or BCL10-CARD11 fusion overnight at 4°C rotating. Sepharose beads were pelleted after incubation (100  $\times$  g, 4 min, 4°C), washed 3x with co-IP buffer, and boiled after the addition of 20  $\mu\text{l}$  2xSDS loading dye (Roti-load). Lysates and ST-PDs were separated by SDS-PAGE and analyzed by Western Blot.

### Western Blot

Proteins were transferred onto PVDF-membranes for immunodetection using an electrophoretic semi-dry transfer system. After transfer, membranes were blocked with 5% BSA for 1 h at RT and incubated with specific primary antibodies (indicated above, diluted 1:1,000 in 2.5% BSA/PBS-T) overnight at 4°C. Membranes were washed in PBS-T before the addition of HRP-coupled secondary antibodies (indicated above, 1:7,000 in 1.25% BSA in PBS-T; 1 h, RT). HRP was detected by enhanced chemiluminescence (ECL) using the LumiGlo reagent (Cell Signaling) according to manufacturer's instructions.

### Electrophoretic Mobility Shift Assay (EMSA)

For EMSAs, double-stranded NF- $\kappa\text{B}$  (H2K: fw: 5'-GATCCA GGGCTGGGGATTCCCCATCTCCACAGG-3', rev: 5'- GAT CCCTGTGGAGATGGGGAATCCCCAGCCCTG-3'), and OCT1 binding sequences (fw: 5'- GATCTGTGCAATGCA AATCACTAGAA-3', rev: 5'-GATCTTCTAGTGATTTGCATT CGACA-3') were labeled with [ $\alpha$ - $^{32}\text{P}$ ] dATP using Klenow Fragment (NEB). To monitor DNA binding, whole cell lysates (3–6  $\mu\text{g}$ ) were incubated for 30 min at RT with shift-buffer [20 mM HEPES pH 7.9, 120 mM KCl, 4% Ficoll, 5 mM DTT, 10  $\mu\text{g}$  BSA and 2  $\mu\text{g}$  poly-dI-dC (Roche)] and radioactive double stranded NF- $\kappa\text{B}$  or OCT1 probes (10,000–20,000 cpm). Samples were separated on a 5% polyacrylamide gel in TBE buffer, vacuum-dried and exposed to autoradiography.

### Confocal Immunofluorescence Microscopy

The localization and distribution of BCL10 was analyzed by seeding U2OS cells in 96-well plates. Cells were transfected using Lipofectamine 3000 Transfection Reagent (Invitrogen) according to the manufacturer's instructions. To optimize cell attachment, CellCarrier-96 black plates (PerkinElmer) were coated with 100  $\mu\text{l}$  poly-D-lysine at a concentration of 50  $\mu\text{g}/\text{ml}$ . Twenty-four hours after transfection, cells were washed with PBS and fixed with 60  $\mu\text{l}$  Methanol ( $-20^\circ\text{C}$ ) for 5–10 min at room temperature and then washed 3x with PBS. For immunostaining, cells were blocked in 2% BSA in PBS. Cells were incubated with primary antibody (anti-StrepTagII) in blocking buffer for 2 h at RT. Cells were washed 3x for

10 min at RT, before incubation with secondary antibody (Alexa Fluor488-donkey anti-mouse) in blocking buffer for 1 h at RT. Cell nuclei were visualized by incubation with Hoechst 33342 dye (Life Technologies) in PBS at a concentration of 0.5 µg/ml for 30 min at RT. Afterwards the cells were washed and covered with PBS, sealed with foil and kept at 4°C in the dark until microscopy. Confocal microscopy was performed with an Operetta high-content imaging system (Perkin-Elmer).

## Labeling and Biotin Pull-Down (PD) of Active MALT1

The biotin-labeled MALT1 activity based probe (MALT1-ABP) has been described previously (19). To investigate MALT1 protease activity, Jurkat T cells ( $3 \times 10^7$ ) were washed with PBS, and lysed in 600 µl co-IP buffer without protease inhibitors for 30 min at 4°C. After clearing the lysates by centrifugation (20,000 × g, 4°C, 15 min), 30 µl were collected as lysate control, mixed with 4x SDS loading buffer and boiled for 5 min at 95°C. To 550 µl of the supernatant 12 µl High Capacity Streptavidin Beads (Thermo Fisher) was added and incubated for 1 h at 4°C for pre-clearing. The beads were pelleted (4,000 rpm, 2 min, 4°C) and 450 µl of supernatant was mixed with MALT1-ABP probe (0.1 µM final concentration). After 1 h rotating at room temperature, 15 µl High Capacity Streptavidin Beads was added before 1–2 h incubation at 4°C (rotating). Beads were collected and washed 3x with co-IP buffer without protease inhibitors. Beads were re-suspended in 22 µl 2x SDS loading buffer and boiled at 95°C for 7 min before SDS-PAGE and Western Blot analysis.

## NF-κB Reporter Assay

For NF-κB luciferase reporter assays,  $8 \times 10^6$  Jurkat cells were transfected by electroporation with 2 µg NF-κB firefly luciferase reporter plasmid, 1 µg renilla luciferase and 6 µg of CARD11 and BCL10-CARD11 fusion constructs using 220 V and 1,000 µF (Gene Pulser X, BioRad). After cultivation for 72 h cells were lysed in passive lysis buffer and luciferase activity measured using a dual luciferase reporter kit according to the manufacturer's protocol (Promega). All luciferase values were calculated in relation to the Renilla control.

## Quantitative Reverse-Transcriptase Polymerase Chain Reaction (qRT-PCR)

RNA was isolated (QIAGEN RNeasy Kit) and equal amounts of RNA (InviTrap Spin Universal RNA Mini Kit, 1060100200, Stratec) were transcribed into cDNA using the Verso cDNA synthesis Kit (AB1453B, Thermo Fisher Scientific). Quantitative real-time (qRT) PCR was performed using KAPA SYBR FAST qPCR Master Mix (KAPA Biosystems) and standard LightCycler protocol on a Roche LightCycler 480. RNA Polymerase II (PolII) served as internal standard. The following primers were used: fw: 5'-CCGCACCTCCACTCCATCC-3' rev: 5'-ACATCAGCACCC AAGGACACC-3'; RPII fw: 5'-GCACCACGTCCAATGACA-3' rev: 5'-GTGCGGCTGCTTCATAA-3'. Results represent the mean and standard error of the mean of three independent experiments.

## Structural Model of CARD11-BCL10 and BCL10-BCL10 Interaction Surfaces

The CARD11-BCL10 CARD/CARD interaction model was prepared under consideration of the surface charge complementarity analysis of the BCL10-MALT1 filament cryo EM structure (EMD-0013, PDB 6GK2) and the crystal structure of the CARD11 domain (PDB 4LWD) (**Supplementary Figure 1**). The CARD11 CARD structure has been superimposed on the BCL10 CARD within the BCL10-MALT1 filament using the align command in PyMOL (The PyMOL Molecular Graphics System, Version 2.0 Schrödinger, LLC). Under consideration that the mutation of residue R35 in CARD11 abolishes the interaction to BCL10 (12), we propose that the mainly positively charged top of the CARD11 CARD interacts with the negatively charged bottom of the Bcl10 filament (**Supplementary Figures 1B,C**). The electrostatic surface was calculated with the program APBS Tool 2.1 implemented in PyMOL (47).

## Statistical Analysis

Data for luciferase reporter assay, quantitative RT-PCR and fluorescence microscopy was analyzed for statistical significance using the unpaired Student's *t*-test ( $**p \leq 0.01$ ,  $***p \leq 0.001$ ). Sample size (*n*) is specified for each experiment and data are shown as mean ± s.e.m.

## AUTHOR CONTRIBUTIONS

TS and SK conceived and performed most experiments, analyzed, and interpreted the data. FS and KL conceived and performed biophysical experiments and provided structural expertise. SW, TG, and SWi generated, verified and analyzed KO cells. DK conceived the study, experiments, wrote the manuscript, and secured funding. All authors read, acknowledged, and helped with the final version of the manuscript.

## FUNDING

Deutsche Krebshilfe (grant no. 70112622) to DK supported work on oncogenic CARD11 signaling. Deutsche Forschungsgemeinschaft SFB 1054 TP A04 to DK and TP B02 to KL supported structural and mechanistic work on CBM complex signaling in T cells.

## ACKNOWLEDGMENTS

We thank Katrin Demski and Kerstin Kutzner for excellent technical assistance.

## SUPPLEMENTARY MATERIAL

The Supplementary Material for this article can be found online at: <https://www.frontiersin.org/articles/10.3389/fimmu.2018.02695/full#supplementary-material>

## REFERENCES

- Juilland M, Thome M. Role of the CARMA1/BCL10/MALT1 complex in lymphoid malignancies. *Curr Opin Hematol.* (2016) 23:402–9. doi: 10.1097/MOH.0000000000000257
- Meininger I, Krappmann D. Lymphocyte signaling and activation by the CARMA1-BCL10-MALT1 signalosome. *Biol Chem.* (2016) 397:1315–33. doi: 10.1515/hsz-2016-0216
- Matsumoto R, Wang D, Blonska M, Li H, Kobayashi M, Pappu B, et al. Phosphorylation of CARMA1 plays a critical role in T Cell receptor-mediated NF-kappaB activation. *Immunity* (2005) 23:575–85. doi: 10.1016/j.immuni.2005.10.007
- Sommer K, Guo B, Pomerantz JL, Bandaranayake AD, Moreno-Garcia ME, Ovechkina YL, et al. Phosphorylation of the CARMA1 linker controls NF-kappaB activation. *Immunity* (2005) 23:561–74. doi: 10.1016/j.immuni.2005.09.014
- Lamason RL, McCully RR, Lew SM, Pomerantz JL. Oncogenic CARD11 mutations induce hyperactive signaling by disrupting autoinhibition by the PKC-responsive inhibitory domain. *Biochemistry* (2010) 49:8240–50. doi: 10.1021/bi101052d
- Lenz G, Davis RE, Ngo VN, Lam L, George TC, Wright GW, et al. Oncogenic CARD11 mutations in human diffuse large B cell lymphoma. *Science* (2008) 319:1676–9. doi: 10.1126/science.1153629
- Bertin J, Wang L, Guo Y, Jacobson MD, Poyet JL, Srinivasula SM, et al. CARD11 and CARD14 are novel caspase recruitment domain (CARD)/membrane-associated guanylate kinase (MAGUK) family members that interact with BCL10 and activate NF-kappa B. *J Biol Chem.* (2001) 276:11877–82. doi: 10.1074/jbc.M010512200
- Gaïde O, Martinon F, Micheau O, Bonnet D, Thome M, Tschoop J. Carma1, a CARD-containing binding partner of Bcl10, induces Bcl10 phosphorylation and NF-kappaB activation. *FEBS Lett.* (2001) 496:121–7. doi: 10.1016/S0014-5793(01)02414-0
- Güet C, Vito P. Caspase recruitment domain (CARD)-dependent cytoplasmic filaments mediate bcl10-induced NF-kappaB activation. *J Cell Biol.* (2000) 148:1131–40. doi: 10.1083/jcb.148.6.1131
- Schaefer BC, Kappler JW, Kupfer A, Marrack P. Complex and dynamic redistribution of NF-kappaB signaling intermediates in response to T cell receptor stimulation. *Proc Natl Acad Sci USA.* (2004) 101:1004–9. doi: 10.1073/pnas.0307858100
- David L, Li Y, Ma J, Garner E, Zhang X, Wu H. Assembly mechanism of the CARMA1-BCL10-MALT1-TRAF6 signalosome. *Proc Natl Acad Sci USA.* (2018) 115:1499–504. doi: 10.1073/pnas.1721967115
- Li S, Yang X, Shao J, Shen Y. Structural insights into the assembly of CARMA1 and BCL10. *PLoS One* (2012) 7:e42775. doi: 10.1371/journal.pone.0042775
- Qiao Q, Yang C, Zheng C, Fontan L, David L, Yu X, et al. Structural architecture of the CARMA1/Bcl10/MALT1 signalosome: nucleation-induced filamentous assembly. *Mol Cell* (2013) 51:766–79. doi: 10.1016/j.molcel.2013.08.032
- Schlauderer F, Seeholzer T, Desfosses A, Gehring T, Strauss M, Hopfner K-P, et al. Molecular architecture and regulation of BCL10-MALT1 filaments. *Nat Commun.* (2018) 9:4041. doi: 10.1038/s41467-018-06573-8
- Egawa T, Albrecht B, Favier B, Sunshine MJ, Mirchandani K, O'Brien W, et al. Requirement for CARMA1 in antigen receptor-induced NF-kappa B activation and lymphocyte proliferation. *Curr Biol.* (2003) 13:1252–8. doi: 10.1016/S0960-9822(03)00491-3
- Hara H, Wada T, Bakal C, Koziarzki I, Suzuki S, Suzuki N, et al. The MAGUK family protein CARD11 is essential for lymphocyte activation. *Immunity* (2003) 18:763–75. doi: 10.1016/S1074-7613(03)00148-1
- Ruland J, Duncan GS, Elia A, del Barco Barrantes I, Nguyen L, Plyte S, et al. Bcl10 is a positive regulator of antigen receptor-induced activation of NF-kappaB and neural tube closure. *Cell* (2001) 104:33–42. doi: 10.1016/S0092-8674(01)00189-1
- Jaworski M, Thome M. The paracaspase MALT1: biological function and potential for therapeutic inhibition. *Cell Mol Life Sci.* (2016) 73:459–73. doi: 10.1007/s00018-015-2059-z
- Eitelhuber AC, Vossyka O, Nagel D, Bogner M, Lenze D, Lammens K, et al. Activity-based probes for detection of active MALT1 paracaspase in immune cells and lymphomas. *Chem Biol.* (2015) 22:129–38. doi: 10.1016/j.chembiol.2014.10.021
- Rebeaud F, Hailfinger S, Posevitz-Fejfar A, Tapernoux M, Moser R, Rueda D, et al. The proteolytic activity of the paracaspase MALT1 is key in T cell activation. *Nat Immunol.* (2008) 9:272–81. doi: 10.1038/ni1568
- McCully RR, Pomerantz JL. The protein kinase C-responsive inhibitory domain of CARD11 functions in NF-kappaB activation to regulate the association of multiple signaling cofactors that differentially depend on Bcl10 and MALT1 for association. *Mol Cell Biol.* (2008) 28:5668–86. doi: 10.1128/MCB.00418-08
- Meininger I, Griesbach RA, Hu D, Gehring T, Seeholzer T, Bertossi A, et al. Alternative splicing of MALT1 controls signalling and activation of CD4(+) T cells. *Nat Commun.* (2016) 7:11292. doi: 10.1038/ncomms11292
- Chan W, Schaffer TB, Pomerantz JL. A quantitative signaling screen identifies CARD11 mutations in the CARD and LATCH domains that induce Bcl10 ubiquitination and human lymphoma cell survival. *Mol Cell Biol.* (2013) 33:429–43. doi: 10.1128/MCB.00850-12
- Noels H, van Loo G, Hagens S, Broeckx V, Beyaert R, Marynen P, et al. A Novel TRAF6 binding site in MALT1 defines distinct mechanisms of NF-kappaB activation by API2middle dotMALT1 fusions. *J Biol Chem.* (2007) 282:10180–9. doi: 10.1074/jbc.M611038200
- Bogner MK, Vincendeau M, Erdmann T, Seeholzer T, Grau M, Linnemann JR, et al. Oncogenic CARMA1 couples NF-kappaB and beta-catenin signaling in diffuse large B-cell lymphomas. *Oncogene* (2016) 35:4269–81. doi: 10.1038/nc.2015.493
- Knies N, Alankus B, Weilemann A, Tzankov A, Brunner K, Ruff T, et al. Lymphomagenic CARD11/BCL10/MALT1 signaling drives malignant B-cell proliferation via cooperative NF-kappaB and JNK activation. *Proc Natl Acad Sci USA.* (2015) 112:E7230–8. doi: 10.1073/pnas.1507459112
- Jattani RP, Tritapoe JM, Pomerantz JL. Intramolecular interactions and regulation of cofactor binding by the four repressive elements in the Caspase Recruitment Domain-containing Protein 11 (CARD11) inhibitory domain. *J Biol Chem.* (2016) 291:8338–48. doi: 10.1074/jbc.M116.717322
- Rossman JS, Stoicheva NG, Langel FD, Patterson GH, Lippincott-Schwartz J, Schaefer BC. POLKADOTS are foci of functional interactions in T-cell receptor-mediated signaling to NF-kappaB. *Mol Biol Cell* (2006) 17:2166–76. doi: 10.1091/mbc.e05-10-0985
- Oeckinghaus A, Wegener E, Weltecke V, Ferch U, Arslan SC, Ruland J, et al. Malt1 ubiquitination triggers NF-kappaB signaling upon T-cell activation. *EMBO J.* (2007) 26:4634–45. doi: 10.1038/sj.emboj.7601897
- Satpathy S, Wagner SA, Beli P, Gupta R, Kristiansen TA, Malinova D, et al. Systems-wide analysis of BCR signalosomes and downstream phosphorylation and ubiquitylation. *Mol Syst Biol.* (2015) 11:810. doi: 10.15252/msb.20145880
- Wu CJ, Ashwell JD. NEMO recognition of ubiquitinated Bcl10 is required for T cell receptor-mediated NF-kappaB activation. *Proc Natl Acad Sci USA.* (2008) 105:3023–8. doi: 10.1073/pnas.0712313105
- Yang YK, Yang C, Chan W, Wang Z, Deibel KE, Pomerantz JL. Molecular determinants of scaffold-induced linear ubiquitylation of B cell lymphoma/leukemia 10 (Bcl10) during T cell receptor and oncogenic Caspase Recruitment Domain-Containing Protein 11 (CARD11) signaling. *J Biol Chem.* (2016) 291:25921–36. doi: 10.1074/jbc.M116.754028
- Yang Y, Kelly P, Shaffer ALIII, Schmitz R, Yoo HM, Liu X, et al. Targeting non-proteolytic protein ubiquitination for the treatment of diffuse large B cell lymphoma. *Cancer Cell* (2016) 29:494–507. doi: 10.1016/j.ccell.2016.03.006
- Yang Y, Schmitz R, Mitala J, Whiting A, Xiao W, Ceribelli M, et al. Essential role of the linear ubiquitin chain assembly complex in lymphoma revealed by rare germline polymorphisms. *Cancer Disc.* (2014) 4:480–93. doi: 10.1158/2159-8290.CD-13-0915
- Lobry C, Lopez T, Israel A, Weil R. Negative feedback loop in T cell activation through IkkappaB kinase-induced phosphorylation and degradation of Bcl10. *Proc Natl Acad Sci USA.* (2007) 104:908–13. doi: 10.1073/pnas.0606982104
- Paul S, Kashyap AK, Jia W, He YW, Schaefer BC. Selective autophagy of the adaptor protein Bcl10 modulates T cell receptor activation of NF-kappaB. *Immunity* (2012) 36:947–58. doi: 10.1016/j.immuni.2012.04.008
- Scharschmidt E, Wegener E, Heissmeyer V, Rao A, Krappmann D. Degradation of Bcl10 induced by T-cell activation negatively

- regulates NF-kappa B signaling. *Mol Cell Biol.* (2004) 24:3860–73. doi: 10.1128/MCB.24.9.3860-3873.2004
38. Moreno-Garcia ME, Sommer K, Rincon-Arango H, Brault M, Ninomiya-Tsuji J, Matesic LE, et al. Kinase-independent feedback of the TAK1/TAB1 complex on BCL10 turnover and NF-kappaB activation. *Mol Cell Biol.* (2013) 33:1149–63. doi: 10.1128/MCB.06407-11
  39. Jeltsch KM, Hu D, Brenner S, Zoller J, Heinz GA, Nagel D, et al. Cleavage of roquin and regnase-1 by the paracaspase MALT1 releases their cooperatively repressed targets to promote T(H)17 differentiation. *Nat Immunol.* (2014) 15:1079–89. doi: 10.1038/ni.3008
  40. Uehata T, Iwasaki H, Vandenbon A, Matsushita K, Hernandez-Cuellar E, Kuniyoshi K, et al. Malt1-induced cleavage of regnase-1 in CD4(+) helper T cells regulates immune activation. *Cell* (2013) 153:1036–49. doi: 10.1016/j.cell.2013.04.034
  41. Arjunaraja S, Nose BD, Sukumar G, Lott NM, Dalgard CL, Snow AL. Intrinsic plasma cell differentiation defects in B cell expansion with NF-kappaB and T cell anergy patient B cells. *Front Immunol.* (2017) 8:913. doi: 10.3389/fimmu.2017.00913
  42. Snow AL, Xiao W, Stinson JR, Lu W, Chaigne-Delalande B, Zheng L, et al. Congenital B cell lymphocytosis explained by novel germline CARD11 mutations. *J Exp Med.* (2012) 209:2247–61. doi: 10.1084/jem.20120831
  43. Hadian K, Griesbach RA, Dornauer S, Wanger TM, Nagel D, Metlitzky M, et al. NF-kappaB essential modulator (NEMO) interaction with linear and lys-63 ubiquitin chains contributes to NF-kappaB activation. *J Biol Chem.* (2011) 286:26107–17. doi: 10.1074/jbc.M111.233163
  44. Bergmann M, Hart L, Lindsay M, Barnes PJ, Newton R. IkappaBalpha degradation and nuclear factor-kappaB DNA binding are insufficient for interleukin-1beta and tumor necrosis factor-alpha-induced kappaB-dependent transcription. Requirement for an additional activation pathway. *J Biol Chem.* (1998) 273:6607–10. doi: 10.1074/jbc.273.12.6607
  45. Cong L, Ran FA, Cox D, Lin S, Barretto R, Habib N, et al. Multiplex genome engineering using CRISPR/Cas systems. *Science* (2013) 339:819–23. doi: 10.1126/science.1231143
  46. Ran FA, Hsu PD, Wright J, Agarwala V, Scott DA, Zhang F. Genome engineering using the CRISPR-Cas9 system. *Nature protocols* (2013) 8:2281–308. doi: 10.1038/nprot.2013.143
  47. Baker NA, Sept D, Joseph S, Holst MJ, McCammon JA. Electrostatics of nanosystems: application to microtubules and the ribosome. *Proc Natl Acad Sci USA.* (2001) 98:10037–41. doi: 10.1073/pnas.181342398

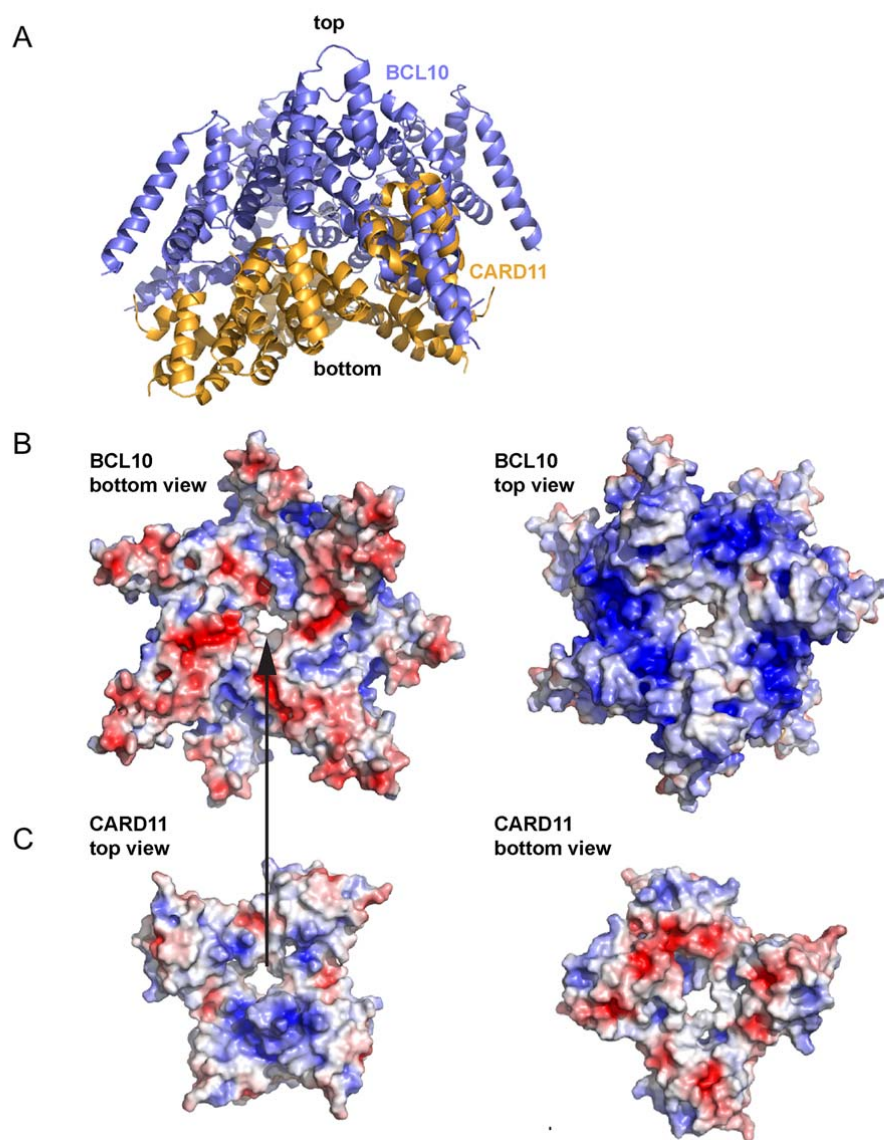
**Conflict of Interest Statement:** The authors declare that the research was conducted in the absence of any commercial or financial relationships that could be construed as a potential conflict of interest.

Copyright © 2018 Seeholzer, Kurz, Schlauderer, Woods, Gehring, Widmann, Lammens and Krappmann. This is an open-access article distributed under the terms of the Creative Commons Attribution License (CC BY). The use, distribution or reproduction in other forums is permitted, provided the original author(s) and the copyright owner(s) are credited and that the original publication in this journal is cited, in accordance with accepted academic practice. No use, distribution or reproduction is permitted which does not comply with these terms.

## SUPPLEMENTARY INFORMATION

Seeholzer et al.

## SUPPLEMENTARY FIGURES AND LEGENDS

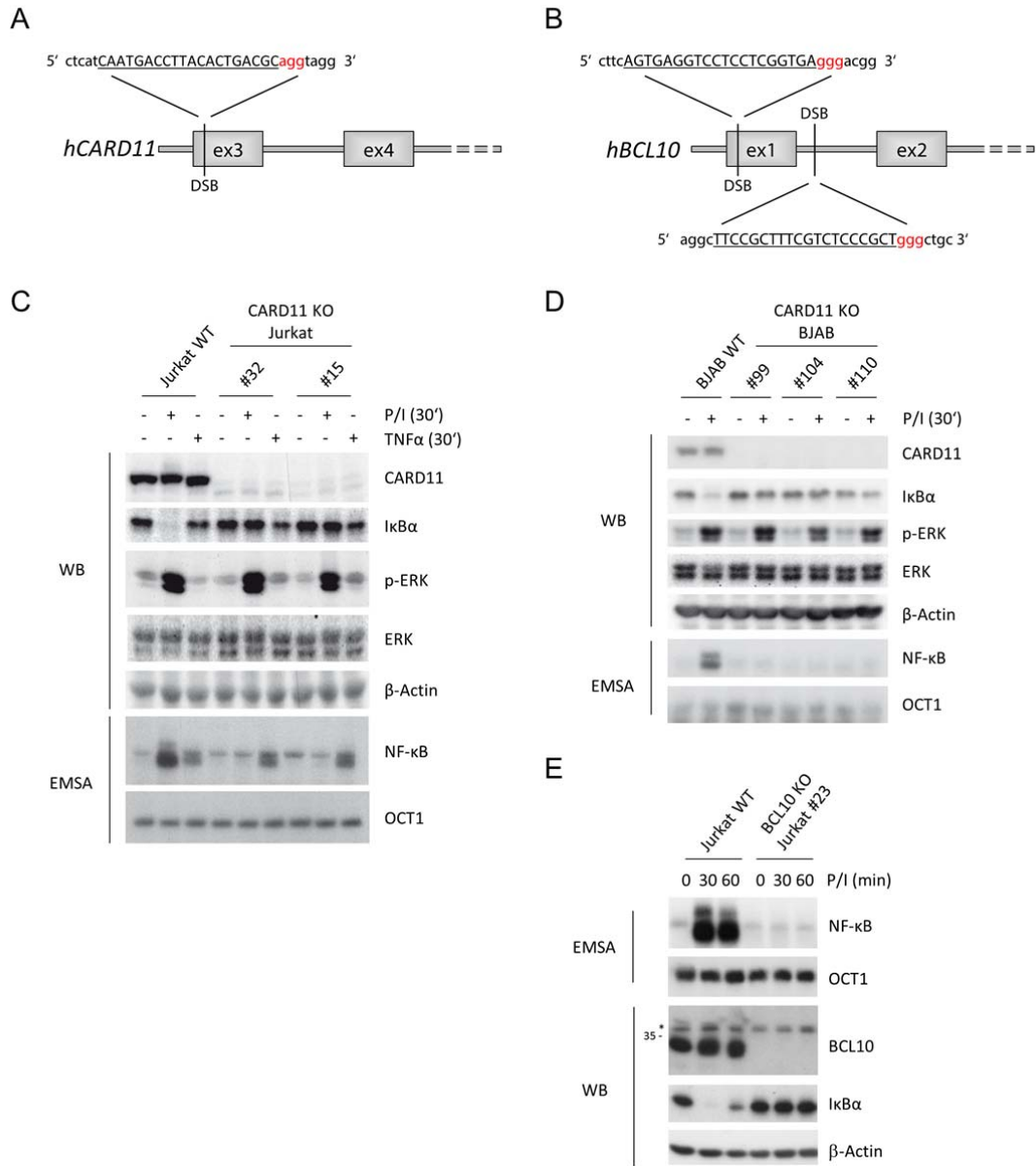


**Supplementary Figure 1: Generation of the CARD11 BCL10 CARD domain interaction model.** (A)

Ribbon model of 5 BCL10 CARD domains (PDB 6GK2) arranged in the filament and colored blue shown together with the superimposed CARD11 CARD domains (PDB:4LWD) colored orange. (B-C)

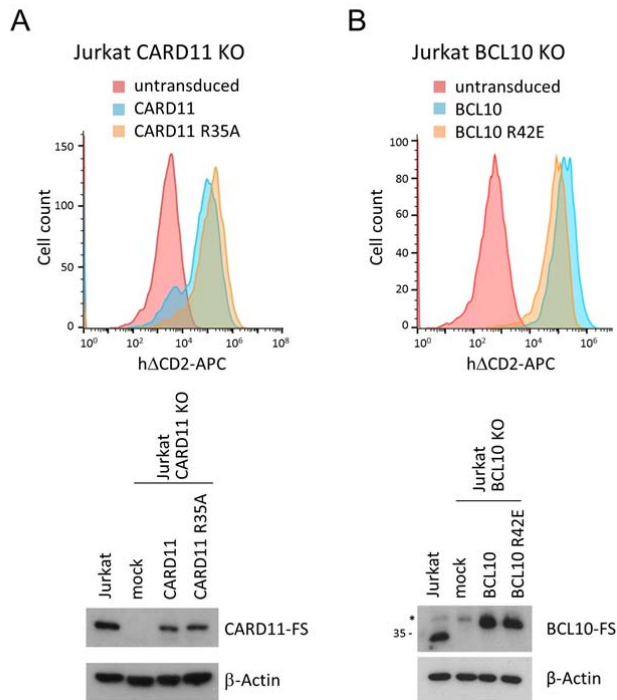
Electrostatic surface potential of the BCL10 filament calculated with APBS and shown from two

opposite views. The bottom of the BCL10 filament is mainly negatively charged (colored red), whereas the blue color of the top view indicates a positively charged surface. (C) Electrostatic surface potential of the CARD11 CARD domain seed model from top and bottom view, respectively. The surfaces indicate that the positively charged top of the CARD11 seed is charged complementary to the negatively charged bottom of the BCL10 filament.

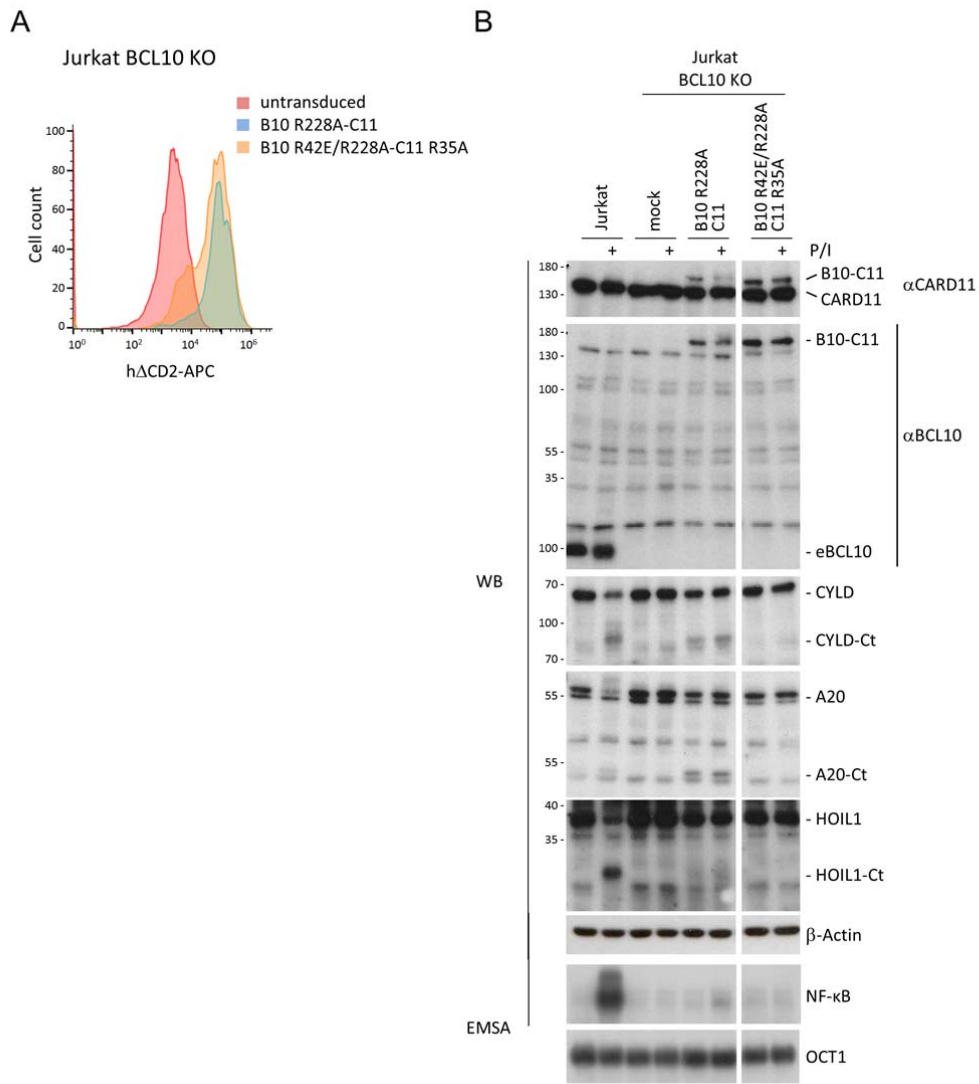


**Supplementary Figure 2: Generation, verification and signaling in *CARD11* and *BCL10* KO cells.** (A and B) Schematic of the Cas9/sgrNA-targeting sites in the *CARD11* gene (A) and *BCL10* gene (B). The sgrNA-targeting sequences are underlined and the protospacer-adjacent motif (PAM) is labeled in red. Induced double-strand breaks are marked with dotted lines. (C) Loss of *CARD11* expression and CBM-driven P/I stimulation, but not CBM-independent TNF stimulation, in two independent *CARD11* KO Jurkat T cell clones. Protein expression, I $\kappa$ B $\alpha$  degradation and phosphorylation of ERK were

analyzed by WB. NF- $\kappa$ B activation was determined by EMSA. (D) Loss of CARD11 expression and CBM-driven P/I stimulation in three independent CARD11 KO BJAB B cell clones. Protein expression, I $\kappa$ B $\alpha$  degradation and pERK were analyzed by WB. NF- $\kappa$ B activation was determined by EMSA. (E) Loss of BCL10 expression and CBM-driven P/I stimulation in a BCL10 KO Jurkat T cell clone. Protein expression and I $\kappa$ B $\alpha$  degradation was analyzed by WB. NF- $\kappa$ B activation was determined by EMSA.



**Supplementary Figure 3: Reconstitution of CARD11 and BCL10 KO Jurkat T cells.** (A) Transduction of CARD11 KO Jurkat T cells with mock, CARD11 WT and CARD11 R35A expressing lentiviruses was analyzed by FACS (ΔCD2 surface marker) and protein expression by WB compared to parental Jurkat T cells. (B) Transduction of BCL10 KO Jurkat T cells with mock, BCL10 WT and BCL10 R42E expressing lentiviruses was analyzed as in A. The asterisk marks an unspecific band in the BCL10 WB.



**Supplementary Figure 4: Reconstitution of BCL10 KO Jurkat T cells with BCL10-CARD11 fusion proteins.** (A) Transduction efficiency of BCL10 KO Jurkat T cells with BCL10-CARD11 (B10-C11) constructs determined by FACS using the surface marker  $\Delta$ CD2. (B) Protein expression of the B10-C11 fusion constructs in BCL10 KO Jurkat T cells, cleavage of MALT1 substrates (CYLD, HOIL1, A20) and NF- $\kappa$ B activity (EMSA) was compared to mock and parental Jurkat T cells with or without P/I stimulation for 30 minutes.

## 5.2 Publication II

Florian Schlauderer\*, **Thomas Seeholzer\***, Ambroise Desfosses\*, Torben Gehring, Mike Strauss, Karl-Peter Hopfner, Irina Gutsche, Daniel Krappmann & Katja Lammens (2018). \* equal contribution

Molecular architecture and regulation of BCL10-MALT1 filaments.

Nat Commun. 2018 Oct 2;9(1):4041. doi: 10.1038/s41467-018-06573-8.

ARTICLE

DOI: 10.1038/s41467-018-06573-8

OPEN

# Molecular architecture and regulation of BCL10-MALT1 filaments

Florian Schlauderer<sup>1</sup>, Thomas Seeholzer<sup>2</sup>, Ambroise Desfosses<sup>3</sup>, Torben Gehring<sup>2</sup>, Mike Strauss <sup>4</sup>, Karl-Peter Hopfner <sup>1</sup>, Irina Gutsche<sup>3</sup>, Daniel Krappmann<sup>2</sup> & Katja Lammens<sup>1</sup>

The CARD11-BCL10-MALT1 (CBM) complex triggers the adaptive immune response in lymphocytes and lymphoma cells. CARD11/CARMA1 acts as a molecular seed inducing BCL10 filaments, but the integration of MALT1 and the assembly of a functional CBM complex has remained elusive. Using cryo-EM we solved the helical structure of the BCL10-MALT1 filament. The structural model of the filament core solved at 4.9 Å resolution identified the interface between the N-terminal MALT1 DD and the BCL10 caspase recruitment domain. The C-terminal MALT1 Ig and paracaspase domains protrude from this core to orchestrate binding of mediators and substrates at the filament periphery. Mutagenesis studies support the importance of the identified BCL10-MALT1 interface for CBM complex assembly, MALT1 protease activation and NF-κB signaling in Jurkat and primary CD4 T-cells. Collectively, we present a model for the assembly and architecture of the CBM signaling complex and how it functions as a signaling hub in T-lymphocytes.

<sup>1</sup>Gene Center, Ludwig-Maximilians University, Feodor-Lynen-Str. 25, 81377 München, Germany. <sup>2</sup>Research Unit Cellular Signal Integration, Institute of Molecular Toxicology and Pharmacology, Helmholtz-Zentrum München - German Research Center for Environmental Health, Ingolstaedter Landstrasse 1, 85764 Neuherberg, Germany. <sup>3</sup>University Grenoble Alpes, CNRS, CEA, Institut de Biologie Structurale IBS, F-38044 Grenoble, France. <sup>4</sup>Department of Anatomy and Cell Biology, McGill University, Montreal, Canada H3A 0C7. These authors contributed equally: Florian Schlauderer, Thomas Seeholzer, Ambroise Desfosses. Correspondence and requests for materials should be addressed to I.G. (email: [irina.gutsche@ibs.fr](mailto:irina.gutsche@ibs.fr)) or to D.K. (email: [daniel.krappmann@helmholtz-muenchen.de](mailto:daniel.krappmann@helmholtz-muenchen.de)) or to K.L. (email: [klammens@genzentrum.lmu.de](mailto:klammens@genzentrum.lmu.de))

The immune stimulation of B-cell and T-cell receptors (TCR and BCR), as well as activating natural killer cell and fungal recognition receptors triggers activation of distinct Caspase recruitment domain (CARD)-containing scaffold proteins, including CARD9, CARD10 (also known as CARMA3), CARD11 (CARMA1), and CARD14 (CARMA2)<sup>1,2</sup>. CARD11, B cell lymphoma 10 (BCL10) and mucosa-associated lymphoid tissue lymphoma translocation protein 1 (MALT1) assemble the CARD11-BCL10-MALT1 (CBM) complex that bridges TCR/BCR proximal signaling to the canonical I $\kappa$ B kinase (IKK)/NF- $\kappa$ B and JNK pathway in lymphocytes<sup>3</sup>. Upon assembly, the CBM complex serves as a scaffolding platform that activates downstream signaling events via association of mediators such as ubiquitin ligases (e.g., TRAF6) and protein kinases (e.g., TAK1 and IKK $\beta$ )<sup>4–6</sup>. Upon activation, IKK $\beta$  phosphorylates I $\kappa$ B $\alpha$  leading to its proteasomal degradation and subsequent release, nuclear translocation and transcriptional activation of NF- $\kappa$ B<sup>7</sup>. Beyond the scaffolding function, MALT1 is a paracaspase and contributes proteolytic activity to the CBM complex, which is key for optimal lymphocyte activation and differentiation<sup>8–10</sup>. Altogether, CBM complex downstream pathways play important roles in regulating the activation, proliferation, and effector functions of lymphocytes in adaptive immunity<sup>11</sup>.

The pathological relevance of CARD11, BCL10, and MALT1 is demonstrated by germline loss-of-function mutations associated with combined immunodeficiency (CID)<sup>12–17</sup>. In contrast, activating mutations in CARD11 promote B-cell proliferation and are frequently found in the malignant activated B-cell-subtype of diffuse large B-cell lymphoma (ABC DLBCL)<sup>18–20</sup>. Furthermore, chromosomal translocations leading to overexpression of BCL10 or MALT1 as well as generation of the API2-MALT1 fusion protein result in oncogenic activation associated with MALT lymphoma<sup>21–23</sup>. The clinical impact of the CBM signalosome has been emphasized by the discovery of MALT1 protease inhibitors that suppress antigen responses in T-cells and kill ABC DLBCL cells that arise from chronic BCR signaling<sup>24–26</sup>.

In resting T-cells CARD11 is kept in an inactive conformation that is activated through phosphorylation by protein kinases including PKC $\theta$  and PKC $\beta$ <sup>27,28</sup>. In the hyper-phosphorylated conformation BCL10-MALT1 complexes are recruited via heterotypic interaction of the CARD11 and BCL10 CARD domains<sup>29,30</sup>. CARD11 acts as a molecular seed that upon binding induces the assembly of BCL10 filaments *in vitro* and in cells<sup>31,32</sup>. While the cryo-EM structure of the BCL10 filaments has been recently determined<sup>31</sup>, no structural information is available for the integration of MALT1 into the BCL10 filaments. MALT1 constitutively associates with BCL10 *in vitro* and in cells. Mutational analyses suggested that regions in the C-terminal Ser/Thr-rich region of BCL10 interact with the N-terminal death domain (DD) and the two Ig (immunoglobulin)-like domains (Ig1/Ig2) of MALT1<sup>33–36</sup>. Nevertheless, the detailed nature of the BCL10-MALT1 interface remains unresolved.

To gain further insight into the CBM complex assembly we determined the cryo-EM structure of the BCL10-MALT1 complex. Our data define the exact interfaces for BCL10 oligomerization as well as the interaction of BCL10 CARD and MALT1 DD. Reconstitution assays of either KO Jurkat T-cells or murine CD4 T-cells from MALT1<sup>-/-</sup> mice highlight the significance of the interaction sites for CBM complex formation and activation of all CBM downstream signaling events.

## Results

**Cryo-EM structure of the BCL10-MALT1 filament.** To provide structural information about the interaction of BCL10 with MALT1 we performed cryo-electron microscopy (cryo-EM) of

the human BCL10 (full length)-MALT1 (T29-G722) complex (Fig. 1a). BCL10 and MALT1 were co-expressed in bacteria and formed a stoichiometric complex that was purified to near homogeneity (Supplementary Fig. 1a). A cleavable GST-fusion at the N-terminus of BCL10 prevented filament assembly during purification and proteolytic removal of the GST-tag initiated oligomerization to a particle size of ~100 nm as determined by dynamic light scattering (DLS) (Supplementary Fig. 1b). An *in vitro* MALT1 cleavage assay revealed that the BCL10-MALT1 complex possesses protease activity (Supplementary Fig. 1c). Visual inspection of cryo-EM images of the purified complex, underpinned by 2D classification and examination of the power spectra, revealed that BCL10-MALT1 assembles into flexible helical filaments of ~29 nm in diameter, with an ordered inner core of ~14 nm in diameter and a less defined periphery (Fig. 1b–d). To calculate the high-resolution structure of the filament interior, the data were processed while limiting the diameter to 21 nm. This analysis was performed on the very first image frames 2–7 (total dose 14 electrons/Å<sup>2</sup>) to avoid sample and image quality deterioration due to radiation damage. This resulted in a 4.9 Å resolution map of BCL10 CARDs tightly decorated by MALT1 DD (Fig. 1e–g).

Our analysis revealed that BCL10-MALT1 is a left-handed helix with a per subunit rotation of 100.8° and a rise of 5.083 Å, resulting in 3.571 subunits of BCL10-MALT1 per helical turn. This helical arrangement agrees with the one observed for the BCL10 (residue 1–115) filament alone, thus indicating that the overall arrangement of the BCL10 CARD core is largely unaltered within the BCL10-MALT1 complex structure (Fig. 2a–f)<sup>31,32</sup>. The 4.9 Å resolution map of the inner filament part enabled us to build a pseudo atomic model of BCL10 residues 10–115 and MALT1 residues (30–121) by flexible fitting of a BCL10 homology model and a related crystal structure of MALT1 DD into the EM density (Fig. 1h, i). Interestingly, the structural comparison with the MALT1 DD X-ray structure (pdb ID: 2G7R) reveals that in the presented EM density helix  $\alpha_6$  is kinked and not forming an extended helix as previously proposed<sup>37</sup>. The observed fold of the kinked MALT1 helix is similar to other CARD family members (Fig. 1i).

## BCL10 filament assembly is critical for CARD11 recruitment.

The BCL10 CARD structure is considerably stabilized in comparison to the NMR structure due to the extensive network of interactions within the BCL10-MALT1 filament assembly (Fig. 2). To obtain a clearer perception of potential rearrangements of BCL10 upon interaction with MALT1, we compared the model of the BCL10 filaments alone, with our model of BCL10 in the BCL10-MALT1 complex<sup>31</sup>. Thereby, we found differences specifically in the amino acid registry that led to altered assignments of key residues involved in BCL10-MALT1 interaction (Supplementary Fig. 2a). Based on the refinement statistics and the FSC (Fourier Shell Correlation) curves assessing the fit between the maps and the models, our model is consistent with both our and the published EM densities<sup>31</sup> and provides reasonable stereochemistry and geometry values (Supplementary Fig. 2b).

The identified BCL10 CARD-CARD interfaces, type I, II, and III as diagrammed in Fig. 2a–f have been previously reported and are shown here to illustrate the composition of the BCL10 core filament<sup>31</sup>. The individual residues involved in the three types of interactions, in the presented structure are highlighted in Fig. 2d–f. Whereas type I and type II interactions are interstrand contacts between the helical turns (Fig. 2c–e), the type III interface exhibits interactions in the helical-strand direction (Fig. 2f). All interfaces identified by the BCL10 filament alone are

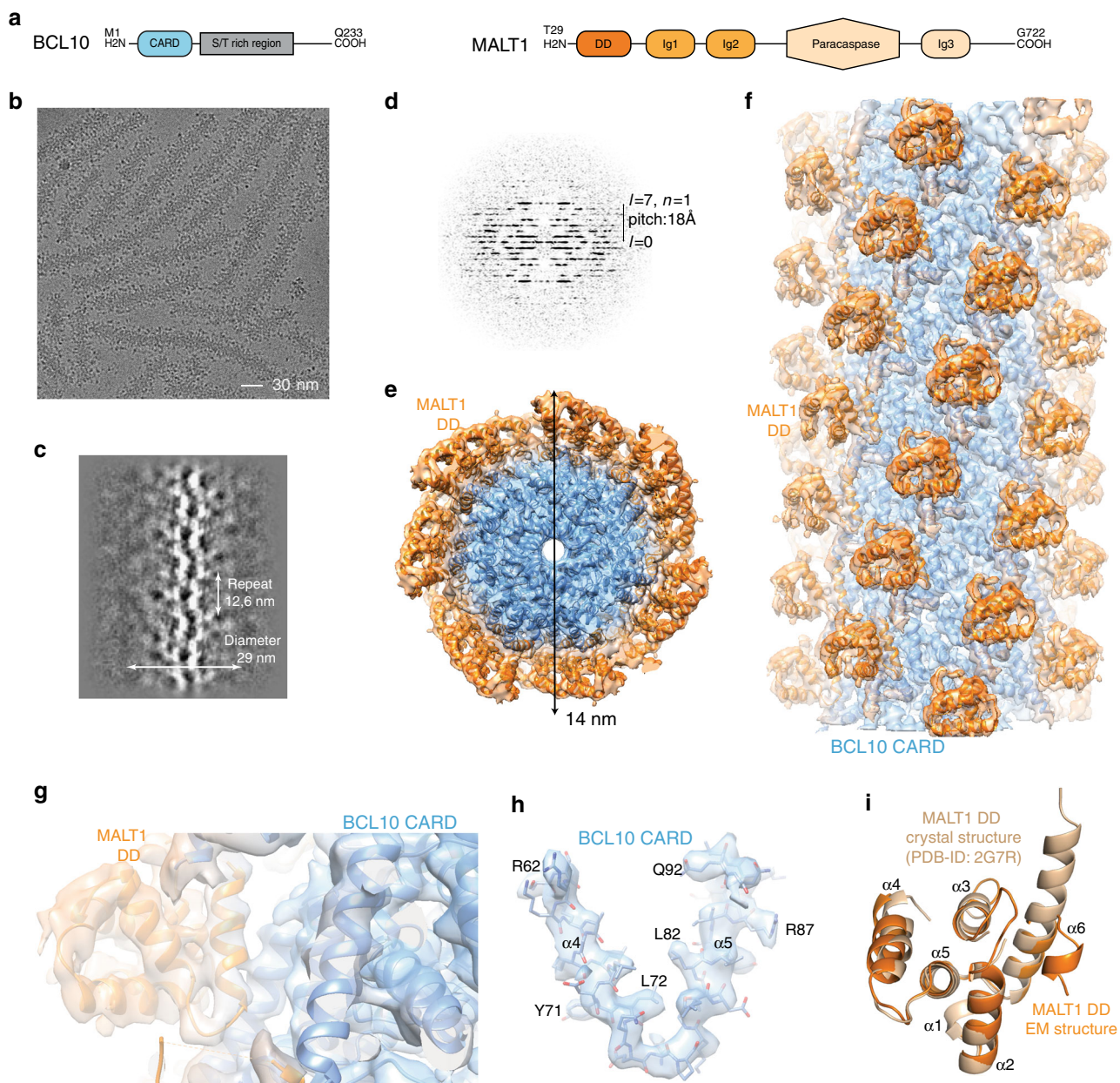


**Fig. 1** Cryo-EM reconstruction and atomic model of the BCL10-MALT1 filament. **a** Domain organization of the BCL10 and MALT1 protein constructs. **b** Example cryo-EM micrograph of the BCL10-MALT1 complex filaments. **c, d** 2D class averages and corresponding power spectra of BCL10-MALT1 filaments used for helical parameter determination. **e, f** Overall architecture of the BCL10-MALT1 filament assembly shown together with the cryo-EM density, clipped top and side view, respectively. The map shows the inner well-structured part of the filament at an overall resolution of 4.9 Å (FSC curve see Supplementary Fig. 8a). This part consists of the BCL10 CARD (residues 10–115) and the MALT1 DD (residues 30–121) colored blue and orange, respectively. **g, h** Example parts of the cryo-EM density map shown together with the BCL10-MALT1 DD and the atomic model of BCL10 shown in ribbon and stick representation, respectively. **i** Overlay of the MALT1 DD cryo-EM and crystal structure (pdb ID: 2g7r) colored orange and beige, respectively

largely conserved within the BCL10-MALT1 complex within the resolution limit of both structures<sup>31,32</sup> (Fig. 2d–f). Thereby, the type I interface comprises the most extensive interactions, with high electrostatic surface complementarity (Fig. 2d). Additionally, we identified residue R42 in interface I and R36 in interface II to be important for BCL10 filament assembly (Fig. 2d, e). To validate the importance of the interfaces we generated site-directed mutants and compared their capability to oligomerize in vitro with those of the wild-type complex. The BCL10 mutations R42E, R49E, and R36E abrogated the ability of the BCL10-MALT1 complex to oligomerize, while the interaction with MALT1 was retained as shown by DLS and co-purification,

respectively (Supplementary Fig. 2c, d). This emphasizes the relevance of the identified interaction regions for filament assembly but not MALT1 interaction.

Previously, the effect of BCL10 interface I-III mutants on NF- $\kappa$ B and MALT1 activation was analyzed upon overexpression<sup>32</sup>. Since filament assembly with recombinant purified BCL10-MALT1 is strongly influenced by local protein concentration, we aimed to investigate the biological effects of BCL10 oligomerization mutants in a clean genetic setting without overexpression or perturbation by endogenous BCL10. To this end we generated BCL10 KO Jurkat T-cells by CRISPR/Cas9 technology using sgRNA targeting Exon1 of human *BCL10*

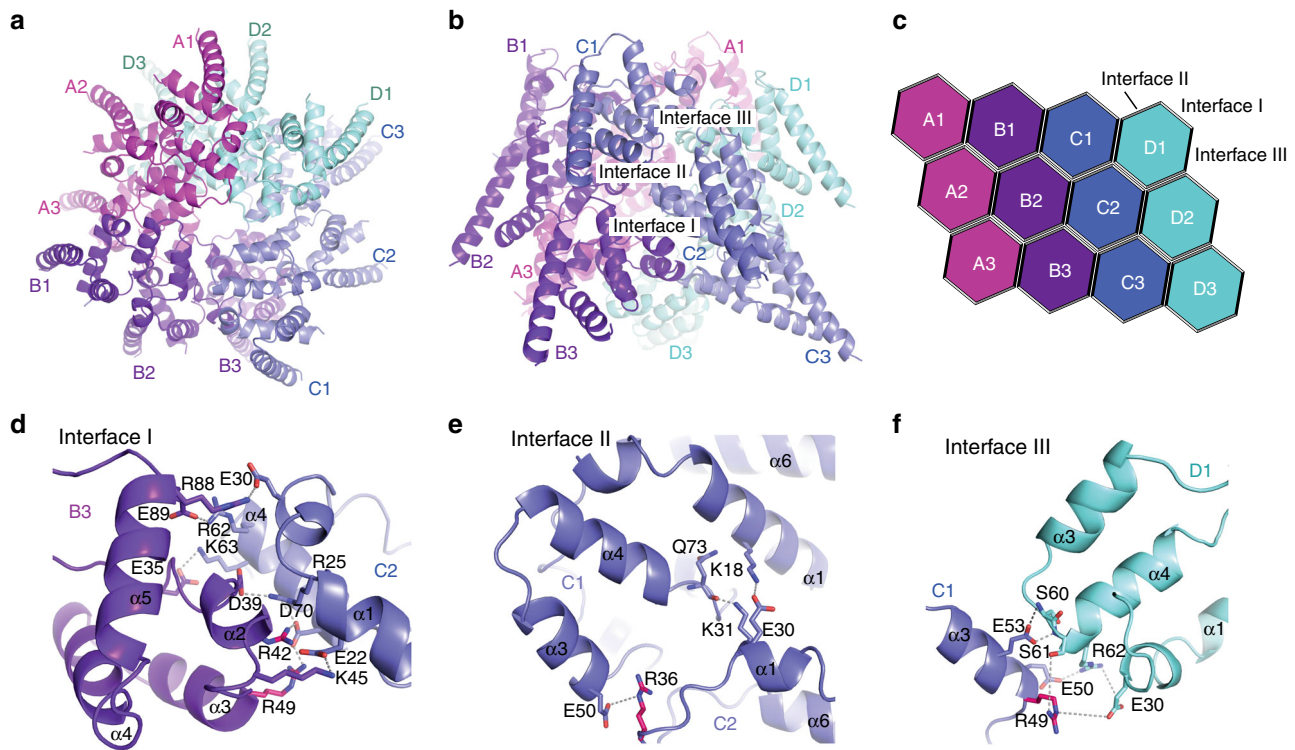


**Fig. 2** Core structure of the BCL10 CARD filament. **a, b** Top and side view of the BCL10 protein model obtained by interpretation of the BCL10-MALT1 complex cryo-EM density. **c** Schematic diagram of the BCL10 helical assembly. Each CARD is represented as a hexagon and the three interfaces are indicated accordingly. **d, f** Detailed view of the three BCL10 interaction surfaces I (**d**), II (**e**), and III (**f**). Interacting residues are shown in stick representation. Sites mutated R42, R36 are highlighted in magenta

(Supplementary Fig. 3a). After limiting dilution, we obtained a BCL10 KO Jurkat T-cell clone, which was reconstituted with BCL10 wt or the BCL10 interface I (R42E) and II (R36E) mutants, which lost the ability to assemble filaments *in vitro*. To exclude that the cellular effects are due to overall conformational alterations in the BCL10 CARD, by changing positively charged arginines to negatively charged glutamic acids, we included the less severe BCL10 R42A substitution (Fig. 3b). Lentiviral infection led to homogenous transduction of Jurkat T-cells as judged by co-expressed surface marker  $\Delta$ CD2 and equivalent expression of all constructs close to endogenous levels in the BCL10 KO cells (Supplementary Fig. 3b–e). Precipitation of BCL10 either by co-IP or StrepTactin pull-down (ST-PD) demonstrated that the mutation in the BCL10 filament interfaces I and II prevented the PMA/Ionomycin (P/I) inducible recruitment of BCL10 to CARD11 and thus stimulus-dependent CBM complex formation (Fig. 3a, b). However, none of the mutants impaired constitutive binding of BCL10 to MALT1, suggesting that the overall protein structure is still intact.

To determine the functional relevance of the BCL10–BCL10 interfaces for T-cell signaling, we stimulated the Jurkat T-cells expressing the distinct BCL10 mutants and analyzed NF- $\kappa$ B signaling and MALT1 protease activation (Fig. 3c, d). Indeed, interface I mutations BCL10 R42E or R42A and interface II mutation R36E completely abolished I $\kappa$ B $\alpha$  phosphorylation and degradation as well as NF- $\kappa$ B DNA binding after P/I stimulation. Likewise, activation of the MALT1 protease was absent in all BCL10 filament mutants as determined by the ability to cleave the substrates BCL10, CYLD, and HOIL1 (Fig. 3c, d). Hence, under physiological conditions the correct assembly of the BCL10 core filament via its CARDS is crucial for stimulus-dependent CARD11 recruitment and thus CBM complex assembly and downstream functions.

**MALT1 binds to BCL10 via DD and CARD interaction.** Besides unravelling the architecture of the BCL10 CARD filaments, the 4.9 Å resolution cryo-EM map provides the detailed molecular structure of the BCL10-MALT1 interaction surface (Fig. 4a–c). The MALT1 DD interacts with BCL10 at the rim of the CARD core filament in a 1:1 stoichiometry. Thereby, the C-termini of MALT1 DD domains are pointing away from the core filament. A close-up view of the BCL10-MALT1 interaction site I (BM-I) illustrates that MALT1 binds to the C-terminal part (BCL10 helix  $\alpha$ 6) of the BCL10 CARD forming a new interface that is distinct from the BCL10 filament interfaces I–III (Fig. 4a–c). Thus, the structure underscores that BCL10 filament assembly is not required for MALT1 association, which agrees with the cellular pre-assembly of the BCL10-MALT1 complex without stimulation (see Fig. 3a, b). In BM-I, the two most central interacting residues of MALT1 are V81 and L82 situated in helix  $\alpha$ 4 (Fig. 4c). The opposing hydrophobic surface in BCL10 is formed by L104, V103 in helix  $\alpha$ 6 and V83 and I96 in helices  $\alpha$ 5 and  $\alpha$ 6, respectively. Several salt bridges stabilize the hydrophobic core contacts (Fig. 4c).

To investigate the significance of the identified BM-I, we mutated residues on both sides of the interface. Co-purification of GST-BCL10 demonstrates a severely reduced binding of MALT1 V81R mutant *in vitro* (Supplementary Fig. 4a). In line, the single mutation V81R completely disrupted the interaction of BCL10 after co-expression in HEK293 (Fig. 4d). Vice versa, BCL10 L104R abolished association of MALT1 to BCL10 (Fig. 4d). Further, the cryo-EM structure indicated a potential second interface between MALT1 DD  $\alpha$ 4 and  $\alpha$ 5 segment and the adjacent BCL10 helix  $\alpha$ 6 at the C-terminus of the core CARD filament (BM-II; Supplementary Fig. 4b, c). However, mutation of potential contact points Q76A/E98R as well as the putative disulfide bond C77–C91 (C77A) in MALT1 did not affect BCL10–

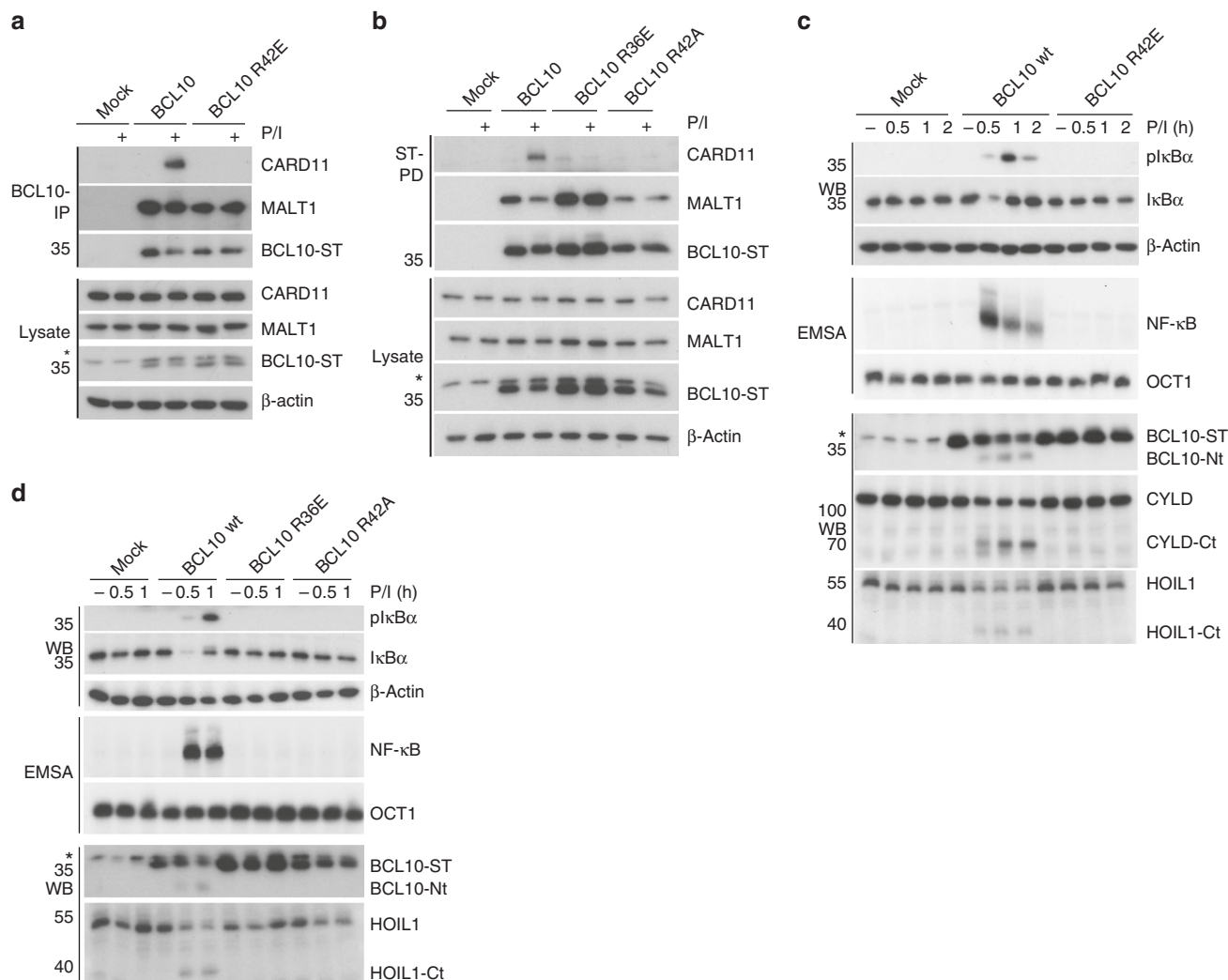


**Fig. 3** Functional analyses of BCL10-BCL10 interfaces in Jurkat T-cells. **a, b** BCL10 KO Jurkat T-cells lentivirally reconstituted with BCL10 wt, R42E, R36E or R42A constructs were stimulated P/I for 20 min and CBM complex formation was monitored by BCL10-IP (**a**) and Strep-tag II (ST) pull down (PD) (**b**). **c, d** BCL10 KO Jurkat T-cells reconstituted with BCL10 wt or BCL10-BCL10 interface mutants were stimulated with P/I for the times indicated. NF- $\kappa$ B activation was determined by I $\kappa$ B $\alpha$  WB and EMSA. Activation of the MALT1 protease was monitored by WB analyses of the substrate cleavage. Asterisks indicate non-specific cross-reactivity of the BCL10 antibody

MALT1 association in co-IPs (Supplementary Fig. 4d), suggesting that BM-II is not essential for BCL10-MALT1 complex formation.

#### CBM assembly and T-cell activation relies on MALT1 binding.

To assess the biological impact of the newly identified BCL10-MALT1 interaction surfaces, we expressed BM-I mutants located on both sides of the interface in BCL10 or MALT1 KO T-cells, respectively (Fig. 5). MALT1 KO Jurkat T-cells were generated by CRISPR/Cas9 technology<sup>38</sup>. In BCL10 we used the single mutation L104R in helix  $\alpha$ 6 of the CARD. In MALT1 we analyzed mutation V81R or L82D in  $\alpha$ 4 of the DD opposite to the BCL10  $\alpha$ 6 helix. Using lentiviral transduction, we obtained Jurkat T-cells that expressed all BCL10 or MALT1 constructs homogeneously at endogenous levels (Supplementary Fig. 5a-f). Indeed, BCL10 co-IP experiments revealed that missense mutation either in BCL10 (L104R) or MALT1 (V81R or L82D) completely abrogate the constitutive binding of BCL10 to MALT1 in resting Jurkat T-cells (Fig. 5a-c). For BCL10 L104R and MALT1 V81R, loss of interaction was also confirmed by ST-PD of BCL10 or MALT1, respectively (Supplementary Fig. 5g-h). Moreover, loss of MALT1

led to a severely reduced BCL10 recruitment to CARD11 after P/I stimulation (Fig. 5b, c). In all BCL10 and MALT1 interface mutants the binding of BCL10 to CARD11 was impaired, providing evidence that the constitutive association of BCL10 and MALT1 is a prerequisite for CBM complex assembly (Fig. 5a-c). Thus, in T-cells the BCL10-MALT1 interaction significantly contributes to the dynamics of CBM complex formation strengthening the importance of interface BM-I.

To determine the functional relevance of the BCL10-MALT1 interface for T-cell signaling and MALT1 activation, we stimulated the Jurkat T-cells expressing the MALT1 and BCL10 BM-I mutants (Fig. 5d-h). In line with its critical role for assembly of the entire CBM complex, I $\kappa$ B $\alpha$  phosphorylation/degradation and NF- $\kappa$ B DNA binding after T-cell stimulation were abolished. Also, activation of the MALT1 protease was absent in the BCL10 L104R (Fig. 5d, e) as well as MALT1 V81R (Fig. 5f, g) or MALT1 L82D (Fig. 5h) mutants, as evident from the lack of substrate cleavage. In contrast, BM-II mutations Q76A/E98R and C77A, which did not significantly impair BCL10-MALT1 association, did not alter NF- $\kappa$ B responses (Supplementary Fig. 4d and 5i). To address the importance of

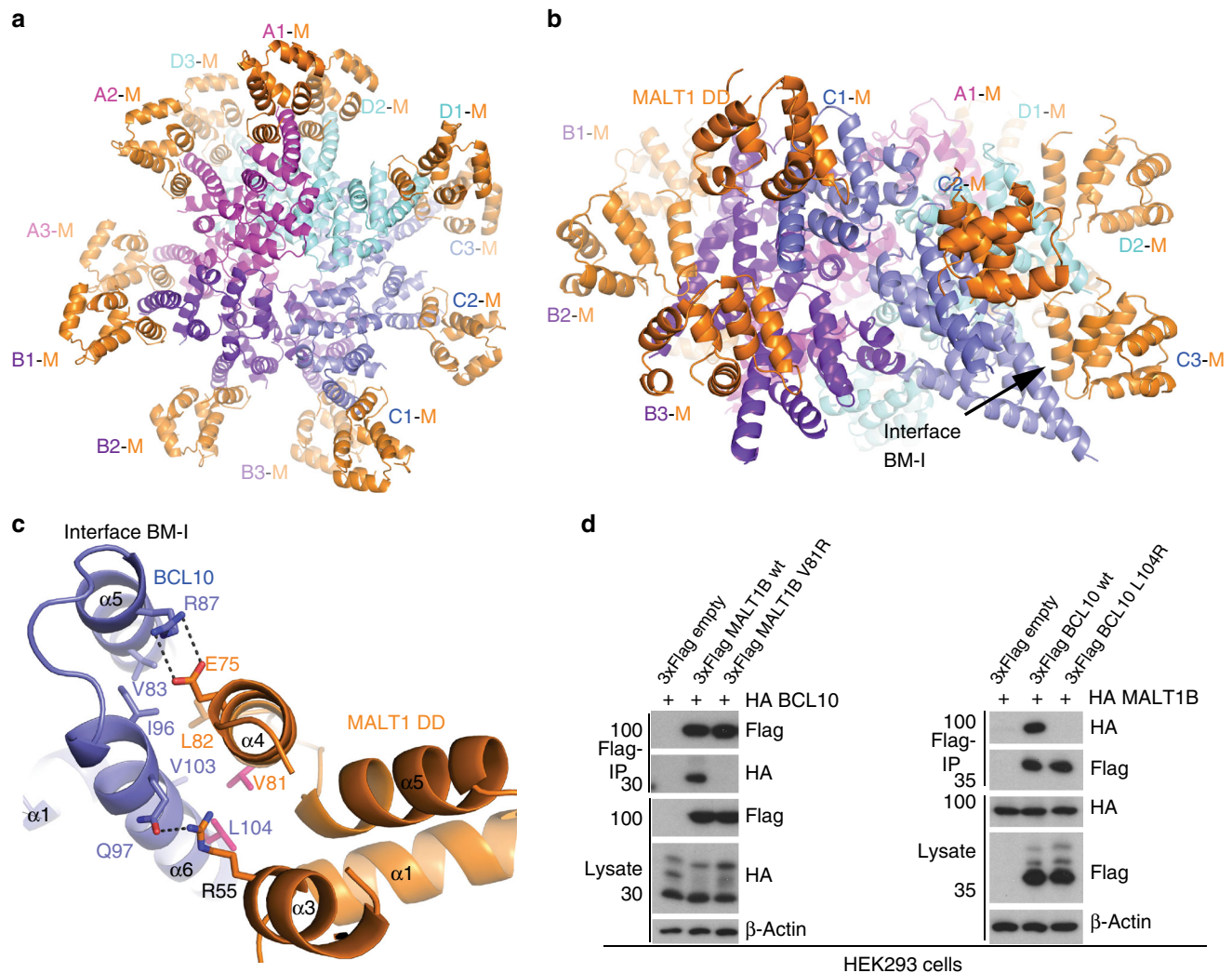
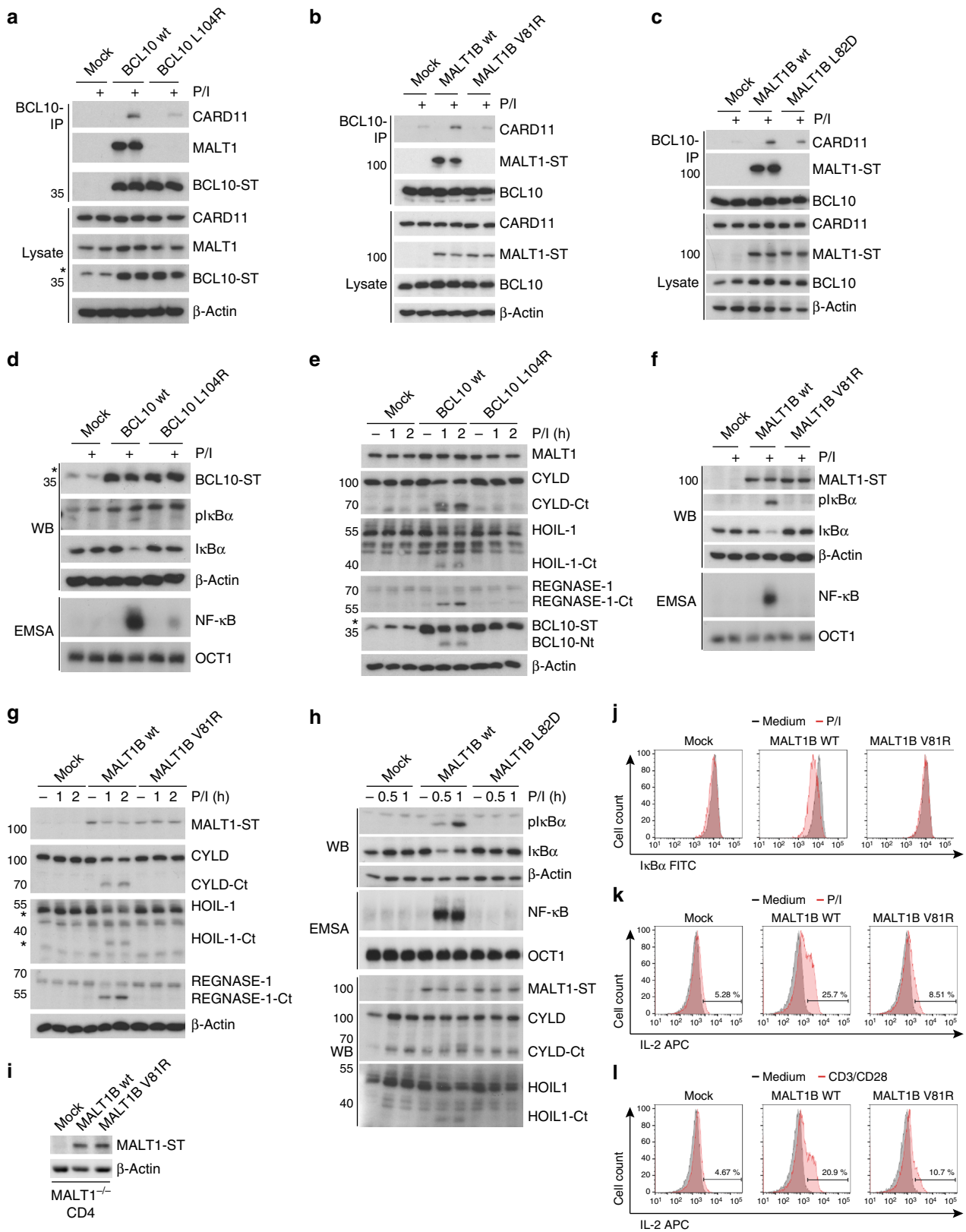


**Fig. 4** Architecture of the BCL10-MALT1 interface. **a, b** Top and side view of one repeat of the BCL10-MALT1 holo-complex as visible in the cryo-EM density. Position of BCL10-MALT1 interface BM-I is indicated in **(b)**. **c** Close up view of the BCL10 and MALT1 interaction site I (BM-I) shown as ribbon model in blue and orange, respectively. The interacting residues are shown in stick representation. Mutations introduced are colored magenta. **d** HEK293 cells were co-transfected with tagged MALT1B and BCL10 wt and mutant constructs as indicated. Co-IP was carried out using anti-Flag antibodies and analyzed by WB for co-precipitation

the BCL10-MALT1 interface BM-I for T-cell activation in a physiological setting, we purified CD4 T-cells from MALT1<sup>-/-</sup> mice and reconstituted the cells with either MALT1 wt or the MALT1 BM-I mutant V81R. Effects on NF- $\kappa$ B signaling and IL-2 production after MALT1 reconstitution were determined by single cell FACS analyses. Retroviral transduction led to equal expression of MALT1 wt and the mutant construct V81R in primary T-cells (Fig. 5i). Infected cells were identified by the surface marker Thy1.1 (Supplementary Fig. 6a-b). As expected, I $\kappa$ B $\alpha$  was not degraded and IL-2 was not significantly induced in Thy1.1-negative MALT1<sup>-/-</sup> T-cells (Supplementary Fig. 6a-b). When gated on the transduced Thy1.1-positive CD4 T-cells population, MALT1 wt but not BM-I interface mutant V81R was able to rescue NF- $\kappa$ B signaling after P/I stimulation as evident from I $\kappa$ B $\alpha$  degradation (Fig. 5j). Further, strong upregulation of IL-2 in response to P/I stimulation or anti-CD3/CD28 co-ligation in CD4 T-cells was impaired in the MALT1 V81R mutant expressing cells as determined by intracellular FACS staining (Fig. 5k, l). Thus, the identified BCL10-MALT1 interface I is essential for bridging TCR stimulation to downstream signaling and T-cell activation.

**Architecture of the BCL10-MALT1 holo-complex.** To gain more information about the structural organisation of the additional MALT1 domains (Ig1-Ig2-paracaspase-Ig3) around the BCL10-MALT1 DD skeleton, the cryo EM data have been analysed by a second approach. The diameter constraints have been relieved to 29 nm and the dose increased to 32 electrons/ $\text{\AA}^2$  (frames 2–16) which yielded an overall 5.9  $\text{\AA}$ , but highly anisotropic resolution reconstruction of the entire BCL10-MALT1 complex domains (Fig. 6 and Supplementary Fig. 8). In the density filtered to 6  $\text{\AA}$  the MALT1 DDs are rigidly attached to the BCL10 core (Fig. 6a, b). The EM density filtered to 8  $\text{\AA}$  depicts that the subsequent MALT1 domain Ig1 is clearly visible and we were able to rigid body dock this domain. The Ig1 domain is pointing away from the BCL10-MALT1 DD core filament separating the C-terminal domains from the inner core of the filament (Fig. 6c, d). Together with the flexible linked Ig2 domain this arrangement supposedly allows for dimerization of the MALT1 paracaspase domains, which is key for MALT1 protease activation<sup>39</sup>. Further, the map with a resolution cut-off at 25  $\text{\AA}$  indicates how a stable inner core formed by BCL10 CARD and the MALT1 DD-Ig1 fragments orchestrates a flexible outer



MALT1 platform (Fig. 6e, f). The top view illustrates a ‘paddle wheel-like’ architecture of the BCL10-MALT1 complex with the MALT1 Ig1-Ig2-paracaspase domains forming the more adaptable periphery of the filament (Fig. 6f). Due to the flexibility of the C-terminal MALT1 domains, we could not provide an unambiguous fit of the MALT1 Ig2-paracaspase-Ig3 domains.

### Discussion

Our cryo-EM structure resolved the inner core of the BCL10-MALT1 assembly at 4.9 Å resolution. We identified the BCL10 CARD and MALT1 DD interface BM-I and cell-based assays provide compelling proof that the filaments channel all CBM downstream signaling events. Since the peripheral C-terminal

**Fig. 5** Functional analyses of the MALT1-BCL10 interface in Jurkat and murine CD4 T-Cells. **a** BCL10 KO Jurkat T-cells were lentivirally reconstituted with BCL10 wt or BM-I mutant L104R constructs. After 20 min P/I stimulation CBM complex formation was investigated by BCL10-IP. Asterisk indicates non-specific cross-reactivity of the BCL10 antibody. **b, c** MALT1 KO Jurkat T-cells were lentivirally reconstituted with MALT1 wt or BM-I mutant constructs V81R (**b**) or L82D (**c**). P/I stimulation and CBM complex formation was investigated as in (a). **d-h** NF- $\kappa$ B signaling (**d, f, h**) and MALT1 protease activation (**e, g, h**) in BCL10 (**d, e**) or MALT1 (**f-h**) BM-I mutant reconstituted Jurkat T-cells after P/I treatment was analyzed by Western Blot ( $\kappa$ B $\alpha$  phosphorylation and degradation) and NF- $\kappa$ B-DNA binding studies (EMSA). Induction of MALT1 protease activity was monitored by cleavage of MALT1 substrates in WB as indicated. **i** Expression of MALT1 wt and BM-I mutant (V81R) was determined by WB after enrichment of infected murine MALT1<sup>-/-</sup> CD4 T-cells. **j** MALT1<sup>-/-</sup> CD4 T-cells transduced with MALT1 wt or BM-I mutant were stimulated for 30 min with P/I. I $\kappa$ B $\alpha$  expression and degradation were measured by FACS and transduced cells were gated by co-staining of Thy1.1 (Supplementary Fig. 6a). **k, l** MALT1<sup>-/-</sup> CD4 T-cells transduced as in (**j**) and stimulated for 5 h with P/I (**k**) or anti-CD3/CD28 (**l**). Intracellular IL-2 production was determined by FACS and transduced cells were gated by co-staining of Thy1.1 (Supplementary Fig. 6b)

regions of MALT1 and BCL10 are flexible, it is unlikely that other surfaces are directly contributing to BCL10 binding. This is remarkable, because previous co-IPs using overexpression suggested that BCL10-MALT1 may associate through a more extended binding surface. BCL10-MALT1 interaction was lost by a small deletion at the C-terminus of the CARD (aa 106–120), which overlaps the MALT1 binding surface that has been identified here by cryo-EM<sup>34</sup>. However, other deletions in the BCL10 C-terminus also impaired the tight association of BCL10 to MALT1<sup>36</sup>. Moreover, on the side of MALT1 it was shown that the DD as well as the Ig1/Ig2 domains are contributing to the BCL10 binding in cells<sup>33</sup>. Thus, we speculate that regions outside the direct BCL10-MALT1 interface are important for the conformation of the CARD and the DD and thus indirectly affect the interaction. In fact, the crystal structure of the MALT1 DD alone indicates that in the absence of the Ig1/Ig2 domains the  $\alpha$ 6 helix is not kinked, which could certainly prevent BCL10 from binding<sup>37</sup>.

Further, we found that MALT1 association to BCL10 is required for the stimulus-dependent recruitment of BCL10 to CARD11. *In vitro* CARD11 and BCL10 form complexes at high concentrations<sup>31,32</sup>. Under physiological conditions, however, only the MALT1-BCL10 complex adopts a conformation that allows efficient CARD11 association. Mechanistically, MALT1 may either facilitate a BCL10 conformation that promotes CARD11 binding or wrapping of BCL10 by MALT1 may stabilize otherwise labile BCL10 core filaments. Clearly, the cryo-EM structure reveals stoichiometric binding of BCL10 to MALT1 and that BCL10 oligomerization is not required for MALT1 association, which is in line with the constitutive pre-assembly of BCL10-MALT1 complexes in cells. Furthermore, BCL10 is decorated with ubiquitin chains and these BCL10 modifications have been suggested to activate downstream signaling partially bypassing the necessity for MALT1<sup>6,40</sup>. However, the absence of a CARD11-BCL10 binding in MALT1 deficient or BM-I mutant cells indicates that signaling competent CARD11-BCL10 sub-complexes do not exist and downstream effects are relying on MALT1 association.

The cellular analyses of structure-guided mutations in the BCL10 filament interfaces I and II highlight the necessity of filament assembly for CARD11 recruitment. Since none of these mutations affect MALT1 association, it is quite unlikely that they destroy the overall conformation of the BCL10 CARD or the interface to CARD11. In line with the modeled CARD11-BCL10 interactions<sup>32</sup>, we propose that the weak affinity of BCL10 monomers for CARD11 needs to be stabilized by BCL10 oligomerization, which augments the affinity by presenting multiple interfaces. In fact, the data implicate that recruitment of BCL10 to CARD11 and BCL10 oligomerization are highly interconnected processes that cannot be uncoupled. Thus, BCL10 oligomerization may boost an initial low affinity interaction leading to rapid CBM complex assembly and threshold responses after stimulation.

Furthermore, an interesting aspect regarding the BCL10-MALT1 core structure is, that BCL10 is degraded upon prolonged T-cell stimulation, leading to CBM complex disassembly and termination of TCR-signaling<sup>41,42</sup>. Proteasomal degradation requires unfolding of the proteins and thus the rigidity of BCL10 core filaments can explain why BCL10 is primarily removed through selective autophagy and lysosomal degradation<sup>41,43</sup>. However, despite the 1:1 stoichiometry of BCL10-MALT1 in the complex, MALT1 is stable and not degraded after stimulation<sup>43</sup>. At present it is unclear how MALT1 is disconnected from the BCL10 filaments. MALT1 auto-cleavage at R149 could certainly release the C-terminal fragment, but there is no evidence for the appearance of a stabilized DD-truncated form of MALT1 after stimulation<sup>44</sup>. The BCL10 C-terminus is most likely flexible and was not visible in the cryo-EM map, but interestingly hyperphosphorylation of BCL10 in this Ser/Thr-rich region impairs binding to MALT1<sup>36</sup>. Thus, post-translational modifications of BCL10 or MALT1 may be involved in the release of MALT1 to separate it from removal by autophagy.

Despite the lower resolution in the outer region of the 29 nm wide BCL10-MALT1 filaments, the cryo-EM map depicts how the C-terminal MALT1 domains are emanating from the BCL10-MALT1 DD core filament forming a ‘paddle wheel-like’ shape. In spite of the moderate resolution of the map of the outer regions in the BCL10-MALT1 complex, the current data allows us to provide a model in which MALT1 C-terminal region covering the Ig2-paracaspase-Ig3 domain is flexibly attached to the BCL10-MALT DD core filaments. The flexibility and positioning of the individual MALT1 molecules in the filament periphery provides a platform for the recruitment of mediators like TRAF6 to foster NF- $\kappa$ B signaling<sup>38</sup>. Further, mono-ubiquitination, substrate binding and paracaspase domain dimerization will promote protease activation<sup>39,45</sup>. Future studies must elucidate the mechanism of MALT1 protease activation in the complex and how the BCL10-MALT1 platform integrates factors like TRAF6, TAK1 and NEMO/IKK $\beta$  to initiate downstream processes.

## Methods

**Expression and purification.** Human MALT1 isoform B amino acids T29 to G722 and the V81R mutant of this construct were cloned by NdeI and NotI restriction sites into a modified pET28a vector (Novagen), containing a N-terminal PreScission Protease (GELifeSciences) cleavable 8  $\times$  -His-tag sequence (Supplementary Table 2). Human BCL10 wt and the respective R36E, R42E, R49E mutants were cloned into pGEX-6P-2 vector (GELifeSciences) using BamHI and XhoI restriction sites (Supplementary Table 3)<sup>36</sup>. The corresponding plasmids were co-transformed in *Escherichia coli* Rosetta™ (DE3) strain (Novagen), protein expression was induced by addition of 0.2 mM IPTG and performed overnight at 18 °C. Cells were resuspended in lysis buffer containing 50 mM Hepes pH = 7.5, 200 mM NaCl, 7 mM Imidazol and 4 mM  $\beta$ -mercaptoethanol. Cells were lysed by sonication and clarified by centrifugation. The BCL10-MALT1 complex was further purified by Ni-NTA affinity chromatography (Qiagen) using the lysis buffer containing 250 mM Imidazol as elution buffer. Subsequently, the NiNTA elution fraction was loaded on a Glutathion-sepharose column (GE-Healthcare) and eluted with lysis buffer containing 20 mM reduced Glutathion. Size exclusion chromatography

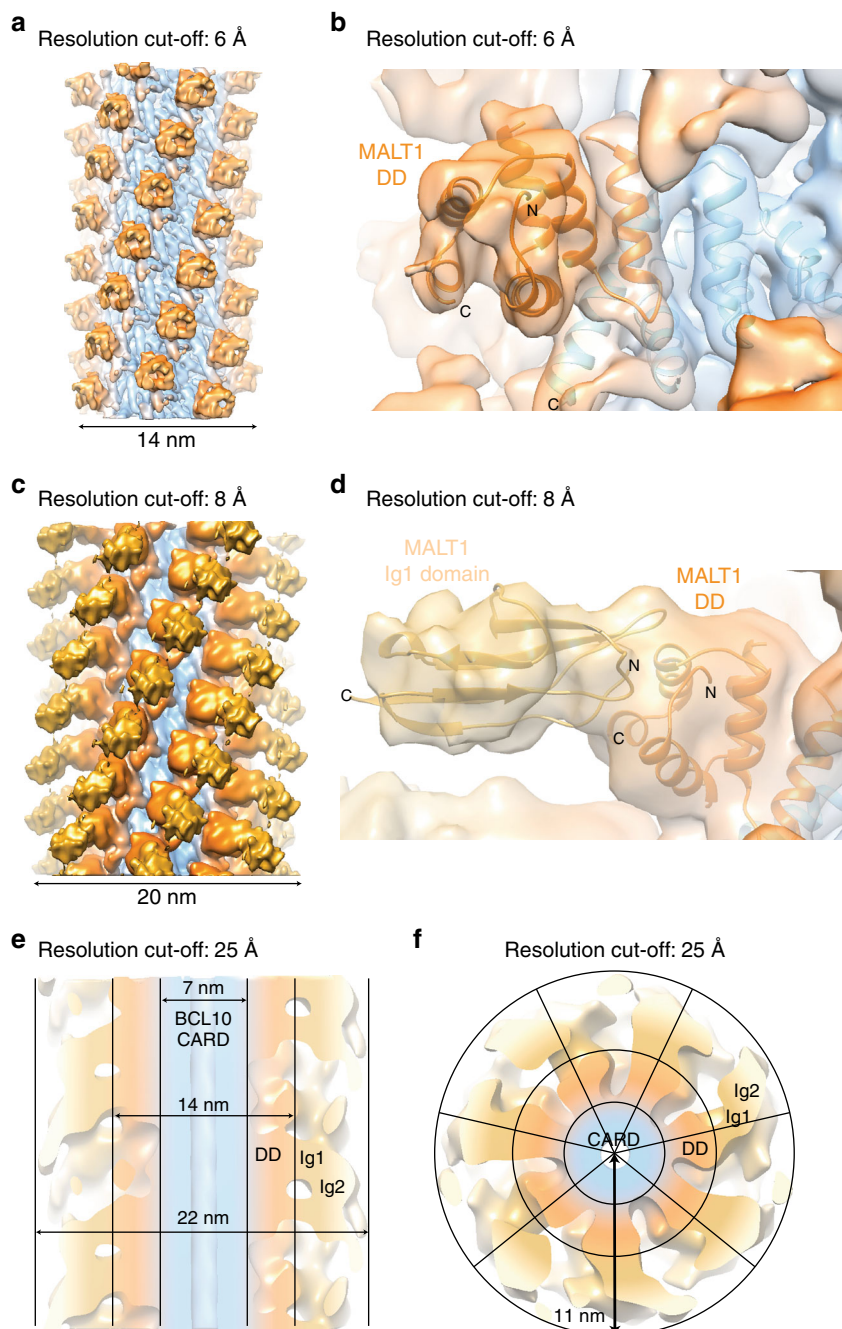


**Fig. 6** Structural organisation of additional MALT1 domains in framework of the BCL10-MALT1 filament. **a, b** EM density map of the well-ordered inner core of the BCL10-MALT1 filament shown together with the atomic model of BCL10 (blue) and MALT1 DD (orange) as built in the 4.9 Å density map (map sharpening B-factor applied:  $-200 \text{ \AA}^2$ ). **c, d** Reconstructed density map filtered to 8 Å indicates the orientation of the MALT1 Ig1 domain shown as ribbon and colored yellow (B-factor applied:  $-100 \text{ \AA}^2$ ). **e, f** Paddle-wheel like architecture of the BCL10-MALT1 filament revealed by the EM-density filtered to 25 Å (B-factor applied:  $0 \text{ \AA}^2$ )

(S200 26/60, GE-Healthcare) was performed to separate BCL10-MALT1 complex fractions. Size exclusion buffer contained 25 mM Hepes pH = 7.5, 200 mM NaCl and 2 mM  $\beta$ -mercaptoethanol.

**MALT1 activity assay.** The MALT1 cleavage assay was performed with 500 nM or 10  $\mu\text{M}$  of BCL10-MALT1 filaments, GST-BCL10-MALT1 species, and MALT1 V81R mutant. Protein samples were incubated in 384-well non-binding microplates and 20  $\mu\text{M}$  of the MALT1 substrate Ac-LRSR-AMC was added. After 2 min incubation at 30 °C, the fluorescence of cleaved AMC was measured over 1 h by a Synergy 2 Microplate Reader (Biotek, US). The MALT1 protease activity is represented in relative fluorescence units and data from at least three independent experiments were used.

**BCL10-MALT1 complex formation analysis.** The BCL10-MALT1 complex fractions were pooled and concentrated to 0.5  $\mu\text{M}$ . Filament formation was initialized by addition of PreScission protease (GE Healthcare) in equimolar amounts. Polymerization of BCL10-MALT1 species was monitored by dynamic light scattering (Viscotek 802 DLS) as a function of time over 100 min. Higher order species (above  $10^4 \text{ nm}$ ) were excluded from data evaluation. Data was analyzed by the OmniSIZE 3.0 software package (Viscotek).

**BCL10-MALT1 complex preparation for cryo electron microscopy.** BCL10-MALT1 complex fractions were concentrated stepwise to 1 mg/ml. Higher molecular species formation was monitored for each concentration step by dynamic light scattering (Viscotek 802 DLS). Filament formation was initialized by addition of equimolar amounts of PreScission Protease (GE Healthcare) and performed

overnight at 12 °C. Analytical size exclusion chromatography (S200 5/150 GL) was performed to separate BCL10-MALT1 filaments from non-oligomerized protein. Directly before blotting Octyl-beta-Glucoside was added to the selected size exclusion fraction with a final concentration of 0.001%. 4.5 µl of the BCL10-MALT1 sample was applied on glow-discharged R1/2 grids (Quantifoil Cu R1/2, 300 mesh). The grids were blotted for 3 s at 95 % humidity and 15 °C and plunge-frozen in liquid ethane using a Leica Plunger (FEI).

**Cryo electron microscopy data collection.** Cryo-EM images of the BCL10-MALT1 complex were collected on a 200 keV Talos Arctica microscope equipped with a Falcon III detector (FEI). In total 662 micrographs were collected automatically using the EPU software (FEI). Micrographs were acquired in nano-probe mode using 49 movie frames with a dose of ~2 electrons/Å<sup>2</sup>/frame resulting in a total dose of 98 electrons per Å<sup>2</sup> at a pixel size of 1.002 Å.

**Helical reconstruction.** In order to obtain both a higher resolution map of the core of the BCL10-MALT1 filaments, and a lower resolution map of the entire assembly, we performed two 3D refinements, varying the diameter limitation used during refinement, and the total dose used prior to particle extraction. For the higher resolution map, the frames 2 to 7 (total dose ~14 electrons/Å<sup>2</sup>) out of a total of 49 frames were motion-corrected and dose-weighted using MotionCor2<sup>46</sup>, while for the lower-resolution map, the frames 2 to 16 (total dose ~32 electrons/Å<sup>2</sup>) were processed. The low dose dataset was used to determine the helical symmetry and to obtain the map of the BCL10-MALT1DD filament core, while the higher dose dataset enabled to get information about the periphery of the filaments.

For both datasets, the defocus estimation was performed with CTFFIND/CTFTILT<sup>47</sup>. In total, 2618 straight sections of filaments were boxed manually using the e2heliboxer submodule of EMAN2<sup>48</sup> from a selected subset of 370 micrographs. The average length of picked BCL10-MALT1 filament sections was ~756 Å and the total length ~0.2 mm (Supplementary Table 1). All subsequent processing steps were performed in the helical reconstruction software package SPRING<sup>49</sup>. In total 25,576 segments were extracted using a segment size of 500 Å and segment step size of 30 Å. For 2D classification and initial symmetry estimation, phase-flipped, verticalized segments were extracted from the low dose dataset, whereas for symmetry refinement and 3D reconstruction, convolved, non-rotated segments were used. The sum of the power-spectra of all verticalized segments was calculated using Segmentexam module, confirming the helical nature of the specimen. Helical parameters were determined as follows. First, 40 class averages were obtained using k-means clustering algorithm from SPARX<sup>50</sup> as implemented in the Segmentclass module. Class averages showed a repetition of the projection pattern along the helical axis every ~126 Å, suggesting that this distance was a close estimate of the repeat *c*. The sum of the power spectra of 2D class averages padded in 1080\*1080 pixels boxes and showing the biggest number of layer lines (11 class-averages) was then calculated for symmetry estimation. Layer lines are positioned at multiples of ~1/126 Å<sup>-1</sup>, confirming the initial estimation of the repeat (Supplementary Fig. 7a). A strong layer line (*l* = 7) with a first intensity maximum near the meridian (Bessel order *n* = 1) was attributed to the pitch *P*, with a height of 1/18 Å<sup>-1</sup>. Worthy of note, other CARD domain assemblies have their layer line corresponding to the pitch at position *l* = 9<sup>51</sup>. Therefore, the structure repeats after 7 helix turns and the possible solutions of the number of units *s* are such that *s*\*7 = *u*; *u* being the integer corresponding to the number of units in the repeat *c*. Given a range of *s* between 1.5 and 4.5, as estimated from the size of the subunit, the pitch, and the reported symmetries for CARD assemblies in the literature, we defined a range of possible values for *u* of 10 to 32. For each *u* in this range, we calculated all ratios *s* = *u*/7, excluding the solutions with *s* integer, as those solutions would correspond to a helix with a repeat *c* equal to *P*. Retained solutions have layer line heights matching those observed in the experimental power spectra, but have different predicted Bessel orders *n* for each layer line. The compatibility between predicted *n*'s and experimental meridional distance of first intensity maximum along layer lines in the sum of power spectra was then assessed, to narrow down the number of possible symmetries. These symmetries were further used to generate low-resolution 3D models from the 2D class-average with most signal in its power spectrum (Supplementary Fig. 7b), with the module Segclassreconstruct. Only one symmetry, with *s* = 3.571 units/turn, gave a plausible model in terms of density distribution (Supplementary Fig. 7c). This symmetry and the corresponding<sup>47</sup> low-resolution model were used as input for 3D refinement using Segrefine3D, with a limitation of diameter of 210 Å applied on the reference model at each iteration, giving an initial map with an average resolution of 5.7 Å. Comparison with existing CARD domain atomic models showed that the helix was left-handed. Importantly, when a cylinder was used as initial model instead of the model constructed from the class-average, the refinement couldn't converge to a correct 3D structure. The helical symmetry was further refined using segrefine3dgrid module, still using a diameter of 210 Å, to a pitch of 18.15 Å and 3.571 subunits per turn, corresponding to a helical rise of 5.083 Å and a helical twist of -100.81°.

Using the refined symmetry parameters and a strong segment selection based on geometrical restraints<sup>49,52</sup> such as calculated filament straightness (60% of straightest filaments kept) and forward x-shift difference (limited to 6 Å), the final map of the filament core was obtained using a refinement diameter of 210 Å, with 8591 segments corresponding to 51,546 asymmetric units after symmetrization.

The overall resolution of this map estimated at Fourier shell correlation (FSC) cutoff of 0.143 was 4.9 Å (Supplementary Table 1, Supplementary Fig. 8). This map was used as an initial model for the processing of the higher dose dataset using an analogous approach, but this time with the symmetry parameters were kept fixed and a higher refinement diameter of 290 Å was used for visualization of the less ordered filament exterior. Selected 8412 segments corresponding to 50,472 asymmetric units after symmetrization resulted in a map of the whole BCL10-MALT1 assembly with an overall resolution of 5.9 Å.

Both 4.9 Å and 5.9 Å resolution raw half maps were symmetrized and used to estimate the local resolution (Supplementary Fig. 8b) and the B-factor using relion\_postprocess. Additionally, in order to assess the resolution of each region of the maps (Bcl10, MALT1 DD, MALT1 Ig1-Ig2-paracaspase domains) FSC curves were calculated between half maps within smooth cylinder masks of various diameters of 0–83 Å, 83–140 Å, and 140–260 Å (Supplementary Fig. 8a). The final higher resolution map of filament core (Fig. 1) used for model building was post-processed using 3Dinspect module in Spring with a b-factor of -200 Å<sup>-2</sup> and a resolution cutoff of 4.9 Å, whereas the lower resolution map of the entire assembly was post-processed with various resolution cut-off and sharpening, as indicated in Fig. 4.

**Model building and refinement.** The BCL10 CARD domains and MALT1 DD were built using Coot<sup>53</sup>. To this end, BCL10 was generated by flexible fitting of a homology model created by the program Phyre<sup>2,54</sup> and under consideration of the BCL10 CARD domain NMR structure (pdb ID: 2MB9). The MALT1 DD was built in the EM density using the related crystal structure (pdb ID: 2G7R) as well as a homology model based on the APAF CARD domain (pdb ID: 2YGS) structure prepared with Modeller<sup>55</sup>. The final model was refined with PHENIX real-space refinement<sup>56</sup>. The similarity of the refined model of BCL10 CARD with the unsharpened, unfiltered map of the filament core was assessed by FSC, after helical symmetrization of the model and calculation of a density map with a voxel size of 1.002 Å using Chimera. Similarly, the refined model and the previously deposited model PDB: 6BZE, were compared to the EMD entry EMD-7314. Final figures were generated with UCSF Chimera and PyMol<sup>57,58</sup>.

**Antibodies and DNA constructs.** The following antibodies were used for immunoprecipitation (IP), Western Blot (WB), and fluorescence activate cell sorting (FACS). WB was done at a dilution of 1:1000 except when otherwise stated. Anti-HA (3F1 (WB), obtained from E. Kremmer); anti-CARD11 (1D12), anti-IκBα (L35A5, FACS 1:50), anti-p-IκBα (5A5) (all Cell Signaling Technology); anti-FLAG-M2 (F3165, Sigma-Aldrich, WB 1:10000, IP 1 µl); anti-hCD2-APC (RPA-2.1.0, eBioscience, FACS 1:200); anti-BCL10 (EP606Y, Abcam, for endogenous BCL10); anti-BCL10 (C-17, IP 2.5 µl) and H-197 (WB for strep-tagged BCL10); anti-MALT1 (B12), anti-β-Actin (C4; WB 1:10000), anti-CYLD (E10) (all Santa Cruz Biotechnology); anti-HOIL-1 (S150D, MRC PPU Reagents); Regnase-1 (604421, R&D; WB 1:500); horseradish peroxidase (HRP)-conjugated secondary antibodies (Jackson ImmunoResearch); anti-mouse IgG1-FITC (A85-1, BD, FACS 1:100), anti-IL-2-APC (JES6-5H4, eBioscience; FACS 1:100) and anti-Thy1.1-APC-Cy7 (HIS51, eBioscience; FACS 1:200) were used. For Jurkat T-cell stimulation anti-human CD3 and CD28 from mouse were used in the presence of anti-murine IgG1 and IgG2a (all BD Pharmingen). For CD4 T-cell stimulation anti-murine CD3 and CD28 (BD Pharmingen) from hamster were used in the presence of plate-bound rabbit anti-hamster (Jackson ImmunoResearch). Oligonucleotides for EMSAs were: H2K (fw: 5'-GATCCAGGGCTGGGGATCCCCATCTCCACAGG-3', rev: 5'-GATCCCTGTGGAGATGGGAATCCCCAGCCCTG-3'), OCT1 (fw: 5'-GATCTGTGCAATGCAAATCACTAGAA-3', rev: 5'-GATCTTCTAGT-GATTTCATTTCGACA-3'). The following DNA constructs were used: 3xFlag and HA tagged MALT1B and BCL10 cDNAs were cloned in the pEF backbone vector (Invitrogen) or pHAGE-ΔCD2-T2A (lentiviral transduction)<sup>59</sup> or pMSCV-IRES-Thy1.1 (retroviral transduction)<sup>4</sup>.

**Cell culture and stimulation.** Cells were grown in DMEM (HEK293, HEK293T (both DSMZ), Phoenix-ECO (ATCC) or RPMI 1640 (Jurkat T-cells; verified by DSMZ) medium supplemented with 10% fetal calf serum and 100 U/ml penicillin/streptomycin (P/S) (all Life Technologies). HEK293 cells were transfected using standard calcium phosphate precipitation protocols. For P/I stimulation of Jurkat T-cells, 200 ng/ml PMA and 300 ng/ml Ionomycin were applied. For CD3/CD28 co-ligation, 0.3 µg anti-CD3 and 1 µg anti-CD28 antibody was used in the presence of 0.5 µg rat anti-mouse IgG1 and IgG2a.

**Generation and reconstitution of KO Jurkat T-cells.** Bicistronic expression vector px458 expressing Cas9 and sgRNA<sup>60,61</sup> was digested with BbsI and the linearized vector was gel purified. Targeting oligonucleotides and generation of MALT1-deficient Jurkat T-cells has been described<sup>38</sup>. For BCL10 two oligonucleotides targeting sites and flanking exon1 (5'AGTGAGGTCCTCCTCGGTGA 3'/5'TTCCGCTTTCGTCTCCCGCT 3' (Supplementary Fig. 4a) were cloned. Jurkat T-cells (4 × 10<sup>6</sup>) were electroporated (220 V and 1000 µF) using a Gene pulser X (Biorad) with px458 plasmids (Addgene #48138; gift F. Zhang) containing sgRNA targeting BCL10 and EGFP expression cassette. Twenty-four hours after electroporation, EGFP-positive cells were sorted using a MoFlo sorting system (Beckman

Coulter). Isolation of clonal cell lines was achieved by serial dilutions and was followed by an appropriate expansion period. KO cell clones were initially identified by anti-BCL10 staining by Western Blot. Clones lacking protein expression were genotyped by genomic PCR using intronic primers flanking targeting sites.

For reconstitution, MALT1 isoform B and BCL10 cDNAs were linked to a C-terminal Flag-Strep-Strep tag and hACD2 by a co-translational processing site T2A<sup>59</sup> and introduced into pHAGE lentiviral expression plasmids. Lentivirus was produced by transfecting HEK293T cells with 1.5 µg psPAX2 (Addgene #12260; gift D. Trono), 1 µg pMD2.G (Addgene #12259; gift D. Trono) and 2 µg transfer vector. Seventy-two hours after transfection, lentivirus encoding MALT1 and BCL10 were collected, filtrated and in the presence of 8 µg/ml polybrene added to MALT1 and BCL10 KO Jurkat T-cells ( $5 \times 10^5$  cells), respectively. After 24 h, virus was replaced by RPMI medium. FACS analysis using an Attune Flow Cytometer (Applied Biosystems) revealed >95% ΔCD2-positive cells after one week in culture.

**Purification and analysis of murine MALT1<sup>-/-</sup> CD4<sup>+</sup>T-cells.** CD4<sup>+</sup> T-cells were MACS-purified from spleen and lymph nodes of MALT1<sup>-/-</sup> mice (MALT1<sup>tm1a(EUCOMM)Hmgua</sup>; ES cell clone HEPD0671\_C08) and stimulated with plate-bound anti-CD3/CD28 antibodies for 48 h. Retroviruses were produced in Phoenix cells transfected with pMSCV retroviral transfer vectors carrying human MALT1-FlagStrepII constructs and Thy1.1 (separated by internal ribosome entry site (IRES) sequence) and viruses were collected after 48 and 72 h. CD4<sup>+</sup> T-cells were incubated for 6 h with retroviral supernatant supplemented with Polybrene (8 µg/ml) and then washed and cultured in RPMI medium supplemented with IL-2 (20 U/ml), 10% heat-inactivated FCS, 1% P/S, 1% NEAA (Life Technologies), 1% HEPES, 1% L-glutamine, 1% sodium pyruvate (Life Technologies) and 0.1% β-mercaptoethanol for 3 days before analysis. Infection efficiencies between 25 and 50% were achieved.

For IκBα degradation, cells were stimulated for 30 min with PMA (200 nM) and Ionomycin (300 nM), fixed with 2% paraformaldehyde and stained for Thy1.1. After permeabilization (0.1% saponine), cells were stained using mouse anti-IκBα antibody (L35A5, CST) and anti-mouse IgG1 FITC (BD). For determination of intracellular IL-2, cells were rested for 12 h and then stimulated with P/I or plate-bound anti-CD3/CD28 (0.5 µg/ml CD3 and 1 µg/ml CD28) antibodies for 5 h in the presence of Brefeldin A. After fixation and permeabilization, cells were stained with anti-IL-2 APC antibody (JES6-5H4, eBioscience). FACS analyses were performed using an Attune Flow Cytometer (Applied Biosystems) and analyzed with FlowJo Software (Treestar).

**Cell lysis and cellular binding studies.** For cellular analyses Jurkat T-cells ( $2-3 \times 10^6$ ) were lysed in co-immunoprecipitations (co-IP) buffer (25 mM HEPES (pH 7.5), 150 mM NaCl, 0.2% NP-40, 10% glycerol, 1 mM DTT, 10 mM sodium fluoride, 8 mM β-glycerophosphate, 300 µM sodium vanadate and protease inhibitor cocktail). For monitoring CBM complex formation after IP or StrepTactin pull-down (ST-PD), Jurkat T-cells ( $1-3 \times 10^7$ ) were lysed in co-IP buffer. Lysate controls were taken up in 4xSDS-loading buffer and boiled for 5 min at 95 °C. IP was carried out using anti-BCL10 C-17 (2.5 µl) or anti-Flag-M2 (1 µl) antibodies overnight at 4 °C. Afterwards Protein G Sepharose (15 µl 1:1 suspension) was administered for 1–2 h at 4 °C to bind antibodies. StrepII-tagged were pulled down (ST-PD) with Strep-Tactin Sepharose (15 µl 1:1 suspension) at 4 °C overnight. For co-IP and ST-PD beads were washed with co-IP buffer and boiled after adding of 22 µl 2x SDS loading buffer. Lysates and precipitated proteins were separated by SDS-PAGE and analyzed by Western blot.

**Western blotting.** Transfer onto PVDF-membranes was performed using electrophoretic semi-dry blotting system. PVDF-membranes were blocked with 5% BSA for 1 h at RT and before primary antibody (indicated above, dilution 1:1000 in 2.5% BSA/PBS-T) were incubated overnight at 4 °C. Membranes were washed in PBS-T and HRP (horse radish peroxidase)-coupled secondary antibodies (indicated above, 1:7000 in 1.25% BSA in PBS-T; 1 h, RT) were used for detection. HRP was visualized by enhanced chemiluminescence (ECL) with LumiGlo reagent (Cell Signaling Technologies) according to the protocol of the manufacturer. Images were cropped for presentation and full size images are presented in Supplementary Fig. 9.

**Electrophoretic mobility shift assay.** Electrophoretic mobility shift assays (EMSA) were carried out using double-stranded NF-κB or OCT1 binding sequences (H2K or OCT1 oligonucleotides; see reagents) which were radioactively labeled using [ $\alpha$ -<sup>32</sup>P] dATP in a Klenow Fragment (NEB) reaction. Whole cell lysates (3–6 µg) were incubated for 30 min at RT with shift-buffer (HEPES pH 7.9 (20 mM), KCl (120 mM), Ficoll (4%), DTT (5 mM), BSA (10 µg) and poly-dI-dC (2 µg, Roche) and radioactive probe (10,000–20,000 cpm) to detect DNA binding of transcription factors. Samples were run on a 5% polyacrylamide gel in TBE buffer and exposed to autoradiography after vacuum-drying. Images were cropped for presentation and full size images are presented in Supplementary Fig. 9.

**Data availability.** The electron density reconstruction and final model were deposited with the EM Data Base (accession codes EMD-0013, PDB ID 6GK2). Other data are available from the corresponding authors upon reasonable request.

Received: 3 May 2018 Accepted: 10 September 2018

Published online: 02 October 2018

## References

- Gehring, T., Seeholzer, T. & Krappmann, D. BCL10 - Bridging CARDs to immune activation. *Front. Immunol.* **9**, 1539 (2018).
- Jiang, C. & Lin, X. Regulation of NF-κappaB by the CARD proteins. *Immunol. Rev.* **246**, 141–153 (2012).
- Meiningner, I. & Krappmann, D. Lymphocyte signaling and activation by the CARMA1-BCL10-MALT1 signalosome. *Biol. Chem.* **397**, 1315–1333 (2016).
- Oeckinghaus, A. et al. Malt1 ubiquitination triggers NF-κB signaling upon T-cell activation. *EMBO J.* **26**, 4634–4645 (2007).
- Sun, L., Deng, L., Ea, C.-K., Xia, Z.-P. & Chen, Z. J. The TRAF6 ubiquitin ligase and TAK1 kinase mediate IKK activation by BCL10 and MALT1 in T lymphocytes. *Mol. Cell* **14**, 289–301 (2004).
- Wu, C.-J. & Ashwell, J. D. NEMO recognition of ubiquitinated Bcl10 is required for T cell receptor-mediated NF-κB activation. *Proc. Natl Acad. Sci.* **105**, 3023–3028 (2008).
- Oeckinghaus, A. & Ghosh, S. The NF-κappaB family of transcription factors and its regulation. *Cold Spring Harb. Perspect. Biol.* **1**, a000034 (2009).
- Coornaert, B. et al. T cell antigen receptor stimulation induces MALT1 paracaspase-mediated cleavage of the NF-κappaB inhibitor A20. *Nat. Immunol.* **9**, 263–271 (2008).
- Rebeaud, F. et al. The proteolytic activity of the paracaspase MALT1 is key in T cell activation. *Nat. Immunol.* **9**, 272–281 (2008).
- Jaworski, M. & Thome, M. The paracaspase MALT1: biological function and potential for therapeutic inhibition. *Cell. Mol. Life Sci.* **73**, 459–473 (2016).
- Thome, M., Charton, J. E., Pelzer, C. & Hailfinger, S. Antigen receptor signaling to NF-κappaB via CARMA1, BCL10, and MALT1. *Cold Spring Harb. Perspect. Biol.* **2**, a003004 (2010).
- Greil, J. et al. Whole-exome sequencing links caspase recruitment domain 11 (CARD11) inactivation to severe combined immunodeficiency. *J. Allergy Clin. Immunol.* **131**, 1376–1383.e1373 (2013).
- Jabara, H. H. et al. A homozygous mucosa-associated lymphoid tissue 1 (MALT1) mutation in a family with combined immunodeficiency. *J. Allergy Clin. Immunol.* **132**, 151–158 (2013).
- McKinnon, M. L. et al. Combined immunodeficiency associated with homozygous MALT1 mutations. *J. Allergy Clin. Immunol.* **133**, 1458–1462 (2014). 1462 e1451-1457.
- Stepensky, P. et al. Deficiency of caspase recruitment domain family, member 11 (CARD11), causes profound combined immunodeficiency in human subjects. *J. Allergy Clin. Immunol.* **131**, 477–485 e471 (2013).
- Torres, J. M. et al. Inherited BCL10 deficiency impairs hematopoietic and nonhematopoietic immunity. *J. Clin. Invest.* **124**, 5239–5248 (2014).
- Ma, C. A. et al. Germline hypomorphic CARD11 mutations in severe atopic disease. *Nat. Genet.* **49**, 1192–1201 (2017).
- Knies, N. et al. Lymphomagenic CARD11/BCL10/MALT1 signaling drives malignant B-cell proliferation via cooperative NF-κappaB and JNK activation. *Proc. Natl Acad. Sci. USA* **112**, E7230–E7238 (2015).
- Lenz, G. et al. Oncogenic CARD11 mutations in human diffuse large B cell lymphoma. *Science* **319**, 1676–1679 (2008).
- Snow, A. L. et al. Congenital B cell lymphocytosis explained by novel germline CARD11 mutations. *J. Exp. Med.* **209**, 2247–2261 (2012).
- Zhang, Q. et al. Inactivating mutations and overexpression of BCL10, a caspase recruitment domain-containing gene, in MALT lymphoma with t(1;14)(p22;q32). *Nat. Genet.* **22**, 63–68 (1999).
- Dierlamm, J. et al. The apoptosis inhibitor gene API2 and a novel 18q gene, MLT, are recurrently rearranged in the t(11;18)(q21;q21) associated with mucosa-associated lymphoid tissue lymphomas. *Blood* **93**, 3601–3609 (1999).
- Sanchez-Izquierdo, D. et al. MALT1 is deregulated by both chromosomal translocation and amplification in B-cell non-Hodgkin lymphoma. *Blood* **101**, 4539–4546 (2003).
- Bardet, M. et al. The T-cell fingerprint of MALT1 paracaspase revealed by selective inhibition. *Immunol. Cell Biol.* **96**, 81–99 (2018).
- Fontan, L. et al. MALT1 small molecule inhibitors specifically suppress ABC-DLBCL in vitro and in vivo. *Cancer Cell* **22**, 812–824 (2012).
- Nagel, D. et al. Pharmacologic inhibition of MALT1 protease by phenothiazines as a therapeutic approach for the treatment of aggressive ABC-DLBCL. *Cancer Cell* **22**, 825–837 (2012).
- Matsumoto, R. et al. Phosphorylation of CARMA1 plays a critical role in T Cell receptor-mediated NF-κappaB activation. *Immunity* **23**, 575–585 (2005).
- Sommer, K. et al. Phosphorylation of the CARMA1 linker controls NF-κappaB activation. *Immunity* **23**, 561–574 (2005).

29. Jang, T. H., Park, J. H. & Park, H. H. Novel disulfide bond-mediated dimerization of the CARD domain was revealed by the crystal structure of CARMA1 CARD. *PLoS ONE* **8**, e79778 (2013).
30. Li, S., Yang, X., Shao, J. & Shen, Y. Structural insights into the assembly of CARMA1 and BCL10. *PLoS ONE* **7**, e42775 (2012).
31. David, L. et al. Assembly mechanism of the CARMA1-BCL10-MALT1-TRAF6 signalosome. *Proc. Natl Acad. Sci. USA* **115**, 1499–1504 (2018).
32. Qiao, Q. et al. Structural architecture of the CARMA1/Bcl10/MALT1 signalosome: nucleation-induced filamentous assembly. *Mol. Cell* **51**, 766–779 (2013).
33. Langel, F. D. et al. Multiple protein domains mediate interaction between Bcl10 and MALT1. *J. Biol. Chem.* **283**, 32419–32431 (2008).
34. Lucas, P. C. et al. Bcl10 and MALT1, independent targets of chromosomal translocation in malt lymphoma, cooperate in a novel NF-kappa B signaling pathway. *J. Biol. Chem.* **276**, 19012–19019 (2001).
35. Uren, A. G. et al. Identification of paracaspases and metacaspases: two ancient families of caspase-like proteins, one of which plays a key role in MALT lymphoma. *Mol. Cell* **6**, 961–967 (2000).
36. Wegener, E. et al. Essential role for IkkappaB kinase beta in remodeling Carma1-Bcl10-Malt1 complexes upon T cell activation. *Mol. Cell* **23**, 13–23 (2006).
37. Qiu, L. & Dhe-Paganon, S. Oligomeric structure of the MALT1 tandem Ig-like domains. *PLoS ONE* **6**, e23220 (2011).
38. Meininger, I. et al. Alternative splicing of MALT1 controls signalling and activation of CD4(+) T cells. *Nat. Commun.* **7**, 11292 (2016).
39. Schlauderer, F. et al. Structural analysis of phenothiazine derivatives as allosteric inhibitors of the MALT1 paracaspase. *Angew. Chem. Int. Ed. Engl.* **52**, 10384–10387 (2013).
40. Yang, Y. K. et al. Molecular determinants of scaffold-induced linear ubiquitinylation of B cell lymphoma/leukemia 10 (Bcl10) during T cell receptor and oncogenic caspase recruitment domain-containing protein 11 (CARD11) signaling. *J. Biol. Chem.* **291**, 25921–25936 (2016).
41. Scharshmidt, E., Wegener, E., Heissmeyer, V., Rao, A. & Krappmann, D. Degradation of Bcl10 induced by T-cell activation negatively regulates NF-kappa B signaling. *Mol. Cell Biol.* **24**, 3860–3873 (2004).
42. Hu, S. et al. cIAP2 is a ubiquitin protein ligase for BCL10 and is dysregulated in mucosa-associated lymphoid tissue lymphomas. *J. Clin. Invest.* **116**, 174–181 (2006).
43. Paul, S., Kashyap, A. K., Jia, W., He, Y. W. & Schaefer, B. C. Selective autophagy of the adaptor protein Bcl10 modulates T cell receptor activation of NF-kappaB. *Immunity* **36**, 947–958 (2012).
44. Baens, M. et al. MALT1 auto-proteolysis is essential for NF-kappaB-dependent gene transcription in activated lymphocytes. *PLoS ONE* **9**, e103774 (2014).
45. Pelzer, C. et al. The protease activity of the paracaspase MALT1 is controlled by monoubiquitination. *Nat. Immunol.* **14**, 337–345 (2013).
46. Zheng, S. Q. et al. MotionCor2: anisotropic correction of beam-induced motion for improved cryo-electron microscopy. *Nat. Methods* **14**, 331–332 (2017).
47. Mindell, J. A. & Grigorieff, N. Accurate determination of local defocus and specimen tilt in electron microscopy. *J. Struct. Biol.* **142**, 334–347 (2003).
48. Ludtke, S. J., Baldwin, P. R. & Chiu, W. EMAN: semiautomated software for high-resolution single-particle reconstructions. *J. Struct. Biol.* **128**, 82–97 (1999).
49. Desfosses, A., Ciuffa, R., Gutsche, I. & Sachse, C. SPRING - an image processing package for single-particle based helical reconstruction from electron cryomicrographs. *J. Struct. Biol.* **185**, 15–26 (2014).
50. Hohn, M. et al. SPARX, a new environment for Cryo-EM image processing. *J. Struct. Biol.* **157**, 47–55 (2007).
51. Xu, H. et al. Structural basis for the prion-like MAVS filaments in antiviral innate immunity. *eLife* **3**, e01489 (2014).
52. Sachse, C. et al. High-resolution electron microscopy of helical specimens: a fresh look at tobacco mosaic virus. *J. Mol. Biol.* **371**, 812–835 (2007).
53. Emsley, P. & Cowtan, K. Coot: model-building tools for molecular graphics. *Acta Crystallogr. D Biol. Crystallogr.* **60**, 2126–2132 (2004).
54. Kelley, L. A., Mezulis, S., Yates, C. M., Wass, M. N. & Sternberg, M. J. The Phyre2 web portal for protein modeling, prediction and analysis. *Nat. Protoc.* **10**, 845–858 (2015).
55. Webb, B. & Sali, A. Protein structure modeling with MODELLER. *Methods Mol. Biol.* **1137**, 1–15 (2014).
56. Adams, P. D. et al. PHENIX: a comprehensive Python-based system for macromolecular structure solution. *Acta Crystallogr. D Biol. Crystallogr.* **66**, (213–221) (2010).
57. Pettersen, E. F. et al. UCSF Chimera--a visualization system for exploratory research and analysis. *J. Comput. Chem.* **25**, 1605–1612 (2004).
58. DeLano, W. L. *The PyMol Molecular Graphics System*. (Delano Scientific, Palo Alto, CA, 2002).
59. Hadian, K. et al. NF-kappaB essential modulator (NEMO) interaction with linear and lys-63 ubiquitin chains contributes to NF-kappaB activation. *J. Biol. Chem.* **286**, 26107–26117 (2011).
60. Cong, L. et al. Multiplex genome engineering using CRISPR/Cas systems. *Science* **339**, 819–823 (2013).
61. Ran, F. A. et al. Genome engineering using the CRISPR-Cas9 system. *Nat. Protoc.* **8**, 2281–2308 (2013).

## Acknowledgements

We thank the MPI of Biochemistry cryo-EM and biophysics core facilities for generous access and support. We are grateful to the IT teams from IBS and EMBL Grenoble, and specifically Aymeric Peuch for help with the usage of the joint IBS/EMBL EM computing cluster which was used as a part of the platforms of the Grenoble Instruct-ERIC Center (ISBG: UMS 3518 CNRS-CEA-UGA-EMBL) with support from FRISBI (ANR-10-INSB-05-02) and GRAL (ANR-10-LABX-49-01) within the Grenoble Partnership for Structural Biology (PSB). We thank Simon Widmann for help with the cell-based assays. K.L. and D.K. are supported by the CRC1054 project B02 and A04, respectively. A.D. is supported by the FRM ARF20160936266 grant. K.-P.H. is supported by the Deutsche Forschungsgemeinschaft (CRC1064, GRK1721), the European Research Council (ERC Advanced Grant ATMMACHINE), the Gottfried-Wilhelm-Leibniz Prize and the Center for Integrated Protein Sciences Munich (CIPSM).

## Author contributions

K.L. and F.S. prepared the cryo-EM samples and collected the data. T.S. performed all cellular experiments. A.D. performed helical reconstruction and helped with structure determination. I.G. helped with EM data analysis. K.L. built atomic models. F.S. prepared the protein complex, the biochemical analysis and participated in structure determination. T.G. established the Jurkat KO T-cells and performed reconstitution of murine MALT1<sup>-/-</sup> CD4 T-cells. M.S. operates the MPI Biochemistry cryo-EM facility, helped with EM data collection and provided general EM advice. K.L., D.K., and K.-P.H. designed the overall study, analyzed the results and wrote the paper with input of A.D. and I.G. and contributions from all other authors.

## Additional information

**Supplementary Information** accompanies this paper at <https://doi.org/10.1038/s41467-018-06573-8>.

**Competing interests:** The authors declare no competing interests.

**Reprints and permission** information is available online at <http://npg.nature.com/reprintsandpermissions/>

**Publisher's note:** Springer Nature remains neutral with regard to jurisdictional claims in published maps and institutional affiliations.



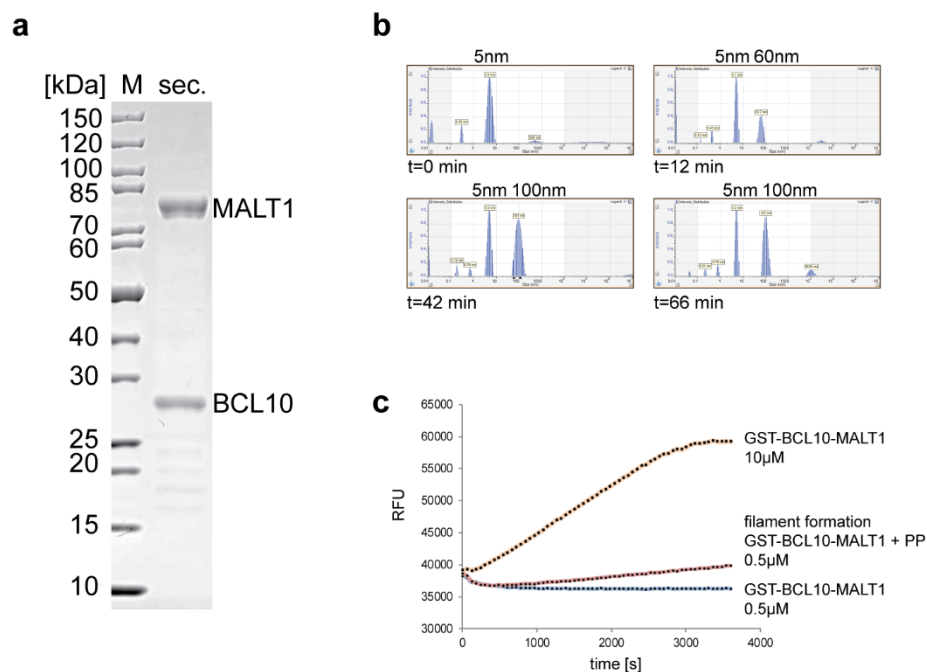
**Open Access** This article is licensed under a Creative Commons Attribution 4.0 International License, which permits use, sharing, adaptation, distribution and reproduction in any medium or format, as long as you give appropriate credit to the original author(s) and the source, provide a link to the Creative Commons license, and indicate if changes were made. The images or other third party material in this article are included in the article's Creative Commons license, unless indicated otherwise in a credit line to the material. If material is not included in the article's Creative Commons license and your intended use is not permitted by statutory regulation or exceeds the permitted use, you will need to obtain permission directly from the copyright holder. To view a copy of this license, visit <http://creativecommons.org/licenses/by/4.0/>.

© The Author(s) 2018

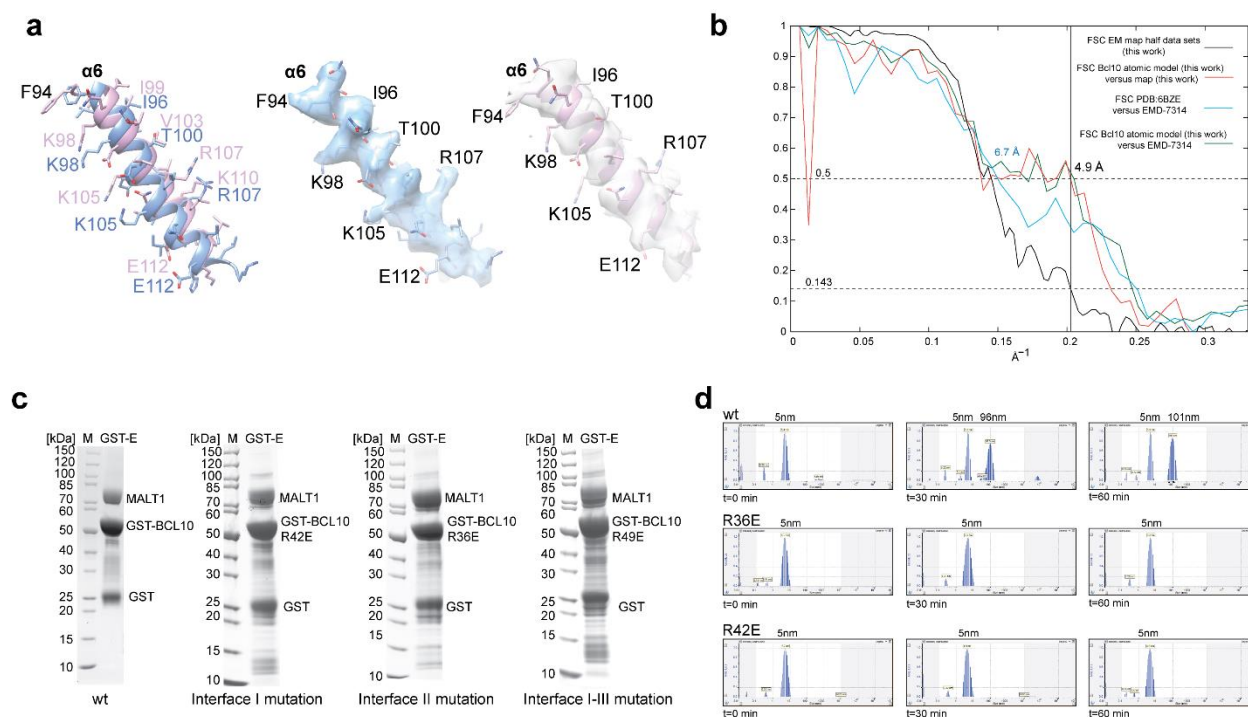
**Supplementary Information for**

**Molecular architecture and regulation of BCL10-MALT1 filaments**

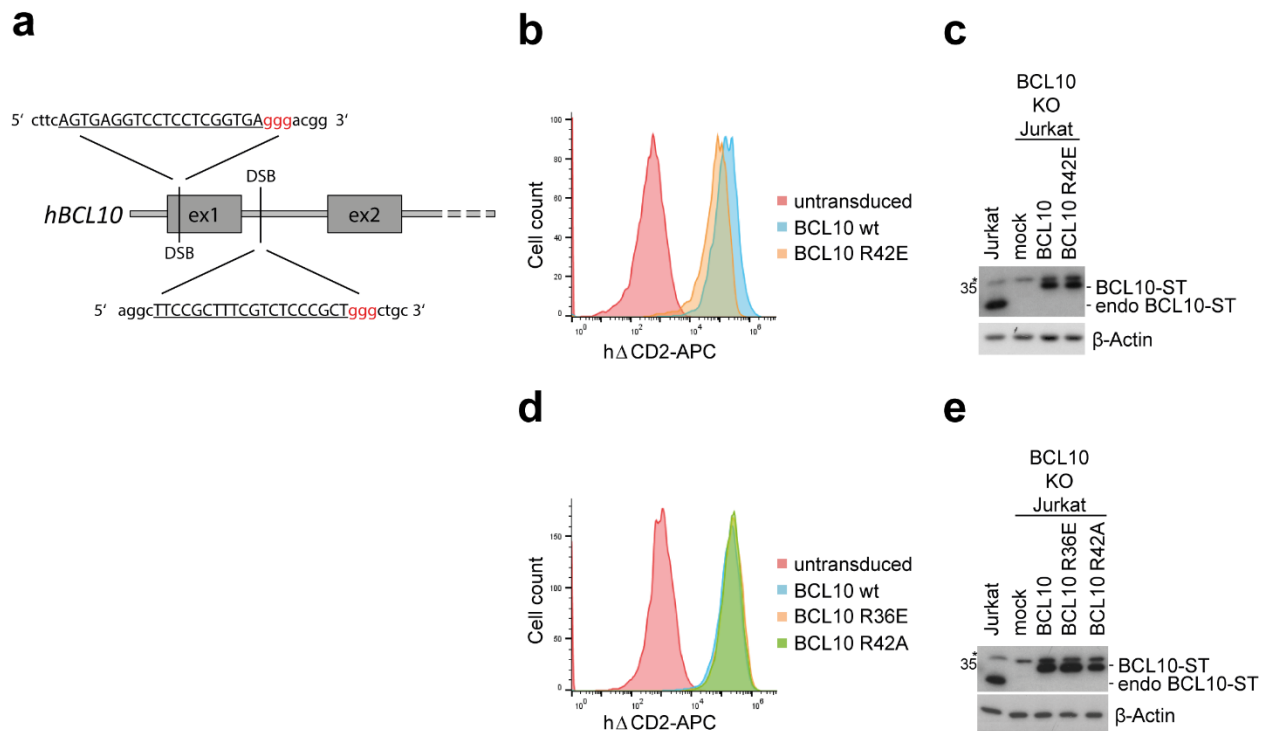
Schlauderer et al.



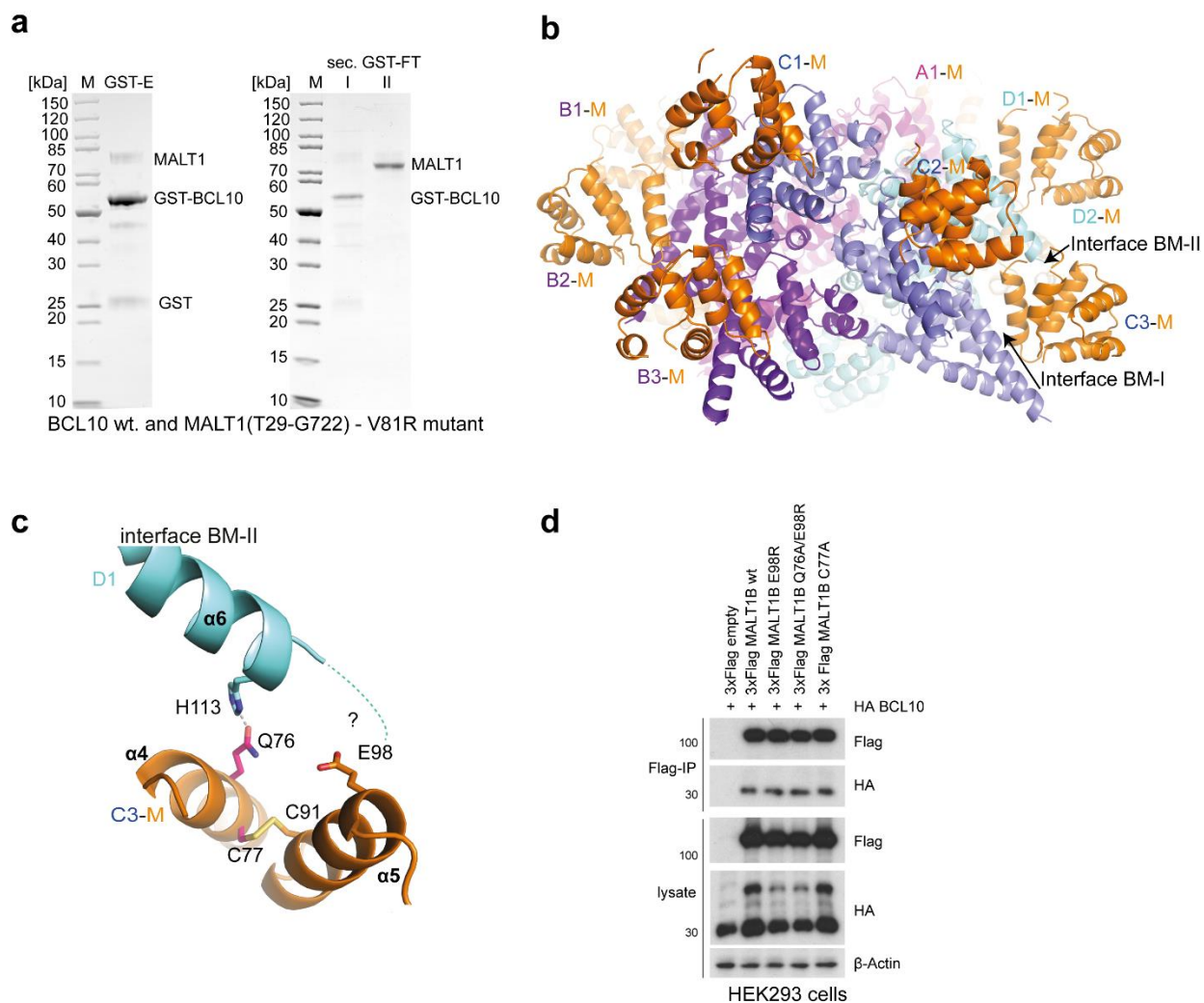
**Supplementary Figure 1:** Biochemical analysis of the recombinant BCL10-MALT1 complex. (a) SDS Page analysis of the purified BCL10-MALT1 protein complex used for cryo-EM grid preparation and biochemical analysis. (b) Dynamic light scattering (DLS) experiment showing the polymerization of the BCL10 MALT1 complex purified from *E. coli* after cleavage of the GST-tag by PreScission protease. (c) Fluorescence activity measurement using the MALT1 substrate Ac-LRSR-AMC. The MALT1 protease activity is represented in relative fluorescence units (RFU).



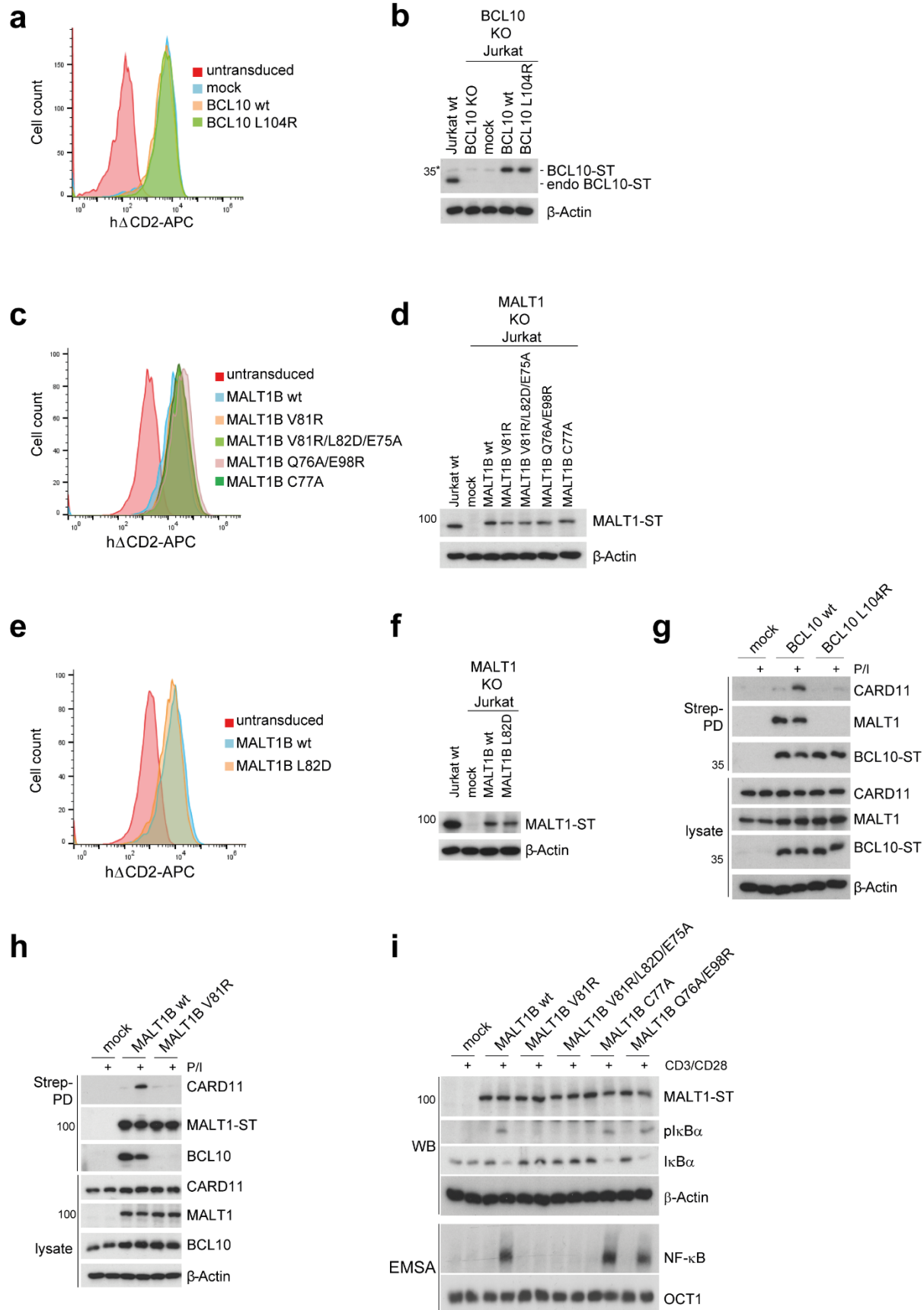
**Supplementary Figure 2:** Biochemical analysis of the recombinant BCL10-MALT1 complex wt and mutants. (a) Comparison of the BCL10 EM structures alone (colored pink) and inside the BCL10-MALT1 complex<sup>31</sup> (colored blue) indicates differences in the amino acid registry in helix  $\alpha 6$  (left). Exemplary model versus map comparison of our BCL10 model and the BCL10 filament structure without MALT1<sup>31</sup> (EMD entry: 7314) middle and right respectively. (b) FSC between refined model and final map. The resolution of 4.9 Å was determined using the 0.143 FSC criterion as indicated by the dotted line. (c) SDS PAGE analysis of GST affinity chromatography elution fractions of BCL10-MALT1 wt and BCL10 mutant proteins. (d) Oligomerization proficiency of wt, R42E and R36E BCL10 mutants monitored by DLS analysis of the respective recombinant BCL10-MALT1 complexes.



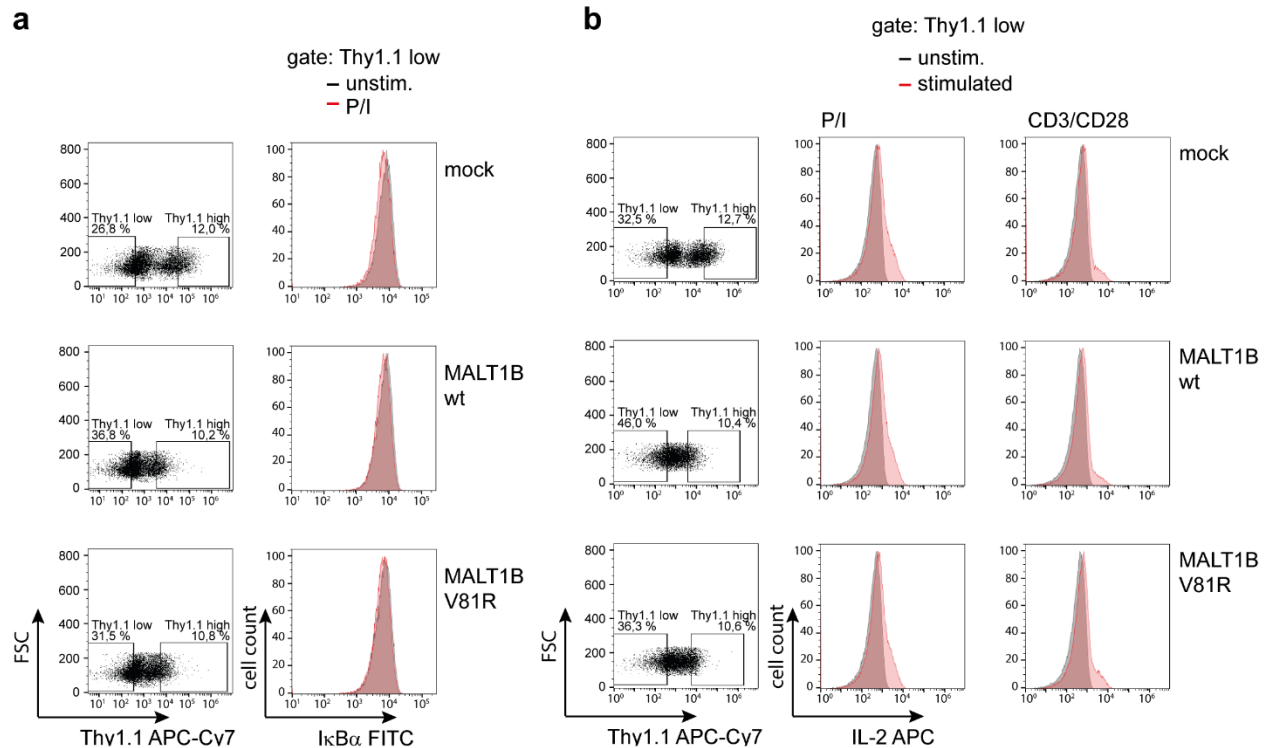
**Supplementary Figure 3:** Generation of BCL10 KO Jurkat T-cells and transduction efficiency of BCL10 constructs. (a) Scheme of genomic organization (ex1-ex2) of human BCL10 gene and depiction of sgRNAs used to delete parts of exon 1 (ex1). (b-e) Transduction efficiency of BCL10 constructs. Infection of BCL10 KO Jurkat T-cells was determined by the co-expressed surface marker h $\Delta$ CD2 in FACS (b, d). Expression of BCL10 and BCL10 mutants in reconstituted BCL10 KO cells compared to parental Jurkat T-cells was analyzed in WB (c, e). Asterisk indicates non-specific cross-reactivity of BCL10 antibody.



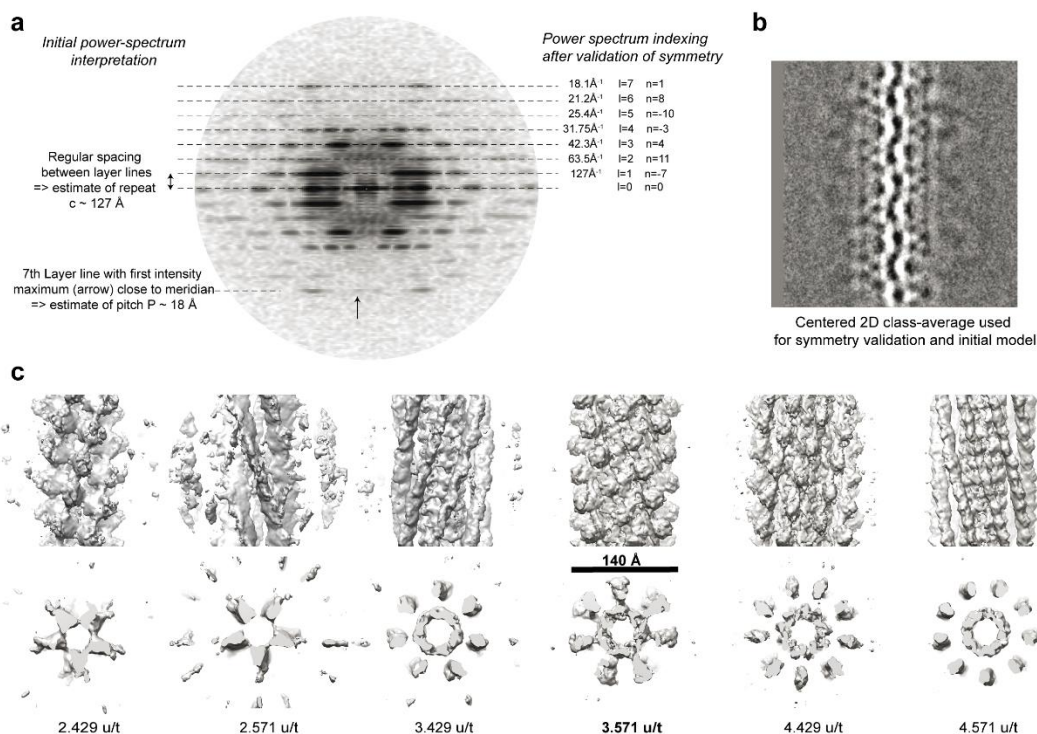
**Supplementary Figure 4:** Structural and functional analyses of BCL10-MALT1 interfaces. (a) SDS PAGE analysis of GST affinity chromatography elution fractions of BCL10 with MALT1 (T29-G722) or MALT1 (T29-G722) V81R. (b) Side view of one repeat of the BCL10-MALT1 holo-complex as visible in the cryo-EM density. Position of the putative interface BM-II is indicated. (c) Close up view of the putative BM-II shown as ribbon model in purple (BCL10) and orange (MALT1). Potentially interacting residues are shown in stick representation. Mutations introduced are colored magenta. (d) HEK293 cells were co-transfected with 3xFLAG MALT1B wt and indicated BM-II mutant constructs and HA BCL10 wt. Co-IP was carried out using anti-Flag antibodies and analyzed by WB.



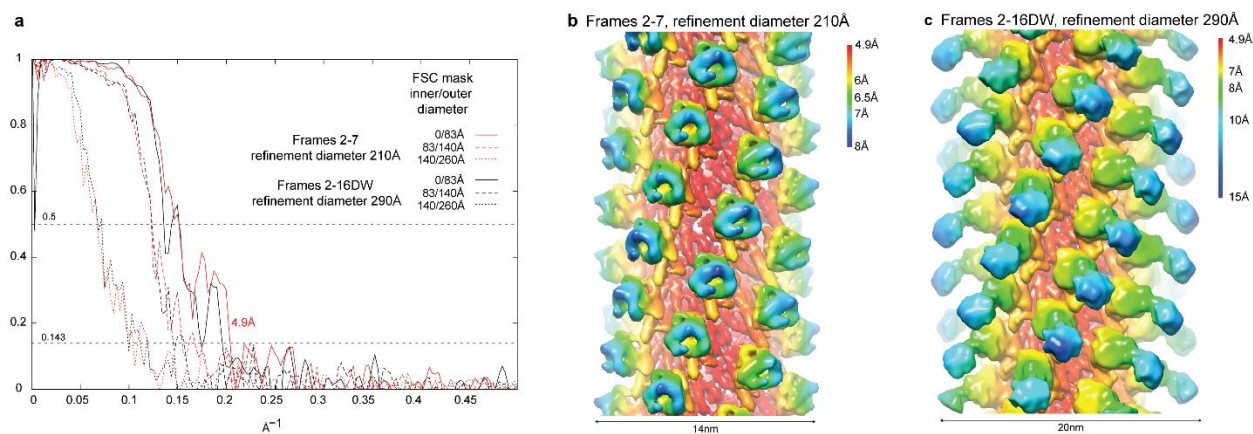
**Supplementary Figure 5:** Transduction efficiency of BCL10 and MALT1 wt and BM-I mutants in Jurkat T-cells. (a) Transduction of BCL10 wt and mutant L104R in BCL10 KO Jurkat T-cells determined by the co-expressed surface marker h $\Delta$ CD2 in FACS. (b) Expression of Strep-tagged BCL10 and BCL10 L104R in reconstituted BCL10 KO cells and comparison to parental Jurkat T-cells in WB. Asterisk indicates non-specific cross-reactivity of BCL10 antibody. (c-f) Transduction of MALT1 constructs in MALT1 KO Jurkat T-cells. Transduction efficiency was determined by the co-expressed surface marker h $\Delta$ CD2 in FACS (c, e). Expression of MALT1 or MALT1 BM-I or BM-II mutant constructs and comparison to parental Jurkat T-cells in WB (d, f). (g) MALT1 KO Jurkat T-cells reconstituted with MALT1 wt or V81R mutant were stimulated for 20 min with P/I stimulation and CBM complex formation was investigated by Strep-PD. (h) BCL10 KO Jurkat T-cells were reconstituted with BCL10 wt or L104R mutant constructs and stimulation and Strep-PD was carried out as described in g. (i) MALT1 KO Jurkat T-cells transduced with MALT1B wt, BM-I or BM-II mutants were stimulated with anti-CD3/28 for 30 minutes. NF- $\kappa$ B signaling was analyzed by WB and EMSA.



**Supplementary Figure 6:** Transduction of MALT1 wt and BM-I mutant V81R in murine MALT1<sup>-/-</sup> CD4 T-cells. (a) Murine MALT1<sup>-/-</sup> CD4 T-cells were retrovirally transduced with mock, MALT1 wt or MALT1 BM-I mutants and the surface marker Thy1.1. For single cells analyses of NF-κB signaling, CD4 T-cells were untreated or stimulated with P/I (20 min) before staining with anti-IκBα (FITC) and Thy1.1-APC. IκBα expression was analyzed in Thy1.1-positive transduced cells or Thy1.1-negative untransduced cells in indicated gates. IκBα staining in the control untransduced Thy1.1-negative T-cell population (MALT1 deficient) is shown in the right histograms and IκBα expression levels in transduced Thy1.1-positive T-cells (mock or MALT1 rescue) is shown in Fig. 5j. (b) MALT1<sup>-/-</sup> CD4 T-cells were retrovirally transduced as in c. For single cells analyses of IL-2 production, CD4 T-cells were untreated or stimulated with P/I or anti-CD3/CD28 for 5 h before staining with anti-IL-2-APC and Thy1.1-APC-Cy7. Intracellular IL-2 production was analyzed in Thy1.1-positive transduced cells or Thy1.1-negative untransduced cells in indicated gates. IL-2 expression staining in the control untransduced Thy1.1-negative T-cell population (MALT1 deficient) is shown in the histograms and IL-2 expression levels in transduced Thy1.1-positive T-cells (mock or MALT1 rescue) are shown in Figure 5k (for P/I) and 5l (for anti-CD3/CD28).



**Supplementary Figure 7:** Sum of the power spectra of selected 2D class-averages, its initial interpretation (left) and the indexing (right) corresponding to the final symmetry (pitch 18.15 Å, 3.571 units/turn) (b) The centered 2D class-average used by the module `segclassreconstruct` to explore plausible symmetries as determined from the initial analysis of the power spectrum shown in (a). (Scale bar = 100 Å). (c). 3D reconstructions obtained from the single 2D class-average shown in (b), for various symmetries for which the predicted layer line positions and their corresponding Bessel function order is compatible with the observed power spectrum. The correct symmetry is indicated in bold.



**Supplementary Figure 8:** (a) Fourier shell correlation (FSC) curves between half-maps from the two refinement procedures, with frames 2-7 (red curves) or 2-16 dose weighted (DW) (black curves). The FSCs were calculated within smooth cylinders of indicated inner and outer diameter. (b-c) Refined maps generated from the high (b) and low (c) resolution data evaluation procedure colored and filtered for local resolution using the indicated color scheme.

Figure 3a

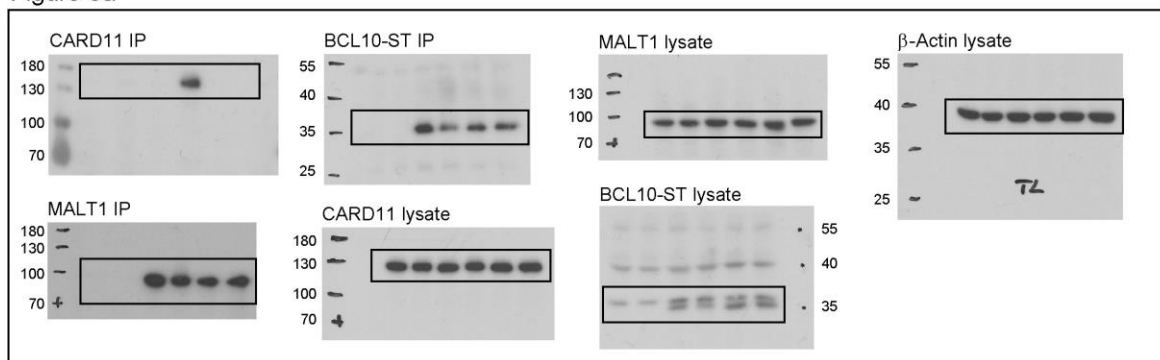


Figure 3b

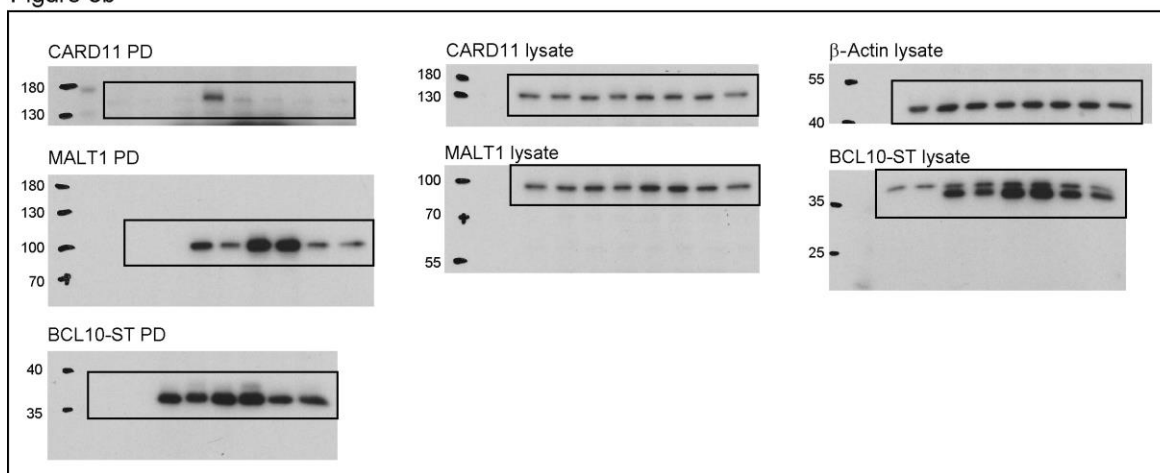
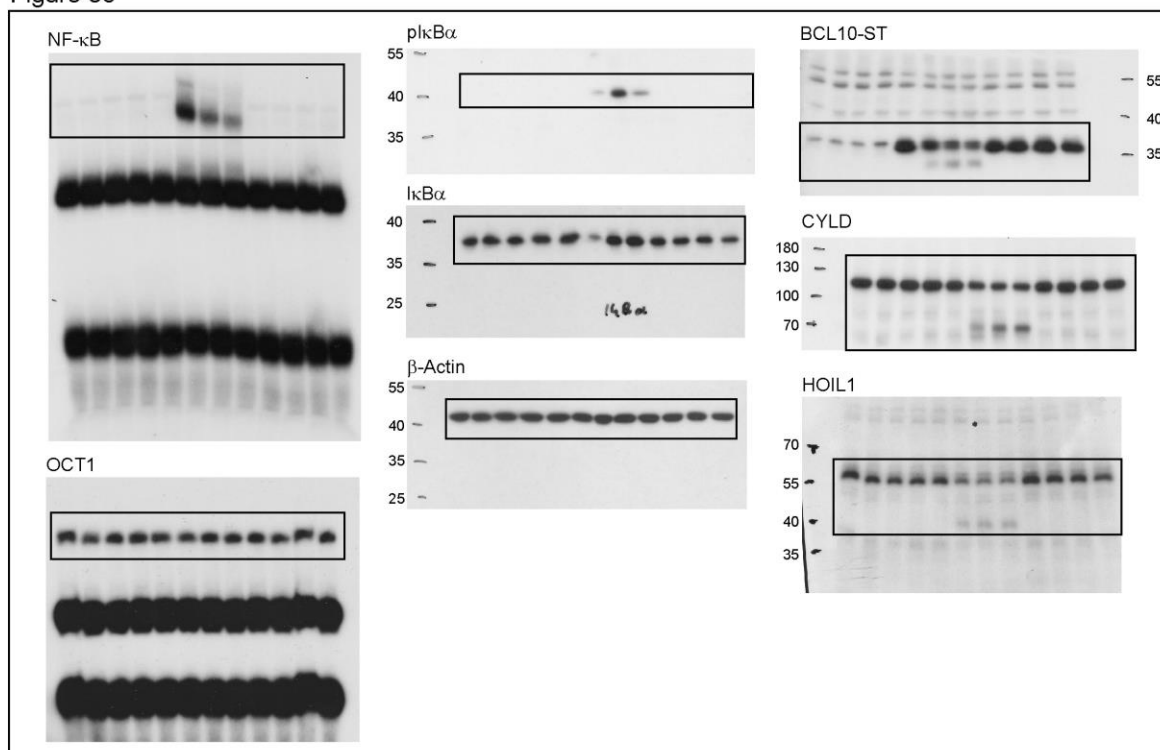


Figure 3c



Supplementary Figure 9: Uncropped images. Boxes highlight approx. area for cropping.

Figure 3d

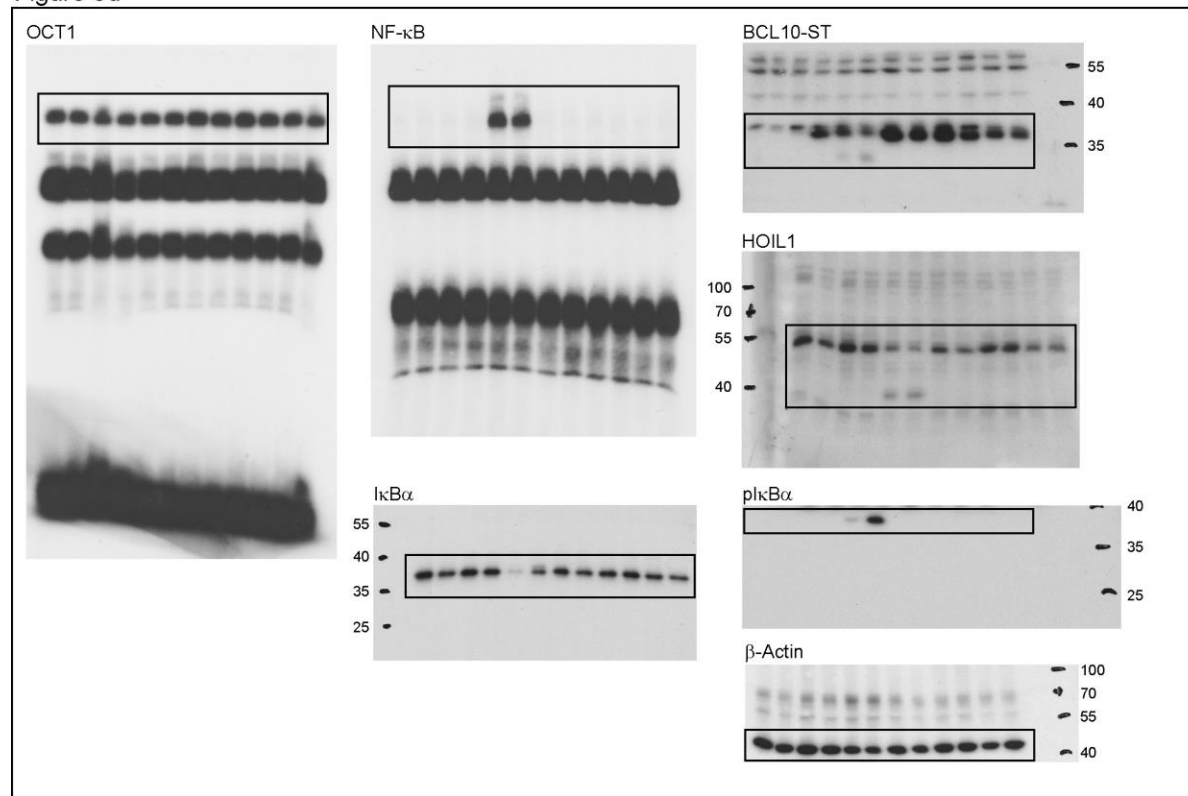
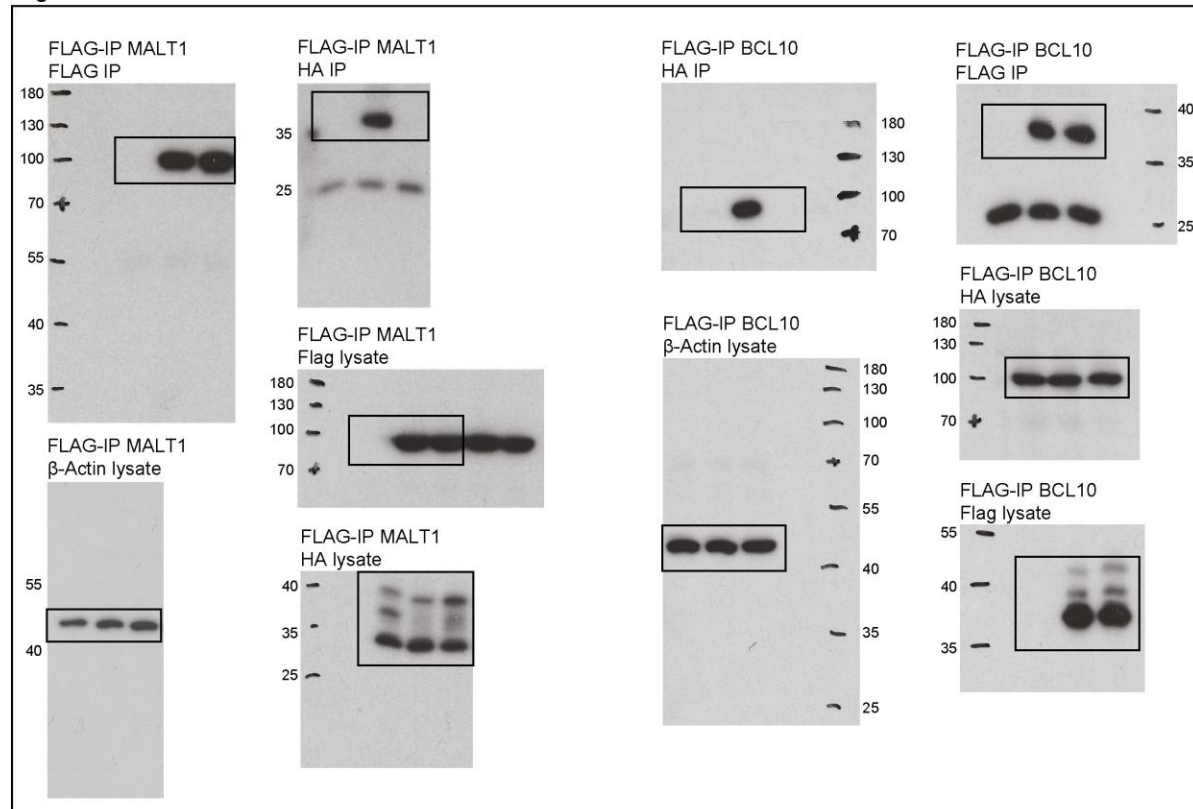


Figure 4d



Supplementary Figure 9: Continued.

Figure 5a

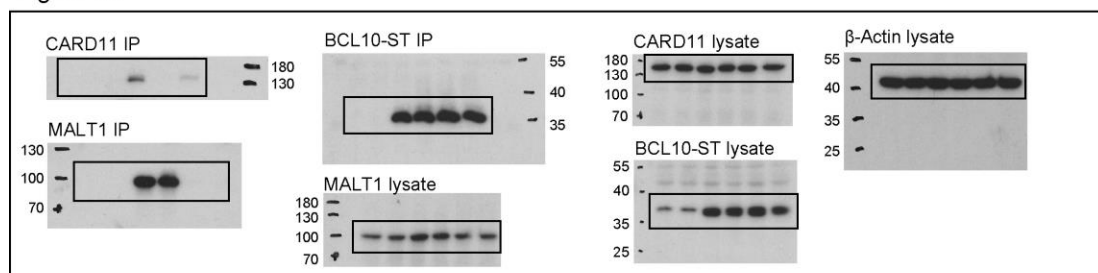


Figure 5b

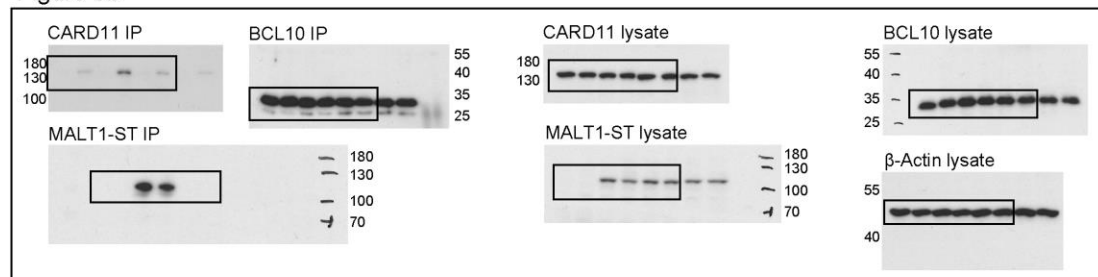


Figure 5c

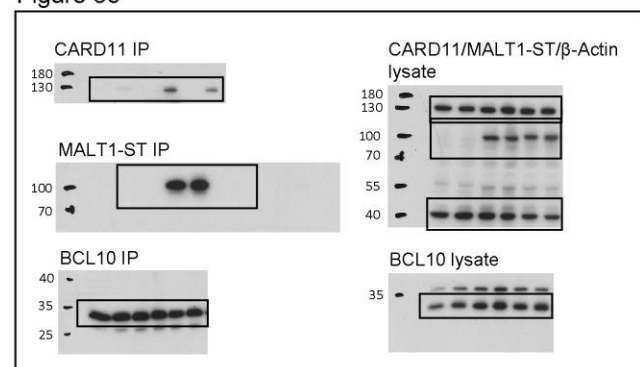


Figure 5d

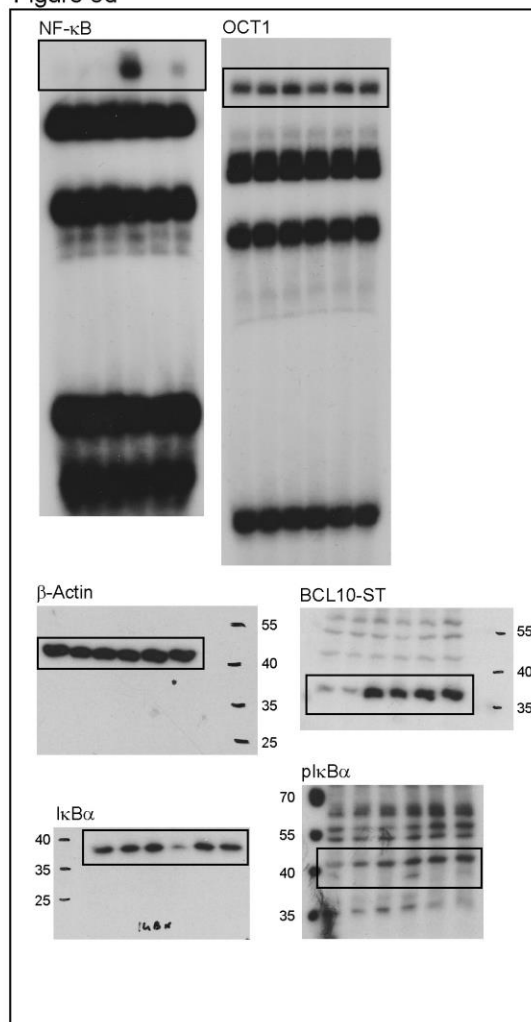
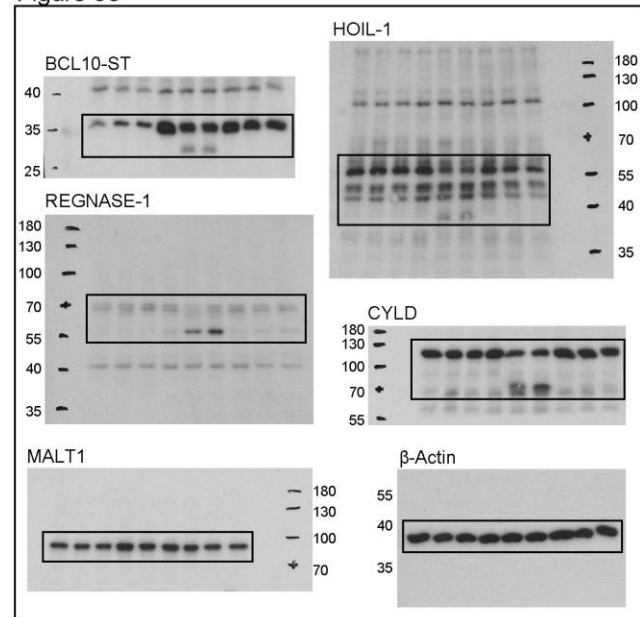


Figure 5e



Supplementary Figure 9: Continued.

Figure 5f

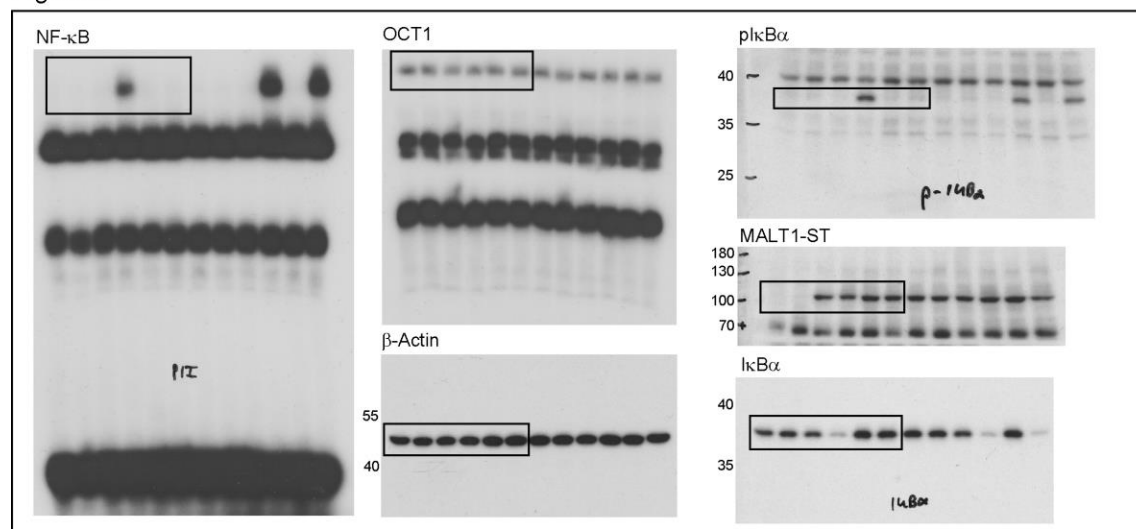


Figure 5g

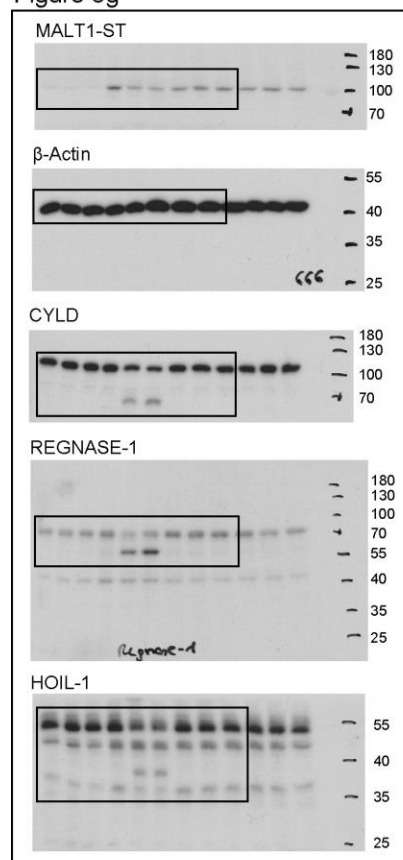


Figure 5h

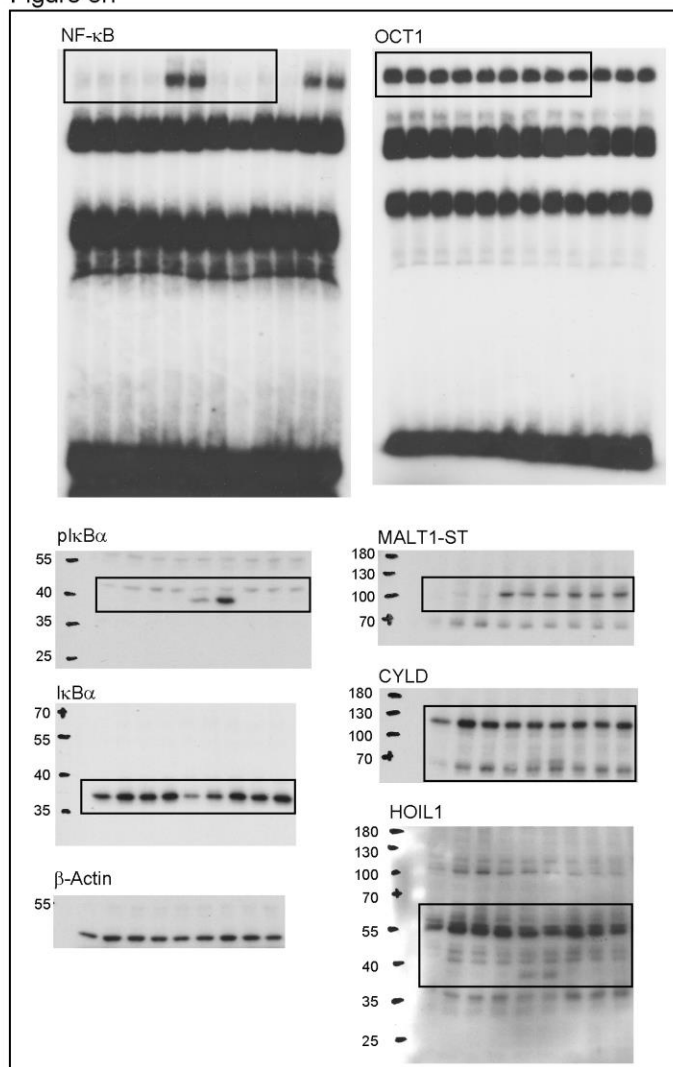
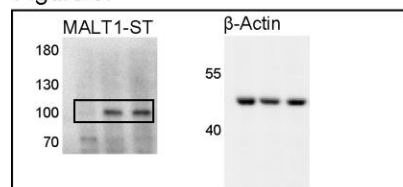


Figure 5i



Supplementary Figure 9: Continued.

Figure S3c

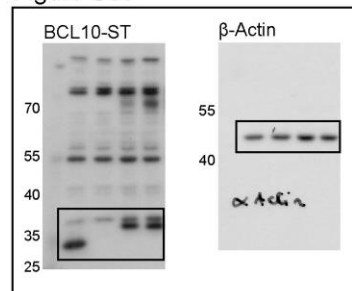


Figure S4d

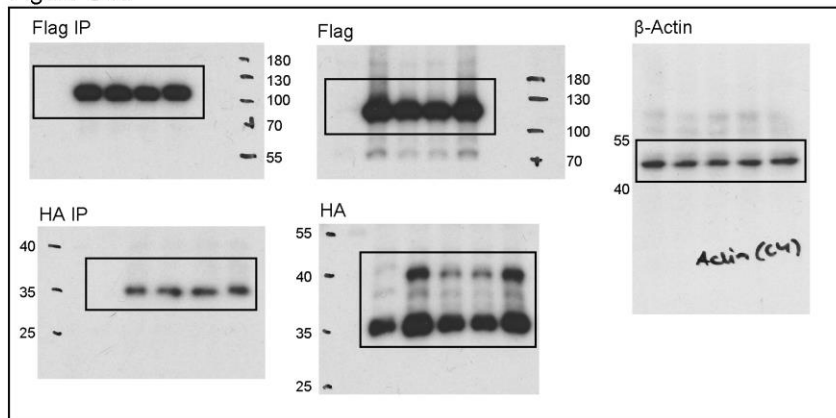


Figure S3e

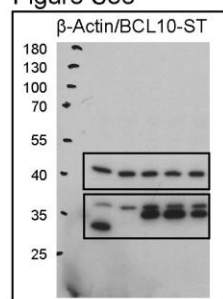


Figure S5b

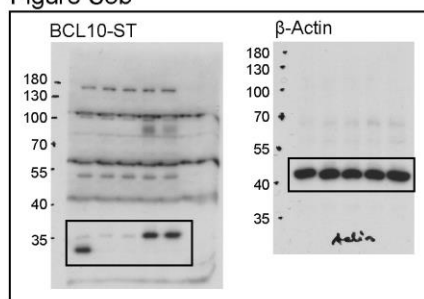


Figure S5g

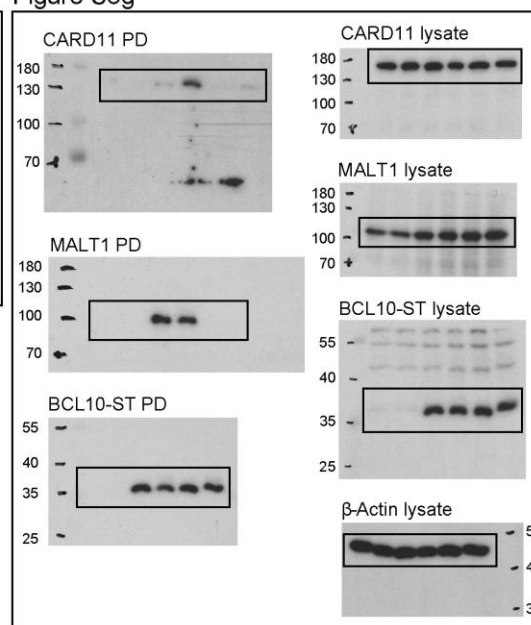


Figure S5d

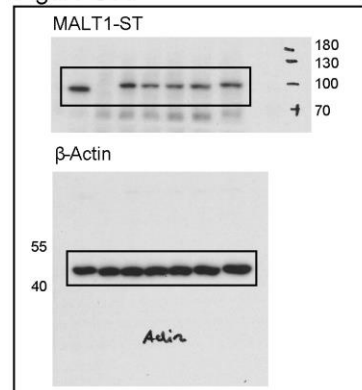


Figure S5f

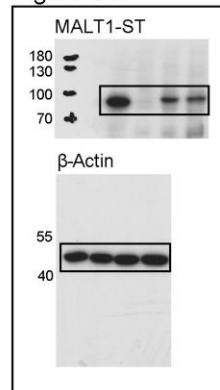
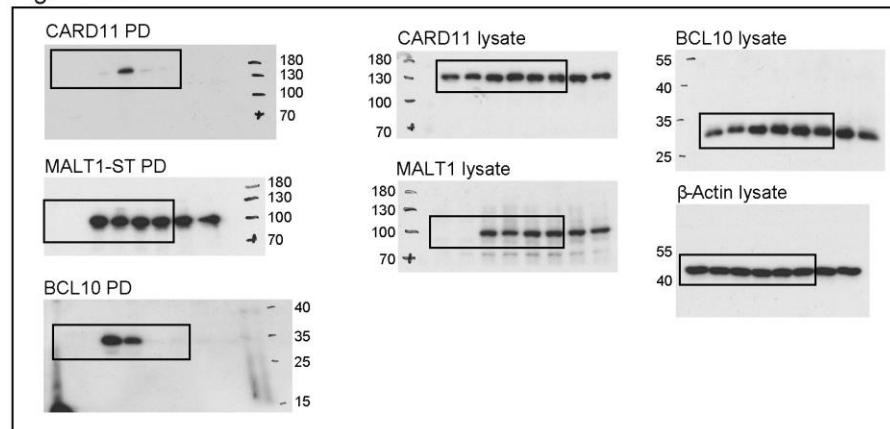


Figure S5h



Supplementary Figure 9: Continued.



**Supplementary Table 1: Cryo-EM data collection, refinement and validation statistics**


---

**Data collection**


---

Voltage (kV)	200
Electron Dose (e-Å <sup>2</sup> )	99.6
Number of Frames	49
Detector	Falcon III
Pixel Size (Å)	1.002
Defocus range (-µm)	1.0-3.5
Total number of micrographs	370
Total number of filaments	2618

**Reconstruction high resolution**


---

Electron Dose (e-Å <sup>2</sup> )	15
Segment size (Å):	500
Segmentation step size (Å):	30
Initial segments:	25576
Final segments:	8591
Diameter (Å):	210
Helical rise (Å):	5.083
Helical twist (°):	-100.8
Map sharpening B factor (Å <sup>2</sup> ):	-200
Final resolution (Å):	6.9/4.9
FSC threshold:	0.5/0.143

**Reconstruction low resolution**


---

Electron Dose (e-Å <sup>2</sup> )	32
Segment size (Å):	500
Segmentation step size (Å):	30
Initial segments:	25576
Final segments:	8412
Diameter (Å):	290
Helical rise (Å):	5.083

Helical twist (°):	-100.8
Final resolution (Å):	7.7/5.9
FSC threshold:	0.5/0.143

### Refinement:

---

Initial models used (PDB code)	2G7R and 2MB9
Model resolution (Å)	4.9
FSC threshold	0.143
Model resolution range (Å)	30-4.9
Map sharpening B factor (Å <sup>2</sup> )	-200
CC Model vs. Map	0.79
Model composition	
Non-hydrogen atoms	196
Protein residues	196
R.m.s. deviations	
Bond lengths (Å)	0.008
Bond angles (°)	0.93
Validation	
MolProbity score	-
Clashscore	
Poor rotamers (%)	0.1*
Ramachandran plot	
Favored (%)	92.8*
Allowed (%)	4.2*
Disallowed (%)	0.0*

---

\*These values are not independent quality criteria, since, during refinement, restraints for rotamers and Ramachandran plot were used

**Supplementary Table 2: Primer list**

<b>Construct</b>	<b>Forward primer</b>	<b>Reverse primer</b>
MALT1 (T29-G722)	5'-CCCTGGGCAGCCAT ATGACCCTCAACCGCCTG-3'	5'-TGCTCGAGTGCGGCC GCTCATCCCAAACCTCGATGCA-3'
MALT1(V81R)	5'-CAGTGTTCTCTTAAG CGACTGGAGCCTGAAG-3'	5'-CTTCAGGCTCCAGTC GCTTAAGAGAACAACACTG-3'
BCL10 (L104R)	5'-ACAGATGAAGTG CGGAAACTTAGAA-3'	5'-TTCTAAGTTTC CGCACTTCATCTGT-3'
BCL10 (R36E)	5'-TCATAGCTGAGGAA CATTTTGATCATCTACGTG-3'	5'-CACGTAGATGATCAAA ATGTTCCCTCAGCTATGA-3'
BCL10 (R42E)	5'-TTTGATCATCTAGAA GCAAAAAAATACTCAG-3'	5'-CTGAGTATTTTTTTTG CTTCTAGATGATCAAA-3'
BCL10 (R49E)	5'- CGTGCAAAAAAAT ACTCAGTGAAGAAGACACT-3'	5'-GTGTCCTTCTTCACTGA GTATTTTTTTTGCACG-3'

**Supplementary Table 3: Oligonucleotide primer for generation of mutations**

<b>Mutation</b>	<b>Mutagenesis primer</b>
MALT1 V81R	5'-CAGTGTTCTCTTAAGCGACTGGAGCCTGAAG-3'
MALT1 L82D	5'-TTCAGGCTCGTCTACCTTAAGAGA-3'
MALT1 E75A/V81R/L82D	5'-AGGCTCATCTCTCTTAAGAGAACAACACTGCGCCAGG-3'
MALT1 E98R	5'-ACTGTGCAACCTTTTCTACCCATTAACCTTCAG-3'
MALT1 Q76A	5'-AGAGAACACGCCTCCAGGTCTAGGC-3'
MALT1 C77A	5'-TACCTTAAGAGAAGCCTGCTCCAGGTCTA-3'
BCL10 R36E	5'-TCATAGCTGAGGAACATTTTGATCATCTACGTG-3'
BCL10 R42E	5'-TTTGATCATCTAGAAGCAAAAAAATACTCAG-3'
BCL10 R49E	5'-CGTGCAAAAAAATACTCAGTGAAGAAGACACT-3'
BCL10 R42A	5'-TTTTTGCAGCTAGATGATCA-3'
BCL10 L104R	5'-TAAGTTTCCGCACTTCATCTGTAAT-3'

### 5.3 Manuscript I

**Thomas Seeholzer**, Andreas Gewies, Thomas J. O'Neill, Carina Graß, Katrin Demski, Aurelia Weber & Daniel Krappmann (in preparation).

**Homoeostatic control of MALT1 protease activity by the ubiquitin ligase TRAF6.**

*In preparation.*

# **Homoeostatic control of MALT1 protease activity by the ubiquitin ligase TRAF6**

Thomas Seeholzer<sup>1</sup>, Andreas Gewies<sup>1</sup>, Thomas J. O'Neill<sup>1</sup>, Carina Graß<sup>1</sup>, Katrin Demski<sup>1</sup>, Aurelia Weber<sup>1</sup> and Daniel Krappmann<sup>1,\*</sup>

1 Research Unit Cellular Signal Integration, Institute of Molecular Toxicology and Pharmacology, Helmholtz Zentrum München - German Research Center for Environmental Health, Ingolstaedter Landstr. 1, 85764 Neuherberg, Germany

\* Corresponding Author:

Phone: +49 (0)89 3187 3461

FAX: +49 (0)89 3187 3449

daniel.krappmann@helmholtz-muenchen.de

## Abstract

MALT1 couples proximal T cell receptor (TCR) engagement to downstream signaling pathways in T lymphocytes, where it serves a dual function. By acting as a molecular scaffold, MALT1 recruits the E3 ligase TRAF6 to the CARD11-BCL10-MALT1 (CBM) complex to trigger canonical IKK (I $\kappa$ B kinase)/NF- $\kappa$ B signaling. Concurrently, induction of MALT1 protease activity leads to cleavage of distinct substrates to augment T cell activation. How scaffolding and protease functions of MALT1 are integrated has remained elusive. Here, we identified the E3 ubiquitin ligase TRAF6 as a negative regulator that maintains MALT1 protease in an inactive state in T cells prior to antigenic stimulation. While TCR/CD28-induced NF- $\kappa$ B activation is defective in TRAF6-deficient Jurkat or primary CD4 T cells, MALT1 protease function is constitutively active in the absence of TRAF6 leading to chronic cleavage of MALT1 substrates. Analogously, disruption of the MALT1-TRAF6 interaction by mutation of TRAF6 binding motifs (T6BMs) in MALT1 induces chronic MALT1 substrate cleavage in T cells. While canonical NF- $\kappa$ B signaling is lost when TRAF6 cannot be recruited to MALT1, MALT1 proteolytic activity is essential for optimal activation of distinct target genes such as *NFKB1Z* and *IL-2*. Thus, the data define a dual function of TRAF6: it not only channels the CBM complex to canonical NF- $\kappa$ B, but is also involved in the homeostatic control of MALT1 paracaspase activity. Chronic MALT1 protease activity in the absence of TRAF6 may explain the hitherto unexplained autoimmune and inflammatory phenotype of mice lacking TRAF6 in T cells.

## Introduction

In adaptive immunity, immune stimulation of the T cell receptor (TCR) triggers lymphocyte activation, proliferation and effector functions (Thome et al. 2010). Concomitant with formation of the CARMA1/CARD11-BCL10-MALT1 (CBM) complex, MALT1 scaffolding function leads to activation of the canonical I $\kappa$ B kinase (IKK)/nuclear factor- $\kappa$ B (NF- $\kappa$ B) and JNK signaling pathway (Meininger and Krappmann 2016). Binding of the E3 ubiquitin ligase TRAF6 (tumor-necrosis factor associated receptor-associated factor 6) promotes K63-linked polyubiquitination of MALT1, thereby facilitating activation of the IKK (I $\kappa$ B kinase) complex (Duwel et al. 2009; Oeckinghaus et al. 2007; Sun et al. 2004). Active IKK $\beta$  phosphorylates the NF- $\kappa$ B inhibitor I $\kappa$ B $\alpha$ , triggering its degradation and releasing NF- $\kappa$ B for its nuclear import (Hayden and Ghosh 2012; Oeckinghaus and Ghosh 2009). Consequently, MALT1 knockout (KO) mice are impaired in NF- $\kappa$ B activation and show severe defects in adaptive immunity.

Beyond its scaffolding function, MALT1 confers proteolytic activity to the CBM complex (Coornaert et al. 2008; Rebeaud et al. 2008). Via its paracaspase domain, MALT1 induces cleavage of substrates

such as the deubiquitinases A20 and CYLD, the RNA regulators Regnase-1 (also known as Zcc3h12a or MCPIP1) and Roquin-1 and -2, or the linear ubiquitin chain assembly complex (LUBAC) subunit HOIL-1, thereby modulating positive and negative regulators of NF- $\kappa$ B signaling and post-transcriptional regulation (Coornaert et al. 2008; Jeltsch et al. 2014; Klein et al. 2015; Staal et al. 2011; Uehata et al. 2013). Although signaling downstream of the CBM complex is not directly controlled by MALT1 protease activity, cleavage of substrates is associated with a variety of functions in T cells, for instance TCR-mediated T cell proliferation and IL-2 production (Bornancin et al. 2015; Gewies et al. 2014; Jaworski et al. 2014; Yu et al. 2015). Interestingly, MALT1 protease mutant (PM) mice develop an autoimmune phenotype. Residual immune activation by the preserved MALT1 scaffolding function accompanied by severely decreased Treg numbers and/or function causes a shift in the equilibrium from peripheral tolerance to autoimmune activation. Hence, MALT1 not only promotes immune activation, but also functions as a critical regulator of immune homeostasis.

Controversial results have been obtained regarding the role of TRAF6 for TCR/CD28-triggered signaling. TRAF6 is required for optimal NF- $\kappa$ B activation in Jurkat T cells (Oeckinghaus et al. 2007; Sun et al. 2004), and TRAF6 binding motifs (T6BMs) on MALT1 are essential for antigen-receptor mediated NF- $\kappa$ B signaling in Jurkat and primary T cells (Meininger et al. 2016; Noels et al. 2007). Alternative splicing of MALT1 leads to expression of two distinct isoforms, MALT1A and MALT1B, which differ in inclusion or exclusion of exon7 encoding an additional TRAF6 binding site (Meininger et al. 2016). While inclusion of exon7 modulates MALT1 scaffolding function by enhancing TRAF6 recruitment and NF- $\kappa$ B signaling, MALT1 protease activation is not affected (Meininger et al. 2016). In contrast, conditional ablation of TRAF6 in CD4 T cells does not affect NF- $\kappa$ B signaling, but induces severe autoimmunity (King et al. 2006), raising the question whether other E3 ligases could compensate for a loss of TRAF6. Recently, association of LUBAC and the E3 ubiquitin ligases cIAP1 and 2 to the CBM complex have been reported (Y. Yang et al. 2016a). LUBAC is the only known E3 ligase complex to date for the generation of linear ubiquitin chains (Ikeda et al. 2011; Kirisako et al. 2006), and its catalytic subunit HOIP/RNF31 was suggested to regulate TCR/CD28-dependent NF- $\kappa$ B signaling in T cells (Dubois et al. 2014; Y. K. Yang et al. 2016b).

Here, we closely investigated the influence of the E3 ligases HOIP and TRAF6 on NF- $\kappa$ B and MALT1 paracaspase activation by generating Jurkat KO T cells using CRISPR/Cas9 technology. We show that activation of MALT1 and NF- $\kappa$ B in Jurkat and murine CD4 T cells exclusively relies on TRAF6. Moreover, we demonstrate an additional function of TRAF6 in maintaining MALT1 in an inactive state in resting T cells and thus in the homeostatic control of MALT1 paracaspase activity.

## Results

### **MALT1 signaling and activity is not relying on HOIP and cIAP1/2.**

To better understand how MALT1 catalytic activity is regulated in T cells, we performed a PMA/Ionomycin (P/I)-induced kinetic in Jurkat T cells and assessed CBM-complex formation, NF- $\kappa$ B signaling and MALT1 protease activation (Fig. 1a). P/I stimulation circumvents upstream TCR signaling by directly activating PKC $\theta$  and increasing cytosolic calcium levels. Immunoprecipitation (IP) of BCL10 revealed that formation of the CBM-complex occurred within approximately five minutes of stimulation, peaked around twelve minutes and was disassembled after 90-240 minutes. NF- $\kappa$ B signaling was maximal after 12-30 minutes of stimulation, as evident from degradation of the inhibitor I $\kappa$ B $\alpha$ . To detect and capture activated MALT1, we used a biotinylated MALT1 activity-based probe (ABP) followed by biotin pulldown (PD) (Eitelhuber et al. 2015). Additionally, we assessed MALT1 protease activity by substrate cleavage (CYLD and Regnase-1). Activation of MALT1 was slightly delayed compared to CBM-complex formation, but showed prolonged activity, independent of the presence of the CBM signalosome (Fig. 1a). Further, cleavage of substrates coincided with the detection of ABP-labelled active MALT1. Interestingly, truncated substrate fragments persisted for up to four hours of stimulation, even though active MALT1 was only detectable up to two hours.

Recently, a role for LUBAC in NF- $\kappa$ B activation during T cell activation was described (Dubois et al. 2014; Y. K. Yang et al. 2016b). However, its potential to regulate CBM-dependent NF- $\kappa$ B and MALT1 paracaspase activation has not been thoroughly investigated yet. To evaluate if HOIP/RNF31, the catalytic subunit of LUBAC, regulates NF- $\kappa$ B and MALT1 catalytic activity in T cells, we used CRISPR/Cas9 technology to generate HOIP KO Jurkat T cells. HOIP was deleted by using a sgRNA targeting exon1 in the *HOIP/RNF31* gene (Supplementary Fig. S1a), and T cell activation was analysed in two Jurkat T cell clones lacking HOIP expression (Fig. 1b). Activation of NF- $\kappa$ B in response to P/I was slightly reduced in HOIP KO cells compared to parental Jurkat T cells. In contrast, MALT1 catalytic activity was slightly increased, as evident from MALT1 ABP PD and cleavage of the substrates CYLD and Regnase-1. Of note, cleavage of LUBAC subunit HOIL-1 was severely reduced, indicating that LUBAC integrity is required for HOIL-1 recruitment and MALT1-catalyzed cleavage.

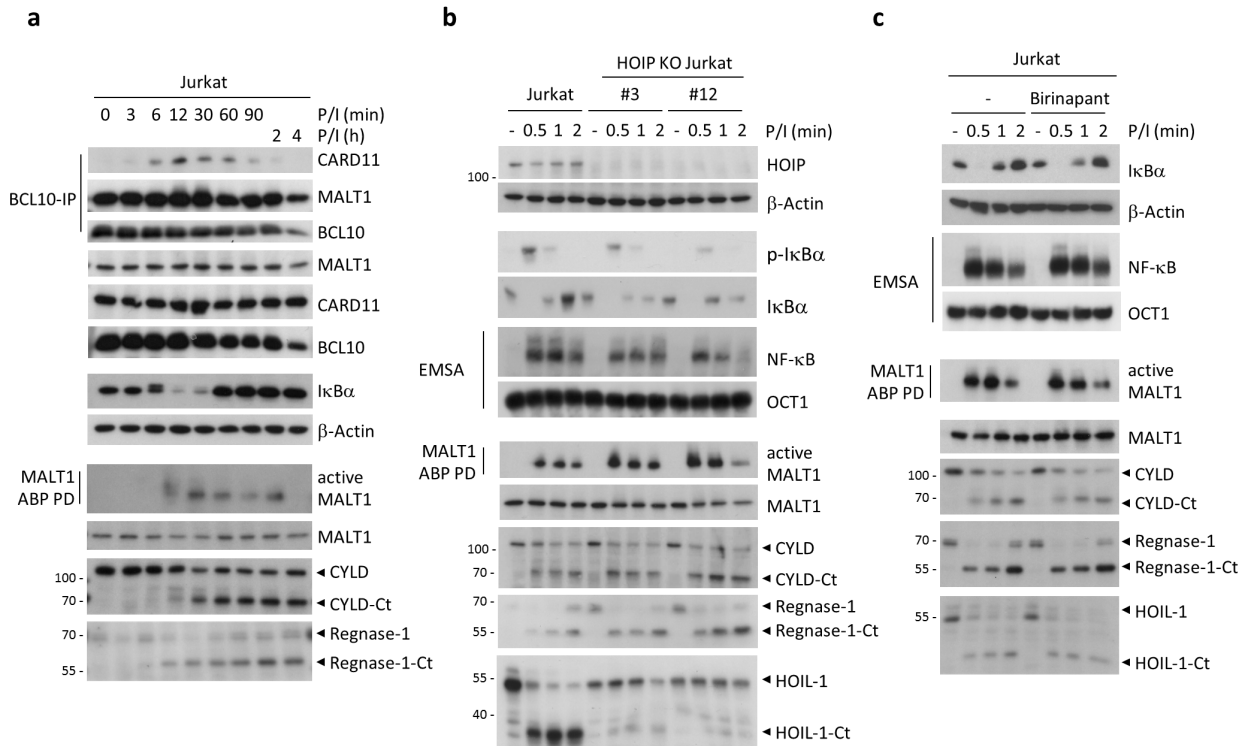


**Fig. 1 | LUBAC does not regulate MALT1 activity in Jurkat T cells.** **a**, Jurkat T cells were stimulated with PMA/Ionomycin (P/I) for the indicated times and CBM complex assembly assessed by BCL10-IP. IκBα phosphorylation and degradation were analysed by western blot (WB) and NF-κB DNA binding was determined by electrophoretic mobility shift assay (EMSA). Active MALT1 prior or after stimulation was detected in extracts with biotin-labelled MALT1-ABP and MALT1-ABP pull-down (PD) followed by WB. Cleavage of MALT1 substrates (CYLD, Regnase-1) was detected by WB. **b**, Jurkat and HOIP KO Jurkat T cells (clone #3 and #12) were treated with P/I for the indicated times. NF-κB and MALT1 activation prior or after stimulation were monitored as described in (a). **c**, Jurkat T cells were pre-treated with Birinapant (2.5μM) for ten minutes and stimulated with P/I for the indicated times. Activation of NF-κB and MALT1 was detected as described in (a).

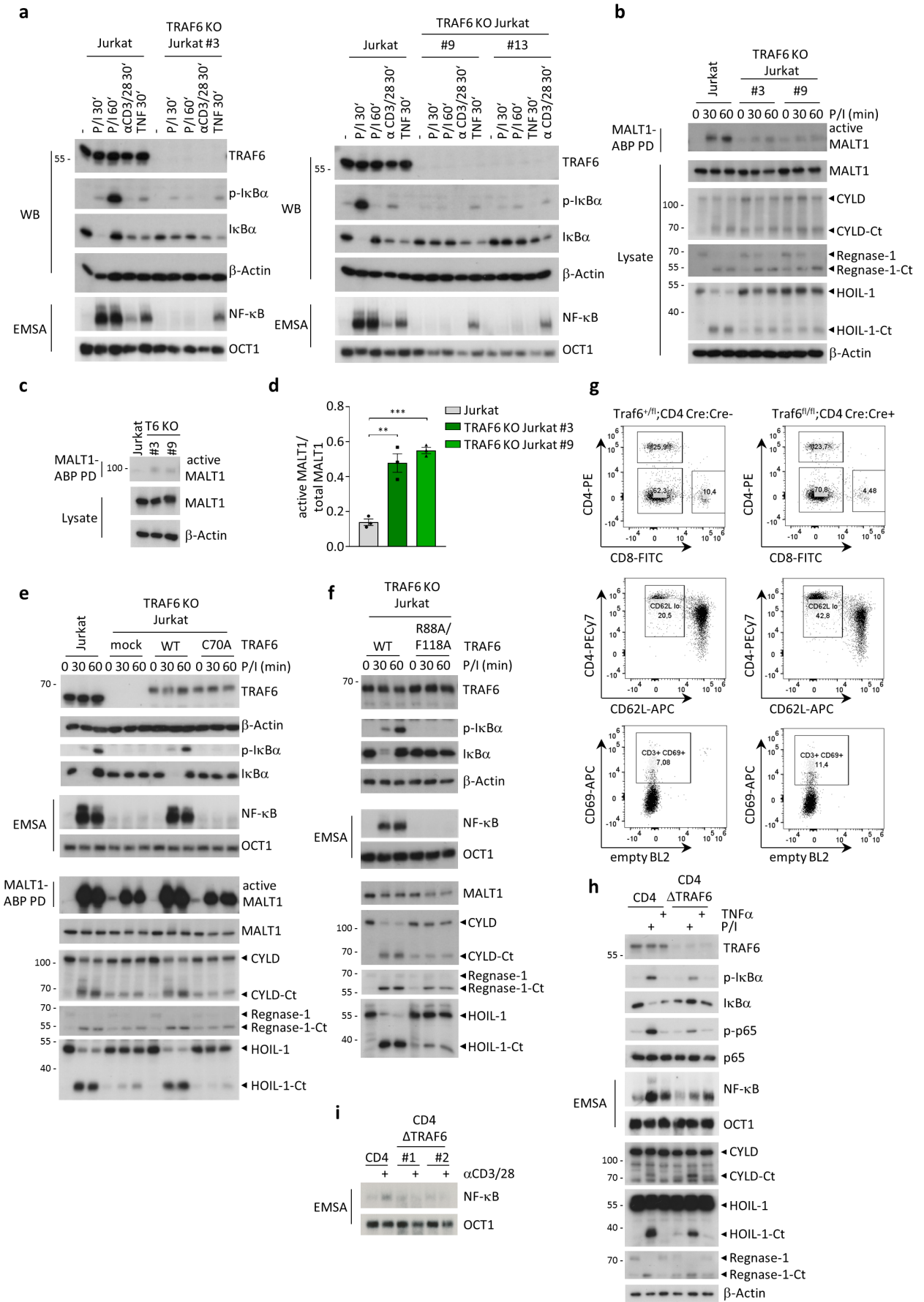
Next, we tested a possible involvement of cIAP1 and 2 in Jurkat T cells on NF-κB and MALT1 catalytic activity. For inhibition of cIAP1 and 2 in Jurkat T cells, we used the second mitochondrial-derived activator of caspases (SMAC) mimetic Birinapant (Allensworth et al. 2013). Indeed, Birinapant treatment of Jurkat T cells induced degradation of cIAP1, while cIAP2 is not expressed in Jurkat T cells (Supplementary Fig. S1b). Birinapant treatment and depletion of cIAP1 did not affect P/I-induced NF-κB or MALT1 activation in Jurkat T cells (Fig. 1c), emphasizing that neither HOIP nor cIAPs significantly contribute to downstream effects of the CBM complex in Jurkat T cells.

### Loss of TRAF6 abolishes NF-κB signaling and induces constitutive MALT1 protease activity in T cells

While TRAF6 knock-down decreases TCR/CD28-triggered NF-κB signaling in Jurkat T cells (Oeckinghaus et al. 2007), TRAF6 ablation in T cells does not impact NF-κB activation (King et al. 2006). To re-evaluate the role of TRAF6 in NF-κB signaling and to test its effect on MALT1 protease

activation, we generated TRAF6 KO Jurkat T cells by CRISPR/Cas9 technology. TRAF6 was deleted by using two sgRNAs targeting exon1 and exon2, respectively (Supplementary Fig. S2a), and several clones were obtained displaying complete loss of TRAF6 protein expression (Fig. 2a). Indeed, TRAF6 deficiency in three independent Jurkat T cell clones abolished P/I- and  $\alpha$ CD3/28-induced NF- $\kappa$ B signaling. In contrast, CBM-independent activation of NF- $\kappa$ B in response to TNF $\alpha$  stimulation did not rely on the presence of TRAF6 (Fig. 2a).

Quite unexpectedly, loss of TRAF6 resulted in a weak but consistent chronic activation of MALT1 protease activity even in the absence of any stimulation, as evident from MALT1 ABP PD and cleavage of the MALT1 substrates CYLD, Regnase-1 and HOIL-1 (Fig. 2b). Interestingly, chronic MALT1 activity was only slightly enhanced upon P/I stimulation. To confirm these findings, we quantified the amount of active MALT1 precipitated by MALT1 ABP PD in unstimulated conditions and found a consistent 2.5 – 3 fold increase in the TRAF6 KO Jurkat T cell clones compared to parental Jurkat T cells (Fig. 2c and d). Thus, the data indicate that TRAF6 not only channels the CBM complex to canonical NF- $\kappa$ B, but is also involved in the homeostatic control of MALT1 activity. To assess if the E3 ligase activity and C-terminal oligomerization of TRAF6 is required for controlling NF- $\kappa$ B signaling and MALT1 protease activity, we rescued TRAF6 KO Jurkat T cells by lentiviral transduction and obtained comparable infection rates as judged by the co-expressed surface marker  $\Delta$ CD2 (Supplementary Fig. S2b). In addition to TRAF6 wild type (WT), we introduced the TRAF6 C70A point mutant, which abrogates the TRAF6-UBC13 interaction and therefore E3 ligase activity, and the TRAF6 R88A/F118A dimerization-deficient mutant (Lamothe et al. 2008; Walsh et al. 2008; Yin et al. 2009). Flag-StrepTagII-TRAF6 WT and mutants were expressed at equivalent amount below endogenous TRAF6 levels in parental Jurkat T cells (Fig. 2e and f). While TRAF6 WT completely rescued NF- $\kappa$ B signaling upon P/I-stimulation to a level comparable to parental Jurkat T cells (Fig. 2e), neither the TRAF6 C70A (Fig. 2e) nor R88A/F118A (Fig. 2f) mutants were able to restore NF- $\kappa$ B activation. Moreover, constitutive MALT1 protease activity as seen by MALT1-ABP PD and substrate cleavage in Jurkat T cells lacking TRAF6 (mock) was lost after re-introduction of TRAF6 (Fig. 2e and f). Full substrate cleavage was obtained after transduction of TRAF6 WT, confirming that both effects are indeed caused by the loss of TRAF6. Again, this effect could not be reverted by the E3 ligase mutant TRAF6 C70A (Fig. 2e) or the dimerization mutant TRAF6 R88A/F118A (Fig. 2f). Hence, induction of canonical NF- $\kappa$ B as well as homeostatic control of MALT1 protease activity by TRAF6 is reliant upon the recruitment of UBC13 to TRAF6 and the N-terminal homo-dimerization of TRAF6.



Mice with conditional deletion of TRAF6 in CD4 T cells (Traf6- $\Delta$ T) have previously been generated, and *ex vivo* stimulation did not show significant alterations in NF- $\kappa$ B signaling upon  $\alpha$ CD3/CD28 or P/I stimulation (King et al. 2006). Given the severe defects in NF- $\kappa$ B and the chronic MALT1 protease activity upon TRAF6 ablation in Jurkat T cells, we wanted to revisit T cell signaling in a murine model where TRAF6 is conditionally deleted in CD4 T cells (Traf6<sup>fl/fl</sup>;CD4-Cre). While King et al. reported splenomegaly and severe multi-organ inflammation in ten week old Traf6- $\Delta$ T mice (King et al. 2006), we did not observe such phenotypes in mice up to the age of 20 weeks (data not shown). Nevertheless, as observed earlier, Traf6<sup>fl/fl</sup>;CD4-Cre mice displayed a decrease in the percentage of CD8 T cells and an increase in activated (CD69<sup>+</sup>) and effector-memory (CD44<sup>hi</sup>, CD62L<sup>lo</sup>) CD4 T cell percentages compared to TRAF6<sup>+/fl</sup>;CD4-Cre control mice at seven weeks of age (Fig. 2g). The absence of severe inflammation may be attributed to different housing conditions. We stimulated CD4 T cells purified from Traf6<sup>+/fl</sup>;CD4-Cre and Traf6<sup>fl/fl</sup>;CD4-Cre mice for *ex vivo* analyses of T cell signaling. As expected, TRAF6 expression is lost in CD4 T cells of Traf6<sup>fl/fl</sup>;CD4-Cre mice (Fig. 2h). Moreover, reminiscent of the situation in TRAF6 KO Jurkat T cells, canonical NF- $\kappa$ B signaling in response to P/I (Fig. 2h) or  $\alpha$ CD3/CD28 (Fig. 2i) stimulation, as evident from I $\kappa$ B $\alpha$  phosphorylation and degradation as well as p65 phosphorylation and NF- $\kappa$ B binding, is strongly diminished in the absence of TRAF6. Of note, NF- $\kappa$ B binding in response to TNF $\alpha$  stimulation was independent of TRAF6 (Fig. 2h). Moreover, stimulus-dependent activation of MALT1 was independent of TRAF6, while ablation of TRAF6 in CD4 T cells induced constitutive activation of the MALT1 cleavage of the substrates CYLD, HOIL-1 and Regnase-1 (Fig. 2h). Thus, TRAF6 is critical for TCR-induced NF- $\kappa$ B signaling in Jurkat and primary T cells, and at the same time loss of TRAF6 induces chronic proteolytic activity and substrate cleavage by MALT1 in T cells.

---

**Fig. 2 | TRAF6 is essential for NF- $\kappa$ B signaling and regulation of MALT1 activity in T cells.** **a**, Jurkat and TRAF6 KO Jurkat T cells (clone #3, #9 and #13) were stimulated with P/I,  $\alpha$ CD3/28 or TNF $\alpha$  for the indicated times. I $\kappa$ B $\alpha$  phosphorylation and degradation were analysed by WB and NF- $\kappa$ B DNA binding was assessed by electrophoretic mobility shift assay (EMSA). **b**, Jurkat and TRAF6 KO cells (clone #3 and #9) were stimulated with P/I as indicated. Active MALT1 was detected with biotin-labelled MALT1-ABP and MALT1-ABP pulldown, followed by WB. Cleavage of MALT1 substrates (CYLD, Regnase-1, HOIL-1) was assessed by WB. **c**, Detection of active MALT1 in unstimulated Jurkat and TRAF6 KO extracts after MALT1-ABP PD, analysed by WB. **d**, Quantification of active MALT1 relative to total MALT1 from unstimulated Jurkat and TRAF6 KO extracts after MALT1-ABP pulldown (mean  $\pm$  s.e.m.; n=3; \*\* $p \leq 0.01$ ; \*\*\* $p \leq 0.001$ ). **e, f** Jurkat and TRAF6 KO cells transduced with StrepTagII (mock) and TRAF6 variants (WT, C70A and R88A/F118A) were stimulated with P/I for the times indicated. NF- $\kappa$ B signaling was analysed by WB and EMSA. Active MALT1 was detected by cleavage of MALT1 substrates (**e, f**) and MALT1-ABP PD (**e**), followed by WB. **g**, Percentages of CD4 and CD8 T cells, and activated CD4 T cells in seven week old Traf6<sup>fl/fl</sup>;CD4 Cre:Cre+ mice compared to Traf6<sup>+/fl</sup>;CD4 Cre:Cre- control animals. Expression of CD44 and CD62L, gated on live CD4, and CD69, gated on live CD3+, was determined by FACS. **h**, Purified CD4 splenic T cells from littermate control (CD4) or Traf6<sup>fl/fl</sup>;CD4 Cre:Cre+ mice (CD4  $\Delta$ TRAF6) were stimulated with P/I or TNF $\alpha$  for 30 minutes. Active MALT1 was assessed by cleavage of substrates (CYLD, HOIL-1 and Regnase-1) on WB. NF- $\kappa$ B activity was monitored by WB (phosphorylation of I $\kappa$ B $\alpha$  and p65) and EMSA. **i**, Purified CD4 splenic T cells from littermate control (CD4) or Traf6<sup>fl/fl</sup>;CD4 Cre:Cre+ mice (CD4  $\Delta$ TRAF6 #1 and #2) were stimulated with  $\alpha$ CD3/28 for 30 minutes and NF- $\kappa$ B activity assessed by EMSA.

## **Recruitment of TRAF6 to MALT1 activates NF- $\kappa$ B and maintains MALT1 in an inactive state**

Three TRAF6 binding motifs (T6BMs) in MALT1 exist that surround the paracaspase domain, with one found in between the Ig2 and paracaspase domain (T6BM1) and two located in the C-terminus (T6BM2 and T6BM3) (Noels et al. 2007; Sun et al. 2004) (Fig. 3a). Only T6BM1 and T6BM3 have been shown to serve as functional TRAF6 binding motifs that control NF- $\kappa$ B signaling in T cells (Meininger et al. 2016). Interestingly, exon7 (aa309-319), containing T6BM1, is prone to alternative splicing and only the longer splice variant MALT1A (824 aa) encodes both T6BM1 and T6BM3, while MALT1B (813 aa) only contains TBM3 (Meininger et al. 2016). To analyse if association of TRAF6 to MALT1 is critical to maintain the MALT1 protease in an inactive state, we investigated the effect of mutating T6BM1 and T6BM3 in MALT1A (E316A/E806A) or T6BM3 in MALT1B (E795A) (Meininger et al. 2016) (Fig. 3a). Viral reconstitution led to equivalent expression of all MALT1 constructs at near endogenous levels (Fig. 3b) (Meininger et al. 2016). MALT1A or MALT1B rescued NF- $\kappa$ B signaling upon P/I-stimulation as evident from I $\kappa$ B $\alpha$  degradation, and NF- $\kappa$ B signaling was completely depending on the functionality of the T6BMs (Fig. 3b). Congruent with the observations in TRAF6-deficient T cells, mutation of the T6BM1/3 in MALT1A or T6BM3 in MALT1 B provoked chronic cleavage of the MALT1 substrates CYLD, Regnase-1 and HOIL-1 (Fig. 3b).

To evaluate the molecular requirements for the chronic activation of MALT1 protease upon loss of TRAF6 binding sites in detail, we generated a series of MALT1 mutants that eliminate BCL10-MALT1 association (MALT1B V81R), abolish the MALT1 dimerization interface (MALT1B K513E) or prevent MALT1 mono-ubiquitination (MALT1B K633R) (Cabalzar et al. 2013; Pelzer et al. 2013; Schlauderer et al. 2018; Wiesmann et al. 2012). Again, viral transduction into MALT1 KO Jurkat T cells led to equivalent expression of MALT1B mutant constructs that contain the mutations alone or in combination with the T6BM E795A mutation (Supplementary Fig. S3a, b). As expected, all mutations abolished (V81R and K513E) or severely reduced (K633R) MALT1 protease activation in response to P/I stimulation as determined by MALT1 ABP PD and substrate cleavage (Fig. 3c and d). Additionally, NF- $\kappa$ B activation upon stimulation was compromised in the E795A and V81R, but not in K513E and K633R mutations, as evident from I $\kappa$ B $\alpha$  degradation. CBM-independent ERK signaling was still functional in all mutants. Moreover, chronic MALT1 activity and substrate cleavage by the lack of TRAF6 association in the T6BM mutant MALT1B E795A was also entirely abrogated by preventing MALT1-BCL10 association (V81R/E795A), MALT1 dimerization (K513E/E795A) or MALT1 mono-ubiquitination (K633R/E795A). Thus, chronic MALT1 proteolytic activity relies on the same mechanisms as inducible MALT1 catalytic activity following T cell activation.

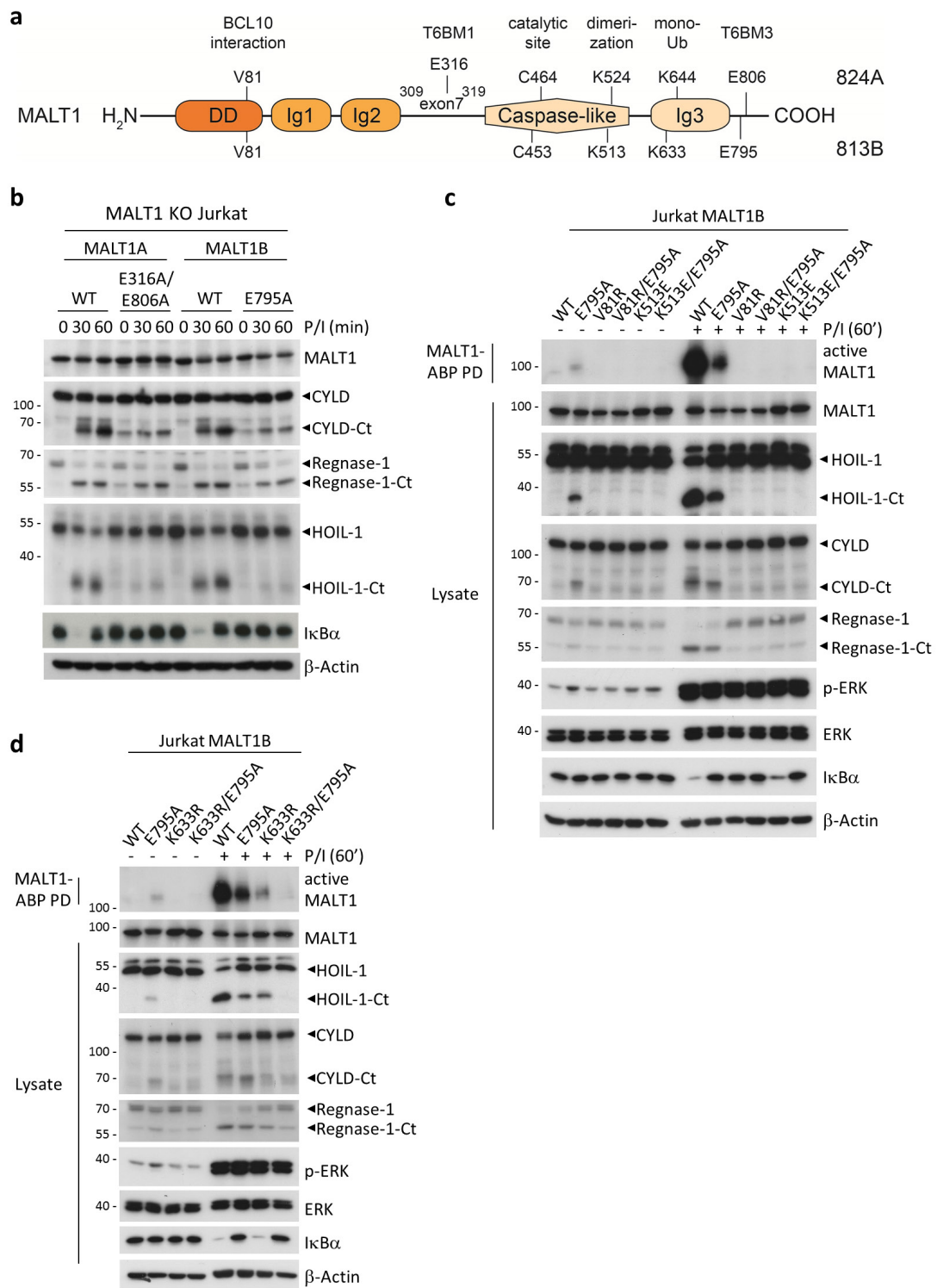


**Fig. 3 | Mutation of TRAF6 binding motifs (T6BMs) in MALT1 induces constitutive MALT1 paracaspase activation.** **a**, Domain structure of MALT1 isoform A and B. TRAF6 binding motifs (T6BMs), BCL10 binding, catalytic, dimerization and monoubiquitination sites are indicated. Protein domains are marked by coloured boxes. DD, death domain, Ig, Immunoglobulin-like domain. **b**, MALT1 KO Jurkat cells were reconstituted with MALT1A and MALT1B wildtype or T6BM mutants, stimulated with P/I for the indicated times, and degradation of IκBα and cleavage of MALT1 substrates assessed by WB. **c, d**, MALT1 KO Jurkat cells were reconstituted with MALT1B wildtype, T6BM mutant (E795A), BCL10 binding mutant (V81R), or MALT1 dimerization mutant (K513E) (**c**) and MALT1 monoubiquitination mutant (K633R) (**d**) solely or in combination with the T6BM mutant (E795A). Cells were tested for active MALT1 prior or after P/I stimulation for 60 minutes in extracts with biotin-labelled MALT1-ABP and MALT1-ABP PD, followed by WB. Cleavage of MALT1 substrates (CYLD, Regnase-1, HOIL-1) was detected by WB.

## **Chronic substrate cleavage in T6BM mutants depends on MALT1 catalytic activity**

MALT1 proteolytic activity is mediated by the active site C453 (MALT1B) in the active center of the paracaspase domain (Wiesmann et al. 2012). To test if constitutive cleavage of substrates is catalysed by the MALT1 active center, we reconstituted MALT1 KO Jurkat T cells with T6BM mutants alone or in combination with a catalytically inactive form (C453A/E795A) (Supplementary Fig. S4a, b). Again, we could label active MALT1 with MALT1-ABPs in the TRAF6 binding mutants of both isoforms in the unstimulated state, while the corresponding WT constructs showed no active MALT1 or substrate cleavage (Fig. 4a, b). Mutation of the catalytic cysteine C453A in MALT1B E795A completely abrogated MALT1 activity, highlighting that indeed MALT1 protease activity is induced. Of note, MALT1B with its single T6BM displayed significantly higher chronic MALT1 activity compared to MALT1A containing two T6BMs (Fig. 4b). In agreement with these results, chronic activity was inhibited by the allosteric MALT1 inhibitor (S)-Mepazine (Nagel et al. 2012), as evident from the absence of the CYLD cleavage fragment (Fig. 4c).

To investigate if CYLD is cleaved by constitutively active MALT1 at its canonical cleavage site R324 as previously described (Staal et al. 2011), we transiently expressed E-Tag CYLD WT or R324A in MALT1 KO Jurkat T cells stably reconstituted with MALT1A and MALT1B WT with or without the respective T6BM mutations (Fig. 4d and e). In cells with MALT1A and MALT1B WT, overexpressed CYLD was cleaved exclusively upon P/I stimulation. As expected, CYLD R324A was resistant to MALT1-catalyzed cleavage. Importantly, E-Tag CYLD was constitutively cleaved in Jurkat T cells expressing MALT1A E316A/E806A or MALT1B E795A and cleavage was not further increased by P/I-stimulation. Again, constitutive cleavage of CYLD was completely depending on R342 (Fig. 4d and e). Hence, constitutively active MALT1 relies on its catalytic center and targets the previously identified canonical cleavage site in CYLD.

Despite the fact that the putative T6BM2 is not involved in mediating NF- $\kappa$ B signaling downstream of MALT1 (Meininger et al. 2016; Noels et al. 2007), we wanted to ensure that it is not involved in counteracting chronic MALT1 activity, since it is positioned in the vicinity of the paracaspase domain. Indeed, expression of MALT1B T6BM2 mutant E642A behaved like MALT1B WT in promoting I $\kappa$ B $\alpha$  degradation and preventing constitutive CYLD substrate cleavage (Fig. 4f). Further, chronic MALT1 activity was not further enhanced in the MALT1B E642A/E795A double mutant compared to the MALT1B E795A mutant (Fig. 4f).

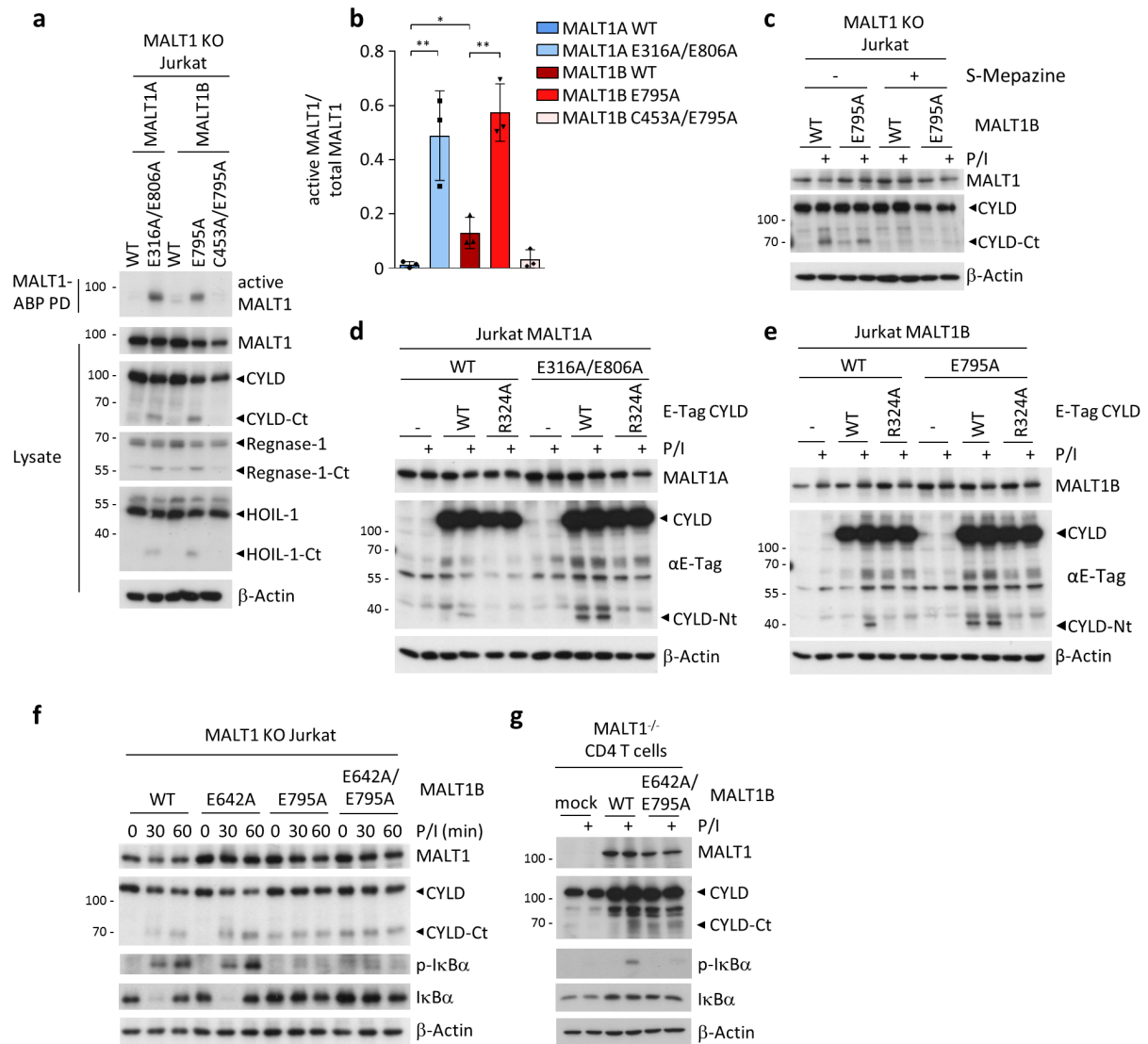


**Fig. 4 | Constitutive substrate cleavage by MALT1 in T6BM mutants relies on its catalytic activity.** **a**, MALT1 KO Jurkat T cells reconstituted with MALT1A and MALT1B wildtype, T6BM mutants or MALT1B catalytic inactive/T6BM double mutant (C453A/E795A) were tested for active MALT1 during basal conditions in extracts with biotin-labelled MALT1-ABP and MALT1-ABP PD, followed by WB. Cleavage of MALT1 substrates (CYLD, Regnase-1, HOIL-1) was detected by WB. **b**, Active MALT1 quantified relative to total MALT1 from unstimulated reconstituted MALT1 KO cell extracts after MALT1-ABP pulldown (mean  $\pm$  s.e.m.;  $n=3$ ; \* $p \leq 0.05$ ; \*\* $p \leq 0.01$ ). **c**, MALT1 KO Jurkat MALT1B WT or T6BM mutant (E795A) reconstituted cells untreated or incubated with S-Mepazine (10  $\mu$ M) for four hours prior to P/I stimulation for 30 minutes. Cleavage of CYLD was assessed by WB. **d**, **e** Transient expression of E-tagged CYLD (WT or R324A) in MALT1A (**d**) or MALT1B (**e**) wildtype or T6BM mutant reconstituted MALT1 KO Jurkat cells. Cleavage of CYLD was assessed after P/I stimulation for 30 minutes on WB with an  $\alpha$ E-Tag antibody targeting the N-terminal (Nt) part of the protein. **f**, MALT1 KO Jurkat T cells transduced with MALT1B WT or MALT1B T6BM mutants were stimulated with P/I for the indicated times. NF- $\kappa$ B (phosphorylation and degradation of I $\kappa$ B $\alpha$ ) and MALT1 proteolytic activity (CYLD cleavage) were determined by WB. **g**, CD4 T cells from MALT1-deficient mice (C57/BL6N) were retrovirally reconstituted with mock, MALT1B WT or MALT1B E642A/E795A T6BM mutant. Transduced cells were enriched and purified by MACS sorting. MALT1 expression levels, phosphorylation of I $\kappa$ B $\alpha$  and cleavage of CYLD were determined by WB.

To confirm the effect of constitutive CYLD cleavage by MALT1B T6BM mutants in primary T cells, we purified CD4 T cells from MALT1-deficient mice and retrovirally transduced with StrepTagII (mock) control, MALT1B WT or MALT1B E642A/E795A. After expansion of T cells, reconstituted cells were enriched using the cell surface marker Thy1.1 (Supplementary Fig. 4c). P/I-induced phosphorylation

of I $\kappa$ B $\alpha$  and cleavage of CYLD was absent in MALT1-deficient CD4 T cells, while reconstitution with MALT1B WT rescued NF- $\kappa$ B signaling and MALT1 protease activity (Fig. 4g). Reconstitution with MALT1B E642A/E795A could not rescue NF- $\kappa$ B activation, but indeed constitutive cleavage of CYLD was induced and this process was not enhanced upon P/I stimulation. Thus, also in primary murine T cells, binding of TRAF6 to MALT1 counteracts chronic MALT1 protease activity.

### **MALT1 scaffolding and protease function orchestrates target gene induction in T cells**

To assess the involvement of MALT1 scaffolding and protease on NF- $\kappa$ B-induced gene transcription, we stably expressed an NF- $\kappa$ B-EGFP reporter in parental or MALT1 KO Jurkat T cells. While EGFP expression was induced in parental Jurkat T cells upon P/I or  $\alpha$ CD3/28 treatment, MALT1 KO Jurkat T cells failed to upregulate the NF- $\kappa$ B-EGFP reporter in response to both T cell stimuli (Supplementary Fig. S5a). To evaluate the requirements of TRAF6 binding and/or MALT1 catalytic activity for NF- $\kappa$ B-dependent gene induction, MALT1 KO Jurkat reporter T cells were reconstituted with MALT1 WT or respective T6BM or catalytic site mutants (Supplementary Figure S5b, c). As seen for MALT1 KO Jurkat T cells, CBM-independent activation of the NF- $\kappa$ B-EGFP reporter by TNF $\alpha$  was not affected by the absence of or missense mutations in MALT1 (Supplementary Fig. S5a, d). While MALT1A or MALT1B WT rescued NF- $\kappa$ B activation upon P/I or  $\alpha$ CD3/28 stimulation, T6BM mutants of MALT1A (E316A/E806A) and MALT1B (E795A) were unable to induce the EGFP reporter (Fig. 5a; Supplementary Fig. S5e, f). In contrast, MALT1B C453A rescued reporter gene induction to the same degree as MALT1B WT, underscoring that catalytic activity of MALT1 is not required for NF- $\kappa$ B transcriptional activity (Fig. 5a). As expected, the double mutant MALT1B C453A/E795A was unable to induce EGFP expression upon stimulation. Thus, usage of an artificial NF- $\kappa$ B reporter proves that direct transcriptional NF- $\kappa$ B gene induction relies on TRAF6 recruitment by MALT1, but not on MALT1 protease activity.

We wanted to evaluate the impact of MALT1 scaffolding versus protease function on induction of two individual target genes *NFKBIA*/I $\kappa$ B $\alpha$  and *NFKBIZ*/I $\kappa$ B $\zeta$ . While *NFKBIA* is a prototype immediate-early transcriptional NF- $\kappa$ B response gene (Whiteside and Israel 1997), *NFKBIZ* is also strongly regulated on the post-transcriptional level by the MALT1 substrate Regnase-1 that destabilizes *NFKBIZ* mRNA by binding to its 3'UTR (Jeltsch et al. 2014; Uehata et al. 2013). In addition, an essential role for NF- $\kappa$ B in I $\kappa$ B $\zeta$  induction upon TLR and IL-1 receptor stimulation has been described (Eto et al. 2003). While destruction of the T6BM in MALT1 E795A or C453A/E795A completely abolished induction of *NFKBIA*, protease inactive MALT1B C453A was still able to confer *NFKBIA*

upregulation, though at a reduced level when compared to MALT1B WT (Fig. 5b). Interestingly, deletion of the T6BM reduced *NFKBIZ* expression at early stimulation time points compared to WT, while, upon prolonged stimulation, MALT1B E795A mutant was able to induce equivalent *NFKBIZ* expression as MALT1B WT (Fig. 5b). In addition, *NFKBIZ* induction was strongly dependent on MALT1 catalytic activity. However,  $\text{I}\kappa\text{B}\zeta$  protein expression was only detectable in MALT1B WT reconstituted cells, which peaked after one hour of P/I-induced stimulation, but not in the mutants E795A or C453A (Fig. 5c), and underscores its dependency on both MALT1 scaffold and protease function. Thus, the data define *NFKBIZ*/ $\text{I}\kappa\text{B}\zeta$  as a response gene in T cells, whose fast induction relies on MALT1 scaffolding and downstream NF- $\kappa$ B activation, while, upon longer stimulation, the MALT1 protease function alone is sufficient to induce its expression.

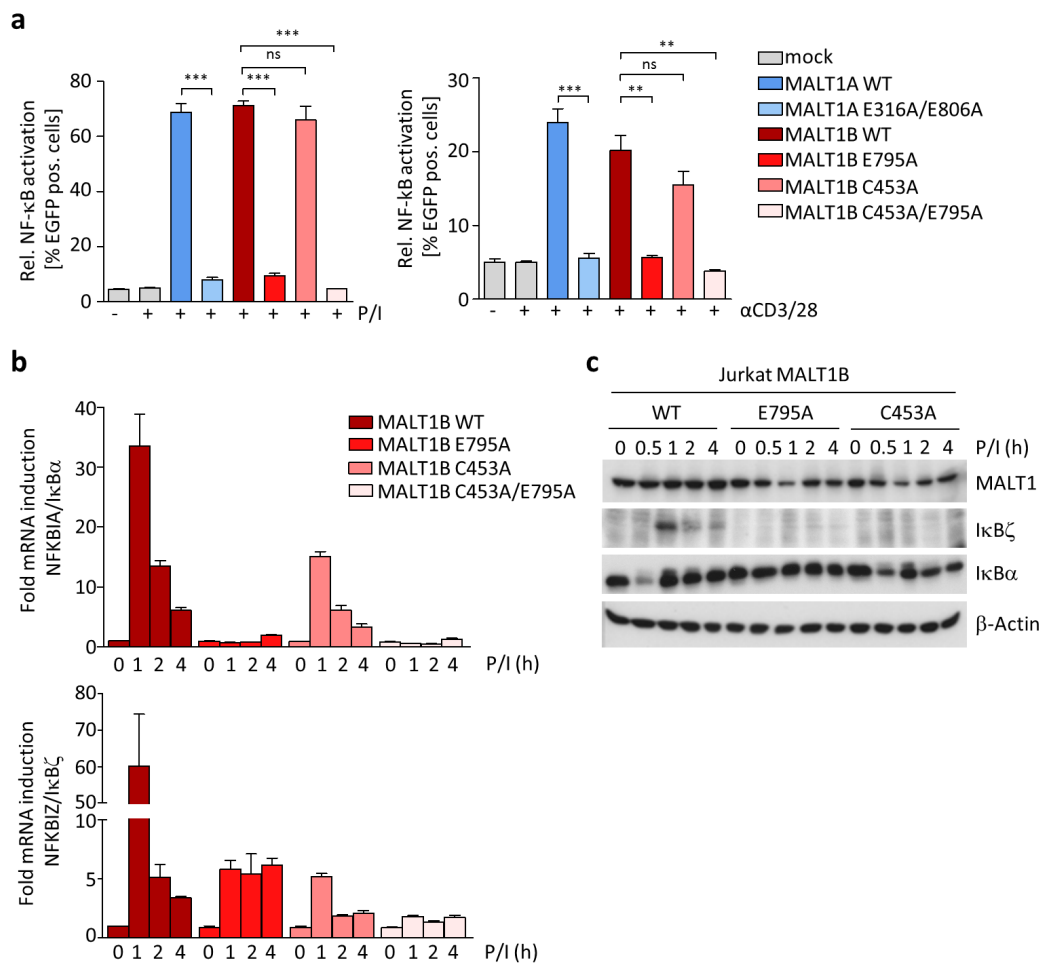


**Fig. 5 | MALT1 T6BMs influence NF- $\kappa$ B and MALT1 target gene expression.** **a**, Reconstituted MALT1 KO Jurkat T cells harbouring an NF- $\kappa$ B-EGFP reporter system were stimulated with P/I or  $\alpha$ CD3/28 for 5 hours and expression of GFP-positive cells analysed by FACS (mean  $\pm$  s.e.m.; n=3). **b**, Expression of *NFKBIA*/ $\text{I}\kappa\text{B}\alpha$  and *NFKBIZ*/ $\text{I}\kappa\text{B}\zeta$  in MALT1B wildtype (WT), T6BM mutant (E795A), catalytic inactive (C453A) or catalytic inactive/T6BM double mutant (C453A/E795A) MALT1 KO Jurkat reconstituted cells was determined by quantitative RT-PCR after stimulation with P/I for the indicated times. All values were normalized to the housekeeping gene RPII and related to MALT1B WT unstimulated samples (mean  $\pm$  s.e.m.; n=3). **c**, Protein expression of  $\text{I}\kappa\text{B}\alpha$  and  $\text{I}\kappa\text{B}\zeta$  upon P/I-stimulation for the indicated time points was determined by WB. \*\* $p \leq 0.01$ ; \*\*\* $p \leq 0.001$ ; ns, not significant.

We wanted to verify the differential requirement of MALT1 scaffolding and protease function for NF- $\kappa$ B activation and T cell activation in primary T cells. For this, primary CD4 T cells were purified from MALT1<sup>-/-</sup> mice and equivalent transduction and expression of MALT1B WT, E795A, C453A or C453A/E795A after viral reconstitution was verified by Thy1.1 staining and Western Blot (Fig. 6a, b). As expected, Thy1.1-negative MALT1<sup>-/-</sup> CD4 T cells did not degrade I $\kappa$ B $\alpha$  or significantly induce IL-2 expression upon stimulation (Supplementary Fig. S6). Just like in Jurkat T cells, NF- $\kappa$ B signaling after P/I stimulation, as detected by I $\kappa$ B $\alpha$  degradation using intracellular FACS staining, was relying on an intact C-terminal TRAF6 binding motif in MALT1B, but not the proteolytic activity (Fig. 6c, d). Since TCR/CD28-induced upregulation of IL-2 requires the concerted action of canonical NF- $\kappa$ B as well as the MALT1 protease function (Bornancin et al. 2015; Gewies et al. 2014; Jain et al. 1995; Jaworski et al. 2014), we determined intracellular IL-2 expression in MALT1B WT and mutant expressing CD4 cells as a marker for T cell activation. Reconstitution of MALT1-deficient CD4 T cells with MALT1 WT strongly enhanced expression of IL-2 in response to P/I (Fig. 6e, f) or  $\alpha$ CD3/CD28 (Fig. 6g, h) stimulation. Interestingly, while the TRAF6-binding defective MALT1B E795A only slightly decreased IL-2 induction in CD4 T cells, lack of MALT1 catalytic activity (C453A) alone had a much more pronounced effect on IL-2 production. In CD4 T cells, the combined mutation of the TRAF6-binding and the catalytic site in MALT1B C453A/E795A caused strongest reduction of IL-2 production (Fig. 6e-h). Hence, orchestrate action of MALT1 scaffolding and protease activity is required to allow optimal activation of CD4 T cells.

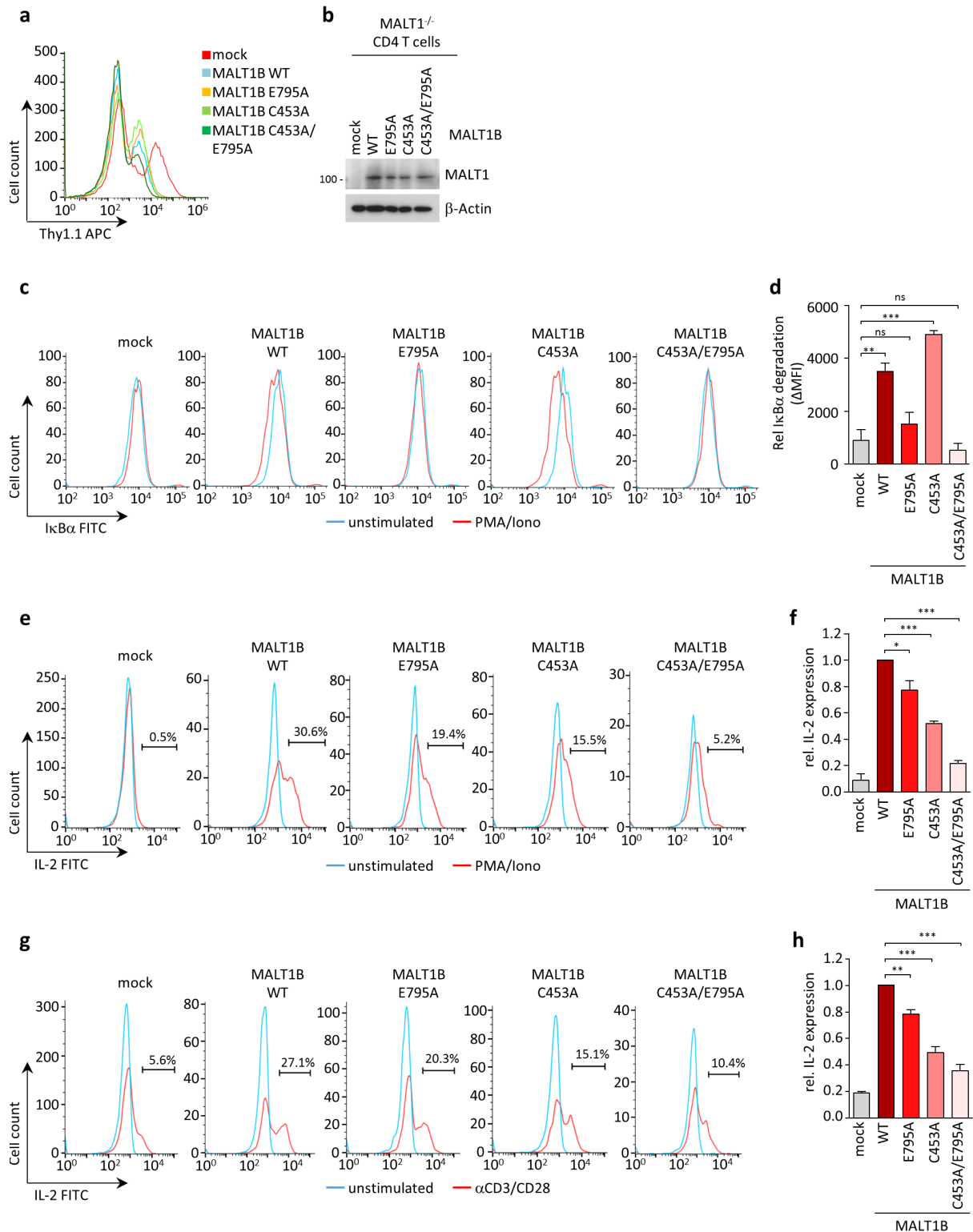


**Fig. 6 | Catalytic activity of MALT1 is critical for IL-2 expression but not NF- $\kappa$ B activation in primary CD4 T cells.** **a-h**, Primary murine MALT1<sup>-/-</sup> CD4 T cells were retrovirally reconstituted with StrepTagII (mock) or MALT1B-StrepTagII variants. **a**, Transduction efficiency of infections was evaluated by co-expression of the Thy1.1 surface marker and analysed by FACS. **b**, Protein expression of transduced cells was analysed by western blot. **c, d**, MALT1B WT or mutant transduced cells were stimulated with P/I for 30 minutes. Expression and degradation of I $\kappa$ B $\alpha$  were measured by FACS (**c**). Transduced cells were gated by co-staining of the surface expression marker Thy1.1 (Supplementary Fig. S6). **d**, Mean  $\Delta$ MFI values from three independent experiments are shown as bar graph (mean  $\pm$  s.e.m.; n=3). **e-h**, Transduced cells were stimulated with P/I (**e, f**) or  $\alpha$ CD3/28 (**g, h**) for 5 hours, and intracellular IL-2 production determined by FACS (**e, g**). Transduced cells were gated by co-staining of Thy1.1 (Supplementary Fig. S6). Bar charts represent values from three independent experiments (**f, h**) (mean  $\pm$  s.e.m.; n=3). \* $p \leq 0.05$ ; \*\* $p \leq 0.01$ ; \*\*\* $p \leq 0.001$ ; ns, not significant.

## Discussion

MALT1 scaffold and protease function controls transduction of CBM signaling and regulation of T cell activation (Juilland and Thome 2018). Integration of TRAF6 into the CBM complex promotes MALT1 ubiquitination and further activation of the IKK complex (Oeckinghaus et al. 2007). Although it was reported that TRAF6 in T cells is dispensable for TCR-induced NF- $\kappa$ B and MAPK activation (King et al. 2006), presence of TRAF6 binding motifs (TBMs) on MALT1 is a prerequisite for proper NF- $\kappa$ B signaling (Meininger et al. 2016), leading to the hypothesis that other E3 ligases may compensate for a loss of TRAF6.

Here, we show that TCR-dependent activation of NF- $\kappa$ B is largely independent of the LUBAC component HOIP or cIAP proteins. However, by generating TRAF6-deficient Jurkat and CD4 T cells, we provide evidence that TRAF6 is indispensable for TCR-induced NF- $\kappa$ B activation, which strictly relies on interaction with UBC13 and C-terminal dimerization. Even more surprising, we determine a new role for TRAF6 in maintaining MALT1 protease inactivity in resting T cells, and either absence of TRAF6 or prevented binding of TRAF6 to MALT1 induces its chronic activation.

Contrary to our findings, King et al. did not observe defective NF- $\kappa$ B activation in response to TCR/CD28 stimulation in TRAF6 KO CD4 T cells (King et al. 2006). The reason for this discrepancy is not clear. Since TRAF6 depletion does not affect TNF $\alpha$ -dependent NF- $\kappa$ B signaling, our knockout strategy for generation of *Traf6*<sup>fl/fl</sup>;CD4-Cre mice does not lead to impairment of canonical NF- $\kappa$ B signaling upon TNF receptor stimulation. This is moreover in line with reports that TRAF6 deficiency does not interfere with TNF $\alpha$ -induced NF- $\kappa$ B activation (Lomaga et al. 1999). As previously observed, T cell-specific deletion of TRAF6 in mice decreases the percentage of CD8 T cells, while activated (CD69<sup>+</sup>) and memory (CD44<sup>hi</sup>, CD62<sup>lo</sup>) T cell populations are increased (King et al. 2006). However, we did not observe phenotypic symptoms for severe autoimmunity until 20 weeks of age, previously reported to occur in twelve week old animals lacking TRAF6 in T cells (King et al. 2006). Differential housing conditions may explain the divergent onset of the disease *in vivo*, and differences in the observed disease severity could explain the inconsistency observed in the *ex vivo* stimulation of CD4 T cells, since pre-activated T cells in heavily burdened mice might contribute to the observed effects. In line with this, reconstitution of Jurkat and murine CD4 MALT1 KO T cells with MALT1 mutated in its TRAF6 binding motifs failed to rescue NF- $\kappa$ B signaling, and thereby show the same results obtained by deletion of TRAF6. Hence, we demonstrate that TRAF6 is an essential factor for TCR-induced NF- $\kappa$ B activation in primary T cells.

Surprisingly, *Traf6<sup>fl/fl</sup>;CD4-Cre* mice develop an activated T cell phenotype in the absence of NF- $\kappa$ B. Ablation of any component of the CBM-complex abolishes NF- $\kappa$ B activation and leads to severe immunodeficiency (Egawa et al. 2003; Hara et al. 2003; Ruefli-Brasse et al. 2003; Ruland et al. 2001; Ruland et al. 2003). Therefore, an additional function of TRAF6, besides its role in NF- $\kappa$ B signaling, must account for the observed phenotype in these mice. Here, we describe a new role for TRAF6 in maintaining MALT1 in an inactive state prior to antigenic stimulation. Absence of TRAF6 leads to constitutively activated MALT1 and cleavage of substrates, and suppression of this constitutive activity depends on catalytic activity and dimerization of TRAF6. In line, preventing interaction between TRAF6 and MALT1 via mutation of T6BMs exhibits similar results. Chronic MALT1 proteolytic activity in absence of TRAF6 critically depends on MALT1-BCL10 association, MALT1 dimerization and MALT1 mono-ubiquitination, and therefore on the same mechanisms as the induced MALT1 catalytic activity upon T cell stimulation (Pelzer et al. 2013; Schlauderer et al. 2018; Wiesmann et al. 2012).

Mechanistically, MALT1 protease inactivity may be maintained prior to antigenic stimulation via the MALT1-TRAF6 interaction or post-translational modifications, either of which could prevent conformational changes within the C-terminal domains of MALT1. MALT1 dimerizes in its ligand-free form, adopting an inactive conformation where the nucleophile of the active-site cysteine is dislocated and therefore catalytically incompetent (Wiesmann et al. 2012). Substrate binding induces rearrangements of the activate site and numerous structural changes throughout the molecule, especially in the C-terminus, triggering MALT1 activation (Wiesmann et al. 2012). Since this region is involved in the interaction with TRAF6, it is tempting to speculate that binding of TRAF6 and ubiquitination of MALT1 affects the structure of the catalytic site, thereby regulating substrate recognition and turnover. For instance, monoubiquitination of MALT1A K644, which is located in an exposed loop structure, induces conformational changes in the caspase-like domain and thereby facilitates MALT1 activation (Pelzer et al. 2013; Wiesmann et al. 2012; Yu et al. 2011). Similar mechanisms could contribute to prevention of conformational changes within or in vicinity of the paracaspase domain of MALT1, thereby restricting protease activity in resting cells.

It is interesting to speculate if chronic MALT1 paracaspase activation might be causative for the development of an autoimmune phenotype in *Traf6<sup>fl/fl</sup>;CD4-Cre* mice despite compromised NF- $\kappa$ B activity. We show that optimal activation of *NFKB1Z/I $\kappa$ B $\zeta$*  critically relies on both MALT1 scaffolding and protease function. It has been shown that T cell-specific deletion of *I $\kappa$ B $\zeta$*  increases the number of IFN $\gamma$ -producing CD4 T cells in three week old mice (Maruyama et al. 2015). Regulatory T cells from these mice exhibit a diminished suppressive function, which indicates a critical role of *I $\kappa$ B $\zeta$*  in their

differentiation from naïve CD4 T cells. Recently, a critical MALT1 protease-dependent role for the CBM complex in the immune-suppressive function of Tregs was also described (Cheng et al. 2019; Di Pilato et al. 2019; Rosenbaum et al. 2019): disruption of CBM complex components or pharmacological inhibition of MALT1 protease activity leads to dysregulation of cytokine expression and induces IFN $\gamma$  secretion, thereby impairing the suppressive functions of Tregs. Interestingly, also T cell-specific Regnase-1 KO or Roquin (sanroque) mutant mice show an enhanced IFN $\gamma$ -producing cell population (Cui et al. 2017). Therefore, chronic MALT1 activity in Traf6<sup>fl/fl</sup>;CD4-Cre mice induces constitutive cleavage of Regnase-1 and Roquin, resulting in dysregulation of *NFKB1Z*/ $\text{I}\kappa\text{B}\zeta$  expression and modified IFN $\gamma$  production. Since we observed normal percentages of Treg cells compared to littermate control mice (data not shown), dysregulation of cytokine expression might diminish suppressor function of Tregs or influence activation of effector cells, which would ultimately contribute to the observed inflammatory phenotype in Traf6<sup>fl/fl</sup>;CD4-Cre mice. Interestingly, human germline-encoded MALT1 missense mutations result in loss or decreased expression of MALT1, impairing NF- $\kappa$ B activation and cell proliferation (Charbit-Henrion et al. 2017; Jabara et al. 2013; McKinnon et al. 2014; Punwani et al. 2015). However, defects in MALT1 also provoked auto-inflammatory responses reminiscent of Traf6<sup>fl/fl</sup>;CD4-Cre mice, and it would be interesting to see if residual MALT1 protease activity could account for the observed phenotype (Charbit-Henrion et al. 2017).

It will be interesting to see if the activated effector T cell repertoire in our Traf6<sup>fl/fl</sup>;CD4-Cre mice will eventually lead to the development of an autoimmune disease as reported earlier for ablation of TRAF6 in T cells (King et al. 2006), and how constitutive MALT1 activity contributes to the observed phenotype. Future studies must elucidate the contribution of both MALT1 scaffold and protease function on the expression of distinct target genes, and how this affects differentiation and activation of different cell types. Generation of T6BM mutant knock-in mice will be crucial to confirm the phenotype observed in Traf6<sup>fl/fl</sup>;CD4-Cre mice and give further insights how scaffolding and paracaspase function of MALT1 regulates immune homeostasis.

## Material and Methods

### Antibodies and reagents

The following antibodies were used for immunoprecipitations (IPs), Western Blot (WB) and FACS. Antibodies for WB were diluted to 1:1000 if not stated otherwise. anti-CARD11 (1D12), anti-I $\kappa$ B $\alpha$  (L35A5), anti-I $\kappa$ B $\alpha$  (phosphor-Ser32/36) (5A5) (all Cell Signaling Technology); anti-BCL10 (C-17, IP 2.5 $\mu$ l), anti-MALT1 (B-12), anti- $\beta$ -Actin (I-19 or C4, both 1:10.000), anti-CYLD (E-10), anti-HOIL-1 (H-1) (all Santa Cruz); anti-Regnase-1; anti-HOIP; anti-clAP1; anti-clAP2; anti-TRAF6 (EP591Y); anti-p65; anti-p65 (phosphor); anti-Roquin, anti-HA (obtained from E. Kremmer); anti-E-tag; horseradish peroxidase (HRP)-conjugated secondary antibodies (Jackson ImmunoResearch); anti-mouse IgG1-FITC (A85-1, BD, 1:100), anti-IL-2-APC (JES6-5H4, eBioscience, 1:100), anti-Thy1.1-APC-Cy7 (HIS51, eBioscience, 1:200), anti-CD2-APC (RPA-2.10, eBioscience, 1:400), anti-CD4-PE (eBioscience, 1:300), anti-CD8-FITC (eBioscience, 1:200), anti-CD44-PECy7 (eBioscience, 1:400), anti-CD62L-APC (eBioscience, 1:300), anti-CD69-APC (eBioscience, 1:200) were used for FACS. The following DNA constructs were used: pHAGE-h $\Delta$ CD2-T2A (lentiviral transduction, (Hadian et al. 2011)) or pMSCV-IRES-Thy1.1 (retroviral transduction, (Oeckinghaus et al. 2007)). The following reagent was used: Birinapant (2597-1, BioVision), recombinant IL-2 (Proleukin<sup>®</sup>S, Novartis Pharma), S-Mepazine (5216177, Hit2lead).

### Cultivation and stimulation of cell lines

All cell lines were maintained in humidified atmosphere (37°C, 5% CO<sub>2</sub>). Jurkat T cells were cultured in RPMI 1640 Medium, HEK293 and HEK293T cells in DMEM. Media were supplemented with 10% fetal calf serum, 100 U/ml penicillin and 100 $\mu$ g/ml streptomycin (all Life Technologies). Jurkat T cells were verified by the Authentication Service of the Leibniz Institute (DSMZ). Primary murine CD4 T cells were isolated from spleen, treated with Red Blood Cell Lysis Solution (Miltenyi) and CD4 T cells purified by using the CD4 T cell isolation kit II (Miltenyi) followed by negative magnetic-activated cell sorting (MACS). CD4 T cells were cultured in primary T cell medium (RPMI 1640, 100 U/ml penicillin, 100 $\mu$ g/ml streptomycin, 10% heat inactivated fetal calf serum, 10mM HEPES pH 7.5, 2mM L-Glutamine, 1mM Sodium-Pyruvate, MEM-NEAA (1x), 50nM  $\beta$ -Mercaptoethanol (all Life Technologies)). For expansion of primary murine CD4 T cells, the medium was supplemented with recombinant IL-2 (1:5000, Proleukin<sup>®</sup>S, Novartis Pharma). Jurkat T cells were stimulated with Phorbol 12-Myristate 13-Acetate (PMA, 200 ng/ml; Merck)/Ionomycin (Iono, 300 ng/ml; Calbiochem), anti-CD3 (0.3  $\mu$ g)/CD28 (1  $\mu$ g) in presence of rat anti-mouse IgG1 and IgG2a (0.5 $\mu$ g) (all BD Pharmingen) or recombinant human TNF $\alpha$  (20 ng/ml, Biomol). CD4 T cells were stimulated with PMA (200 ng/ml)/Iono (300 ng/ml) or anti-CD3 (0.5  $\mu$ g/ml)/CD28 (1  $\mu$ g/ml) on rabbit anti-hamster IgG (Jackson ImmunoResearch) pre-coated plates.

### **Generation and reconstitution of HOIP-, TRAF6- and MALT1-deficient Jurkat T cells**

Jurkat KO cell lines were generated as described before (Seeholzer et al. 2018). Shortly, targeting oligos (RNF31/HOIP: 5' – GAGAGCTGGCTAGTAGCGGC – 3'; TRAF6: 5' – TGTTACAGCGCTACAGGAGC – 3' and 5' – ATGGTGAAATGTCCAAATGA – 3') as depicted in Supplementary Fig. S1a and S2a were ligated in the linearized bicistronic expression vector px458 (Cong et al. 2013; Ran et al. 2013), electroporated in Jurkat T cells and sorted for GFP-expressing cells using a MoFlow sorting system. After serial dilution and expansion of single clones, KO cell lines were confirmed by protein expression on western blot and genotyping by genomic PCR. Generation of MALT1-deficient Jurkat T cells has been described earlier (Meininger et al. 2016).

For reconstitution of TRAF6- and MALT1-deficient T cells, TRAF6 and MALT1 constructs were linked to h $\Delta$ CD2 by a co-translational processing site T2A (Hadian et al. 2011) and introduced into a pHAGE transfer vector.  $2 \times 10^6$  HEK293T cells were seeded in 10 cm<sup>2</sup> dish and transfected with 1.5  $\mu$ g psPAX2 (Addgene #12260; gift D. Trono), 1  $\mu$ g pMD2.G (Addgene #12259; gift D. Trono) and 2  $\mu$ g transfer vector using X-tremeGENE HP DNA Transfection Reagent (Roche). For transduction, virus-containing supernatant was applied to  $5 \times 10^5$  Jurkat T cells, mixed with Polybrene (8  $\mu$ g/ml) and incubated for 24 hours. After transduction, cells were washed with PBS, resuspended in RPMI, cultured for ten days and expression of h $\Delta$ CD2 determined by FACS. Protein expression was confirmed by WB.

### **Generation of Traf6<sup>fl/fl</sup>;CD4-Cre mice**

Traf6 floxed mice were derived from the EUCOMM ES cell clone Traf6<sup>tm2a(EUCOMM)</sup>Wtsi (EPD0530\_9\_H08). Frozen embryos were delivered by Infrafrontiers, Biocenter Oulu. For generating the floxed locus, the IRES-lacZ and Neo resistance cassettes were deleted by crossing to flp delete mice. Subsequently, the floxed locus was crossed to CD4-Cre mice for T cell specific deletion of exons 4 and 5 of the Traf6 gene, which encode part of the RING finger domain and a major part of the zinc finger region. In addition, deletion of exon 4 and exon 5 result in a downstream frame shift.

### **Reconstitution of MALT1-deficient murine CD4 T cells**

MACS-purified splenic CD4 T cells from MALT1-deficient mice (MALT1<sup>tm1a(EUCOMM)</sup>Hmgu; ES cell clone HEPD0671\_C08) were stimulated with hamster anti-murine CD3 (0.5  $\mu$ g/ml)/CD28 (2.5  $\mu$ g/ml) antibodies on rabbit anti-hamster IgG pre-coated plates for 48 hours. HEK293T cells were transfected by standard calcium phosphate precipitation protocols with pMSCV retroviral transfer vectors carrying human MALT1-FlagStrepII constructs and Thy1.1 (separated by an internal ribosome entry site (IRES) sequence) and virus produced for 72 hours. CD4 T cells were incubated with retrovirus-containing supernatant supplemented with Polybrene (8  $\mu$ g/ml) for six hours post spin-infection for one hour. Cells were washed with PBS, resuspended in T cell medium supplemented

with IL-2 (1:5000) and analyzed for Thy1.1 expression after three days. For enrichment of Thy1.1 positive cells by MACS separation, a CD90.1 MicroBeads kit was used according to the manufacturer's instructions (Miltenyi Biotec).

### **Flow cytometry (FACS)**

For analysis of the hΔCD2 surface expression marker after lentiviral transduction, Jurkat T cells were incubated with anti-CD2-APC (1:400, RPA-2.10, eBioscience) for 15 minutes at room temperature (RT). For staining of Thy1.1 expression, primary murine CD4 T cells were treated with anti-Thy1.1-APC (1:200, HIS51, eBioscience) for 20 min at 4 °C. Samples were washed, resuspended in FACS buffer (PBS + 3% FCS) and analyzed using the Attune Acoustic Focusing Flow Cytometer.

For intracellular IL-2 staining, primary murine CD4 T cells were rested for one day in T cell medium without IL-2.  $2 \times 10^6$  cells were stimulated with P/I or anti-CD3/CD28 for 5 hours in presence of Brefeldin-A (10 ng/ml, Sigma) to prevent exocytosis of signaling molecules. Cells were fixed with 2% PFA (in PBS) for 15 minutes at RT, permeabilized with IC buffer for seven minutes at RT (0.1% saponin in PBS) and treated with anti-CD16/32 (1:50 in IC buffer, eBioscience) for 10 min at 4 °C to preclude unspecific antibody binding to Fc receptors. After incubation with anti-IL-2 FITC antibody (1:100, JES6-5H4, eBioscience) for 30 minute on ice, cells were washed (15 minutes in IC buffer at RT) and resuspended in FACS buffer. For intracellular IκBα staining, cells were treated with P/I for 20 minutes and prepared as described for IL-2 staining. IκBα was stained with anti-IκBα antibody for 30 minutes at 4°C (1:100, L35A5, Cell Signaling), followed by incubation with anti-mouse-IgG1 FITC antibody (1:300, A85-1, BD) for 20 minutes at 4°C. Cells were analyzed by using the Attune Acoustic Focusing Flow Cytometer.

For intracellular CD4, CD8, CD44, CD62L and CD69 staining of splenic lymphocytes of Traf6<sup>+/fl</sup>;CD4 Cre:Cre<sup>-</sup> and Traf6<sup>fl/fl</sup>;CD4 Cre:Cre<sup>+</sup> mice, cells were washed 2x with PBS and treated with Fixable Viability DyeFluor 780 (1:1000 in PBS) for 30 minutes at 4°C for life/dead staining. Cells were treated with anti-CD16/32 (1:400 in FACS buffer) for 20 minutes at RT, and incubated with the respective staining antibodies for 20 minutes in the dark at RT. After washing with FACS buffer, cells were analyzed by using the Attune Acoustic Focusing Flow Cytometer.

### **Generation and analysis of NF-κB-EGFP reporter cells**

For the generation of NF-κB-EGFP reporter cells, six copies of the NF-κB/Rel-binding site of the immunoglobulin κ light chain enhancer (ATCTGGGGATTCCCCA), and the conalbumin (cona) minimal promoter upstream of a hygromycin-EGFP-fusion gene were cloned into a lentiviral pHAGE vector backbone. The resulting pHAGE-Igκ(6x)cona-HygEGFP construct induces NF-κB-dependent EGFP-expression (NF-κB-EGFP reporter) (Schmidt-Ullrich et al. 1996). For generation of a stable NF-κB-

EGFP reporter cell line, MALT1 KO Jurkat T cells were lentivirally transduced with the pHAGE-Igκ(6x)cona-HygEGFP construct as described above. Transduction efficiency was assessed by EGFP expression upon TNFα stimulation. Subsequent transduction of the MALT1 KO NF-κB-EGFP reporter cell line with pHAGE-hΔCD2-T2A-MALT1 constructs and analysis of transduction efficiency via hΔCD2 by FACS and protein expression on western blot was done as described earlier. Stimulation of NF-κB-EGFP reporter was performed in 500μl medium in 24-well plates at 37°C, and EGFP expression assessed and quantified by FACS.

### **Cell Lysis and Precipitations**

For cellular analysis via WB, Jurkat T cells ( $2-3 \times 10^6$ ) were lysed in co-immunoprecipitations (co-IP) buffer (25 mM HEPES pH 7.5, 150 mM NaCl, 0.2% NP-40, 10% glycerol, 1 mM DTT, 10 mM NaF, 8 mM β-glycerophosphate, 300 μM sodium vanadate and protease inhibitor cocktail mix (Roche)) for 20 minutes at 4°C. For monitoring CBM-complex formation after IP or StrepTactin pulldown (Strep-PD),  $1-3 \times 10^7$  Jurkat T cells were lysed in co-IP buffer. For cellular lysis of EMSA samples, a high salt buffer was used (20 mM HEPES pH 7.9, 350 mM NaCl, 20% glycerol, 1 mM MgCl<sub>2</sub>, 0.5 mM EDTA, 0.1 mM EGTA, 1% NP-40, 1 mM DTT, 10 mM sodium fluoride, 8 mM β-glycerophosphate, 300 μM sodium vanadate and Roche protease inhibitor cocktail mix). Lysate controls were mixed with 4xSDS loading dye and boiled for five minutes at 95°C. For StrepTactin pull-downs (Strep-PD), lysates were incubated with Strep-Tactin Sepharose beads (15μl 1:1 suspension, IBA) overnight at 4°C. For BCL-IP, lysates were treated with anti-BCL10 antibody (C-17, Santa Cruz, 2.5μl) at 4°C overnight, and incubated with protein-G-sepharose beads (15μl 1:1 suspension, Thermo Fisher) for 1-2 hours at 4°C to bind antibodies. Beads were washed 3x with co-IP buffer, resuspended in 22μl 2x SDS loading buffer, boiled for eight minutes at 95°C, separated by SDS-PAGE and analyzed by WB.

### **Western Blotting**

An electrophoretic semi-dry blotting system was used to transfer SDS-PAGE separated proteins onto PVDF-membranes (Merck Millipore). After transfer, membranes were blocked with 5% BSA (Sigma-Aldrich) or 5% milk (Roth) in PBS-Tween (0.01% Tween) for 1 hour at RT. Primary antibodies were diluted as indicated above in 2.5% BSA or milk in PBS-T and membranes incubated overnight at 4°C. Membranes were washed 3x 15 minutes with PBS-T and treated with HRP-coupled secondary antibodies (1:7000 in 1.25% BSA or milk in PBS-T) for 1 hour at RT. HRP was detected by enhanced chemiluminescence using the LumiGlo reagent kit (Cell Signaling Technologies) according to the manufacturer's specifications and visualized on ECL Amersham Hyperfilms (GE Healthcare). Images were cropped for presentation.

### **Electrophoretic Mobility Shift Assay (EMSA)**

EMSAs were carried out using double stranded NF- $\kappa$ B (H2K fwd: 5'-GATCCAGGGCTGGGGATTCCCCATCTCCACAGG-3', H2K rev: 5'-GATCCCTGTGGAGATGGGGAATCCCCAGCCCTG-3') and OCT1 (fwd: 5'-GATCTGTGCAATGCAAATCACTAGAA-3', rev: 5'-GATCTTCTAGTGATTTGCATTCGACA-3') binding sequences which were radioactively labeled with [ $\alpha$ -<sup>32</sup>P] dATP using Klenow Fragment (NEB). Whole cell lysates (6-10  $\mu$ g) were incubated for 30 minutes with shift-buffer (20 mM HEPES pH 7.9, 120 mM KCl, 4% Ficoll, 5 mM DTT, 10  $\mu$ g BSA and 2  $\mu$ g poly-dI-dC (Roche)) and radioactively labelled double stranded probes (10.000-20.000 cpm). Samples were applied on a 5% polyacrylamide gel in TBE buffer, vacuum-dried and exposed to Amersham autoradiography films (GE Healthcare).

### **Detection of active MALT1 by activity based probes (ABP)**

Generation and application of biotin-labeled MALT1 activity based probes (MALT1-ABPs) has been described previously (Eitelhuber et al. 2015). Jurkat T cells ( $3 \times 10^7$ ) were washed with PBS and lysed in 600  $\mu$ l co-IP buffer without protease inhibitors for 25 minutes at 4°C. Cleared lysates (>20.000 x g, 4°C, 10 minutes) were used to collect lysate control (60 $\mu$ l) or incubated with High Capacity Streptavidin Beads (Thermo Fisher, 12 $\mu$ l) for 1 hour at 4°C for pre-clearing (490 $\mu$ l). Beads were pelleted (1700 x g, 2 minutes, 4°C) and 420  $\mu$ l of supernatant mixed with biotin-labeled MALT1-ABP at a final concentration of 0.1  $\mu$ M). After 50 minutes rotating at RT, High Capacity Streptavidin Beads (Thermo Fisher, 15 $\mu$ l) were incubated and samples incubated for 1-2 hours at 4°C (rotating). Beads were collected (1700 x g, 2 minutes, 4°C), washed 3x with co-IP buffer without protease inhibitors, resuspended in 22  $\mu$ l 2x SDS loading buffer, boiled at 95°C for 7 minutes and analyzed by WB.

### **RNA isolation and quantitative PCR (qPCR)**

RNA was isolated (QIAGEN RNeasy Kit) and reverse transcribed into cDNA (Verso cDNA synthesis Kit, Thermo Fisher) according to the manufacturer's instructions. qPCR was performed on a Roche LightCycler 480 using KAPA SYBR FAST qPCR Master Mix (KAPA Biosystems). The following primers were used: *NFKBIA* (I $\kappa$ B $\alpha$ ) fwd: 5'-AGGACGGGGACTCGTTCCTG-3', *NFKBIA* (I $\kappa$ B $\alpha$ ) rev: 5'-CAAGTGGAGTGGAGTCTGCTG-3', *NFKBIZ* (I $\kappa$ B $\zeta$ ) fwd: 5'-TCCGACTTCTCTCTGCCTCGTC-3', *NFKBIZ* (I $\kappa$ B $\zeta$ ) rev: 5'-GAAGCCTTCTGTTTATGACTTC-3', RPII fwd: 5'-GTTCGGAGTCCTGAGTCCGGATG-3', RPII rev: 5'-CCTGCCTCGGGTCCATCAGC-3'.

### **Statistical Analysis**

Data was analyzed for statistical significance using an unpaired student's *t*-test (\* $p \leq 0.05$ , \*\* $p \leq 0.01$ , \*\*\* $p \leq 0.001$ ). Sample size (n) is indicated for each experiment and data are shown as mean  $\pm$  s.e.m.

## References

- Allensworth, J. L., et al. (2013), 'Smac mimetic Birinapant induces apoptosis and enhances TRAIL potency in inflammatory breast cancer cells in an IAP-dependent and TNF-alpha-independent mechanism', *Breast Cancer Res Treat*, 137 (2), 359-71.
- Bornancin, F., et al. (2015), 'Deficiency of MALT1 paracaspase activity results in unbalanced regulatory and effector T and B cell responses leading to multiorgan inflammation', *J Immunol*, 194 (8), 3723-34.
- Cabalzar, K., et al. (2013), 'Monoubiquitination and activity of the paracaspase MALT1 requires glutamate 549 in the dimerization interface', *PLoS One*, 8 (8), e72051.
- Charbit-Henrion, F., et al. (2017), 'Deficiency in Mucosa-associated Lymphoid Tissue Lymphoma Translocation 1: A Novel Cause of IPEX-Like Syndrome', *J Pediatr Gastroenterol Nutr*, 64 (3), 378-84.
- Cheng, L., et al. (2019), 'Malt1 Protease Is Critical in Maintaining Function of Regulatory T Cells and May Be a Therapeutic Target for Antitumor Immunity', *J Immunol*, 202 (10), 3008-19.
- Cong, L., et al. (2013), 'Multiplex genome engineering using CRISPR/Cas systems', *Science*, 339 (6121), 819-23.
- Coornaert, B., et al. (2008), 'T cell antigen receptor stimulation induces MALT1 paracaspase-mediated cleavage of the NF-kappaB inhibitor A20', *Nat Immunol*, 9 (3), 263-71.
- Cui, X., et al. (2017), 'Regnase-1 and Roquin Nonredundantly Regulate Th1 Differentiation Causing Cardiac Inflammation and Fibrosis', *J Immunol*, 199 (12), 4066-77.
- Di Pilato, M., et al. (2019), 'Targeting the CBM complex causes Treg cells to prime tumours for immune checkpoint therapy', *Nature*, 570 (7759), 112-16.
- Dubois, S. M., et al. (2014), 'A catalytic-independent role for the LUBAC in NF-kappaB activation upon antigen receptor engagement and in lymphoma cells', *Blood*, 123 (14), 2199-203.
- Duwel, M., et al. (2009), 'A20 negatively regulates T cell receptor signaling to NF-kappaB by cleaving Malt1 ubiquitin chains', *J Immunol*, 182 (12), 7718-28.
- Egawa, T., et al. (2003), 'Requirement for CARMA1 in antigen receptor-induced NF-kappa B activation and lymphocyte proliferation', *Curr Biol*, 13 (14), 1252-8.
- Eitelhuber, A. C., et al. (2015), 'Activity-based probes for detection of active MALT1 paracaspase in immune cells and lymphomas', *Chem Biol*, 22 (1), 129-38.
- Eto, A., et al. (2003), 'Essential roles for NF-kappa B and a Toll/IL-1 receptor domain-specific signal(s) in the induction of I kappa B-zeta', *Biochem Biophys Res Commun*, 301 (2), 495-501.
- Gewies, A., et al. (2014), 'Uncoupling Malt1 threshold function from paracaspase activity results in destructive autoimmune inflammation', *Cell Rep*, 9 (4), 1292-305.
- Hadian, K., et al. (2011), 'NF-kappaB essential modulator (NEMO) interaction with linear and lys-63 ubiquitin chains contributes to NF-kappaB activation', *J Biol Chem*, 286 (29), 26107-17.
- Hara, H., et al. (2003), 'The MAGUK family protein CARD11 is essential for lymphocyte activation', *Immunity*, 18 (6), 763-75.
- Hayden, M. S. and Ghosh, S. (2012), 'NF-kappaB, the first quarter-century: remarkable progress and outstanding questions', *Genes Dev*, 26 (3), 203-34.
- Ikeda, F., et al. (2011), 'SHARPIN forms a linear ubiquitin ligase complex regulating NF-kappaB activity and apoptosis', *Nature*, 471 (7340), 637-41.

- Jabara, H. H., et al. (2013), 'A homozygous mucosa-associated lymphoid tissue 1 (MALT1) mutation in a family with combined immunodeficiency', *J Allergy Clin Immunol*, 132 (1), 151-8.
- Jain, J., Loh, C., and Rao, A. (1995), 'Transcriptional regulation of the IL-2 gene', *Curr Opin Immunol*, 7 (3), 333-42.
- Jaworski, M., et al. (2014), 'Malt1 protease inactivation efficiently dampens immune responses but causes spontaneous autoimmunity', *EMBO J*, 33 (23), 2765-81.
- Jeltsch, K. M., et al. (2014), 'Cleavage of roquin and regnase-1 by the paracaspase MALT1 releases their cooperatively repressed targets to promote T(H)17 differentiation', *Nat Immunol*, 15 (11), 1079-89.
- Juilland, M. and Thome, M. (2018), 'Holding All the CARDs: How MALT1 Controls CARMA/CARD-Dependent Signaling', *Front Immunol*, 9, 1927.
- King, C. G., et al. (2006), 'TRAF6 is a T cell-intrinsic negative regulator required for the maintenance of immune homeostasis', *Nat Med*, 12 (9), 1088-92.
- Kirisako, T., et al. (2006), 'A ubiquitin ligase complex assembles linear polyubiquitin chains', *EMBO J*, 25 (20), 4877-87.
- Klein, T., et al. (2015), 'The paracaspase MALT1 cleaves HOIL1 reducing linear ubiquitination by LUBAC to dampen lymphocyte NF-kappaB signalling', *Nat Commun*, 6, 8777.
- Lamothe, B., et al. (2008), 'The RING domain and first zinc finger of TRAF6 coordinate signaling by interleukin-1, lipopolysaccharide, and RANKL', *J Biol Chem*, 283 (36), 24871-80.
- Lomaga, M. A., et al. (1999), 'TRAF6 deficiency results in osteopetrosis and defective interleukin-1, CD40, and LPS signaling', *Genes Dev*, 13 (8), 1015-24.
- MaruYama, T., et al. (2015), 'Control of IFN-gamma production and regulatory function by the inducible nuclear protein I kappa B-zeta in T cells', *J Leukoc Biol*, 98 (3), 385-93.
- McKinnon, M. L., et al. (2014), 'Combined immunodeficiency associated with homozygous MALT1 mutations', *J Allergy Clin Immunol*, 133 (5), 1458-62, 62 e1-7.
- Meininger, I. and Krappmann, D. (2016), 'Lymphocyte signaling and activation by the CARMA1-BCL10-MALT1 signalosome', *Biol Chem*, 397 (12), 1315-33.
- Meininger, I., et al. (2016), 'Alternative splicing of MALT1 controls signalling and activation of CD4(+) T cells', *Nat Commun*, 7, 11292.
- Nagel, D., et al. (2012), 'Pharmacologic inhibition of MALT1 protease by phenothiazines as a therapeutic approach for the treatment of aggressive ABC-DLBCL', *Cancer Cell*, 22 (6), 825-37.
- Noels, H., et al. (2007), 'A Novel TRAF6 binding site in MALT1 defines distinct mechanisms of NF-kappaB activation by API2middle dotMALT1 fusions', *J Biol Chem*, 282 (14), 10180-9.
- Oeckinghaus, A. and Ghosh, S. (2009), 'The NF-kappaB family of transcription factors and its regulation', *Cold Spring Harb Perspect Biol*, 1 (4), a000034.
- Oeckinghaus, A., et al. (2007), 'Malt1 ubiquitination triggers NF-kappaB signaling upon T-cell activation', *EMBO J*, 26 (22), 4634-45.
- Pelzer, C., et al. (2013), 'The protease activity of the paracaspase MALT1 is controlled by monoubiquitination', *Nat Immunol*, 14 (4), 337-45.
- Punwani, D., et al. (2015), 'Combined immunodeficiency due to MALT1 mutations, treated by hematopoietic cell transplantation', *J Clin Immunol*, 35 (2), 135-46.

- Ran, F. A., et al. (2013), 'Genome engineering using the CRISPR-Cas9 system', *Nat Protoc*, 8 (11), 2281-308.
- Rebeaud, F., et al. (2008), 'The proteolytic activity of the paracaspase MALT1 is key in T cell activation', *Nat Immunol*, 9 (3), 272-81.
- Rosenbaum, M., et al. (2019), 'Bcl10-controlled Malt1 paracaspase activity is key for the immune suppressive function of regulatory T cells', *Nat Commun*, 10 (1), 2352.
- Ruefli-Brasse, A. A., French, D. M., and Dixit, V. M. (2003), 'Regulation of NF-kappaB-dependent lymphocyte activation and development by paracaspase', *Science*, 302 (5650), 1581-4.
- Ruland, J., et al. (2003), 'Differential requirement for Malt1 in T and B cell antigen receptor signaling', *Immunity*, 19 (5), 749-58.
- Ruland, J., et al. (2001), 'Bcl10 is a positive regulator of antigen receptor-induced activation of NF-kappaB and neural tube closure', *Cell*, 104 (1), 33-42.
- Schlauderer, F., et al. (2018), 'Molecular architecture and regulation of BCL10-MALT1 filaments', *Nat Commun*, 9 (1), 4041.
- Schmidt-Ullrich, R., et al. (1996), 'NF-kappaB activity in transgenic mice: developmental regulation and tissue specificity', *Development*, 122 (7), 2117-28.
- Seeholzer, T., et al. (2018), 'BCL10-CARD11 Fusion Mimics an Active CARD11 Seed That Triggers Constitutive BCL10 Oligomerization and Lymphocyte Activation', *Front Immunol*, 9, 2695.
- Staal, J., et al. (2011), 'T-cell receptor-induced JNK activation requires proteolytic inactivation of CYLD by MALT1', *EMBO J*, 30 (9), 1742-52.
- Sun, L., et al. (2004), 'The TRAF6 ubiquitin ligase and TAK1 kinase mediate IKK activation by BCL10 and MALT1 in T lymphocytes', *Mol Cell*, 14 (3), 289-301.
- Thome, M., et al. (2010), 'Antigen receptor signaling to NF-kappaB via CARMA1, BCL10, and MALT1', *Cold Spring Harb Perspect Biol*, 2 (9), a003004.
- Uehata, T., et al. (2013), 'Malt1-induced cleavage of regnase-1 in CD4(+) helper T cells regulates immune activation', *Cell*, 153 (5), 1036-49.
- Walsh, M. C., et al. (2008), 'TRAF6 autoubiquitination-independent activation of the NFkappaB and MAPK pathways in response to IL-1 and RANKL', *PLoS One*, 3 (12), e4064.
- Whiteside, S. T. and Israel, A. (1997), 'I kappa B proteins: structure, function and regulation', *Semin Cancer Biol*, 8 (2), 75-82.
- Wiesmann, C., et al. (2012), 'Structural determinants of MALT1 protease activity', *J Mol Biol*, 419 (1-2), 4-21.
- Yang, Y., et al. (2016a), 'Targeting Non-proteolytic Protein Ubiquitination for the Treatment of Diffuse Large B Cell Lymphoma', *Cancer Cell*, 29 (4), 494-507.
- Yang, Y. K., et al. (2016b), 'Molecular Determinants of Scaffold-induced Linear Ubiquitylation of B Cell Lymphoma/Leukemia 10 (Bcl10) during T Cell Receptor and Oncogenic Caspase Recruitment Domain-containing Protein 11 (CARD11) Signaling', *J Biol Chem*, 291 (50), 25921-36.
- Yin, Q., et al. (2009), 'E2 interaction and dimerization in the crystal structure of TRAF6', *Nat Struct Mol Biol*, 16 (6), 658-66.
- Yu, J. W., et al. (2011), 'Crystal structure of the mucosa-associated lymphoid tissue lymphoma translocation 1 (MALT1) paracaspase region', *Proc Natl Acad Sci U S A*, 108 (52), 21004-9.

Yu, J. W., et al. (2015), 'MALT1 Protease Activity Is Required for Innate and Adaptive Immune Responses', *PLoS One*, 10 (5), e0127083.

## **Acknowledgments**

We thank Prof. Dr. Rudi Beyaert for kindly providing human CYLD and CYLD-R324A constructs. This work was supported by the Deutsche Forschungsgemeinschaft CRC1054 project A04.

## **Author contributions**

TS designed and performed most of experiments. CG, TJO, AG, KD and AW performed or contributed to specific experiments. DK conceived the project and designed the experiments. TS and DK wrote the paper. All authors have read and approved the final version of the manuscript.

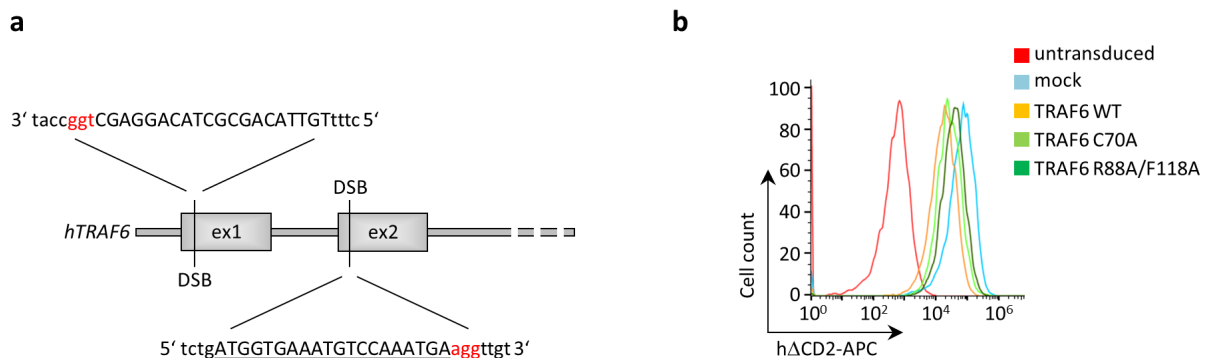
## **Competing interests**

The authors declare that there is no competing financial interest.

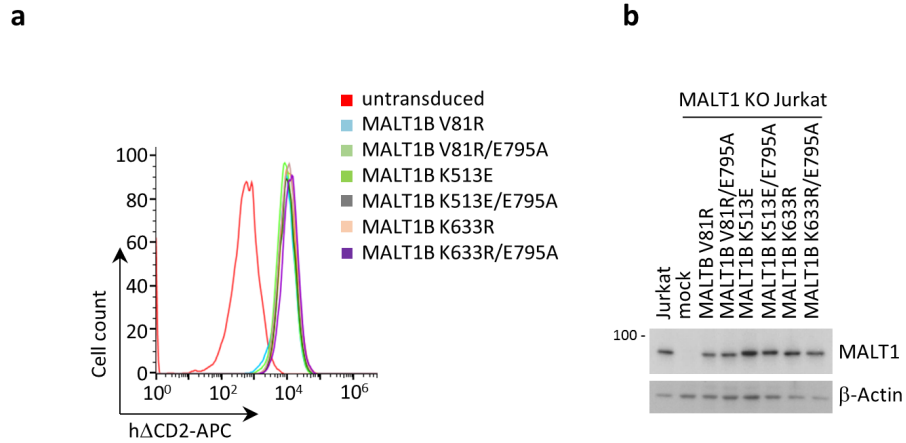
## Supplementary information



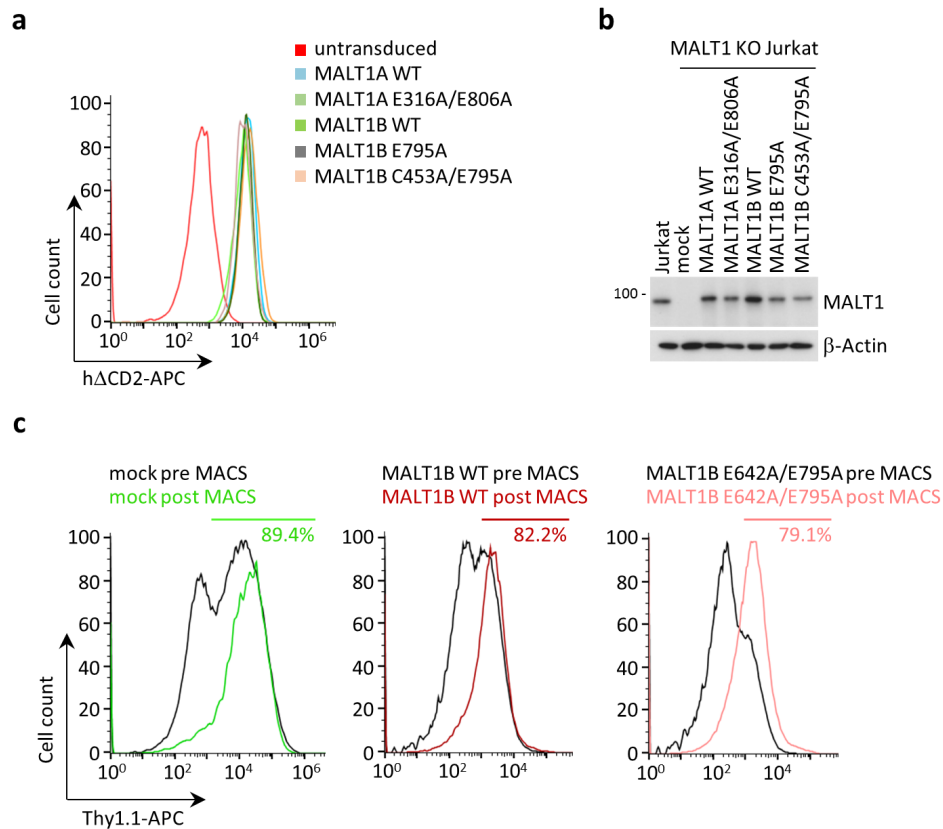
**Supplementary Fig. S1 | Targeting of the E3 ubiquitin ligases HOIP, cIAP1 and cIAP2 in Jurkat T cells.** **a**, Schematic of the Cas9/sgrNA-targeting sites in the *HOIP/RNF31* gene for generation of HOIP KO Jurkat T cells. The sgRNA-targeting sequences are underlined, the protospacer-adjacent motif (PAM) is coloured in red and induced double-strand break (DSB) is marked. **b**, Jurkat cells were treated for ten minutes with different concentration of Birinapant as indicated and expression of cIAP1 and cIAP2 analysed by WB.



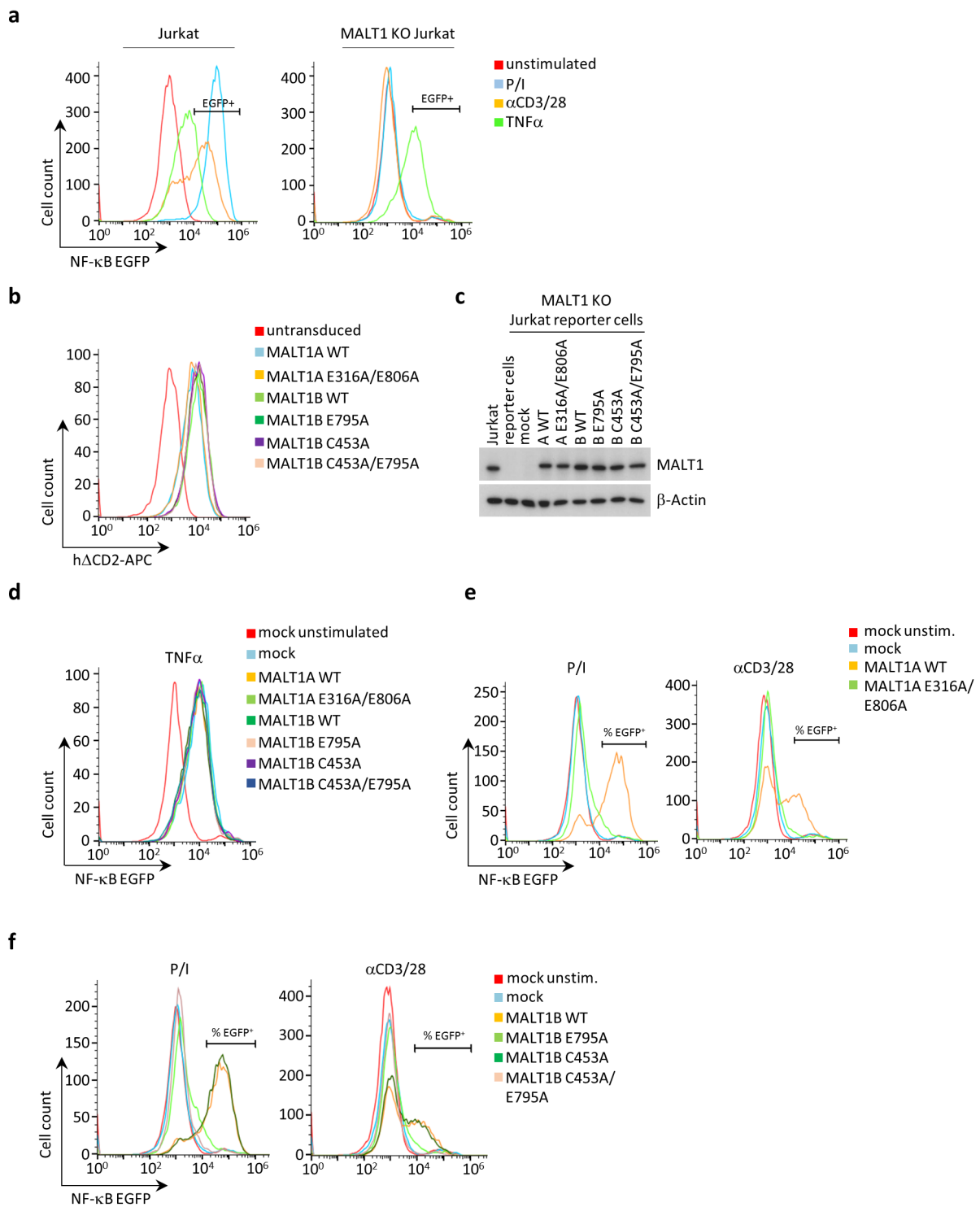
**Supplementary Fig. S2 | Generation and reconstitution of TRAF6 KO Jurkat cells.** **a**, Schematic of the Cas9/sgrNA-targeting sites in the *TRAF6* gene. The protospacer-adjacent motif (PAM) is coloured in red and the sgRNA-targeting sequences are underlined. Induced double-strand breaks (DSB) are indicated. **b**, Transduction of TRAF6 KO Jurkat T cells with mock, TRAF6 WT, TRAF6 C70A and TRAF6 R88A/F118A expressing lentiviruses. Transduction efficiency was determined by co-expression of the surface marker hΔCD2 by FACS.



**Supplementary Fig. S3 | Transduction efficiency of MALT1 WT and mutants in Jurkat cells. a,** Transduction of MALT1B WT and mutant constructs (untagged) in MALT1 KO Jurkat cells, determined by FACS analysis by the co-expressed surface marker hΔCD2. **b,** Protein expression of MALT1 WT and MALT1 single or double mutants in reconstituted MALT1 KO Jurkat cells in comparison to parental Jurkat T cells on WB.

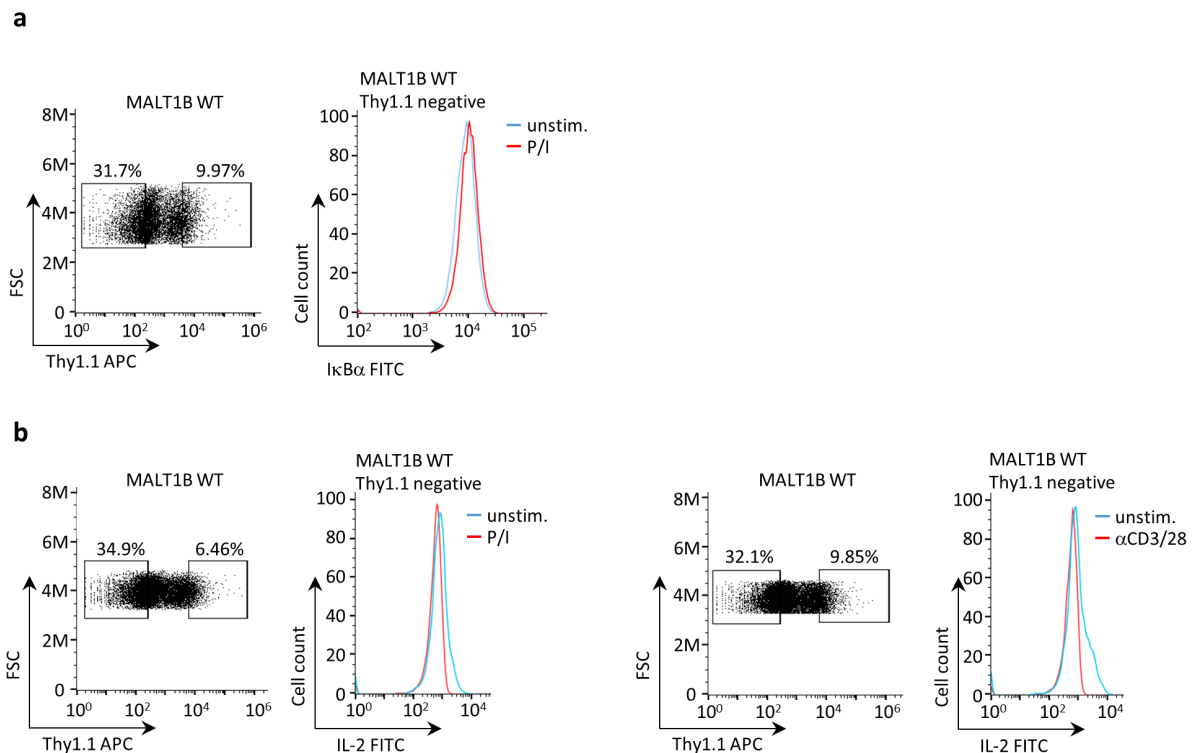


**Supplementary Fig. S4 | Transduction efficiency of MALT1 WT and mutants in Jurkat and primary T cells.** **a**, Transduction efficiency of untagged MALT1B WT and mutant constructs in MALT1 KO Jurkat cells, determined by co-expression of the surface marker hΔCD2. **b**, Protein expression of MALT1 WT and MALT1 mutants in reconstituted MALT1 KO Jurkat cells in comparison to parental Jurkat T cells on WB. **c**, CD4 T cells from MALT1<sup>-/-</sup> mice were retrovirally reconstituted with MALT1 expression constructs. Transduction efficiency was determined by staining for co-expressed Thy1.1 on the cell surface pre and post magnetic cell sorting (MACS) and analysed by FACS. 80-90% of cell populations were positive for Thy1.1 after sorting.



**Supplementary Fig. S5 | Generation of NF-κB-EGFP reporter cells and gating strategy for quantification of NF-κB activity.** **a**, Parental (left) or MALT1 KO (right) Jurkat T cells were lentivirally transduced with an NF-κB-EGFP reporter construct and transduction efficiency determined by EGFP expression (EGFP+) upon P/I, αCD3/28 and TNFα stimulation for five hours, respectively, and analysed by FACS. **b**, NF-κB-EGFP reporter MALT1 KO Jurkat T cells were lentivirally reconstituted with MALT1A or MALT1B WT or mutant constructs and analysed for expression of the hΔCD2 surface

marker by FACS. **c**, Protein expression of reconstituted MALT1 KO Jurkat reporter cells compared to parental Jurkat cells was determined by WB. **d**, FACS analysis of EGFP expressing reconstituted MALT1 KO Jurkat reporter cells upon 5 hours of TNF $\alpha$  stimulation. **e, f**, EGFP expression of MALT1A (**e**) and MALT1B (**f**) WT and mutant reconstituted MALT1 KO Jurkat reporter cells upon P/I and  $\alpha$ CD3/28 stimulation for 5 hours, respectively. Gating for EGFP positive cells (% EGFP+) is indicated.



**Supplementary Fig. S6 | Single cell analysis of I $\kappa$ B $\alpha$  degradation and IL-2 expression in Thy1.1-negative murine MALT1<sup>-/-</sup> CD4 T cells.** **a**, CD4 T cells from MALT1<sup>-/-</sup> mice were retrovirally reconstituted with MALT1B WT expression construct. Transduction efficiency was determined by staining for co-expressed Thy1.1 on the cell surface. Thy1.1-negative (left box) and Thy1.1-positive (right box) cell populations are indicated. Expression of I $\kappa$ B $\alpha$  in Thy1.1-negative cells before and after P/I stimulation for 30 minutes is shown in the histogram. **b**, MALT1<sup>-/-</sup> CD4 T cells transduced as described in (**a**). For IL-2 expression staining, Thy1.1-negative cells were stimulated with or without P/I or  $\alpha$ CD3/28 for five hours and IL-2 production assessed by FACS analysis.

## 6 DISCUSSION

### 6.1 Structural and functional insights into the architecture of the CBM complex

#### 6.1.1 Formation of the CARD11 seed and BCL10 filaments are highly interconnected processes

Structural data and *in vitro* assays indicate that CARD11 acts as a seed, nucleating BCL10 assembly and formation of filaments via homo- and heterotypic CARD-CARD interactions. However, the relevance of these findings for assembly of the CBM signalosome remains poorly defined.

As noted earlier, CARD11 phosphorylation upon TCR or BCR ligation induces conformational changes throughout the protein, especially its N-terminal CARD domain (Matsumoto et al. 2005; Sommer et al. 2005). A basic patch of amino acids within the exposed CARD of CARD11 subsequently recruits pre-assembled BCL10-MALT1 complexes through interaction with an acidic patch in the CARD of BCL10 (Li et al. 2012). By these heterotypic CARD-CARD interactions, CARD11 is able to nucleate the aggregation of BCL10, inducing its oligomerization and formation of filaments (David et al. 2018; Qiao et al. 2013). For instance, R35 on the side of CARD11 is a critical residue for the interaction with residues of BCL10, including E53, and site-directed mutagenesis of these residues strongly impairs NF- $\kappa$ B and MALT1 activation upon overexpression (Li et al. 2012). This highlights the critical importance of the CARD surfaces for heterotypic CARD-CARD association and downstream signaling.

Upon nucleation, BCL10 assembles into helical filaments, with a left-handed symmetry comprising three to four BCL10 subunits per helical turn (Publication II) (Figure 6.1). By solving the cryo-EM structure of the BCL10-MALT1 core filament (Publication II), we were able to confirm the previously reported homotypic BCL10 CARD-CARD interfaces within the filament (David et al. 2018; Qiao et al. 2013). Three homotypic BCL10-BCL10 CARD interfaces could be observed (Figure 6.1): in contrast to type I and type II interactions, which are interstrand contacts between the helical turns, the type III interface mediates contact in the helical-strand direction. Likewise to the critical need of heterotypic CARD-CARD interfaces for the interaction between CARD11 and BCL10, overexpression of BCL10 mutated in residues of interface I (e.g. R42) or interface II (e.g. E53) abolishes BCL10 filament formation, NF- $\kappa$ B activation and MALT1 protease activity (Qiao et al. 2013). Of note, it has been described that type II interactions between BCL10-BCL10 molecules, for instance via residue E53, also confer CARD11-BCL10 interaction, while type I interactions are not competent for heterotypic interactions with CARD11 (Qiao et al. 2013). However, this study did not address the impact of the respective interfaces upon antigenic activation when expressed at endogenous levels.

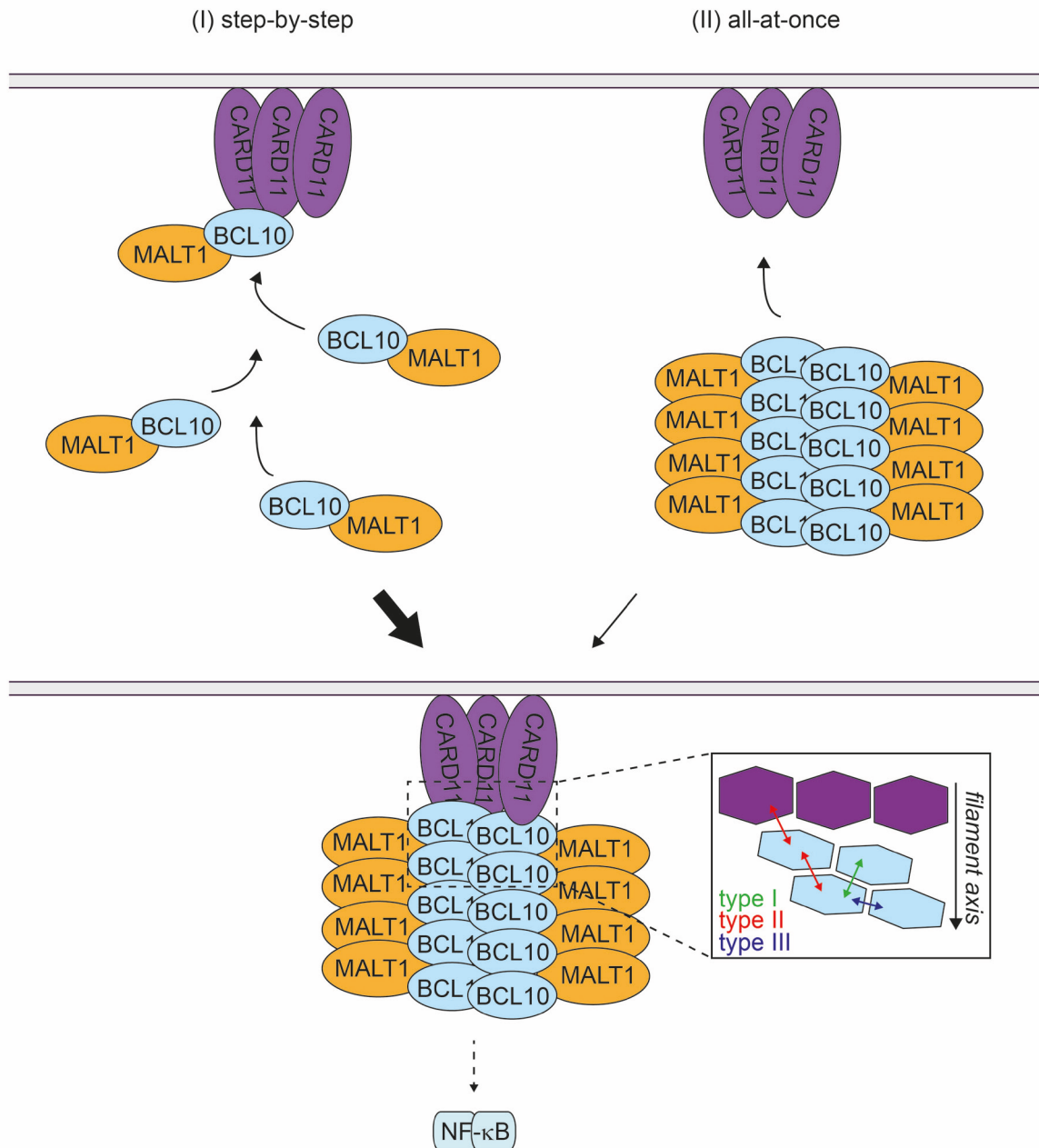


**Figure 6.1: Modes of CBM complex formation.**

Two modes for the assembly of the CBM signalosome could be considered. By a step-by-step mechanism, pre-assembled BCL10-MALT1 dimers are recruited to CARD11 one by one (I). In an all-at-once mechanism, already pre-formed BCL10 filaments are recruited to oligomerized CARD11 (II). The box shows a schematic diagram of the CARD11 seed (purple) and the BCL10 helical assembly (blue). Each CARD domain of CARD11 and BCL10 is represented as a hexagon. The different types of homotypic interstrand (type I and II) or intrastrand (type III) CARD-CARD interactions are indicated with coloured double-headed arrows. Homotypic type II interactions, but not type I and III, additionally contribute to heterotypic CARD-CARD interactions between CARD11 and BCL10, and ultimately lead to the activation of NF-κB.

By using CRISPR/Cas9 generated Jurkat CARD11 and BCL10 KO T cells and lentiviral reconstitution at endogenous protein levels, we were able to demonstrate the functional impact of missense mutation in the CARDS of CARD11 and BCL10 in a clean genetic setup (Publication I). Both the described CARD mutations R35A in CARD11, which abolishes CARD11-BCL10 interaction (Bognar et

al. 2016; Li et al. 2012) and R42E in BCL10 (Qiao et al. 2013; Schlauderer et al. 2018), which destroys BCL10-BCL10 interaction, were unable to rescue NF- $\kappa$ B signaling and MALT1 paracaspase activity in CARD11 and BCL10 KO cells, and proof their functional necessity for hetero- and homotypic interactions. Interestingly, we found that the R42E mutation in the BCL10-BCL10 interface I not only lead to a loss of BCL10 filament assembly, but also abolished the recruitment of BCL10 to CARD11 and therefore abrogated CBM complex formation.

This is rather surprising, since the CARD-CARD interaction between CARD11 and BCL10, modelled in consideration of our BCL10-MALT1 filament cryo-EM structure (Publication II) and the crystal structure of CARD11, predicts that residue R42 is buried within interface I and is therefore not able to contribute to the CARD11-BCL10 interaction. To confirm that the R42E mutation does indeed not affect direct binding to CARD11, we also tested the milder mutation R42A (Publication II). However, all mutations had the same outcome and the structure of the BCL10 filaments clearly shows that this interface is neither directly contributing to the CARD11 interface nor that mutation disrupts the overall conformation of the CARD domain of BCL10. Additionally, an intact BCL10 CARD is also evident from the fact that mutation of R42 to glutamic acid (R42E) or alanine (R42A) did not disrupt binding to MALT1. This raises the question if CARD11 oligomerization and seeding function induce BCL10 filament formation, or if an already assembled initial BCL10 filament is necessary for its recruitment to CARD11. However, our data clearly shows that single mutations of the CARD11-BCL10 or BCL10-BCL10 interfaces alone are insufficient to resolve this question. Therefore, by covalently fusing the two proteins, we generated a system that bypasses the inducible association of BCL10 to CARD11 (Publication I).

Using the BCL10-CARD11 fusion not only allowed us to bypass the necessity to seed BCL10 via the CARD11 CARD: by using structure-guided mutations in the CARDS of BCL10 and CARD11, we could investigate the impact of abrogated BCL10 filament formation or CARD11-BCL10 interaction in the fusion protein. In the BCL10-CARD11 fusion construct, BCL10 filament assembly is possible via both the BCL10 and CARD11 CARD domain. Destructive mutation of the BCL10-BCL10 interface I residue in the BCL10 R42E-CARD11 construct allows BCL10 filament assembly only on the CARD domain of CARD11. In contrast, mutation of the CARD11-BCL10 interface in the BCL10-CARD11 R35A construct restricts filament formation to the BCL10 CARD. By destructive mutation of both BCL10-BCL10 and CARD11-BCL10 interfaces in the fusion construct BCL10 R42E-CARD11 R35A, no BCL10 filament on either CARD can form. In reconstituted CARD11 KO cells, the fusion constructs can either induce oligomerization of endogenous BCL10 or they may self-assemble.

Indeed, expression of the BCL10-CARD11 construct induced strong and chronic NF- $\kappa$ B and MALT1 activation (Publication I). Interestingly, this constitutive activation strictly relied on the presence of the BCL10-BCL10 interface I, since the construct with the oligomerization-defective BCL10 CARD, that impairs filament formation, was no longer constitutively active. However, stimulation-dependent recruitment of endogenous BCL10 to an intact CARD11 CARD, also in absence of a functional BCL10 interface I, was still able to mediate activation. In contrast, mutation of the CARD11-BCL10 interface did not impact chronic MALT1 and NF- $\kappa$ B activity, and mutation of both the BCL10-BCL10 and CARD11-BCL10 interfaces promoted neither constitutive nor stimulus-dependent activation of MALT1 or NF- $\kappa$ B. Hence, we provide evidence that covalent fusion of BCL10 to CARD11 is sufficient to induce MALT1 activity and NF- $\kappa$ B signaling, which strictly relies on the oligomerization interface of BCL10 and recruitment of endogenous BCL10. This strongly supports the concept that CARD11 nucleates BCL10 to induce filament formation.

In addition, transient expression of the fusion protein in Jurkat T cells triggered NF- $\kappa$ B activation to a similar extent as the oncogenic CARD11 variant L225LI or CARD11 without its negative regulatory linker region (Lamason et al. 2010; Lenz et al. 2008; McCully and Pomerantz 2008). Similarly, stable expression of the BCL10-CARD11 construct in CRISPR/Cas9-generated CARD11 KO BJAB B cells induces constitutive NF- $\kappa$ B and MALT1 activity to comparable levels as oncogenic variants of CARD11 (Bognar et al. 2016; Knies et al. 2015; Lamason et al. 2010; Lenz et al. 2008). These oncogenic mutations interfere with the closed, inactive conformation of CARD11, rendering its CARD accessible for heterotypic interaction with the CARD of BCL10. In the fusion protein, the proximity of BCL10 and CARD11 alone seems to be sufficient to overcome its auto-inhibitory functions, for instance by the CARD11 linker, and to activate downstream NF- $\kappa$ B signaling. This provides compelling evidence that a seeding function of CARD11 boosts lymphocyte activation.

There are several lines of evidence that additionally argue for a function of CARD11 as a seed: for instance, although BCL10 filaments form in the absence of CARD11 in a cell free system *in vitro*, CARD11 promotes initiation of BCL10 clustering by reducing the lag time for BCL10 nucleation (David et al. 2018). However, the extension rate of the forming BCL10 filaments is independent of CARD11, which is in line with a role of CARD11 in nucleating BCL10 oligomerization. In addition, EM and fluorescence imaging show that CARD11 is located solely at one side on the tip of the BCL10 filaments, and the observation of star-like or multi-armed filament structure further suggests that each CARD11 seed has the potential to nucleate not only one, but several BCL10 filaments (David et al. 2018; Qiao et al. 2013). Since the minimal nucleus size of the BCL10 filament is at least three molecules, one could speculate that also a trimer of CARD11 may serve as a minimal nucleation

platform. However, it has been shown recently that also CARD11 forms helical filaments *in vitro* (Holliday et al. 2019). The requirement of this helical assembly for BCL10 nucleation suggests that formation of CARD11 filaments precedes BCL10 filament formation and thereby directly templates BCL10 oligomerization. In contrast, earlier studies did not show that higher-order oligomerization of CARD11 is required to nucleate BCL10 filament formation (Qiao et al. 2013), and future studies will have to illuminate the exact degree of oligomerized CARD11 to act as a seed *in vivo*.

Nevertheless, the question if initial oligomerization of BCL10 precedes its recruitment to CARD11 or if BCL10 filaments only form upon nucleation by CARD11 remains difficult to be answered. Two modes of action could be considered (Figure 6.1): (1) In a step-by-step mechanism, pre-assembled BCL10-MALT1 dimers are recruited to CARD11, and the initial weak affinity is stabilized by the growing BCL10 filament. However, both processes are highly interconnected. (2) In an all-at-once mechanism, pre-formed BCL10 filaments are recruited to oligomerized CARD11. Fractionation of the CBM components by gel-filtration does not indicate the presence of pre-assembled BCL10-MALT1 filaments in the absence of CARD11 (Oeckinghaus et al. 2007), arguing for the first mode, albeit the inability to resolve the recruitment of single molecules and the fast and high cooperativity of the interconnected processes preclude a clear answer. In addition, the weak and unstable binding of un-oligomerized BCL10 (e.g. BCL10 R42E) to CARD11 may not be detectable by current methods.

Our data indicates that the initial weak heterotypic interactions of the monomeric CARDS of BCL10 and CARD11 need to be further stabilized by interactions from the oligomerized CARD11 seed and the BCL10 filaments. Since oligomerization and interaction are interconnected, a single mutation will exert effects on both functionalities. This could be delineated by the following analogy: two people are rock climbing and the person on top wants to lift the second person to the summit. If both people create a bond between two hands and two hands, this will result in a strong interaction. However, by losing contact between one of the hands, the interaction would become much weaker and the person on top might not be able to lift the second person to the peak. Analogous, if BCL10 cannot oligomerize due to mutation in the BCL10-BCL10 interface, its interaction to CARD11 will also become much weaker. Hence, formation of additional contact points within the complex in combination with the structural solidity of the BCL10-MALT1 core filament are essential to boost the initial low affinity interaction, leading to rapid CBM complex assembly and downstream signaling upon stimulation. Interestingly, also in the BCL10-MALT1 interface mutants (Publication II) the binding of BCL10 to CARD11 was severely compromised. Therefore, also constitutive association of BCL10 to MALT1 seems to be a prerequisite for CBM complex formation and significantly contributes to the dynamics during the formation of the CBM signalosome. Binding of MALT1 to BCL10 may

either stabilize otherwise labile BCL10 core filaments, or particular conformational changes within BCL10 upon MALT1 interaction could increase the affinity of BCL10 towards CARD11. Initial and weak binding of BCL10 to CARD11 might also be important for recruitment of additional accessory factors like adhesion and degranulation-promoting adapter protein (ADAP) and AhR interacting protein (AIP) to support optimal structural rearrangements of CARD11 and thereby sustain CBM complex formation (Medeiros et al. 2007; Schimmack et al. 2014).

Of note, stable expression, in contrast to transient expression, of the BCL10-CARD11 fusion protein led to an unresponsiveness in Jurkat T cells regarding constitutive and inducible NF- $\kappa$ B activation, although MALT1 paracaspase activity was not affected. On the contrary, activation of NF- $\kappa$ B was not affected after expression of the fusion construct in BJAB B cells. This resembles the phenotype of the so called B cell expansion with NF- $\kappa$ B and T cell anergy (BENTA) disease, where germline CARD11 mutations induce activation and expansion of B cells, driving constitutive NF- $\kappa$ B activation. In contrast, these germline mutations induced an unresponsive, anergic phenotype in T cells (Arjunaraja et al. 2017; Snow et al. 2012). Interestingly, congruent to the stable expression of the fusion construct, reconstituting CARD11 KO Jurkat T cells with the oncogenic CARD11 mutants L225LI and L244P led to blunted NF- $\kappa$ B signaling, but did not affect MALT1 paracaspase activation (unpublished data). However, which cell-intrinsic regulatory mechanisms could counteract activation of the NF- $\kappa$ B pathway by the active BCL10-CARD11 fusion or oncogenic CARD11 mutants in T cells, but not in B cells, need further investigations.

In addition, both stable and transient expression of the BCL10-CARD11 fusions in Jurkat T or BJAB B cells containing a functional CARD were expressed at lower levels compared to the filament defective R42E mutant, which may indicate additional counter-selection mechanisms keeping expression of the active fusion protein in check. Especially the combination of the fusion construct with the oncogenic driver mutation L225LI in BJAB cells showed a very weak expression. Despite its low expression, this oncogenic fusion construct induced strong NF- $\kappa$ B activation and acted as a “super-activator” to further boost CBM signaling. This counter-selection may be attributed to the chronic MALT1 paracaspase activity which is induced by the fusion constructs. Constitutive cleavage of the post-transcriptional regulators Regnase-1 and Roquin-1/2 by MALT1 may alter the gene expression of cytokines and transcription factors and thereby could induce mechanisms that control expression of the fusion construct (Jeltsch et al. 2014; Uehata et al. 2013).

### 6.1.2 Dynamics of BCL10 filament formation

By mutation of residues in the BCL10-BCL10 interface we could show that formation of the BCL10 core structure via its CARD domains is indispensable for CBM complex assembly and downstream signaling (Publication I and II). Recently, the BCL10 filament structure excluding MALT1 was solved with a similar resolution (David et al. 2018). Both BCL10 filaments with or without MALT1 (Publication II)(David et al. 2018) show the same helical arrangement, indicating that the overall conformation of the BCL10 CARD within the filaments is not influenced by the integration of MALT1 into the complex. In line, also the three identified BCL10 CARD-CARD interfaces I, II and III are largely conserved between the BCL10 filament alone (David et al. 2018) and the BCL10-MALT1 complex (Publication II). *In vitro* time-lapse confocal microscopy of BCL10 polymerization showed a unidirectional growth of the BCL10 filaments with CARD11 residing at one end (David et al. 2018). Correlating the BCL10 CARD within the filament with a monomeric BCL10 CARD nuclear magnetic resonance (NMR) structure highlights the largely positively charged surfaces in the growing filaments and how these interact with the largely negatively charged surface of the monomeric BCL10, explaining the course of polymerization: in the first step, the positively charged surface of CARD11 recruits the negatively charged surface of the first BCL10 molecule. Conformational changes within BCL10 lead to the exposure of its basic, positively charged surface, which is able to interact with the next BCL10 monomer via its negatively charged surface, thereby dictating the route of polymerization (David et al. 2018). Indeed, these results were confirmed by modelling the CARD11 BCL10 CARD-CARD interaction by using the BCL10-MALT1 filament cryo-EM structure and the crystal structure of CARD11 (Publication I).

Interestingly, the existence of diverse scaffolding platforms can commonly be observed in cells. For instance, the mode of directional nucleation resembles mechanistically the polymerization of the cytoskeleton: assembly of microtubules is nucleated by so called microtubule-organizing centers (MTOCs). The (-) end of each microtubule stays fixed in the MTOC, while the (+) end is facing away from it (Roostalu and Surrey 2017). In addition, formation of the CBM complex mechanistically also resembles the activation of the Nacht, LRR and PYD domains-containing protein 3 (NLRP3) inflammasome (Guo et al. 2015). In general, inflammasomes serve as a scaffolding platform to recruit pro-caspase-1, inducing its autoproteolytic cleavage and activation by oligomerization (X. Yang et al. 1998). Activated caspase-1 proteolytically activates pro-inflammatory cytokines like interleukin-1 $\beta$  (IL-1 $\beta$ ) and thereby induces inflammation as part of the innate immune system (Martinon et al. 2002). For activation of the NLRP3 inflammasome, NLRP3 oligomerizes and forms, comparable to CARD11, a seed to nucleate the apoptosis-associated speck-like protein containing a CARD (ASC), which forms filamentous structures (Guo et al. 2015). Finally, pro-caspase-1 binds via

CARD-CARD interactions to the formed ASC filaments, thereby allowing auto-proteolytic activation of caspase-1. Hence, similar to the formation of BCL10 filaments in the CBM complex, the ASC filaments provide a platform for integration and activation of mediators during inflammation.

### 6.1.3 Structural organization and function of BCL10-MALT1 filaments

Our 4.9 Å resolution cryo-EM map of the inner core of the BCL10-MALT1 filament shows how the BCL10 CARDS are tightly decorated by the MALT1 DD in a 1:1 stoichiometry. In addition, we resolved for the first time the exact BCL10-MALT1 interaction site. This interface is distinct from the homotypic BCL10-BCL10 interfaces within the filament, explaining why mutations which abrogate BCL10 filament formation (e.g. R42E) are not affecting binding to MALT1. This also highlights that for pre-assembly of MALT1 to BCL10 in unstimulated conditions BCL10 filament formation is not required. In addition, we were also able to gain structural information on the C-terminal MALT1 domains (Ig1-Ig2-paracaspase-Ig3), although with lower resolution (Figure 6.2). The EM density filtered to 8 Å depicts that the Ig1 domain is pointing away from the core filament followed by the flexible linked Ig2 domain, thereby separating the C-terminal domains from the BCL10-MALT1 DD core. A resolution cut-off to 25 Å allowed us to gain information how the stable inner core formed by the CARD of BCL10 and the MALT1 DD-Ig1 fragments is able to orchestrate the flexible outer MALT1 platform: all domains are pointing away from the BCL10-MALT1 DD core filament and form an architecture that resembles a “paddle wheel” (Figure 6.2). The stable inner core which is formed by the CARD of BCL10 and the DD-Ig1 domains of MALT1 thereby orchestrates the C-terminal MALT1 domains, which are able, due to their high flexibility, to provide a platform for the recruitment and integration of additional mediators to foster downstream signaling events. Since the periphery of the BCL10-MALT1 filament is rather flexible, it is unlikely that C-terminal regions of MALT1 contribute to the binding of BCL10.

The high flexibility in the C-terminal domains of MALT1 with its TRAF6 binding motifs provides a docking station for the recruitment of the E3 ubiquitin ligase TRAF6 to foster NF-κB signaling (Meininger et al. 2016). Since activated TRAF6 initiates K63-linked polyubiquitination of MALT1, this provides an additional platform for the recruitment of the IKK complex (Oeckinghaus et al. 2007). Indeed, all of the reported post-translational modifications of MALT1 occur in its C-terminal region (Figure 3.2) (Oeckinghaus et al. 2007; Pelzer et al. 2013; Wegener et al. 2006), which is reasonable due to the inaccessibility of the inner core fragment. Since also JNK signaling critically relies on CARD11 and MALT1 (Gewies et al. 2014; Hara et al. 2003; Meininger et al. 2016), the CBM signalosome may facilitate the recruitment of kinases that mediate JNK phosphorylation and activation, thereby mediating the crosstalk to the JNK pathway.

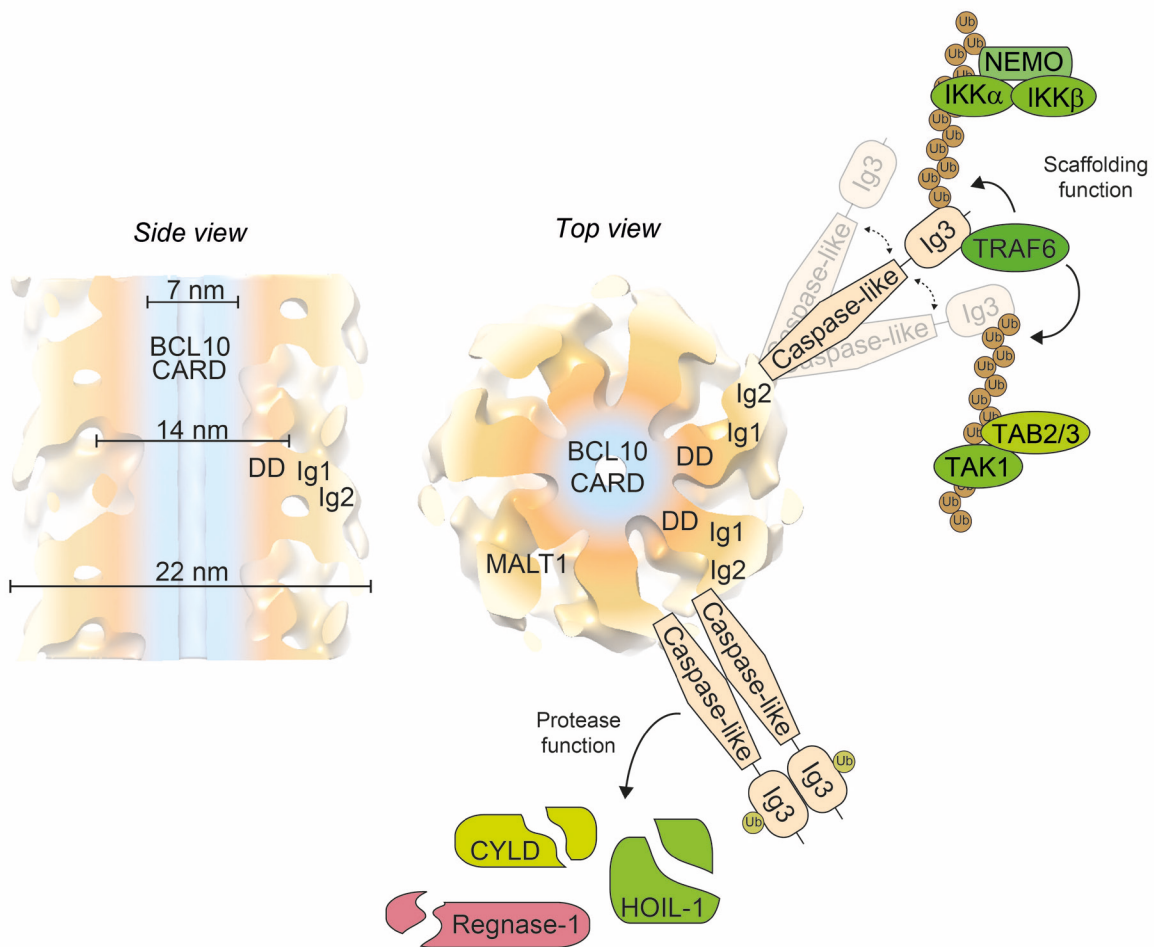


**Figure 6.2: "Paddle wheel-like" architecture of the BCL10-MALT1 filament.**

The Cryo-EM structure of the BCL10-MALT1 filament at a resolution of 25 Å from side (left) and top (right) view depicts how the stable inner core fragment is formed by the CARD of BCL10 (blue) and the DD-Ig1 domains of MALT1 (orange). Flexible outer regions are formed by the C-terminal domains of MALT1 (Ig2-Caspase-like-Ig3) and thereby promote MALT1 scaffolding and protease function. The flexible outer MALT1 platform allows recruitment of additional mediators like TRAF6, the IKK complex and the TAB/TAK1 complex to foster downstream signaling. In addition, dimerization of MALT1 paracaspase domains, which are prerequisite for MALT1 protease activation, induces cleavage of substrates. Abbreviations: CARD, caspase recruitment domain; DD, death domain; Ig, immunoglobulin-like; nm, nanometer.

More recently, integration of LUBAC and the E3 ubiquitin ligases cIAP1 and cIAP2 into the CBM signalosome was suggested to induce attachment of linear or K63-linked ubiquitin chains on BCL10 that contribute to the activation of NF- $\kappa$ B (Y. K. Yang et al. 2016b; Y. Yang et al. 2016a). However, all the described ubiquitination sites are located in the CARD domain of BCL10 and therefore buried in the core filament and probably difficult to be accessed by LUBAC. Therefore, it seems unlikely that BCL10 is modified by K63-linked or linear ubiquitin chains in its filamentous, but rather its monomeric form. Another possibility could be that BCL10 is solely ubiquitinated at the tip of the growing filament. How this would be in line with further downstream signaling is unclear. Most of the experiments regarding BCL10 ubiquitination relied solely on functional cell assays like NF- $\kappa$ B luciferase reporter assays, and rather showed a decrease than complete abolishment of NF- $\kappa$ B

activation in lymphocytes (Dubois et al. 2014; Y. K. Yang et al. 2016b). In contrast to these reports, we observe only mild effects on NF- $\kappa$ B activation when ablating the catalytic LUBAC subunit HOIP in Jurkat T cells (Manuscript I). In line, also degradation of cIAP1/2 by the SMAC mimetic Birinapant had no impact on the activation of NF- $\kappa$ B in Jurkat T cells (Manuscript I). This suggests that linear ubiquitination by LUBAC or K63-linked ubiquitination by cIAP1/2 in T cells has, if at all, rather a fine tuning role in NF- $\kappa$ B activation. This is completely in line with our cryo-EM data that clearly demonstrate the inaccessibility of the BCL10 CARD within the inner core of the filament. It therefore seems to be spatially impossible for LUBAC or other E3 ligases to reach the CARD domain of oligomerized BCL10, and strongly argues against a role of BCL10 ubiquitination during CBM-dependent NF- $\kappa$ B signaling.

Since activation of the paracaspase function of MALT1 relies on its dimerization, the BCL10-MALT1 filaments might facilitate the contact of monomeric MALT1 molecules to promote their dimerization and proteolytic activation (Wiesmann et al. 2012; J. W. Yu et al. 2011). While the ordered inner core of the BCL10-MALT1 filaments measures  $\sim 14$  nm in diameter, the more flexible parts of the helical filament enlarge the complex to a diameter of  $\sim 29$  nm. Since the outer periphery in our cryo-EM structure is less defined, it is challenging to determine if BCL10 oligomerization is sufficient to induce MALT1 dimerization or if additional modifications of MALT1 or integration of additional signaling proteins are required. Interestingly, it was shown that MALT1 decorates BCL10 filaments in a dramatic all-or-none interaction, leading to either solely BCL10 filaments or fully decorated MALT1-BCL10 filaments (David et al. 2018). Similar to MALT1, also the E3 ligase TRAF6 decorates the CBM filaments in an all-or-none mechanism (David et al. 2018). Further studies will be needed to elicit the exact mechanism of MALT1 protease activation within the complex. For instance, it has been described that monoubiquitination of K644 in the Ig3 domain of MALT1 is a critical step for its paracaspase activation upon T cell stimulation (Pelzer et al. 2013), but it is currently unclear which ligase catalyzes this monoubiquitination or if a initially formed polyubiquitin chain is reduced to the monomeric form by recruitment of an additional DUB. In addition, also recruitment and integration of TRAF6 into the CBM filaments might be a critical requirement for optimal activation of the MALT1 paracaspase activity.

Additionally, the BCL10-MALT1 platform might facilitate the recruitment and cleavage of MALT1 substrates upon MALT1 protease activation. It has been described that the DUB A20 negatively regulates NF- $\kappa$ B signaling by removing K63-linked ubiquitin chains from MALT1 (Duwel et al. 2009). By its integration into the BCL10-MALT1 filament, its cleavage by MALT1 may therefore be facilitated by induced proximity (Coornaert et al. 2008). In line, also recruitment of LUBAC to the CBM complex

might facilitate the physical accessibility of MALT1 to HOIL-1 to induce its cleavage (Dubois et al. 2014; Klein et al. 2015). However, it is not clear how and where in the cell active MALT1 encounters its substrates. Gel filtration experiments suggest that MALT1, upon CARD11-dependent activation, can be active outside the CBM complex in its full length form and that substrates do not necessarily need to be recruited to the higher order filaments (Eitelhuber et al. 2015). The MALT1 substrate Regnase-1 localizes to processing (P) bodies and the endoplasmic reticulum to regulate mRNAs (Mino et al. 2015; Suzuki et al. 2011). Also Roquin-1 is primarily found in P bodies and stress granules (Mino et al. 2015). Therefore, active MALT1 might target these post-translational modifiers at distinct foci in the cell. Interestingly, it has been shown that MALT1 contains two nuclear export signals (NES) in its paracaspase domain, and treatment with a NES-specific inhibitor retained MALT1 in the nucleus (Nakagawa et al. 2005). This indicates that MALT1 is able to shuttle between nucleus and cytoplasm, and it is tempting to speculate that MALT1 is able to target yet unidentified substrates in the nucleus. However, further studies will be needed to evaluate if active MALT1 could localize to the nucleus and how MALT1 activity is maintained in absence of the CBM complex.

#### **6.1.4 *In vivo* relevance of BCL10 filaments for signal propagation in lymphocytes**

Although formation of BCL10-MALT1 filaments provide a signaling platform and facilitate the initiation of downstream processes, there is some controversy if cellular BCL10 forms oligomers/filaments and that oligomerization is a prerequisite for signaling *in vivo*, or if filament formation is only observed with recombinant BCL10 or after overexpression of BCL10 *in vitro*. However, strong evidence supports the existence and functional role of BCL10 filaments in cells.

Upon overexpression in cells, BCL10 assembles into clusters and extended filaments, and strictly relies on its CARD domain since BCL10 lacking the CARD region shows a non-filamentous but diffuse distribution (Bertin et al. 2001; Guet and Vito 2000). In line, indirect confocal immunofluorescence microscopy showed that mutation of R42 to glutamic acid (R42E) abrogates formation of cellular clusters upon overexpression in U2OS cells (Publication II). In addition, endogenous BCL10 and BCL10-YFP form oligomeric structures in antigen-stimulated T cells termed “punctuated and oligomeric killing or activating domains transducing signals” (POLKADOTS) and point mutations in the CARD of BCL10 that abolish POLKADOT formation also impair NF- $\kappa$ B activation (Rossman et al. 2006; Schaefer et al. 2004). It was also shown by EM that the CBM complex purified from ABC DLBCL is able to form filaments *in vitro* (Qiao et al. 2013). Size exclusion chromatography in ABC DLBCL or stimulated Jurkat T cells show that all components of the CBM signalosome assemble into a complex with an apparent molecular weight of 1-2 Mio. Dalton, which is much higher than expected if all components were in their monomeric state (Oeckinghaus et al. 2007). Also the existence of diverse

scaffolding platforms like microtubuli, inflammasomes or apoptosomes in a variety of signaling pathways emphasizes the critical role of large oligomeric protein complexes in efficiently mediating cellular processes (Bao and Shi 2007; Guo et al. 2015; Roostalu and Surrey 2017).

Since assembly of filaments with recombinant purified BCL10 is largely influenced by the local protein abundance, increasing concentrations of BCL10 may “force” artifactual filament formation *in vitro* rather than taking place in living cells. Indeed, the nature and relevance of cellular BCL10 filaments has not been completely resolved. Also our CARD11-BCL10 fusion protein is in line with a model where CARD11-BCL10 association, but not BCL10 oligomerization is critical to promote signaling in lymphocytes (Publication I). It is questionable if the BCL10-CARD11 fusion itself is able to form long filaments in the absence of endogenous BCL10, and its activation in BCL10 KO Jurkat T cells might indicate that dimerization or short oligomerization may be sufficient to activate downstream signaling. So far, the cellular morphology with a high nucleus to cytoplasm ratio hampered imaging in lymphocytes. For future studies, new imaging techniques with high resolution will be required to resolve the extent of BCL10 oligomerization/filament formation and the exact cellular architecture of these clusters *in vivo*.

### 6.1.5 Disassembly of the CBM complex

For post-inductive termination of CBM complex signaling, its disassembly is required. TCR-induced K63-linked ubiquitination of BCL10 leads to its depletion by p62/Sequestosome-1-dependent selective autophagy, followed by lysosomal degradation (Paul et al. 2012; Scharschmidt et al. 2004). In addition, a role for BCL10 phosphorylation inducing its proteasomal degradation was suggested (Lobry et al. 2007). However, since the high-order BCL10 filaments form cellular clusters with high rigidity, it is unlikely that oligomerized BCL10 is degraded by the proteasome, which would require precedent unfolding of the proteins. Interestingly, despite its constitutive association with BCL10, MALT1 is not degraded upon stimulation and seems to be excluded from selective autophagy (Paul et al. 2012). How MALT1 is disconnected from the CBM complex and spared from degradation is currently unknown. BCL10 is hyperphosphorylated by IKK $\beta$  in its S/T-rich region at several serine residues, thereby impairing binding to MALT1, and therefore might explain how MALT1 is released from the CBM complex prior to BCL10 degradation (Wegener et al. 2006). Dissociation of MALT1 from BCL10 may additionally destabilize the BCL10 core filament which thereby becomes accessible for K63-linked ubiquitination and association with the autophagy adaptor p62 (Paul et al. 2012).

In addition, MALT1 auto-cleavage at R149 upon stimulation would release a C-terminal fragment without the BCL10-MALT1 binding interface from the CBM complex (Baens et al. 2014), but evidence for the existence of a stable DD-truncated form of MALT1 after stimulation is still missing.

Nevertheless, post-translational modifications of both BCL10 and MALT1 may induce their disengagement and thereby protect MALT1 from autophagy. Finally, also CARD11 K48 ubiquitination and its proteasomal degradation, or mono-ubiquitination and its dissociation from BCL10, were suggested to disassemble the CBM complex (Kojo et al. 2009; Moreno-Garcia et al. 2010). However, since only a minor fraction of CARD11 might be degraded, a decrease in total CARD11 protein levels may be difficult to detect.

## 6.2 Regulation of NF- $\kappa$ B and MALT1 activity by TRAF6

### 6.2.1 TRAF6 is essential for NF- $\kappa$ B activation in Jurkat and primary CD4 T cells

Controversial results have been obtained regarding the role of TRAF6 for TCR/CD28-triggered signaling. For instance, expression of a dominant-negative mutant of TRAF6 in Jurkat T cells severely reduces phosphorylation of I $\kappa$ B $\alpha$  upon  $\alpha$ CD3/28 stimulation (L. Sun et al. 2004). In line, siRNA-mediated knockdown of TRAF6 delays I $\kappa$ B $\alpha$  degradation and impairs NF- $\kappa$ B signaling in Jurkat T cells (Bidere et al. 2006; Oeckinghaus et al. 2007). Additionally, TRAF6 binding motifs on both isoforms of MALT1 are essential for the recruitment of TRAF6 and the activation of NF- $\kappa$ B in Jurkat and primary T cells (Meininger et al. 2016; Noels et al. 2007). In contrast, conditional ablation of TRAF6 in CD4 T cells was suggested to not affect NF- $\kappa$ B signaling, but induces severe autoimmunity in mice (King et al. 2006). This led to the assumption that other E3 ligases could compensate for a loss of TRAF6 in T cells.

By generating TRAF6 deficient Jurkat T cells, we provide evidence that TRAF6 is essential for proper NF- $\kappa$ B activation, and rescue of NF- $\kappa$ B signaling by lentiviral reconstitution relies on the interaction with the E2 conjugating enzyme UBC13 and N-terminal dimerization (Manuscript I). Also, in primary CD4 T cells we find that NF- $\kappa$ B signaling in response to antigen receptor stimulation is strongly compromised in absence of TRAF6 (Manuscript I). In line with previous results, TNF $\alpha$ -dependent NF- $\kappa$ B signaling was not affected by TRAF6 depletion, indicating that our knockout strategy is not impairing NF- $\kappa$ B signaling in general (Lomaga et al. 1999). Contrary to our findings, King et al. did not observe defective NF- $\kappa$ B activation in response to TCR/CD28 stimulation in TRAF6 KO CD4 T cells (King et al. 2006). Of note, T cell specific deletion of the E2 conjugating enzyme UBC13 strongly inhibits TCR-induced NF- $\kappa$ B signaling (Yamamoto et al. 2006). The reason for this discrepancy is not clear. As previously observed, T cell specific ablation of TRAF6 in mice decreases the percentage of CD8 T cells and increases the percentage of activated (CD69<sup>+</sup>) and memory (CD44<sup>hi</sup>, CD62<sup>lo</sup>) T cells and therefore show an activated T cell phenotype (King et al. 2006). However, we did not observe symptoms for severe autoimmunity up to 20 weeks of age as described earlier for ten week old TRAF6- $\Delta$ T mice (King et al. 2006). Differential housing conditions could explain the divergent onset

of the disease *in vivo* and could be the reason why the mice by King et al. develop the autoimmune phenotype already after twelve weeks. This may also explain the difference observed during *ex vivo* stimulations. King et al. did not indicate at what age they investigated the effect of TRAF6 absence on NF- $\kappa$ B or MAP kinase activation. Possibly the T cells displayed pre-activated T cells in heavily burdened mice, although NF- $\kappa$ B activation might be compromised also in their CD4 T cells. However, this raises the interesting question, why T cell specific deletion of TRAF6 leads to chronic T cell activation and potentially an autoimmune phenotype, albeit NF- $\kappa$ B activation is strongly compromised. Therefore, an additional function of TRAF6 besides its role in NF- $\kappa$ B signaling must account for the observed phenotype in these mice.

In conclusion, we clearly demonstrate by a set of independent assays that TRAF6 is an essential factor in TCR signaling for proper NF- $\kappa$ B activation: deletion of TRAF6 in Jurkat or murine primary CD4 T cells completely abolishes NF- $\kappa$ B signaling in these cells. These results are reflected by deletion of TRAF6 binding motifs in MALT1, since reconstitution of Jurkat or murine CD4 MALT1 KO T cells with the respective TBM mutants fail to rescue NF- $\kappa$ B signaling (Manuscript I)(Meininger et al. 2016). Hence, in addition to its essential role in signaling pathways triggered by a various set of immune receptors such as the IL-1R, TLR or receptor activator of NF- $\kappa$ B ligand (RANKL) (H. Wu and Arron 2003), we provide compelling evidence that TRAF6 is also essential for regulation of NF- $\kappa$ B in response to TCR engagement.

### **6.2.2 TRAF6 counteracts constitutive MALT1 paracaspase activity in T cells**

By deletion of TRAF6 in Jurkat and murine primary CD4 T cells, we clarified the controversial results regarding the role of TRAF6 in TCR-mediated NF- $\kappa$ B signaling. In addition, we made the surprising finding that TRAF6 keeps MALT1 in an inactive state prior to antigenic stimulation, and thereby define a new role for TRAF6 (Figure 6.3). In resting T cells, BCL10 constitutively associates with MALT1 via an interface between the CARD of BCL10 and the DD of MALT1 (Publication II). Upon TCR stimulation, CARD11 oligomerization leads to the recruitment of pre-assembled BCL10-MALT1 heterodimers, inducing the assembly of BCL10-MALT1 filaments (Figure 6.3 lower part). Further, integration of TRAF6 into the complex might boost MALT1 paracaspase activity by sustaining dimerization and activation of MALT1. Moreover, TRAF6 induces MALT1 ubiquitination and fosters downstream signaling to NF- $\kappa$ B activation. In addition to its role in activating MALT1 paracaspase activity and NF- $\kappa$ B signaling upon stimulation, we attribute a new, second role to TRAF6 (Figure 6.3 upper part): in resting cells, TRAF6 retains MALT1 paracaspase activity, and loss of TRAF6 or its abolished binding to MALT1 via T6BMs leads to constitutively activated MALT1 and cleavage of substrates. Suppression of this constitutive activity depends on catalytic activity and dimerization of

TRAF6. Hence, binding of TRAF6 to MALT1 and modification of MALT1 or another substrate by TRAF6 prevents the formation of a pre-activated form of MALT1, which in absence of TRAF6 is able to dimerize and induce the cleavage of substrates also in absence of any stimuli.

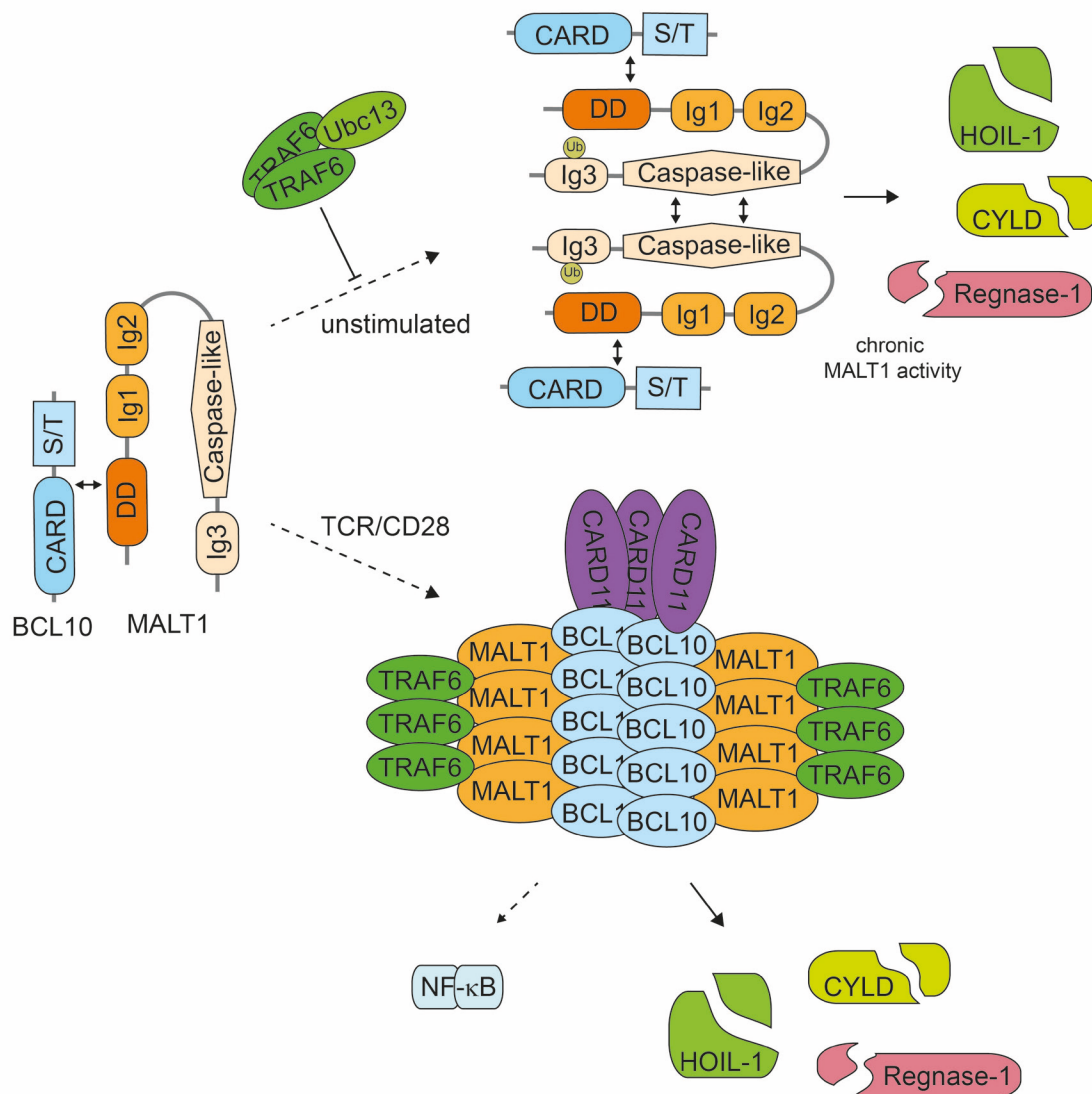


**Figure 6.3: Model for the dual function of the E3 ubiquitin ligase TRAF6.**

BCL10 and MALT1 constitutively associate via their CARD and DD. Upon TCR/CD28-induced cell activation (lower part), oligomerization of CARD11 induces formation of the CBM complex. Integration of TRAF6 into the signalosome triggers NF- $\kappa$ B and full MALT1 paracaspase activity. In resting cells (upper part), TRAF6, in dependency of its oligomerization and interaction to UBC13, suppresses constitutive MALT1 paracaspase activation. Chronic MALT1 paracaspase activity and cleavage of substrates in absence of TRAF6 relies on MALT1-BCL10 interaction, dimerization of the caspase-like domain and mono-ubiquitination in Ig3. Double-headed arrows indicate protein-protein interactions. Abbreviations: CARD, caspase recruitment domain; S/T-rich, Serine/Threonine-rich; DD, death domain; Ig, immunoglobulin-like.

Indeed, the mode of action by which TRAF6 counteracts constitutive MALT1 activity might resemble the action of so called inhibitors of apoptosis (IAPs) in the intrinsic pathway of apoptosis (Verhagen et al. 2001). In absence of apoptotic stimuli, these cytosolic proteins bind to and prevent activation of spontaneously activated pro-caspases. Only upon activation of the apoptotic pathway, release of

anti-IAP proteins repress the activity of IAPs, and allows induction of the caspase cascade. IAPs therefore set a barrier to prevent unintentional activation of caspases to maintain cell homeostasis.

Further, we show the molecular requirements for constitutively active MALT1. Chronic substrate cleavage in T6BM mutants is strictly dependent on MALT1 catalytic activity, since additional mutation of its catalytic center or treatment with the allosteric MALT1 inhibitor S-Mepazine (Nagel et al. 2012) completely abolished its constitutive activity. Of note, mutation of T6BMs does not affect CBM complex formation upon stimulation (Meininger et al. 2016). However, constitutively active MALT1 in T6BM mutants relies on its constitutive association with BCL10 via the MALT1-BCL10 interface I, but may be independent of CARD11, since CBM complex relies on stimulus-dependent phosphorylation and activation of CARD11 (Matsumoto et al. 2005; Meininger and Krappmann 2016), and we see no evidence for a pre-formed CBM complex. However, since mutation of the MALT1-BCL10 interface I also abolishes stimulus dependent recruitment of CARD11 to BCL10 (Publication II) we cannot exclude that an initial weak binding of CARD11 or another CARD protein to BCL10 might indeed be a pre-requisite for constitutive MALT1 paracaspase activation.

Additionally, constitutive MALT1 activity in absence of T6BMs strictly depends on its dimerization interface, which is also indispensable for MALT1 paracaspase activation upon stimulation (Wiesmann et al. 2012). Although MALT1 dimerizes in its ligand-free form, it adopts an inactive conformation. In this conformation, the nucleophile of the active-site cysteine is dislocated. Regions within the caspase-domain, which are necessary for substrate recognition, are not able to bind substrates and therefore keep MALT1 in an auto-inhibited state. Rearrangement of the active site, induced by substrate binding, triggers MALT1 activation. This is accompanied by numerous structural changes throughout the molecule, especially in the C-terminus including the third Ig-like domain (Wiesmann et al. 2012). Since this region is involved in the interaction with TRAF6, it is tempting to speculate that binding of TRAF6 and ubiquitination of MALT1 affects the structure of the catalytic site, thereby regulating substrate recognition and turnover. Structural rearrangements within the TRAF6 mutants C70A and R88A/F118A, which are either unable to bind to UBC13 or to dimerize, may coincide with a loss of MALT1 binding, explaining the constitutively active MALT1 in these constructs.

However, also post-translational modification of MALT1 or another factor by the E3 ubiquitin-ligase activity of TRAF6, which is compromised in the C70A and R88A/F118A mutants, seem to contribute to keep MALT1 in its inactive conformation (Manuscript I). For instance, MALT1A K644 is located at an exposed loop structure, and its mono-ubiquitination upon stimulation induces conformational changes of the caspase-like domain, thereby facilitating its activation (Pelzer et al. 2013; Wiesmann et al. 2012; J. W. Yu et al. 2011). Indeed, also constitutive activity of MALT1B E795A relies on the

presence of the monoubiquitination site. However, binding of TRAF6 to MALT1 or post-translational modifications may prevent conformational changes within the catalytic site of MALT1 prior to antigenic stimulation, thereby maintaining MALT1 protease inactive.

Our data shows that TRAF6 is necessary for the homeostatic control of MALT1 paracaspase activity in resting cells by preventing its spontaneous activation. However, for full activation of MALT1 and proper substrate cleavage upon stimulation, integration of TRAF6 into the CBM signalosome is essential, and moreover prerequisite to trigger NF- $\kappa$ B activation. Recently, it has been shown that ectopic expression of TRAF6 is sufficient to induce MALT1 activity in Jurkat T cells, independently of CARD11 or BCL10 (Bardet et al. 2018; Ginster et al. 2017). Interestingly, overexpression of BCL10 alone is able to induce MALT1 activity by spontaneously assembling filaments independently of CARD11 (David et al. 2018; Qiao et al. 2013). Moreover, also spontaneous aggregation of overexpressed TRAF6 could be observed (Yin et al. 2009). Hence, spontaneous cluster formation of TRAF6 by its overexpression may be sufficient to integrate MALT1 into a TRAF6-MALT1 complex, thereby inducing conformational changes and promoting its activation rather than inhibition.

Interestingly, presence of an additional binding motif in MALT1A leads to a significant reduction of active MALT1 prior to stimulation. Thus, repression of a basal paracaspase activity by TRAF6 may differ in the two MALT1 isoforms. Interestingly, both isoforms are differentially expressed in murine tissues: while both isoforms are present in murine brain and liver, lymphoid organs like spleen or thymus almost exclusively express MALT1B (Meininger et al. 2016). Therefore, T6BMs in MALT1 may influence homeostatic control in different organs due to diverging repression of MALT1 paracaspase activity in the two isoforms. However, upon T cell stimulation, MALT1 catalytic activity is activated to the same extent in both isoforms, showing that MALT1 protease activation is not influenced by the additional T6BM in MALT1A (Meininger et al. 2016).

In conclusion, we clearly demonstrate that TRAF6 keeps MALT1 in an inactive state prior to antigenic stimulation, and therefore attribute a new role to TRAF6. Chronic MALT1 proteolytic activity depends on the same mechanisms as the induced MALT1 catalytic activity upon T cell stimulation, and MALT1-BCL10 association, MALT1 dimerization and MALT1 mono-ubiquitination are critical to maintain chronic MALT1 activity in absence of TRAF6.

### 6.2.3 The autoimmune phenotype in *Traf6<sup>fl/fl</sup>;CD4-Cre* mice

*Traf6<sup>fl/fl</sup>;CD4-Cre* mice have an activated T cell phenotype, albeit NF- $\kappa$ B signaling is clearly compromised in these cells (Manuscript I). This is quite surprising, since ablation of any component of the CBM complex, which also abolishes NF- $\kappa$ B signaling, leads to severe immunodeficiency (Egawa et al. 2003; Hara et al. 2003; Ruefli-Brasse et al. 2003; Ruland et al. 2001; Ruland et al. 2003). Therefore the question arises, how *Traf6<sup>fl/fl</sup>;CD4-Cre* mice possibly develop an autoimmune phenotype, although they clearly lack NF- $\kappa$ B activity in their CD4 T cells.

When naïve T cells become activated during an immune reaction, they differentiate into effector T cells (Teffs), for instance  $T_H1$  and  $T_H17$  cells which boost the immune response, and regulatory T cells (Tregs) (Figure 6.4). Key function of Tregs is the suppression of proliferation as well as activation of effector T cells to maintain immunological self-tolerance and prevent development of autoimmune disease (Chaudhry et al. 2009; Koch et al. 2009; Sakaguchi et al. 1985). Both MALT1 scaffolding and protease function contribute to and maintain the equilibrium between Teffs and Tregs in a functional immune system. However, by destruction of both scaffold and protease function of MALT1, for instance in MALT1-deficient mice, NF- $\kappa$ B signaling, IL-2 production and proliferation of T cells are heavily compromised, leading to a reduced number of Teffs (Jaworski et al. 2014; Ruefli-Brasse et al. 2003; Ruland et al. 2003) (Figure 6.4). In line, also Treg numbers are strongly decreased in these mice. However, due to the impaired generation of Teffs, MALT1 absence leads to a strong immune suppression. MALT1 protease mutant (PM) knock-in in mice, which possess MALT1 scaffolding function but are deficient in MALT1 protease function, show compromised IL-2 production and proliferation of T cells similar to MALT1 KO mice (Bornancin et al. 2015; Gewies et al. 2014; Jaworski et al. 2014; J. W. Yu et al. 2015) (Figure 6.4). In contrast to the MALT1 KO mice, MALT1 PM mice show normal NF- $\kappa$ B signaling independently of MALT1 protease activity, and Teffs in PM mice exhibit an activated phenotype with increased secretion levels of cytokines like interferon gamma (IFN $\gamma$ ). However, just like in the MALT1 KO mice, development of Tregs is strongly compromised in absence of MALT1 proteolytic activity. This is in line with recent reports showing that CBM signaling, in dependency of MALT1 proteolytic activity, is necessary for the suppressive effector functions of Tregs (Brustle et al. 2017; Di Pilato et al. 2019; Rosenbaum et al. 2019). Since MALT1 protease defective mice have a preserved MALT1 scaffolding function, the residual immune activation cannot be counterbalanced due to the reduced Treg numbers and their reduced effector function, inducing a spontaneous autoimmune phenotype (Jaworski et al. 2014).

Interestingly, our data shows a dual function of TRAF6 in T cells: upon antigen stimulation, MALT1 scaffolding function and activation of NF- $\kappa$ B critically depends on TRAF6. Moreover, TRAF6 controls

MALT1 protease activity in resting cells and prevents constitutive paracaspase activation and cleavage of substrates (Manuscript I). Therefore, by ablation of TRAF6 in murine CD4 T cells, MALT1 loses its scaffolding function, but retains its proteolytic function, which is even constitutively activated. Interestingly, albeit the severely reduced NF- $\kappa$ B activation in *Traf6<sup>fl/fl</sup>*;CD4-Cre mice, the number of activated Teffs is strongly increased and possibly leads to the development of an autoimmune phenotype (Figure 6.4).

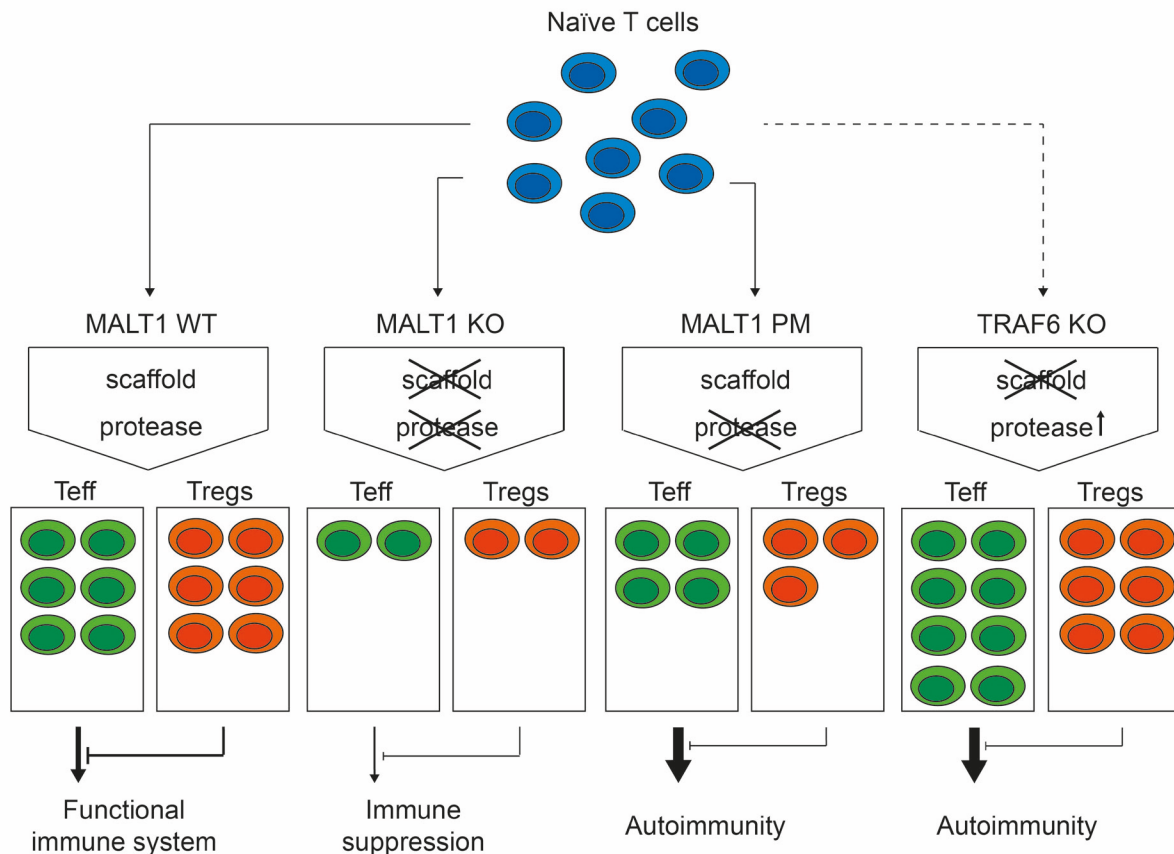


**Figure 6.4: Model for MALT1 scaffold and protease function in balancing activation of immune cells.**

Immune reactions activate naïve T cells and induce their differentiation into effector T cells (Teffs) and suppressive regulatory T cells (Tregs). Both MALT1 scaffold and protease function contribute to the equilibrium between Teffs and Tregs and thereby shape a functional immune system (MALT1 WT). In absence of MALT1, both MALT1 scaffold and protease functions are compromised (MALT1 KO). Generation of Teffs and Tregs is strongly impaired and therefore leads to immune suppression. Abolishment of MALT1 protease function solely (MALT1 PM) reduces number of both Teffs and Tregs. However, residual activation of Teffs by the preserved MALT1 scaffolding function can't be counterbalanced by the strongly reduced Treg numbers and functions, thereby promoting autoimmunity. Loss of MALT1 scaffold function but preserved and constitutive ( $\uparrow$ ) protease activity does not affect the number of Tregs and shows increased numbers of activated Teffs. However, Tregs are unable to suppress Teff cell functions and induce development of an autoimmune phenotype.

Of note, we observed normal numbers of Treg cells in these mice (data not shown). Since development and differentiation of the regulatory T cell lineage largely depends on CBM proteins (Barnes et al. 2009; Brustle et al. 2017; Molinero et al. 2009; Schmidt-Supprian et al. 2004), residual NF- $\kappa$ B activity in CD4 TRAF6 KO cells may be sufficient for their genesis. However, Tregs in

Traf6<sup>fl/fl</sup>;CD4-Cre mice seems not to be able to counteract the expansion of activated Tregs and are therefore unable to prevent the autoimmune phenotype. Interestingly, we show that optimal activation of distinct target genes, for instance *NFKBIZ*/I $\kappa$ B $\zeta$ , critically relies on both MALT1 scaffolding and protease activity (Manuscript I). It has been described that T cell specific deletion of *NFKBIZ*/I $\kappa$ B $\zeta$  increases the number of IFN $\gamma$ -producing CD4 T cells in 3-week old mice (Maruyama et al. 2015). In addition, regulatory T cells from these mice exhibit a diminished immunoregulatory capacity and suggest a role of I $\kappa$ B $\zeta$  in their differentiation from naïve CD4 T cells. Recently, a critical role for the CBM complex, in a MALT1 protease-dependent manner, for the immune-suppressive function of Tregs was described (Cheng et al. 2019; Di Pilato et al. 2019; Rosenbaum et al. 2019): disruption of the CBM complex components or inhibition of MALT1 protease activity induces dysregulation of cytokine expression, for instance induction of IFN $\gamma$  secretion, thereby oppressing the suppressive functions of Tregs. Interestingly, *NFKBIZ*/I $\kappa$ B $\zeta$  mRNA transcripts are targeted by the posttranscriptional regulators Regnase-1 and Roquin, and T cell-specific Regnase-1 KO or Roquin mutant (sanroque) mice, show an enhanced IFN $\gamma$ -producing cell population (Cui et al. 2017). Of note, Treg-specific TRAF6-deficient mice revealed that TRAF6 is essential for the maintenance of Tregs, thereby suppressing autoimmunity (Muto et al. 2013).

Therefore, chronic MALT1 activity in absence of NF- $\kappa$ B activation might lead to reduced Regnase-1 and Roquin protein levels, attendant with a dysregulation of *NFKBIZ*/I $\kappa$ B $\zeta$  expression, thereby increasing IFN $\gamma$  production and diminishing suppressor function of Tregs, which ultimately contributes to the observed inflammatory phenotype in Traf6<sup>fl/fl</sup>;CD4-Cre mice. However, IFN $\gamma$  production might not be sufficient to suppress different Treg subsets to the same degree. Therefore, dysregulation of target gene expression might also influence activation of effector T cells. Indeed, control CD4<sup>+</sup>CD25<sup>+</sup> Treg cells were unable to efficiently suppress proliferation of proinflammatory cytokine-producing responder T cells in mice with conditional ablation of TRAF6 in CD4 T cells, suggesting that TRAF6 negatively regulates T cell activation (King et al. 2006).

Recently, we also generated knock-in mice which express mutated T6BMs in MALT1. These mice suffer from severe autoimmunity three weeks after birth, and therefore much earlier than the Traf6<sup>fl/fl</sup>;CD4-Cre mice (data not shown). However, also in these mice we observe high levels of activated T effector cells, accompanied by increased levels of IFN $\gamma$ , while the percentages of Tregs are comparable to littermate control animals (data not shown). Due to the largely concurrent phenotypes it seems likely that deregulated MALT1 paracaspase activity in both mouse models could contribute to the loss of immune homeostasis attended by the development of autoimmunity.

### 6.3 Conclusion and outlook

In these studies, we present data on the assembly and architecture of the CBM signalosome and how it provides a signaling platform in lymphocytes. The recruitment of BCL10-MALT1 to CARD11 and the formation of BCL10-MALT1 filaments upon TCR or BCR engagement are highly interconnected processes. For formation of a stable CBM complex, the weak initial heterotypic interactions need to be stabilized by additional contact points by the oligomerized CARD11 seed and the helical BCL10 filaments (Publication I). Our cryo-EM structure resolved the inner core of the BCL10-MALT1 filament at a 4.9 Å resolution and revealed the exact binding interfaces between the BCL10 CARD and the MALT1 DD (Publication II). In spite of the lower resolution of the cryo-EM map in the outer region of the BCL10-MALT1 filaments, our structure shows how the C-terminal regions of MALT1 emanate from the BCL10-MALT1 DD core filament, forming a “paddle wheel-like” architecture. The high flexibility of the C-terminal regions of MALT1, comprising its Ig2, paracaspase and Ig3 domains, provide a platform for the recruitment of additional mediators to foster NF-κB signaling. Additionally, positioning of the individual MALT1 molecules in the outer rim of the filament allows efficient post-translational modifications, substrate binding and paracaspase domain dimerization to promote MALT1 protease activation. Future studies will have to show how additional factors like TRAF6, TAK1 or NEMO/IKKβ are integrated into the BCL10-MALT1 platform and contribute to the dynamics of the CBM signalosome to initiate downstream processes. In addition, the exact requirements and mechanisms of MALT1 protease activation in the complex must be elucidated, for instance if post-translational modifications are a prerequisite for paracaspase dimerization and activation.

Moreover, we present evidence for the dual function of the E3 ubiquitin ligase TRAF6 (Manuscript I). TRAF6-deficient Jurkat or primary CD4 T cells highlight the necessity of TRAF6 for TCR/CD28-induced NF-κB activation. Moreover, MALT1 protease is constitutively activated in the absence of TRAF6 and induces the chronic cleavage of substrates. Similar results have been obtained by disruption of the MALT1-TRAF6 interaction by mutation of T6BMs in MALT1, which induces chronic MALT1 activation, but abolishes NF-κB signaling upon stimulation. Therefore, we define a new role for TRAF6 in keeping MALT1 protease inactive in resting cells.

Interestingly, *Traf6<sup>fl/fl</sup>*;CD4-Cre mice show an activated T cell phenotype in absence of NF-κB activity, which may be in line with the autoimmune phenotype in TRAF6-ΔT mice described by King et al. (King et al. 2006). However, which exact mechanisms contribute to the development of the activated T cell phenotype in *Traf6<sup>fl/fl</sup>*;CD4-Cre mice and if these develop autoimmunity at later stages similar to the mice reported by King et al. needs to be further investigated. Constitutive MALT1 activity may

account for the observed phenotype, and it would be interesting to see if administration of the MALT1 inhibitor S-Mepazine could block chronic MALT1 activation and thereby attenuate the activation of effector T cells. Moreover, also regulatory T cells could be affected by the constitutive MALT1 activity in absence of TRAF6. Since percentage of Treg numbers in *Traf6<sup>fl/fl</sup>;CD4-Cre* mice seems to be unaffected, defects in their suppressor function might contribute to the observed phenotype, which could be possibly rescued by adoptive transfer of functional Tregs.

Also the recently generated knock-in mouse line expressing the T6BM mutant form of MALT1 will give valuable insights into the function of the MALT1 paracaspase in regulating immune homeostasis. However, further investigations are required to determine if chronic MALT1 activity in these mice accounts for the observed phenotype. Crossing MALT1 PM mice with the generated T6BM mutant mice will clarify if the constitutive MALT1 paracaspase activity contributes to the autoimmune phenotype. In addition, generation of CD4- and Treg-specific T6BM mutant knock-in mouse lines will help to understand how regulation of MALT1 by TRAF6 contributes to differentiation and activation of effector and regulatory T cells, and thereby sustains immune homeostasis.

---

## 7 REFERENCES

- Akiyama, T., et al. (2005), 'Dependence of self-tolerance on TRAF6-directed development of thymic stroma', *Science*, 308 (5719), 248-51.
- Alarcon, B., Mestre, D., and Martinez-Martin, N. (2011), 'The immunological synapse: a cause or consequence of T-cell receptor triggering?', *Immunology*, 133 (4), 420-5.
- Arch, R. H., Gedrich, R. W., and Thompson, C. B. (1998), 'Tumor necrosis factor receptor-associated factors (TRAFs)--a family of adapter proteins that regulates life and death', *Genes Dev*, 12 (18), 2821-30.
- Arjunaraja, S., et al. (2017), 'Intrinsic Plasma Cell Differentiation Defects in B Cell Expansion with NF-kappaB and T Cell Anergy Patient B Cells', *Front Immunol*, 8, 913.
- Baens, M., et al. (2014), 'MALT1 auto-proteolysis is essential for NF-kappaB-dependent gene transcription in activated lymphocytes', *PLoS One*, 9 (8), e103774.
- Bao, Q. and Shi, Y. (2007), 'Apoptosome: a platform for the activation of initiator caspases', *Cell Death Differ*, 14 (1), 56-65.
- Bardet, M., et al. (2018), 'MALT1 activation by TRAF6 needs neither BCL10 nor CARD11', *Biochem Biophys Res Commun*, 506 (1), 48-52.
- Barnes, M. J., et al. (2009), 'Commitment to the regulatory T cell lineage requires CARMA1 in the thymus but not in the periphery', *PLoS Biol*, 7 (3), e51.
- Bertin, J., et al. (2001), 'CARD11 and CARD14 are novel caspase recruitment domain (CARD)/membrane-associated guanylate kinase (MAGUK) family members that interact with BCL10 and activate NF-kappa B', *J Biol Chem*, 276 (15), 11877-82.
- Bhatt, D. and Ghosh, S. (2014), 'Regulation of the NF-kappaB-Mediated Transcription of Inflammatory Genes', *Front Immunol*, 5, 71.
- Bidere, N., et al. (2006), 'Caspase-8 regulation by direct interaction with TRAF6 in T cell receptor-induced NF-kappaB activation', *Curr Biol*, 16 (16), 1666-71.
- Blonska, M., et al. (2007), 'The CARMA1-Bcl10 signaling complex selectively regulates JNK2 kinase in the T cell receptor-signaling pathway', *Immunity*, 26 (1), 55-66.
- Bognar, M. K., et al. (2016), 'Oncogenic CARMA1 couples NF-kappaB and beta-catenin signaling in diffuse large B-cell lymphomas', *Oncogene*, 35 (32), 4269-81.
- Bonilla, F. A. and Oettgen, H. C. (2010), 'Adaptive immunity', *J Allergy Clin Immunol*, 125 (2 Suppl 2), S33-40.
- Bonizzi, G. and Karin, M. (2004), 'The two NF-kappaB activation pathways and their role in innate and adaptive immunity', *Trends Immunol*, 25 (6), 280-8.
- Bornancin, F., et al. (2015), 'Deficiency of MALT1 paracaspase activity results in unbalanced regulatory and effector T and B cell responses leading to multiorgan inflammation', *J Immunol*, 194 (8), 3723-34.
- Brohl, A. S., et al. (2015), 'Germline CARD11 Mutation in a Patient with Severe Congenital B Cell Lymphocytosis', *J Clin Immunol*, 35 (1), 32-46.
- Brustle, A., et al. (2017), 'MALT1 is an intrinsic regulator of regulatory T cells', *Cell Death Differ*, 24 (7), 1214-23.

- Brustle, A., et al. (2012), 'The NF-kappaB regulator MALT1 determines the encephalitogenic potential of Th17 cells', *J Clin Invest*, 122 (12), 4698-709.
- Buchbinder, D., et al. (2015), 'Mild B-cell lymphocytosis in patients with a CARD11 C49Y mutation', *J Allergy Clin Immunol*, 136 (3), 819-21 e1.
- Burger, J. A. and Wiestner, A. (2018), 'Targeting B cell receptor signalling in cancer: preclinical and clinical advances', *Nat Rev Cancer*, 18 (3), 148-67.
- Cabalzar, K., et al. (2013), 'Monoubiquitination and activity of the paracaspase MALT1 requires glutamate 549 in the dimerization interface', *PLoS One*, 8 (8), e72051.
- Cambier, J. C., Pleiman, C. M., and Clark, M. R. (1994), 'Signal transduction by the B cell antigen receptor and its coreceptors', *Annu Rev Immunol*, 12, 457-86.
- Casadevall, A. and Pirofski, L. A. (2003), 'Antibody-mediated regulation of cellular immunity and the inflammatory response', *Trends Immunol*, 24 (9), 474-8.
- Chang, J. T., Wherry, E. J., and Goldrath, A. W. (2014), 'Molecular regulation of effector and memory T cell differentiation', *Nat Immunol*, 15 (12), 1104-15.
- Charbit-Henrion, F., et al. (2017), 'Deficiency in Mucosa-associated Lymphoid Tissue Lymphoma Translocation 1: A Novel Cause of IPEX-Like Syndrome', *J Pediatr Gastroenterol Nutr*, 64 (3), 378-84.
- Chaudhry, A., et al. (2009), 'CD4+ regulatory T cells control TH17 responses in a Stat3-dependent manner', *Science*, 326 (5955), 986-91.
- Chen, W., et al. (2003), 'Conversion of peripheral CD4+CD25- naive T cells to CD4+CD25+ regulatory T cells by TGF-beta induction of transcription factor Foxp3', *J Exp Med*, 198 (12), 1875-86.
- Cheng, L., et al. (2019), 'Malt1 Protease Is Critical in Maintaining Function of Regulatory T Cells and May Be a Therapeutic Target for Antitumor Immunity', *J Immunol*, 202 (10), 3008-19.
- Coornaert, B., et al. (2008), 'T cell antigen receptor stimulation induces MALT1 paracaspase-mediated cleavage of the NF-kappaB inhibitor A20', *Nat Immunol*, 9 (3), 263-71.
- Crabtree, G. R. (1999), 'Generic signals and specific outcomes: signaling through Ca<sup>2+</sup>, calcineurin, and NF-AT', *Cell*, 96 (5), 611-4.
- Cui, X., et al. (2017), 'Regnase-1 and Roquin Nonredundantly Regulate Th1 Differentiation Causing Cardiac Inflammation and Fibrosis', *J Immunol*, 199 (12), 4066-77.
- Curotto de Lafaille, M. A., et al. (2004), 'CD25- T cells generate CD25+Foxp3+ regulatory T cells by peripheral expansion', *J Immunol*, 173 (12), 7259-68.
- Dal Porto, J. M., et al. (2004), 'B cell antigen receptor signaling 101', *Mol Immunol*, 41 (6-7), 599-613.
- David, L., et al. (2018), 'Assembly mechanism of the CARMA1-BCL10-MALT1-TRAF6 signalosome', *Proc Natl Acad Sci U S A*, 115 (7), 1499-504.
- Davis, R. E., et al. (2001), 'Constitutive nuclear factor kappaB activity is required for survival of activated B cell-like diffuse large B cell lymphoma cells', *J Exp Med*, 194 (12), 1861-74.
- Davis, R. E., et al. (2010), 'Chronic active B-cell-receptor signalling in diffuse large B-cell lymphoma', *Nature*, 463 (7277), 88-92.
- Deshaies, R. J. and Joazeiro, C. A. (2009), 'RING domain E3 ubiquitin ligases', *Annu Rev Biochem*, 78, 399-434.
- Di Pilato, M., et al. (2019), 'Targeting the CBM complex causes Treg cells to prime tumours for immune checkpoint therapy', *Nature*, 570 (7759), 112-16.

- Dong, C., et al. (2000), 'JNK is required for effector T-cell function but not for T-cell activation', *Nature*, 405 (6782), 91-4.
- Dubois, S. M., et al. (2014), 'A catalytic-independent role for the LUBAC in NF-kappaB activation upon antigen receptor engagement and in lymphoma cells', *Blood*, 123 (14), 2199-203.
- Duwel, M., et al. (2009), 'A20 negatively regulates T cell receptor signaling to NF-kappaB by cleaving Malt1 ubiquitin chains', *J Immunol*, 182 (12), 7718-28.
- Egawa, T., et al. (2003), 'Requirement for CARMA1 in antigen receptor-induced NF-kappa B activation and lymphocyte proliferation', *Curr Biol*, 13 (14), 1252-8.
- Eitelhuber, A. C., et al. (2015), 'Activity-based probes for detection of active MALT1 paracaspase in immune cells and lymphomas', *Chem Biol*, 22 (1), 129-38.
- Elton, L., et al. (2016), 'MALT1 cleaves the E3 ubiquitin ligase HOIL-1 in activated T cells, generating a dominant negative inhibitor of LUBAC-induced NF-kappaB signaling', *FEBS J*, 283 (3), 403-12.
- Emmerich, C. H., Schmukle, A. C., and Walczak, H. (2011), 'The emerging role of linear ubiquitination in cell signaling', *Sci Signal*, 4 (204), re5.
- Ferch, U., et al. (2009), 'Inhibition of MALT1 protease activity is selectively toxic for activated B cell-like diffuse large B cell lymphoma cells', *J Exp Med*, 206 (11), 2313-20.
- Fu, M. and Blackshear, P. J. (2017), 'RNA-binding proteins in immune regulation: a focus on CCCH zinc finger proteins', *Nat Rev Immunol*, 17 (2), 130-43.
- Gaide, O., et al. (2002), 'CARMA1 is a critical lipid raft-associated regulator of TCR-induced NF-kappa B activation', *Nat Immunol*, 3 (9), 836-43.
- Gerondakis, S., et al. (2014), 'NF-kappaB control of T cell development', *Nat Immunol*, 15 (1), 15-25.
- Gewies, A., et al. (2014), 'Uncoupling Malt1 threshold function from paracaspase activity results in destructive autoimmune inflammation', *Cell Rep*, 9 (4), 1292-305.
- Ginster, S., et al. (2017), 'Two Antagonistic MALT1 Auto-Cleavage Mechanisms Reveal a Role for TRAF6 to Unleash MALT1 Activation', *PLoS One*, 12 (1), e0169026.
- Glasmacher, E., et al. (2010), 'Roquin binds inducible costimulator mRNA and effectors of mRNA decay to induce microRNA-independent post-transcriptional repression', *Nat Immunol*, 11 (8), 725-33.
- Greil, J., et al. (2013), 'Whole-exome sequencing links caspase recruitment domain 11 (CARD11) inactivation to severe combined immunodeficiency', *J Allergy Clin Immunol*, 131 (5), 1376-83 e3.
- Guiet, C. and Vito, P. (2000), 'Caspase recruitment domain (CARD)-dependent cytoplasmic filaments mediate bcl10-induced NF-kappaB activation', *J Cell Biol*, 148 (6), 1131-40.
- Guo, H., Callaway, J. B., and Ting, J. P. (2015), 'Inflammasomes: mechanism of action, role in disease, and therapeutics', *Nat Med*, 21 (7), 677-87.
- Ha, H., Han, D., and Choi, Y. (2009), 'TRAF-mediated TNFR-family signaling', *Curr Protoc Immunol*, Chapter 11, Unit11 9D.
- Hachmann, J., et al. (2012), 'Mechanism and specificity of the human paracaspase MALT1', *Biochem J*, 443 (1), 287-95.
- Hailfinger, S., et al. (2009), 'Essential role of MALT1 protease activity in activated B cell-like diffuse large B-cell lymphoma', *Proc Natl Acad Sci U S A*, 106 (47), 19946-51.

- Hailfinger, S., et al. (2011), 'Malt1-dependent RelB cleavage promotes canonical NF-kappaB activation in lymphocytes and lymphoma cell lines', *Proc Natl Acad Sci U S A*, 108 (35), 14596-601.
- Hara, H., et al. (2004), 'The molecular adapter Carma1 controls entry of IkappaB kinase into the central immune synapse', *J Exp Med*, 200 (9), 1167-77.
- Hara, H., et al. (2015), 'Clustering of CARMA1 through SH3-GUK domain interactions is required for its activation of NF-kappaB signalling', *Nat Commun*, 6, 5555.
- Hara, H., et al. (2003), 'The MAGUK family protein CARD11 is essential for lymphocyte activation', *Immunity*, 18 (6), 763-75.
- Harwood, N. E. and Batista, F. D. (2010), 'Early events in B cell activation', *Annu Rev Immunol*, 28, 185-210.
- Hayden, M. S. and Ghosh, S. (2012), 'NF-kappaB, the first quarter-century: remarkable progress and outstanding questions', *Genes Dev*, 26 (3), 203-34.
- Hinz, M. and Scheidereit, C. (2014), 'The IkappaB kinase complex in NF-kappaB regulation and beyond', *EMBO Rep*, 15 (1), 46-61.
- Holliday, M. J., et al. (2019), 'Structures of autoinhibited and polymerized forms of CARD9 reveal mechanisms of CARD9 and CARD11 activation', *Nat Commun*, 10 (1), 3070.
- Hulpiau, P., et al. (2016), 'MALT1 is not alone after all: identification of novel paracaspases', *Cell Mol Life Sci*, 73 (5), 1103-16.
- Ikeda, F. (2015), 'Linear ubiquitination signals in adaptive immune responses', *Immunol Rev*, 266 (1), 222-36.
- Isakov, N. and Altman, A. (2002), 'Protein kinase C(theta) in T cell activation', *Annu Rev Immunol*, 20, 761-94.
- Jabara, H. H., et al. (2013), 'A homozygous mucosa-associated lymphoid tissue 1 (MALT1) mutation in a family with combined immunodeficiency', *J Allergy Clin Immunol*, 132 (1), 151-8.
- Janeway, C. A., Jr. and Medzhitov, R. (2002), 'Innate immune recognition', *Annu Rev Immunol*, 20, 197-216.
- Jang, T. H., Park, J. H., and Park, H. H. (2013), 'Novel disulfide bond-mediated dimerization of the CARD domain was revealed by the crystal structure of CARMA1 CARD', *PLoS One*, 8 (11), e79778.
- Jattani, R. P., Tritapoe, J. M., and Pomerantz, J. L. (2016), 'Intramolecular Interactions and Regulation of Cofactor Binding by the Four Repressive Elements in the Caspase Recruitment Domain-containing Protein 11 (CARD11) Inhibitory Domain', *J Biol Chem*, 291 (16), 8338-48.
- Jaworski, M., et al. (2014), 'Malt1 protease inactivation efficiently dampens immune responses but causes spontaneous autoimmunity', *EMBO J*, 33 (23), 2765-81.
- Jeltsch, K. M., et al. (2014), 'Cleavage of roquin and regnase-1 by the paracaspase MALT1 releases their cooperatively repressed targets to promote T(H)17 differentiation', *Nat Immunol*, 15 (11), 1079-89.
- Jung, D., et al. (2006), 'Mechanism and control of V(D)J recombination at the immunoglobulin heavy chain locus', *Annu Rev Immunol*, 24, 541-70.
- King, C. G., et al. (2006), 'TRAF6 is a T cell-intrinsic negative regulator required for the maintenance of immune homeostasis', *Nat Med*, 12 (9), 1088-92.

- Kirisako, T., et al. (2006), 'A ubiquitin ligase complex assembles linear polyubiquitin chains', *EMBO J*, 25 (20), 4877-87.
- Klein, T., et al. (2015), 'The paracaspase MALT1 cleaves HOIL1 reducing linear ubiquitination by LUBAC to dampen lymphocyte NF-kappaB signalling', *Nat Commun*, 6, 8777.
- Knies, N., et al. (2015), 'Lymphomagenic CARD11/BCL10/MALT1 signaling drives malignant B-cell proliferation via cooperative NF-kappaB and JNK activation', *Proc Natl Acad Sci U S A*, 112 (52), E7230-8.
- Koch, M. A., et al. (2009), 'The transcription factor T-bet controls regulatory T cell homeostasis and function during type 1 inflammation', *Nat Immunol*, 10 (6), 595-602.
- Kojo, S., et al. (2009), 'Mechanisms of NKT cell anergy induction involve Cbl-b-promoted monoubiquitination of CARMA1', *Proc Natl Acad Sci U S A*, 106 (42), 17847-51.
- Lam, L. T., et al. (2005), 'Small molecule inhibitors of IkappaB kinase are selectively toxic for subgroups of diffuse large B-cell lymphoma defined by gene expression profiling', *Clin Cancer Res*, 11 (1), 28-40.
- Lamason, R. L., et al. (2010), 'Oncogenic CARD11 mutations induce hyperactive signaling by disrupting autoinhibition by the PKC-responsive inhibitory domain', *Biochemistry*, 49 (38), 8240-50.
- Lamothe, B., et al. (2008), 'The RING domain and first zinc finger of TRAF6 coordinate signaling by interleukin-1, lipopolysaccharide, and RANKL', *J Biol Chem*, 283 (36), 24871-80.
- Langel, F. D., et al. (2008), 'Multiple protein domains mediate interaction between Bcl10 and MALT1', *J Biol Chem*, 283 (47), 32419-31.
- Lenz, G. and Staudt, L. M. (2010), 'Aggressive lymphomas', *N Engl J Med*, 362 (15), 1417-29.
- Lenz, G., et al. (2008), 'Oncogenic CARD11 mutations in human diffuse large B cell lymphoma', *Science*, 319 (5870), 1676-9.
- Leppek, K., et al. (2013), 'Roquin promotes constitutive mRNA decay via a conserved class of stem-loop recognition motifs', *Cell*, 153 (4), 869-81.
- Li, S., et al. (2012), 'Structural insights into the assembly of CARMA1 and BCL10', *PLoS One*, 7 (8), e42775.
- Lobry, C., et al. (2007), 'Negative feedback loop in T cell activation through IkappaB kinase-induced phosphorylation and degradation of Bcl10', *Proc Natl Acad Sci U S A*, 104 (3), 908-13.
- Lomaga, M. A., et al. (1999), 'TRAF6 deficiency results in osteopetrosis and defective interleukin-1, CD40, and LPS signaling', *Genes Dev*, 13 (8), 1015-24.
- Lucas, P. C., et al. (2001), 'Bcl10 and MALT1, independent targets of chromosomal translocation in malt lymphoma, cooperate in a novel NF-kappa B signaling pathway', *J Biol Chem*, 276 (22), 19012-9.
- Macian, F. (2005), 'NFAT proteins: key regulators of T-cell development and function', *Nat Rev Immunol*, 5 (6), 472-84.
- Martinon, F., Burns, K., and Tschopp, J. (2002), 'The inflammasome: a molecular platform triggering activation of inflammatory caspases and processing of proIL-beta', *Mol Cell*, 10 (2), 417-26.
- MaruYama, T., et al. (2015), 'Control of IFN-gamma production and regulatory function by the inducible nuclear protein IkappaB-zeta in T cells', *J Leukoc Biol*, 98 (3), 385-93.
- Matsumoto, R., et al. (2005), 'Phosphorylation of CARMA1 plays a critical role in T Cell receptor-mediated NF-kappaB activation', *Immunity*, 23 (6), 575-85.

- Matsushita, K., et al. (2009), 'Zc3h12a is an RNase essential for controlling immune responses by regulating mRNA decay', *Nature*, 458 (7242), 1185-90.
- Maul, R. W. and Gearhart, P. J. (2010), 'AID and somatic hypermutation', *Adv Immunol*, 105, 159-91.
- Mc Guire, C., et al. (2014), 'Pharmacological inhibition of MALT1 protease activity protects mice in a mouse model of multiple sclerosis', *J Neuroinflammation*, 11, 124.
- McCully, R. R. and Pomerantz, J. L. (2008), 'The protein kinase C-responsive inhibitory domain of CARD11 functions in NF-kappaB activation to regulate the association of multiple signaling cofactors that differentially depend on Bcl10 and MALT1 for association', *Mol Cell Biol*, 28 (18), 5668-86.
- McKinnon, M. L., et al. (2014), 'Combined immunodeficiency associated with homozygous MALT1 mutations', *J Allergy Clin Immunol*, 133 (5), 1458-62, 62 e1-7.
- Medeiros, R. B., et al. (2007), 'Regulation of NF-kappaB activation in T cells via association of the adapter proteins ADAP and CARMA1', *Science*, 316 (5825), 754-8.
- Meininger, I. and Krappmann, D. (2016), 'Lymphocyte signaling and activation by the CARMA1-BCL10-MALT1 signalosome', *Biol Chem*, 397 (12), 1315-33.
- Meininger, I., et al. (2016), 'Alternative splicing of MALT1 controls signalling and activation of CD4(+) T cells', *Nat Commun*, 7, 11292.
- Metzger, M. B., et al. (2014), 'RING-type E3 ligases: master manipulators of E2 ubiquitin-conjugating enzymes and ubiquitination', *Biochim Biophys Acta*, 1843 (1), 47-60.
- Mino, T., et al. (2015), 'Regnase-1 and Roquin Regulate a Common Element in Inflammatory mRNAs by Spatiotemporally Distinct Mechanisms', *Cell*, 161 (5), 1058-73.
- Molinero, L. L., et al. (2012), 'T cell receptor/CARMA1/NF-kappaB signaling controls T-helper (Th) 17 differentiation', *Proc Natl Acad Sci U S A*, 109 (45), 18529-34.
- Molinero, L. L., et al. (2009), 'CARMA1 controls an early checkpoint in the thymic development of FoxP3+ regulatory T cells', *J Immunol*, 182 (11), 6736-43.
- Moreno-Garcia, M. E., et al. (2010), 'MAGUK-controlled ubiquitination of CARMA1 modulates lymphocyte NF-kappaB activity', *Mol Cell Biol*, 30 (4), 922-34.
- Morgan, J. A., et al. (1999), 'Breakpoints of the t(11;18)(q21;q21) in mucosa-associated lymphoid tissue (MALT) lymphoma lie within or near the previously undescribed gene MALT1 in chromosome 18', *Cancer Res*, 59 (24), 6205-13.
- Muto, G., et al. (2013), 'TRAF6 is essential for maintenance of regulatory T cells that suppress Th2 type autoimmunity', *PLoS One*, 8 (9), e74639.
- Nagel, D., et al. (2014), 'Mechanisms and consequences of constitutive NF-kappaB activation in B-cell lymphoid malignancies', *Oncogene*, 33 (50), 5655-65.
- Nagel, D., et al. (2012), 'Pharmacologic inhibition of MALT1 protease by phenothiazines as a therapeutic approach for the treatment of aggressive ABC-DLBCL', *Cancer Cell*, 22 (6), 825-37.
- Naito, A., et al. (1999), 'Severe osteopetrosis, defective interleukin-1 signalling and lymph node organogenesis in TRAF6-deficient mice', *Genes Cells*, 4 (6), 353-62.
- Nakagawa, M., et al. (2005), 'MALT1 contains nuclear export signals and regulates cytoplasmic localization of BCL10', *Blood*, 106 (13), 4210-6.
- Narciso, J. E., et al. (2011), 'Analysis of the antibody structure based on high-resolution crystallographic studies', *N Biotechnol*, 28 (5), 435-47.

- Noels, H., et al. (2007), 'A Novel TRAF6 binding site in MALT1 defines distinct mechanisms of NF-kappaB activation by API2middle dotMALT1 fusions', *J Biol Chem*, 282 (14), 10180-9.
- Oeckinghaus, A. and Ghosh, S. (2009), 'The NF-kappaB family of transcription factors and its regulation', *Cold Spring Harb Perspect Biol*, 1 (4), a000034.
- Oeckinghaus, A., et al. (2007), 'Malt1 ubiquitination triggers NF-kappaB signaling upon T-cell activation', *EMBO J*, 26 (22), 4634-45.
- Oh-hora, M. and Rao, A. (2008), 'Calcium signaling in lymphocytes', *Curr Opin Immunol*, 20 (3), 250-8.
- Parkin, J. and Cohen, B. (2001), 'An overview of the immune system', *Lancet*, 357 (9270), 1777-89.
- Paul, S. and Schaefer, B. C. (2013), 'A new look at T cell receptor signaling to nuclear factor-kappaB', *Trends Immunol*, 34 (6), 269-81.
- Paul, S., et al. (2012), 'Selective autophagy of the adaptor protein Bcl10 modulates T cell receptor activation of NF-kappaB', *Immunity*, 36 (6), 947-58.
- Pelzer, C., et al. (2013), 'The protease activity of the paracaspase MALT1 is controlled by monoubiquitination', *Nat Immunol*, 14 (4), 337-45.
- Qiao, Q., et al. (2013), 'Structural architecture of the CARMA1/Bcl10/MALT1 signalosome: nucleation-induced filamentous assembly', *Mol Cell*, 51 (6), 766-79.
- Rebeaud, F., et al. (2008), 'The proteolytic activity of the paracaspase MALT1 is key in T cell activation', *Nat Immunol*, 9 (3), 272-81.
- Reiley, W. W., et al. (2007), 'Deubiquitinating enzyme CYLD negatively regulates the ubiquitin-dependent kinase Tak1 and prevents abnormal T cell responses', *J Exp Med*, 204 (6), 1475-85.
- Roostalu, J. and Surrey, T. (2017), 'Microtubule nucleation: beyond the template', *Nat Rev Mol Cell Biol*, 18 (11), 702-10.
- Rosebeck, S., et al. (2011), 'Cleavage of NIK by the API2-MALT1 fusion oncoprotein leads to noncanonical NF-kappaB activation', *Science*, 331 (6016), 468-72.
- Rosenbaum, M., et al. (2019), 'Bcl10-controlled Malt1 paracaspase activity is key for the immune suppressive function of regulatory T cells', *Nat Commun*, 10 (1), 2352.
- Rossman, J. S., et al. (2006), 'POLKADOTS are foci of functional interactions in T-Cell receptor-mediated signaling to NF-kappaB', *Mol Biol Cell*, 17 (5), 2166-76.
- Rothe, M., et al. (1994), 'A novel family of putative signal transducers associated with the cytoplasmic domain of the 75 kDa tumor necrosis factor receptor', *Cell*, 78 (4), 681-92.
- Ruefli-Brasse, A. A., French, D. M., and Dixit, V. M. (2003), 'Regulation of NF-kappaB-dependent lymphocyte activation and development by paracaspase', *Science*, 302 (5650), 1581-4.
- Ruland, J., et al. (2003), 'Differential requirement for Malt1 in T and B cell antigen receptor signaling', *Immunity*, 19 (5), 749-58.
- Ruland, J., et al. (2001), 'Bcl10 is a positive regulator of antigen receptor-induced activation of NF-kappaB and neural tube closure', *Cell*, 104 (1), 33-42.
- Sakaguchi, S., et al. (1985), 'Organ-specific autoimmune diseases induced in mice by elimination of T cell subset. I. Evidence for the active participation of T cells in natural self-tolerance; deficit of a T cell subset as a possible cause of autoimmune disease', *J Exp Med*, 161 (1), 72-87.
- Satpathy, S., et al. (2015), 'Systems-wide analysis of BCR signalosomes and downstream phosphorylation and ubiquitylation', *Mol Syst Biol*, 11 (6), 810.

- Schaefer, B. C., et al. (2004), 'Complex and dynamic redistribution of NF-kappaB signaling intermediates in response to T cell receptor stimulation', *Proc Natl Acad Sci U S A*, 101 (4), 1004-9.
- Scharschmidt, E., et al. (2004), 'Degradation of Bcl10 induced by T-cell activation negatively regulates NF-kappa B signaling', *Mol Cell Biol*, 24 (9), 3860-73.
- Schimmack, G., et al. (2014), 'AIP augments CARMA1-BCL10-MALT1 complex formation to facilitate NF-kappaB signaling upon T cell activation', *Cell Commun Signal*, 12, 49.
- Schlauderer, F., et al. (2018), 'Molecular architecture and regulation of BCL10-MALT1 filaments', *Nat Commun*, 9 (1), 4041.
- Schlauderer, F., et al. (2013), 'Structural analysis of phenothiazine derivatives as allosteric inhibitors of the MALT1 paracaspase', *Angew Chem Int Ed Engl*, 52 (39), 10384-7.
- Schmidt-Supprian, M., et al. (2004), 'Differential dependence of CD4+CD25+ regulatory and natural killer-like T cells on signals leading to NF-kappaB activation', *Proc Natl Acad Sci U S A*, 101 (13), 4566-71.
- Schmitz, M. L. and Krappmann, D. (2006), 'Controlling NF-kappaB activation in T cells by costimulatory receptors', *Cell Death Differ*, 13 (5), 834-42.
- Schulze-Luehrmann, J. and Ghosh, S. (2006), 'Antigen-receptor signaling to nuclear factor kappa B', *Immunity*, 25 (5), 701-15.
- Shaffer, A. L., 3rd, Young, R. M., and Staudt, L. M. (2012), 'Pathogenesis of human B cell lymphomas', *Annu Rev Immunol*, 30, 565-610.
- Shambharkar, P. B., et al. (2007), 'Phosphorylation and ubiquitination of the IkappaB kinase complex by two distinct signaling pathways', *EMBO J*, 26 (7), 1794-805.
- Shinohara, H., et al. (2007), 'IkappaB kinase beta-induced phosphorylation of CARMA1 contributes to CARMA1 Bcl10 MALT1 complex formation in B cells', *J Exp Med*, 204 (13), 3285-93.
- Smith-Garvin, J. E., Koretzky, G. A., and Jordan, M. S. (2009), 'T cell activation', *Annu Rev Immunol*, 27, 591-619.
- Snipas, S. J., et al. (2004), 'Characteristics of the caspase-like catalytic domain of human paracaspase', *Biol Chem*, 385 (11), 1093-8.
- Snow, A. L., et al. (2012), 'Congenital B cell lymphocytosis explained by novel germline CARD11 mutations', *J Exp Med*, 209 (12), 2247-61.
- Sommer, K., et al. (2005), 'Phosphorylation of the CARMA1 linker controls NF-kappaB activation', *Immunity*, 23 (6), 561-74.
- Staal, J., et al. (2011), 'T-cell receptor-induced JNK activation requires proteolytic inactivation of CYLD by MALT1', *EMBO J*, 30 (9), 1742-52.
- Stepensky, P., et al. (2013), 'Deficiency of caspase recruitment domain family, member 11 (CARD11), causes profound combined immunodeficiency in human subjects', *J Allergy Clin Immunol*, 131 (2), 477-85 e1.
- Sun, L., et al. (2004), 'The TRAF6 ubiquitin ligase and TAK1 kinase mediate IKK activation by BCL10 and MALT1 in T lymphocytes', *Mol Cell*, 14 (3), 289-301.
- Sun, S. C. (2010), 'CYLD: a tumor suppressor deubiquitinase regulating NF-kappaB activation and diverse biological processes', *Cell Death Differ*, 17 (1), 25-34.
- Suzuki, H. I., et al. (2011), 'MCPIP1 ribonuclease antagonizes dicer and terminates microRNA biogenesis through precursor microRNA degradation', *Mol Cell*, 44 (3), 424-36.

- Tanner, M. J., et al. (2007), 'CARMA1 coiled-coil domain is involved in the oligomerization and subcellular localization of CARMA1 and is required for T cell receptor-induced NF-kappaB activation', *J Biol Chem*, 282 (23), 17141-7.
- Thome, M., et al. (2010), 'Antigen receptor signaling to NF-kappaB via CARMA1, BCL10, and MALT1', *Cold Spring Harb Perspect Biol*, 2 (9), a003004.
- Tokunaga, F. and Iwai, K. (2012), 'LUBAC, a novel ubiquitin ligase for linear ubiquitination, is crucial for inflammation and immune responses', *Microbes Infect*, 14 (7-8), 563-72.
- Torres, J. M., et al. (2014), 'Inherited BCL10 deficiency impairs hematopoietic and nonhematopoietic immunity', *J Clin Invest*, 124 (12), 5239-48.
- Turvey, S. E., et al. (2014), 'The CARD11-BCL10-MALT1 (CBM) signalosome complex: Stepping into the limelight of human primary immunodeficiency', *J Allergy Clin Immunol*, 134 (2), 276-84.
- Uehata, T., et al. (2013), 'Malt1-induced cleavage of regnase-1 in CD4(+) helper T cells regulates immune activation', *Cell*, 153 (5), 1036-49.
- Uren, A. G., et al. (2000), 'Identification of paracaspases and metacaspases: two ancient families of caspase-like proteins, one of which plays a key role in MALT lymphoma', *Mol Cell*, 6 (4), 961-7.
- Verhagen, A. M., Coulson, E. J., and Vaux, D. L. (2001), 'Inhibitor of apoptosis proteins and their relatives: IAPs and other BIRPs', *Genome Biol*, 2 (7), REVIEWS3009.
- Vyas, J. M., Van der Veen, A. G., and Ploegh, H. L. (2008), 'The known unknowns of antigen processing and presentation', *Nat Rev Immunol*, 8 (8), 607-18.
- Walsh, M. C., et al. (2008), 'TRAF6 autoubiquitination-independent activation of the NFkappaB and MAPK pathways in response to IL-1 and RANKL', *PLoS One*, 3 (12), e4064.
- Wang, D., et al. (2004), 'CD3/CD28 costimulation-induced NF-kappaB activation is mediated by recruitment of protein kinase C-theta, Bcl10, and IkappaB kinase beta to the immunological synapse through CARMA1', *Mol Cell Biol*, 24 (1), 164-71.
- Wang, H., et al. (2010), 'ZAP-70: an essential kinase in T-cell signaling', *Cold Spring Harb Perspect Biol*, 2 (5), a002279.
- Warrington, R., et al. (2011), 'An introduction to immunology and immunopathology', *Allergy Asthma Clin Immunol*, 7 Suppl 1, S1.
- Weaver, C. T., et al. (2007), 'IL-17 family cytokines and the expanding diversity of effector T cell lineages', *Annu Rev Immunol*, 25, 821-52.
- Weber, C. H. and Vincenz, C. (2001), 'The death domain superfamily: a tale of two interfaces?', *Trends Biochem Sci*, 26 (8), 475-81.
- Wegener, E., et al. (2006), 'Essential role for IkappaB kinase beta in remodeling Carma1-Bcl10-Malt1 complexes upon T cell activation', *Mol Cell*, 23 (1), 13-23.
- Weil, R. and Israel, A. (2004), 'T-cell-receptor- and B-cell-receptor-mediated activation of NF-kappaB in lymphocytes', *Curr Opin Immunol*, 16 (3), 374-81.
- Wiesmann, C., et al. (2012), 'Structural determinants of MALT1 protease activity', *J Mol Biol*, 419 (1-2), 4-21.
- Wu, C. J. and Ashwell, J. D. (2008), 'NEMO recognition of ubiquitinated Bcl10 is required for T cell receptor-mediated NF-kappaB activation', *Proc Natl Acad Sci U S A*, 105 (8), 3023-8.
- Wu, H. and Arron, J. R. (2003), 'TRAF6, a molecular bridge spanning adaptive immunity, innate immunity and osteoimmunology', *Bioessays*, 25 (11), 1096-105.

- Wucherpennig, K. W., et al. (2010), 'Structural biology of the T-cell receptor: insights into receptor assembly, ligand recognition, and initiation of signaling', *Cold Spring Harb Perspect Biol*, 2 (4), a005140.
- Yamamoto, M., et al. (2006), 'Key function for the Ubc13 E2 ubiquitin-conjugating enzyme in immune receptor signaling', *Nat Immunol*, 7 (9), 962-70.
- Yang, X., Chang, H. Y., and Baltimore, D. (1998), 'Autoproteolytic activation of pro-caspases by oligomerization', *Mol Cell*, 1 (2), 319-25.
- Yang, Y., et al. (2016a), 'Targeting Non-proteolytic Protein Ubiquitination for the Treatment of Diffuse Large B Cell Lymphoma', *Cancer Cell*, 29 (4), 494-507.
- Yang, Y. K., et al. (2016b), 'Molecular Determinants of Scaffold-induced Linear Ubiquitylation of B Cell Lymphoma/Leukemia 10 (Bcl10) during T Cell Receptor and Oncogenic Caspase Recruitment Domain-containing Protein 11 (CARD11) Signaling', *J Biol Chem*, 291 (50), 25921-36.
- Ye, H., et al. (2002), 'Distinct molecular mechanism for initiating TRAF6 signalling', *Nature*, 418 (6896), 443-7.
- Yin, Q., et al. (2009), 'E2 interaction and dimerization in the crystal structure of TRAF6', *Nat Struct Mol Biol*, 16 (6), 658-66.
- Yoshida, H., et al. (2005), 'The tumor suppressor cylindromatosis (CYLD) acts as a negative regulator for toll-like receptor 2 signaling via negative cross-talk with TRAF6 AND TRAF7', *J Biol Chem*, 280 (49), 41111-21.
- Yu, D., et al. (2007), 'Roquin represses autoimmunity by limiting inducible T-cell co-stimulator messenger RNA', *Nature*, 450 (7167), 299-303.
- Yu, J. W., et al. (2011), 'Crystal structure of the mucosa-associated lymphoid tissue lymphoma translocation 1 (MALT1) paracaspase region', *Proc Natl Acad Sci U S A*, 108 (52), 21004-9.
- Yu, J. W., et al. (2015), 'MALT1 Protease Activity Is Required for Innate and Adaptive Immune Responses', *PLoS One*, 10 (5), e0127083.
- Zhu, J. and Paul, W. E. (2008), 'CD4 T cells: fates, functions, and faults', *Blood*, 112 (5), 1557-69.

## 8 ABBREVIATIONS

Å	Ångström
ABC	activated B cell
ABP	activity-based probe
ADAP	adhesion and degranulation-promoting adapter protein
AIP	AhR interacting protein
AP-1	activator protein-1
APC	antigen presenting cell
ASC	apoptosis-associated speck-like protein containing a CARD
BCL10	B cell lymphoma 10
BCR	B cell receptor
BENTA	B cell expansion with NF- $\kappa$ B and T cell anergy
BLNK	B cell linker
BTK	bruton's tyrosine kinase
CARD	caspase recruitment domain
CARD11	CARD-containing coiled-coil protein 11
CBM	CARD11-BCL10-MALT1
CC	coiled-coil
CD	cluster of differentiation
clAP	cellular inhibitor of apoptosis protein
CID	combined immunodeficiency
cryo-EM	cryogenic electron microscopy
CYLD	cylindromatosis
DAG	diacylglycerol
DD	death domain
DLBCL	diffuse large B cell lymphoma
DUB	deubiquitinase
EAE	experimental autoimmune encephalomyelitis
EGFP	enhanced green fluorescent protein
EMSA	electrophoretic mobility shift assay
ERK	extracellular signal-regulated kinase
FACS	fluorescence-activated cell sorting
FoxP3	forkhead box P3
FYN	fibroblast yes-related non receptor kinase
GCB	germinal center B cell
GUK	guanylate kinase
HOIL-1	heme-oxidized IRP2 ubiquitin ligase 1
HOIP	HOIL-1-interacting protein
IAP	inhibitor of apoptosis
IFN	interferon
Ig	immunoglobulin
IKK	I $\kappa$ B kinase
IL	interleukin
IP	immunoprecipitation
IP <sub>3</sub>	inositol-1,4,5-triphosphate
ITAM	immunoreceptor tyrosine-based activation motif
I $\kappa$ B	inhibitor of NF- $\kappa$ B
JNK	c-Jun N-terminal kinase
kDa	kilodalton
KO	knockout
LAT	linker for the activation of T cells

---

LCK	lymphocyte-specific protein tyrosine kinase
LUBAC	linear ubiquitin chain assembly complex
LYN	Lck/Yes-related novel protein tyrosine kinase
MAGUK	membrane associated guanylate kinase
MALT1	mucosa-associated lymphoid tissue lymphoma translocation protein 1
MATH	Meprin and TRAF6 homology
MHC	major histocompatibility complex
MTOC	microtubule-organizing center
MyD88	myeloid differentiation primary response gene 88
NEMO	NF- $\kappa$ B essential modulator
NF- $\kappa$ B	nuclear factor kappa B
NFAT	nuclear factor of activated T cells
NHL	non-Hodgkin lymphoma
NIK	NF- $\kappa$ B-inducing kinase
NK	natural killer
NLS	nuclear localization sequence
nm	nanometer
NMR	nuclear magnetic resonance
PMA	Phorbol 12-myristate 13-acetate
PD	pulldown
PDK1	phosphoinositide-dependent kinase 1
PDZ	PSD95, Dlg1, ZO-1
PIP <sub>2</sub>	phosphatidylinositol-4,5-bisphosphate
PKC	protein kinase C
PLC $\gamma$	phospholipase C $\gamma$
PM	protease mutant
POLKADOTS	punctate and oligomeric killing or activating domains transducing signals
PRR	pattern-recognition receptors
P/I	PMA/Ionomycin
RANKL	receptor activator of NF- $\kappa$ B ligand
Ras	rat sarcoma
RING	really interesting new gene
RNA	<i>ribonucleic acid</i>
sgRNA	single guide RNA
SH3	Src homology 3
SHARPIN	Shank-associated RH domain-interacting protein
SLP-76	SH2 containing leukocyte phosphoprotein of 76 kDa
SMAC	second mitochondrial-derived activator of caspases
SOS	son of sevenless
Src	sarcoma
SYK	spleen tyrosine kinase
S/T	Serine/Threonine
TCR	T cell receptor
Teff	effector T cells
T <sub>H</sub>	T helper
TLR	toll-like receptor
TNF $\alpha$	tumor necrosis factor alpha
TNFR	tumor necrosis factor receptor
TRAF	tumor necrosis factor receptor associated factor
Treg	regulatory T cell
T6BM	TRAF6 binding motif

UBC	ubiquitin-conjugating enzyme
UTR	untranslated region
WB	western blot
WT	wildtype
Z	Zinc finger
ZAP70	zeta-chain-associated protein kinase 70 kDa

---

## 9 APPENDIX

### 9.1 Declaration of individual contribution

#### Publication I

**Thomas Seeholzer\***, Susanne Kurz\*, Florian Schlauderer, Simone Woods, Torben Gehring, Simon Widmann, Katja Lammens, Daniel Krappmann (2018). BCL10-CARD11 Fusion Mimics an Active CARD11 Seed That Triggers Constitutive BCL10 Oligomerization and Lymphocyte Activation. *Front. Immunol.* 9:2695. \* equal contribution

In this first-author publication, Thomas Seeholzer, together with Susanne Kurz as an equal co-author, clarified the role of CARD11 seeding function and BCL10 filament formation for lymphocyte activation. Thomas Seeholzer supervised Susanne Kurz during her master's thesis, and both conceived and performed most experiments, analysed and interpreted the data. Experiments during the revision process were solely performed by Thomas Seeholzer. Initial experiments with homotypic CARD-CARD BCL10 interface mutants were performed by Thomas Seeholzer (Fig. 1F, Fig. 2D+E, Fig. S2E, Fig. S3B). Susanne Kurz cloned the BCL10-CARD11 fusion constructs, reconstituted Jurkat and BJAB CARD11 KO cells and performed cellular experiments (Fig. 2B+C, Fig. 3, Fig. 4A, Fig. 5, Fig.6, Fig. S3A, Fig. 4). Thomas Seeholzer performed transient expression experiments of the BCL10-CARD11 fusion proteins (Fig. 5B-D), and both Thomas Seeholzer and Susanne Kurz conducted and quantified confocal immunofluorescence experiments (Fig. 1E).

## Publication II

Florian Schlauderer\*, **Thomas Seeholzer\***, Ambroise Desfosses\*, Torben Gehring, Mike Strauss, Karl-Peter Hopfner, Irina Gutsche, Daniel Krappmann, Katja Lammens (2018). Molecular architecture and regulation of BCL10-MALT1 filaments. *Nat Commun.* 9:4041. \* equal contribution

In this co-authorship, first author Florian Schlauderer, with equal contribution from Thomas Seeholzer and Ambroise Desfosses, investigated the molecular architecture and regulation of BCL10-MALT1 filaments. Florian Schlauderer prepared the cryo-EM samples, collected the data and determined the structural model of the BCL10-MALT1 filament (Fig. 1, Fig. 2, Fig. 4a-c, Fig. 6, Fig. S1, Fig. S2, Fig. S4a-c). Ambroise Desfosses performed helical reconstruction and thereby contributed significantly to the determination of the cryo-EM structure (Fig. S7, Fig. S8). Thomas Seeholzer performed all cellular experiments for the functional analysis of BCL10-BCL10 (Fig. 3, Fig. S3) and BCL10-MALT1 interfaces (Fig. 4d, Fig. 5a-h, Fig. S4d, Fig. S5) in Jurkat T cells and thereby determined their essential role for CBM-complex formation, MALT1 protease activation and downstream NF- $\kappa$ B signaling in cells.

## Manuscript I

**Thomas Seeholzer**, Andreas Gewies, Thomas J. O'Neill, Carina Graß, Katrin Demski, Aurelia Weber, Daniel Krappmann (in preparation). Homeostatic control of MALT1 protease activity by the Ubiquitin ligase TRAF6. *In preparation*.

Thomas Seeholzer generated TRAF6 KO Jurkat T cells and performed all experiments, except generation of *Traf6<sup>fl/fl</sup>;CD4-Cre* mice (Andreas Gewies) and their FACS analysis (Andreas Gewies and Thomas O'Neill, Fig. 2g). Aurelia Weber generated HOIP KO Jurkat T cells (Fig. S2a) and Katrin Demski performed experiments for quantitative PCR (Fig. 5b, c). Carina Graß generated the NF- $\kappa$ B-EGFP reporter construct. Thomas Seeholzer and Daniel Krappmann conceived the study, analyzed and interpreted the data, and wrote the manuscript.

---

## 9.2 Further publications

Cho JJ, Xu Z, Parthasarathy U, Drashansky TT, Helm EY, Zuniga AN, Lorentsen KJ, Mansouri S, Cho JY, Edelmann MJ, Duong DM, Gehring T, **Seeholzer T**, Krappmann D, Uddin MN, Califano D, Wang RL, Jin L, Li H, Lv D, Zhou D, Zhou L, Avram D (2019): Hectd3 promotes pathogenic Th17 lineage through Stat3 activation and Malt1 signaling in neuroinflammation. *Nat Commun.* 10: 701

Bardet M, **Seeholzer T**, Unterreiner A, Woods S, Krappmann D, Bornancin F (2018): MALT1 activation by TRAF6 needs neither BCL10 nor CARD11. *Biochemical and biophysical research communications* 506: 48-52

Gehring T, **Seeholzer T**, Krappmann D (2018): BCL10 - Bridging CARDS to Immune Activation. *Front Immunol* 9: 1539

Bognar MK, Vincendeau M, Erdmann T, **Seeholzer T**, Grau M, Linnemann JR, Ruland J, Scheel CH, Lenz P, Ott G, Lenz G, Hauck SM, Krappmann D (2016): Oncogenic CARMA1 couples NF-kappaB and beta-catenin signaling in diffuse large B-cell lymphomas. *Oncogene* 35: 4269-81

Meininger I, Griesbach RA, Hu D, Gehring T, **Seeholzer T**, Bertossi A, Kranich J, Oeckinghaus A, Eitelhuber AC, Greczmiel U, Gewies A, Schmidt-Supprian M, Ruland J, Brocker T, Heissmeyer V, Heyd F, Krappmann D (2016): Alternative splicing of MALT1 controls signalling and activation of CD4(+) T cells. *Nat Commun* 7: 11292

### 9.3 Acknowledgments

First, I want to thank my doctoral thesis supervisor **Daniel Krappmann** for providing me the opportunity to perform this project in his group, and all his excellent help and mentoring to guide me through my dissertation. Thank you very much for having me.

I also want to thank all members of my thesis committee for critically reviewing my thesis.

Special thanks go to the members of my HELENA thesis committee for fruitful discussions and great advices: Vigo Heissmeyer and Katja Lammens.

Further, I want to thank our collaboration partners Florian Schlauderer, Ambroise Desfosses, Irina Gutsche, Katja Lammens and all other co-authors for contributing to this work. Special thanks go to **Susanne Kurz**: best master's student ever!

I want to thank all present and former members of the Krappmann lab and other groups at the Institute for Molecular Toxicology and Pharmacology for permanent support and motivation. I want to express my gratitude especially to **Aurelia Weber**, who is, and always will be, the greatest.

The most important at the end: friends and family, thanks for everything!